

Understanding motor control and impairment: An upper-limb model for muscular assessment

Présentée le 5 juin 2023

Faculté des sciences et techniques de l'ingénieur
Chaire Fondation Bertarelli en neuro-ingénierie translationnelle
Programme doctoral en mécanique

pour l'obtention du grade de Docteur ès Sciences

par

Tristan Jean Robin BARJAVEL

Acceptée sur proposition du jury

Prof. F. Gallaire, président du jury
Prof. S. Micera, directeur de thèse
Prof. A. Roby-Brami, rapporteuse
Prof. M. Casadio, rapporteuse
Prof. F. Hummel, rapporteur

Acknowledgements

I am usually not really good with expressing gratitude and showing how those who have helped me are important for the challenging yet rewarding journey to concluding this PhD dissertation. These acknowledgements, if not extensive, give me this opportunity.

First and foremost, I would like to express my most heartfelt gratitude to Prof. Silvestro Micera for having me join the amazing TNE lab. You gave me quite some cherished independence but kept me on track with your profound knowledge, insightful guidance regarding numerous aspects of my thesis without forgetting your understanding and patience while I was facing difficulties in this research. I consider myself fortunate to have been able to work under your supervision.

I would like to extend my gratitude to the rest of my thesis committee, Prof. Friedhelm Hummel, Prof. Agnès Roby-Brami, Prof. Maura Casadio and Prof. François Gallaire for your time reviewing my dissertation. Your expertise and insightful comments have significantly enhanced the quality and scope of my work.

Throughout my thesis, I have been working within the best possible environment, the TNE lab and all my colleagues clearly have made my work there more enjoyable. The cool and friendly ambiance has been a constant source of motivation and inspiration with all the discussions and brainstorming sessions. Even as PhD students have come and gone, I am thankful for the connections we have forged and the enduring sense of community that has persisted. I know you will recognize yourselves, and you know me, I won't cite all of you, but I deeply hope that we will keep interacting in the future.

To my friends, here again, I cannot name you all, but I would first like to apologize for my absence in the past few months (even year maybe ?). I guess I might have had to finish this thesis... Anyway, this is also the perfect time to thank you all, I clearly felt both understanding and support from you guys and you were always a good source of enjoyment and fun. Special thanks to Barthok and Francis.

I am also grateful to my parents, Marie-Noëlle and Jacques, without forgetting Jean-Louis. Clearly, I would not have been able to start this journey without your support from my earliest years. My whole family has always been there for me and pushed me toward possible success. Especially my brothers and sister Pierre-Loup, Pol-Rémy and

Lye-Jade. I could not forget my nieces and nephew, Valence, Joséphine, and Marius. I hope the best for your future.

Finally, I want to express my deepest thank to Vildana, who endured my ups and downs with kindness and for being so encouraging, without forgetting my dog Abou, who was of great support, especially during the pandemic.

Un grand merci à tous !

T. B.

Abstract

The human upper limb is a complex musculoskeletal system that can still perform various tasks with impressive efficacy thanks to the ability of the central nervous system to control and modulate the activation of more than 40 muscles.

Stroke is a leading cause of long-term disability, and individuals who have experienced a stroke often show unusual muscle activation patterns in the limb that was affected. A thorough understanding of these changes in muscle activation is crucial for the development of efficient rehabilitation plans.

So far, the study of the recorded electromyographic (EMG) signals has been the primary option for investigating muscle activation during movement.

Unfortunately, given the number of muscles acting on the shoulder and arm and their positions with respect to each other, a complete upper-limb's muscles EMG recording is not feasible in practice. Numerical musculoskeletal model could represent a very useful alternative approach to gather this kind of information.

This thesis aims at extending an existing upper-limb musculoskeletal model, to capture the overall muscle activations of a subject from its scaled recorded kinematics and a limited number of recorded muscle EMG.

The original model was force-based and its aim was to obtain the muscle forces from inverse dynamics (ID). However, these could not always be physiologically feasible, indeed, after modeling the musculotendon dynamics with a Hill-type model we further reduced their boundaries leading to unfeasible activations solutions. The ID was then reformulated to be activation based ensuring feasible activation and force given the muscle state. Moreover studying patients performing reaching tasks with an exoskeleton can lead to non-smooth kinematics, further restricting the ID possible solutions. A flexible formulation allowing for tolerance of torques at the joints was added.

The purpose of this thesis is to present a tool that can be used to study variations in muscle activations from healthy and stroke patients during their rehabilitation. This means that a large dataset with multiple repetitions of the different tasks and subjects

has to be simulated which would not be practical with the initial model. However, with a rigid tendon muscle assumption as well as the precomputation of multiple functions of the model, the computation time could be reduced by almost 2 orders of magnitude when studying multiple movements.

In the last part of the thesis I could show how the model could help with a quantified evaluation and functional diagnosis of stroke patients which is in contrast to current assessment methods. It also establishes a study of the muscle co-contractions and synergies given the full set of muscles acting on the shoulder and arm.

I also developed a forward dynamics methods of the model which aims was at first to be solely driven by muscle activations, but without the closed-loop formulation, it is too unstable in its current state because of the accumulation of numerical errors over a simulation. It is however setting the ground for possible further development.

A graphical user interface was also developed for simpler and adaptable use of the model, in the forward and inverse modes, and for the study of multiple subjects and repetitions.

The achievements presented in the thesis can provide a tool to better understand the mechanisms underlying upper limb control as well as its impairments. Moreover, it sets a framework for future developments to be in terms used in the clinics.

Key words

musculoskeletal model, human motor control, shoulder biomechanics, inverse dynamics, forward dynamics, muscle activation, muscle synergies, stroke, rehabilitation,

Résumé

Le membre supérieur humain est un système musculo-squelettique complexe qui peut cependant accomplir diverses tâches avec une efficacité impressionnante grâce à la capacité du système nerveux central à contrôler et moduler l'activation de plus de 40 muscles.

L'accident vasculaire cérébral (AVC) est l'une des principales causes d'invalidité à long terme, et les personnes ayant subi un AVC présentent souvent des schémas d'activation musculaire inhabituels dans le membre touché. Une compréhension approfondie de ces changements dans l'activation musculaire est cruciale pour le développement de plans de réhabilitation efficaces.

Jusqu'à présent, l'étude des signaux électromyographiques (EMG) enregistrés a été la principale option pour étudier l'activation musculaire pendant le mouvement.

Cependant, étant donné le nombre de muscles agissant sur l'épaule et le bras et leurs positions les uns par rapport aux autres, un enregistrement EMG complet des muscles du membre supérieur n'est pas réalisable en pratique. Un modèle musculo-squelettique numérique pourrait représenter une approche alternative très utile pour recueillir ce type d'informations.

Cette thèse vise à étendre un modèle musculo-squelettique existant du membre supérieur, afin de capturer les toutes activations musculaires d'un sujet à partir de sa cinématique et d'un nombre limité d'EMG musculaires enregistrés.

Le modèle original était basé sur l'évaluation de forces et son objectif était d'obtenir ces dernières à partir de la dynamique inverse (ID). Cependant, celles-ci ne sont pas toujours physiologiquement possible. En effet, après avoir modélisé la dynamique du musculotendon avec un modèle de type Hill, leurs limites physiologiques ont encore été réduites. Cela a conduit à des solutions irréalisables. L'ID a alors été reformulée pour être basée sur l'activation, garantissant une activation et une force réalisables compte tenu de l'état du muscle.

De plus, l'étude de patients effectuant des tâches visant à atteindre des cibles avec un exosquelette peut entraîner une cinématique très irrégulière, ce qui restreint encore les

solutions possibles de l'ID. Une formulation flexible permettant une certaine tolérance au niveau des couples au niveau des articulations a été ajoutée.

L'objectif de cette thèse est de présenter un outil qui peut être utilisé pour étudier les variations des activations musculaires de personnes saines et de patients victimes d'un accident vasculaire cérébral (AVC) au cours de leur rééducation. Cela signifie qu'un grand ensemble de données avec de multiples répétitions des différentes tâches et des différents sujets doit être simulé, ce qui n'aurait pas été faisable avec le modèle initial. Cependant, avec l'hypothèse d'un tendon rigide ainsi que le pré-calcul de plusieurs fonctions du modèle, le temps de calcul a pu être diminué de près de deux ordres de grandeur lors de l'étude de plusieurs mouvements.

Dans la dernière partie de la thèse, j'ai pu montrer comment le modèle pouvait aider à une évaluation quantifiée et à un diagnostic fonctionnel des patients victimes d'un accident vasculaire cérébral, ce qui contraste avec les méthodes d'évaluation actuelles qui sont plus qualitatives pour la plupart.

J'ai également développé une méthode de dynamique directe du modèle qui visait au départ à être uniquement piloté par les activations musculaires, mais sans la formulation en boucle fermée, cette dernière est trop instable en raison de l'accumulation d'erreurs numériques au cours d'une simulation. Elle pose cependant les bases d'un éventuel développement ultérieur et d'autres possibles utilisations du modèle.

Une interface utilisateur graphique a également été développée pour une utilisation plus simple et adaptable du modèle, en mode direct et inverse, et pour l'étude de multiples sujets et répétitions.

Les réalisations présentées dans cette thèse peuvent fournir un outil pour mieux comprendre les mécanismes qui sont sous-jacents au contrôle du membre supérieur ainsi que ses déficiences. De plus, elle établit un cadre pour les développements futurs afin d'être en termes utilisés dans les cliniques.

Mots clefs :

modèle musculo-squelettique, contrôle moteur humain, biomécanique de l'épaule, dynamique inverse, dynamique directe, activation musculaire, synergies musculaires, accident vasculaire cérébral, rééducation,

Contents

| | |
|---|-------------|
| Acknowledgements | i |
| Abstract (English/Français) | iii |
| List of figures | xi |
| List of tables | xiii |
| 1 Introduction | 1 |
| 1.1 Upperlimb physiological aspects | 1 |
| 1.1.1 Anatomy and functionality | 1 |
| 1.1.2 Control of upper-limb movement physiological mechanisms . . | 4 |
| 1.1.3 Muscle synergy principles | 8 |
| 1.1.4 Physiological assessment methods and limitations | 11 |
| 1.2 Stroke impairments | 13 |
| 1.3 State of the art and existing upper limb models for muscle assessment | 15 |
| 1.4 Objectives and outline of the thesis | 16 |
| 2 Upper limb numerical model | 17 |
| 2.1 Musculoskeletal modeling | 17 |
| 2.2 Musculokeletal geometry | 18 |
| 2.2.1 Equations of movement | 21 |
| 2.3 Musculotendon dynamics | 23 |
| 2.3.1 Musculotendon contraction dynamics | 26 |
| 2.3.2 Activation dynamics | 26 |
| 2.3.3 Contraction dynamics | 27 |
| 2.3.4 Rigid-tendon model | 31 |
| 2.4 Inverse dynamics formulation | 32 |
| 2.5 Forward dynamics formulation | 35 |
| 2.6 GUI visualization and reduced model | 36 |
| 2.7 Future possibilities | 40 |
| | vii |

| | | |
|----------|---|-----------|
| 3 | Biomechanical model and healthy subjects muscle activation assessment | 43 |
| 3.1 | Abstract | 44 |
| 3.2 | Introduction | 45 |
| 3.3 | Methods | 48 |
| 3.3.1 | Numerical model | 48 |
| 3.3.2 | Experimental set-up and recorded data | 48 |
| 3.3.3 | Data initialization | 49 |
| 3.3.4 | EMG signals preprocessing and activation dynamics | 50 |
| 3.3.5 | Activation estimation | 51 |
| 3.3.6 | Model results validation | 55 |
| 3.4 | Results | 56 |
| 3.4.1 | Raw comparison of activations for a specific target | 56 |
| 3.4.2 | Error evaluation in joint moments and activations estimations | 57 |
| 3.4.3 | Mean activation for all targets | 59 |
| 3.5 | Discussion | 60 |
| 3.6 | Conclusion | 62 |
| 4 | Impairment and improvement of muscle assessments through activation modeling | 65 |
| 4.1 | Abstract | 67 |
| 4.2 | Introduction | 67 |
| 4.3 | Material and methods | 69 |
| 4.3.1 | Subjects | 69 |
| 4.3.2 | Experimental protocol | 70 |
| 4.3.3 | Muscle activations estimations | 70 |
| 4.3.4 | Impairment estimation | 72 |
| 4.3.5 | Muscle co-contractions evaluations | 75 |
| 4.3.6 | Muscle synergies evaluation | 76 |
| 4.4 | Results | 78 |
| 4.4.1 | Validation of the impairment assessment | 78 |
| 4.4.2 | Muscle co-contraction between healthy and patients groups | 80 |
| 4.4.3 | Muscle synergy analysis | 82 |
| 4.5 | Discussion | 85 |
| 4.6 | Conclusion | 86 |
| 5 | Conclusion and perspectives | 89 |
| 5.1 | Summary | 90 |
| 5.2 | Limitations and future developments | 91 |
| A | Appendix | 95 |
| A.1 | Appendix chapter 3 | 96 |
| A.1.1 | Joint moment reconstruction and error | 96 |
| A.1.2 | Means of activation computed per target reached | 98 |

| | | |
|-------------------------|---|------------|
| A.1.3 | Levels of activation computed per muscle and target reached . . . | 105 |
| A.1.4 | Leave-one-out cross-validation for all subjects | 105 |
| A.2 | Appendix chapter 4 | 106 |
| A.2.1 | Rotations observed per target reached | 106 |
| A.2.2 | Tables of RMSE between healthy and patients activations while reaching targets | 110 |
| Bibliography | | 140 |
| Curriculum Vitae | | 141 |

List of Figures

| | | |
|-----|--|----|
| 1.1 | Joints considered and their corresponding bones | 2 |
| 1.2 | Upper limb muscles considered | 3 |
| 1.3 | Voluntary motor control pathways | 5 |
| 1.4 | Muscular contraction and relaxation | 6 |
| 1.5 | Muscle synergy principle | 9 |
| 2.1 | MRI scan used for bony structures reconstructions, model and joints definitions | 19 |
| 2.2 | The musculoskeletal model | 24 |
| 2.3 | Hill-type musculotendon model and normalized functions | 28 |
| 2.4 | Graphical user interface for inverse dynamics of a single movement . . | 38 |
| 2.5 | Graphical user interface for inverse dynamics of a multiple movements | 39 |
| 2.6 | Graphical user interface for forward dynamics | 40 |
| 3.1 | General overview of the presented estimation model and methodologies | 47 |
| 3.2 | Illustrations representing ALEx RS exoskeleton and musculoskeletal model performing a task in the virtual environment. | 51 |
| 3.3 | Means of muscle activations across the 5 repetitions for all 5 subjects while reaching target 13 | 57 |
| 3.4 | Results of activations levels and intermuscle leave-one-out errors . . . | 60 |
| 4.1 | General overview of the present study, to evaluate impairment | 71 |
| 4.2 | Musculoskeletal joints and targets to reach | 73 |
| 4.3 | Illustrations presenting the importance of having metrics for the level of activations. On the top, two sinusoids are generated with one delayed and scaled up, this aims at showing two signals that should not be considered as completely dissimilar. However, they present a RMSE and a Pearson's coefficient R very low. With the introduction of the cumulative sum of the signals on the bottom, the levels of activations are considered and a Pearson's coefficient is more representative of this level of activation. | 76 |
| 4.4 | Number of synergies determination from VAF curves | 77 |

| | | |
|------|---|-----|
| 4.5 | Muscle co-contraction while performing reaching tasks | 81 |
| 4.6 | Synergy weights and dot products from reference cluster based on the target reached | 83 |
| 4.7 | Synergy weights and dot products from reference cluster | 84 |
| A.1 | Measured and recomputed joint moments with the EMG-assisted and static-optimization methods | 97 |
| A.2 | Means of the estimated muscles activations while reaching target: 1 . . | 99 |
| A.3 | Means of the estimated muscles activations while reaching target: 3 . . | 100 |
| A.4 | Means of the estimated muscles activations while reaching target: 5 . . | 101 |
| A.5 | Means of the estimated muscles activations while reaching target: 7 . . | 102 |
| A.6 | Means of the estimated muscles activations while reaching target: 10 . | 103 |
| A.7 | Means of the estimated muscles activations while reaching target: 13 . | 104 |
| A.8 | Levels of activations of muscles per target reached: first part | 107 |
| A.9 | Levels of activations of muscles per target reached: second part | 108 |
| A.10 | leave-one-out cross-validation for all subjects | 109 |

List of Tables

| | | |
|------|---|-----|
| 3.1 | Table of the overall errors from estimations and recorded data for each of the 6 targets reached | 58 |
| 4.1 | Demographics of the stroke population recruited in the study. | 69 |
| 4.2 | Main agonist and antagonist muscle per target reached | 74 |
| 4.3 | RMSE between healthy and patients activations | 78 |
| 4.4 | Pearsons's correlation coefficients between the cumulative sums of healthy and patients activations | 79 |
| A.1 | Table of the rotated joint angles per target reached | 106 |
| A.2 | RMSE between healthy and patients activations while reaching target 1 | 111 |
| A.3 | RMSE between healthy and patients activations while reaching target 3 | 112 |
| A.4 | RMSE between healthy and patients activations while reaching target 5 | 113 |
| A.5 | RMSE between healthy and patients activations while reaching target 7 | 114 |
| A.6 | RMSE between healthy and patients activations while reaching target 10 | 115 |
| A.7 | RMSE between healthy and patients activations while reaching target 13 | 116 |
| A.8 | Pearson's correlation coefficient from cumulated activations between healthy and patients' ones for each muscle while reaching the target 1 . | 117 |
| A.9 | Pearson's correlation coefficient from cumulated activations between healthy and patients' ones for each muscle while reaching the target 3 . | 118 |
| A.10 | Pearson's correlation coefficient from cumulated activations between healthy and patients' ones for each muscle while reaching the target 5 . | 119 |
| A.11 | Pearson's correlation coefficient from cumulated activations between healthy and patients' ones for each muscle while reaching the target 7 . | 120 |
| A.12 | Pearson's correlation coefficient from cumulated activations between healthy and patients' ones for each muscle while reaching the target 10 | 121 |
| A.13 | Pearson's correlation coefficient from cumulated activations between healthy and patients' ones for each muscle while reaching the target 13 | 122 |
| A.14 | Pearson's coefficients for recorded EMG, for Targets (1,3,5) | 123 |
| A.15 | Pearson's coefficients for recorded EMG, for Targets (7,10,13) | 124 |
| A.16 | RMSE between healthy and patients' ones for the recorded muscles (T=1,3,5) | 125 |

A.17 RMSE between healthy and patients' ones for the recorded muscles
(T=1,3,5) 126

1 Introduction

1.1 Upperlimb physiological aspects

1.1.1 Anatomy and functionality

The human upper limb is a complex system that allows for the orientation and position of the hand, which is the primary component of physical interaction with the environment. Anatomically speaking, this can be performed via a combined motion of the shoulder, elbow and wrist joints and in particular, the coordinated movements of each bone involved in these articulations; the clavicle, scapula, humerus, ulna, radius and finally the bones of the hand.

In this thesis, we will focus mainly on the shoulder and elbow joints responsible of the upper-limb reaching tasks. The complex shoulder joint is a combination of three synovial joints acting as ball and sockets, sternoclavicular, acromioclavicular and glenohumeral connecting the clavicle to the sternum, the scapula acromion to the clavicle and the glenoid of the scapula to the humeral head respectively. The elbow articulation, is similarly a combination of the ulnohumeral joint, between the ulna and humerus, the radio humeral joint, between the radius and humerus and the proximal radioulnar joint, between the radius and ulna allowing for the pronation and supination movements. Fig 1.1 represents the bones and joint configuration.

The mentioned bones are kept interconnected via a combined action of various soft tissues; (i) the cartilage, a thin, strong, flexible, and smooth surface on each bone at the point of contact allowing for smooth movement between them, absorbing shocks and reducing friction between the bones, (ii) the ligaments, a firm rope like tissue connecting passively the bones to each other or forming capsules around the articulations containing synovial fluid. Finally, (iii) the tendons, connecting the muscles acting on the joints to the bones, providing further support and moving them. Additionally,

the bony shapes also play an important role in the movement, for instance, there is a perfect fit between the ulna's trochlear notch and the trochlea of the humerus.

The articulations concerned act as ball and socket joints, if small translation between these might occur, it will not be addressed in the scope of this thesis apart from the stability of the glenohumeral joint.

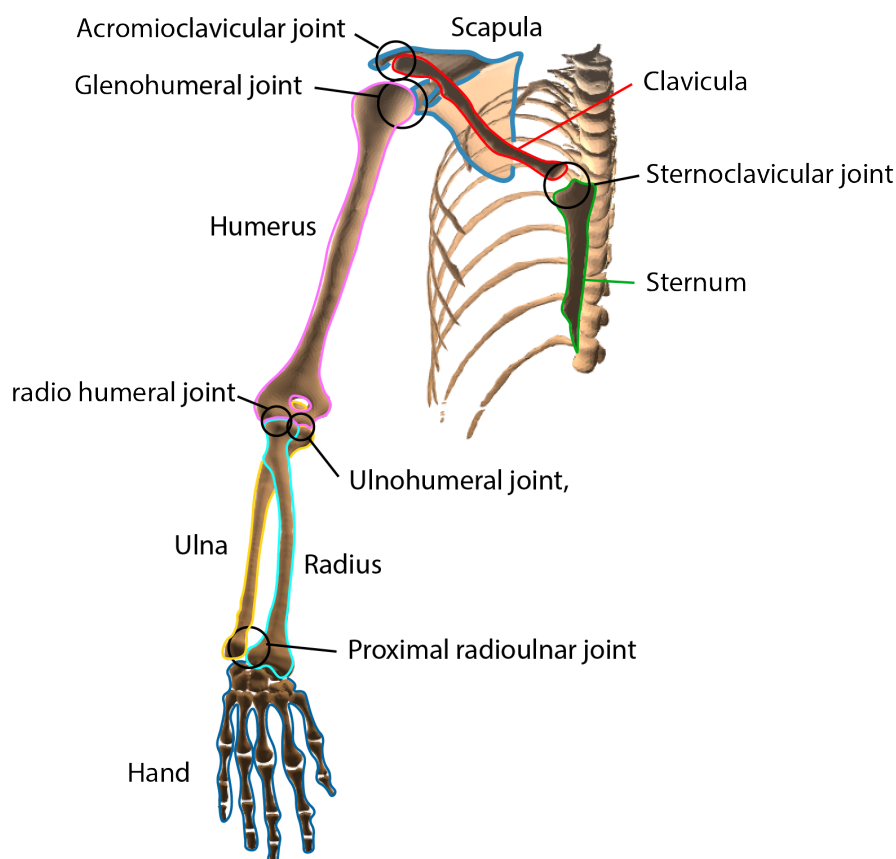


Figure 1.1: Joints considered and their corresponding bones.

42 muscles parts spanning the upper-limb joints described before are considered in this thesis including subclavius, serratus anterior upper, middle and lower parts, trapezius C1-C6/C7/T1/T2-T7, elevator scapulae, rhomboid minor, rhomboid major T1-T2 and T3-T4, pectoralis minor, pectoralis major clavicular sternal and ribs, latissimus dorsi thoracic, lumbar and iliac, deltoid clavicular, acromial and scapular, supraspinatus, infraspinatus, subscapularis, teres minor and major, coracobrachialis, triceps brachii long, medial and lateral, biceps brachii short and long, brachialis, brachioradialis, supinator, pronator Teres, flexor carpi radialis and ulnaris, extensor carpi radialis long and brevis, and extensor carpi ulnaris.

Their positions can be found in figure 1.2.

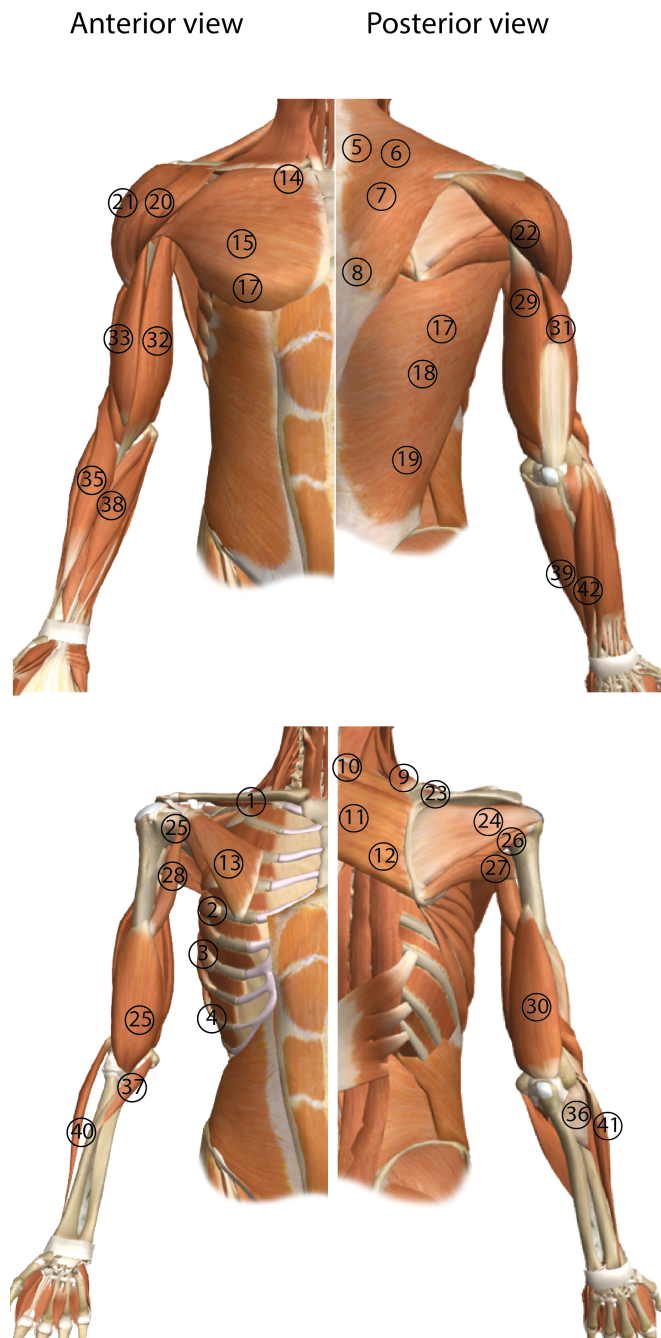


Figure 1.2: Muscles considered and their corresponding placements. subclavius (1), serratus anterior upper (2)/middle (3)/lower (4), trapezius C1-C6 (5)/C7 (6)/T1 (7)/T2-T7 (8), levator scapulae (9), rhomboid minor (10)/major T1-T2 (11)/major T3-T4 (12), pectoralis minor (13)/major clavicular (14)/major sternal (15)/major ribs (16), latissimus dorsi thoracic (17)/lumbar (18)/Iliac (19), deltoid clavicular (20)/acromial (21)/scapular (22), supraspinatus (23), infraspinatus (24), subscapularis (25), teres minor (26)/major (27), coracobrachialis (28), triceps brachii long (29)/medial (30)/lateral (31), biceps brachii short (32)/long (33), brachialis (34), brachioradialis (35), supinator (36), pronator Teres (37), flexor carpi radialis (38)/ulnaris (39), and extensor carpi radialis long (40)/radialis berris (41)/ulnaris (42).

1.1.2 Control of upper-limb movement physiological mechanisms

The human body is a complex system composed of numerous interconnected components. The nervous system is the primary coordination and regulation mechanism for these interactions. It receives information from sensors located throughout the body and transmits signals to the muscles and glands in order to induce a reaction. The nervous system consists of two main parts: the central nervous system (CNS), which consists of the brain and spinal cord, and the peripheral nervous system (PNS), which consists of sensory neurons, ganglia, and nerves that link to the CNS. The brain is the primary control center and interprets all the information received from the PNS. The PNS is subdivided into the somatic nervous system and the autonomic nervous system. The somatic system governs voluntary movements, while the autonomic system controls involuntary activities such as breathing and blood pressure. This categorization enables us to comprehend the qualities of human control and the manner in which the body's many systems cooperate to create movement. Figure 1.3 represents the voluntary motor control pathway.

In this thesis, we focus on the somatic nervous system and especially the control of upper limb movements.

First, the primary motor cortex of the brain engages motor commands that are connected with voluntary movements. The motor-related signals, from the upper motoneurons, go through the pyramidal tract whose main component is the corticospinal tract a descending pathway to the brainstem and the ventral horn of the spinal cord [102, 113]. Of note, there exist alternative descending pathways from the brainstem, the extrapyramidal tracts, but are mostly involved in involuntary movements such as balance, locomotion, and postural control. Voluntary movements are also influenced by the extrapyramidal tracts through an increase or decrease in muscle tone respectively facilitating or inhibiting voluntary movement [97]. Additionally, the basal ganglia and the cerebellum play a significant role in the control of voluntary motor commands, in adjusting their activation or their timing with respect to sensory feedback for proper limb coordination [4, 108].

The motor-related signals exit the spinal cord via the lower motor neurons to the muscles, in particular to the muscle fibers where the lower motor neurons synapses. To be more specific, a neurotransmitter called acetylcholine is released, and it attaches to the receptors on the muscle fibers. The term motor unit denotes a single motor neuron and the muscle fibers it innervates, and neural drive its action potential. [43] The latter will cause the muscle fibers to depolarize, which in turn generates an action potential that travels down the muscle fibers and causes the muscle fibers to contract. The term "muscle activation" is used to denote this muscle fiber action potential. It triggers the release of calcium ions Ca^{2+} from the sarcoplasmic reticulum, which will then bind to the troponin protein on the muscle fibers leading to a conformational

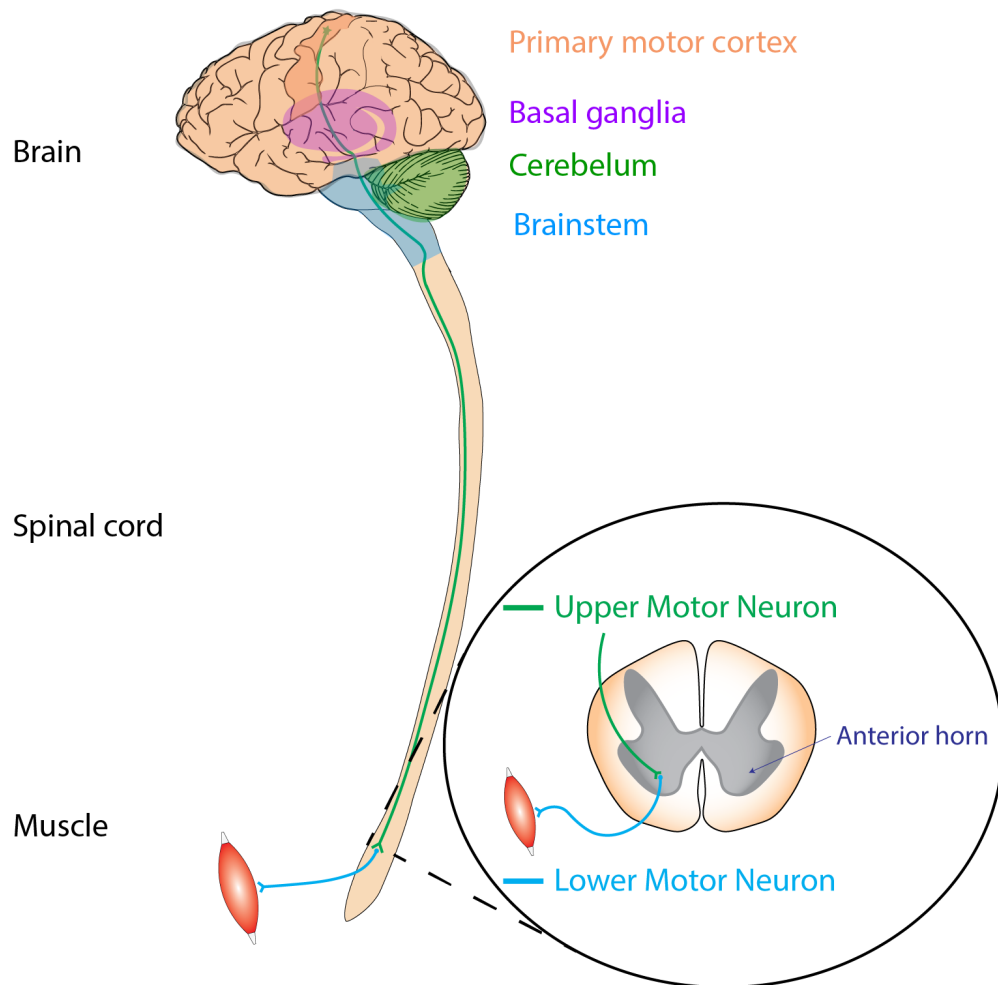


Figure 1.3: Schematic representation of the systems and pathways leading to voluntary motor control. Greatly modified from Wikimedia. This file is licensed under the Creative Commons 4.0 license.

change in another protein, tropomyosin. In other words, this Ca^{2+} release, causes a change in the shape of the troponin-tropomyosin complex leading to the liberation of the previously covered binding site between the myosin and the actin. A more detailed explanation can be obtained in the following figure 1.4

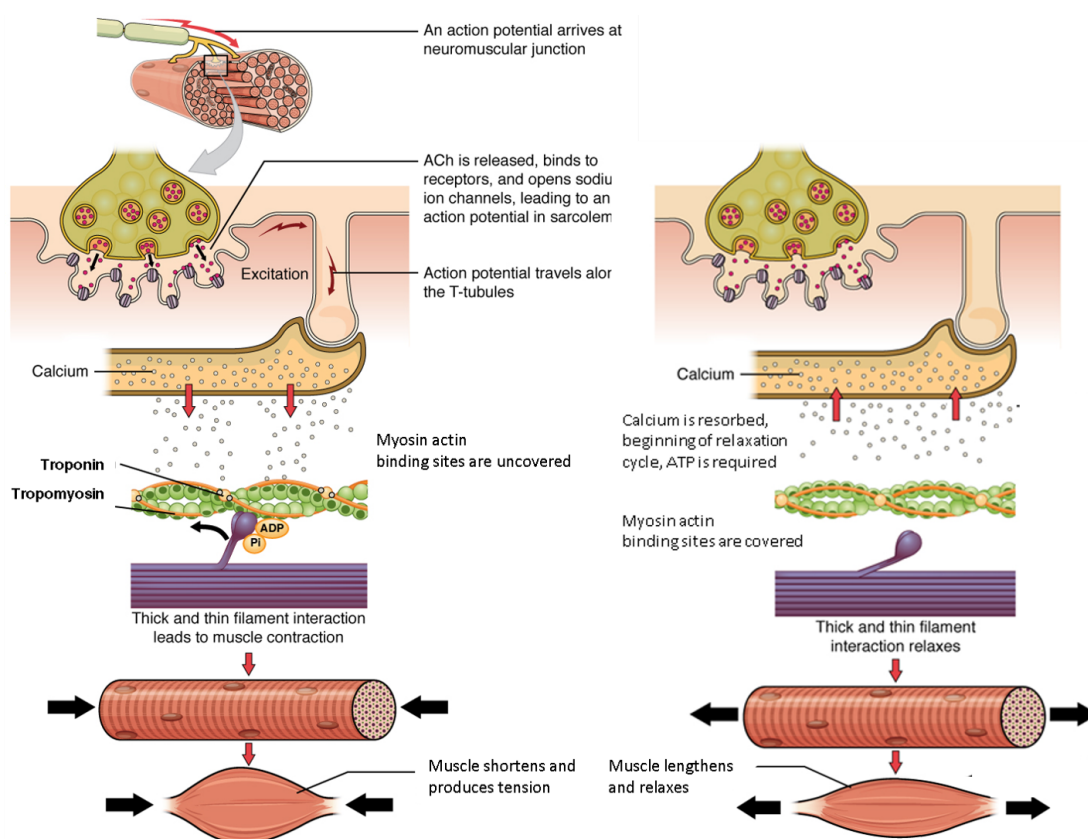


Figure 1.4: Representation of the muscle contraction (on the left) and relaxation (on the right) mechanisms. This is a modified combination of two files from Wikimedia. These files are licensed under the Creative Commons 4.0 license.

A muscle is innervated by multiple motor units, forming a motor nucleus or a motor unit pool, with populations ranging from a few tens to several hundreds [42, 48, 122]. The force production of a single muscle can be fine-tuned either spatially or temporally with the recruitment of the motor units within the motor pool and the rate at which action potential is discharged. It was observed that there is a recruitment pattern occurring to optimize muscle efficiency; The smallest muscle fibers are recruited initially, followed by bigger ones when greater force is required. This recruitment pattern was shown to maximize muscular efficiency. The "size principle" refers to this procedure [59, 154]. Muscles that produce large and powerful movements usually contain motor units with large numbers of fibers while the small, precise muscles typically have fewer fibers per motor unit.

Other elements, such as the availability of energy (in the form of adenosine triphosphate, or ATP), the quantity of calcium ions in the muscle fibers, and the presence of certain enzymes that serve to control muscular contraction as well as the current muscle fiber lengths are also important in the process of muscle contraction. In addition, muscular fatigue can play a part in the contraction of muscles. When muscles are used

for prolonged periods of time or at a high intensity, they begin to fatigue, which results in a reduction in their capacity to create force. This is related to the depletion of energy sources, accumulation of metabolic by-products, and alterations in the muscle fibers themselves.

1.1.3 Muscle synergy principles

The human body's ability to generate movement is a complex process requiring coordination between hundreds of muscles and thus to thousands of motor units by the central nervous system. Moreover, it must process the musculoskeletal properties, such as the muscles' strengths, their contraction velocities, stiffness, fiber sizes, and stiffness, as well as the many requirements of the dynamics and limitations impacting movement. More importantly, there are more muscles spanning each degree of freedom of the system than are technically required from a mechanical standpoint, which means that, in theory, an endless variety of recruitment patterns are feasible. This issue is often referred to as the redundancy problem [36] the force-sharing problem [44].

One way for the central nervous system to complete this extensive task from a vast set of control possibilities would be to generate motor instructions by combining motor primitives or motor modules [11, 13, 25]. Studies and analyses of electromyography signals in the literature have further demonstrated that those modules can be represented as muscle synergies that would correspond to muscle co-activation patterns [12, 25, 33, 65, 144, 165, 168]. Those would constrain how muscle groups are recruited spatially and temporally as separate units. In other words, the concept of muscle synergy relates to the notion that the nervous system regulates movement by engaging a particular combination of muscle groups, as opposed to commanding each muscle separately. This concept is unproven and may require additional research, as the extracted synergies may represent regularities in the activities if there is limited variability in the recorded tasks or in the possibilities in the subspace of the motor commands arising from possible muscle lengths and contractions while performing the activity, leading to the question of whether or not the extracted synergies are of neural origin.[1, 25, 89]

identifying muscle synergies

In order to identify muscles involved in a group as well as the different synergies, the electromyography signals of multiple muscles are studied. The main principle is to apply a dimensionality reduction algorithm to these signals. There are two main approaches that were adopted, a linear transformation of preprocessed EMG signals and the decomposition of the preprocessed EMG signals in time-varying activation waveforms.[34, 35, 77]. In this review, we will focus on the first one with its larger adoption, and its use within the thesis. Methods such as Nonnegative matrix factorization (NNMF), principal component analysis (PCA) and independent component analysis (ICA) have been mainly employed in the literature for that purpose.[34, 95, 121, 159, 167, 178]. There is not a clear consensus of which algorithm would be the most appropriate one [135, 178] and they mostly differ by assumptions and implementations. PCA.

These algorithms assume that the muscle activity can be described by a linear combination of these synergies, and ICA can identify non-linear relationships. PCA and NNMF were shown to perform similarly on EMG and joint motion data outperforming ICA in reconstructing simple 2d examples [92]. The NNMF's nonnegativity condition for activation of basis vectors, on the other hand, is a beneficial feature in detecting physiologically relevant synergies, especially with numerical models with constrained values for muscle activations. Moreover, NNMF was shown to handle sparse data and noisy data more effectively with respect to ICA [109]. Therefore, NNMF factorization techniques will be picked in this thesis.

The EMGs are filtered and rectified and their envelope are collected into a matrix \mathbf{M} as column vectors and decomposed into two matrices, \mathbf{C} and \mathbf{W} , composed of synergies temporal coefficients vectors c_i and muscle synergies weights w_i . With \mathbf{R} , the unexplained residuals leading to the following equation 1.1 and the explanatory figure 1.5.

$$\mathbf{M} = \mathbf{C}\mathbf{W}^T + \mathbf{R} = \sum c_i w_i^T + \mathbf{R} \quad (1.1)$$

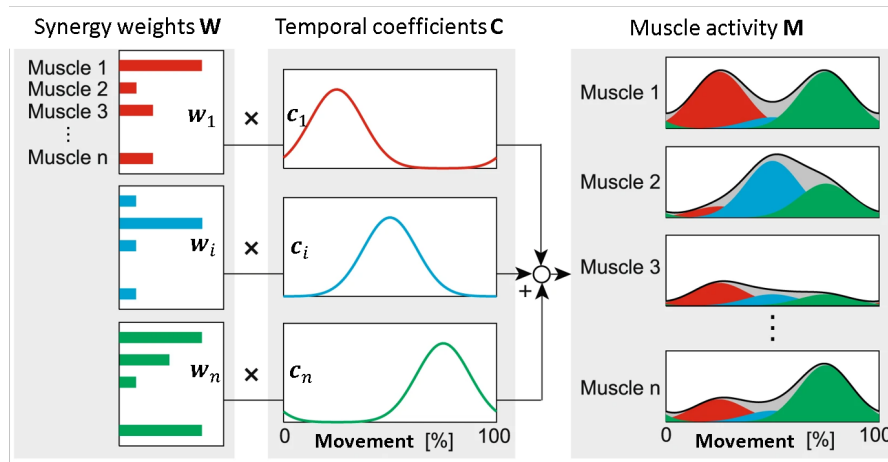


Figure 1.5: Schematic model of muscle synergy principle, with the muscle activities explained by the linear combination of a reduced number of weights and temporal coefficients signals. Modified from [3]. This file is licensed under the Creative Commons 4.0 license.

If the residuals \mathbf{R} are negligible and if the number of synergies is less than the number of muscles we can assume that the initial dataset of EMGs can be mapped into a lower-dimensional space. This can be represented with the so-called VAF (variance accounted for), which quantifies the percentage of variability that is accounted for by the extracted synergies. If the VAF is high, the EMGs are well reconstructed otherwise, the synergies do not sufficiently explain the EMG variance. VAF is typically computed

as with r_i the residuals components (elements of \mathbf{R}) and u_i , the signals from EMGs.

$$VAF = 1 - \frac{\sum r_i^2}{\sum u_i^2} \quad (1.2)$$

The number of synergies is obtained in general from a study of this VAF. Most of the time, it is based via a threshold level (e.g., 90%, 95%) [27, 130, 166, 175] or with the "elbow" method. The latter is based on the principle that as the number of synergies increases, the ability of the algorithm to fit the muscle activity data will also increase. However, at some point, adding additional synergies will not significantly improve the fit of the data. When plotting the VAF against the number of synergies, a sharp inflection occurs at a specific point, this point actually is viewed as the dividing line between "structured" and noise-dependent variability, and so it may be used to determine the minimal amount of synergies required to adequately define task-related characteristics. In general, this number is determined as the minimum number of muscle synergies able to capture the structural variation of the dataset, so that, by adding one more synergy, it will only add noise to the reconstructed dataset [35]. Notably, the preprocessing of EMGs has a substantial effect on the VAF values and curve, making comparisons across studies difficult. Preprocessing should be performed in the same manner within a study, for a VAF analysis of the number of synergies to be accurate. [83, 167]

1.1.4 Physiological assessment methods and limitations

As mentioned before, the electromyographic signal represents the electric field generated by the depolarization of the outer muscle fiber membrane (sarcolemma). Every time a motor unit from a motor pool fires, it generates an electrical signal; a motor unit action potential leading to a force output in the motor unit, called a force twitch. The muscles are composed of many motor units activated usually at the same times and the recorded EMG signal represents the total of the action potentials of the various motor units. This signal can be measured by applying conductive elements or electrodes to the skin surface, or invasively within the muscle with surface electrodes and needle electrodes respectively. The EMG signal is very intricate, and its properties are influenced by a wide variety of factors. These factors include the anatomical and physiological properties, as well as the characteristics of the apparatus that is used to detect and evaluate the signal. A list of non-exhaustive elements influencing the EMG signal :

- Physiological properties
 - Blood flow and temperature
 - Muscle fiber conduction velocity
 - Number of motor units
 - Type of contraction
 - Degree of motor unit synchronization
- Geometrical and anatomical
 - Electrode size
 - Electrode shape
 - Electrode distance from muscle-tendon junctions
 - Thickness of skin and subcutaneous fat
 - Misalignment between electrodes and fiber alignment

In this thesis we will focus on the surface EMG signals, their processing and analysis. The main reasons behind this choice is that intramuscular EMG are invasive, limited to low force levels and to a few motor units only which limits the study of the overall muscle force, and contraction behaviour whereas the surface electrodes record the sum of multiple motor unit action potentials [86, 103]. In the typical recording methodology, we measure the electrical potential difference between two points (bipolar electrode configuration). The electrode should be placed on the muscle of interest in the direction of the predominant fiber direction, and the subject is grounded by placing an electrode in an inactive region of the body.

To accurately record EMG signals and study them in a meaningful way, their placement and their processing should be done in a systematic way, following a set of recommendations.

Due to the fact that EMG signals result from neuromuscular activity, they may be used in the diagnosis of nerve and muscle injuries as well as dysfunctions brought on by neurological and musculoskeletal conditions.

1.2 Stroke impairments

Although the study of muscle activations is not limited to stroke patients and could be applied to other neurological diseases that impair the neuromusculoskeletal system, the research presented in this thesis focused on the stroke population; however, future research could implement this for other populations as well. In this part, we will discuss Stroke disease and the current level of knowledge about its impairments and recovery. A stroke occurs when there is a disruption in the blood flow within the brain. The latter can be caused by a blood clot (ischemic stroke) or bleeding (hemorrhagic stroke) and its severity can vary depending on the location and extent of the damage. Research has demonstrated that a focal lesion, such as one that is caused by a stroke, has far-reaching effects within the brain and its associated networks [60]. The ischemic stroke lesion usually consists of a core of dead neurons and a surrounding area with a limited blood flow, the penumbra [140] that could be potentially saved if treated rapidly via thrombolysis to dissolve blood clots or endovascular thrombectomy to remove them, preventing further clinical outcomes. The first priority is therefore to rapidly restore blood flow. With hemorrhagic stroke blood accumulate within the brain tissue which leads to rapidly developing neurological dysfunction due to the mass effect [143]. Compared to ischemic stroke, morbidity and mortality are higher in hemorrhagic stroke patients. The main goal is to rapidly stop further bleeding.

If most survivors, experience a direct reduced motor control, due to muscle strengths, somatosensory sensations and muscle recruitment selectivity, [20] spontaneous neurobiomechanical recovery occurs within the first weeks after the accident [20, 90]. However, an impairment of the upper-limb is experienced by 70 to 80% of survivors [136] and nearly one-third of all stroke survivors will have significant long-term disability placing it as one of the main causes of long-term disability in adults [170]. Although different treatments are administered to the two types of strokes during the hyperacute phase, research has shown that the recovery of motor function and overall outcome following a stroke is not type of stroke dependant [17, 160]. This implies that the deficits observed in behavior, as well as their progression, may be caused by shared neurobiological mechanisms that occur after a stroke.

A key goal is to improve the spontaneous neurobiomechanical recovery occurring during this period with rehabilitation interventions. Assessing stroke patients' impairments and determining their impact on mobility and function loss are essential steps in their rehabilitation journey. Medical practitioners rely heavily on the evaluation and functional diagnosis of stroke patients to create rehabilitation objectives and develop physical therapy plans. The severity of the impairments, such as the loss of sensation, strength, and control, as well as how they contribute to mobility and function loss, help medical practitioners understand the patient's condition and design effective treatment plans.

The current state-of-the-art methods to estimate the patient's impairment primarily involve qualitative evaluations by therapists, robot-assisted therapies, or surface electromyography (EMG) recordings of selected muscles. Clinical scales, such as the Fugl-Meyer Assessment (FMA) [49], are commonly used to assess therapy effectiveness. The FMA evaluates upper-limb mobility, muscle tone, reflexes, and coordination and assigns a score depending on the patient's level of function. It has been extensively evaluated in the stroke population and is acknowledged as a tool for assessing changes in motor impairment after stroke.

However, the sensitivity of clinical tests may not accurately reflect the patient's actual improvements. The reliability of clinical tests is also limited by the clinicians' inter-rater and intra-rater reliability and by floor and ceiling effects. These limitations may result in underestimating or overestimating the patient's progress during the rehabilitation process. The impact of training on the spontaneous mechanism and how the exercise therapies affects the recovery is still an open question [20]

To address these limitations, clinicians have begun using recorded EMG signals to help quantify muscle activity and track recovery. EMG recordings are non-invasive and provide valuable insights into muscle function and activation patterns during movement. They also allow clinicians to quantify muscle strength and evaluate the efficacy of rehabilitation interventions. However, obtaining the overall muscle EMG is not currently feasible in practice with non invasive procedures. This thesis aims at providing the clinicians with the overall muscle activations to this extend.

1.3 State of the art and existing upper limb models for muscle assessment

Over the last decades, a number of musculoskeletal models have been proposed to predict parameters that could not be measured (in particular forces and neurological controls) and aimed at improving diagnoses, pathologies estimations and treatments processes. [37]. The most acknowledged musculoskeletal model including at least the shoulder and elbow are the Delft shoulder and elbow model [67, 68], The Garner and Pandy model [53, 54], Anybody model[36] the OpenSim model [73], the Waterloo model [40], the Case model [14], the Portuguese model [134] and the dynamic arm simulator [22]. In all these models, the muscle are represented as sets of lines, in other proposed models, muscles are represented as volumes with Finite Element methods [171, 179] but consider a limited number of muscles greatly reducing the applications since it cannot be representative of the complex shoulder model. Moreover, if surface-based and volumetric finite element muscle models are appealing with a better representation of the muscles and their geometry, they are time-consuming (with 30min of computation time for simulating 10s of motion[126], or 12 hours and more[171]) which would not be optimal for a study including large dataset comparison between subjects and movements.

The pioneer in the field was the Delft musculoskeletal model[67, 68], which could estimate muscle and joint forces using inverse dynamics. Over time, models have focused on accurate anatomical representation of muscles and bones, as well as new algorithms and methods to improve the estimation of muscle forces and joint forces, particularly to address the redundancy problem. Two main methods have been used in the models: the first is to determine the muscle forces at each instant of the movement using inverse dynamics and optimize these forces to minimize the muscle stresses (or other physiological cost functions). While the second seeks to reduce the difference between the measured and estimated activation signals by using forces derived from the muscle contraction dynamics to predict the movement.

1.4 Objectives and outline of the thesis

The objective of the thesis is to develop a numerical model that will try to help us further understand the underlying mechanisms for motor control and give us a tool to evaluate a neurological patient's impairment to potentially improve his rehabilitation program.

This main objective can be subdivided into multiple parts

- Develop an existing musculoskeletal upper-limb model that can predict physiological muscle activations. This part is presented in **Chapter 2**. In this chapter, I also present the forward dynamics formulation and potential use for further development. I also show a GUI, developed to ease the use of the model, with a limited need for coding.
- Confront these activations to recorded EMG with healthy subjects performing a set of 3d reaching tasks while wearing an exoskeleton. The aim is to validate the model and to obtain realistic muscle activation with data collected from healthy subjects' data within a clinical environment. This work is presented in **Chapter 3**.
- Present a quantitative impairment measurement tool from recorded kinematics and a limited number of recorded EMG. This corresponds to the first part of **Chapter 4**. This was done with stroke patients performing the same tasks as for **Chapter 3**
- Evaluate the muscle synergies while reaching different targets, and show that having the overall muscle activations helps us better understand patients' rehabilitation with respect to healthy data. This corresponds to the second part of **Chapter 4**

Finally, **Chapter 5** provides a summary/conclusion of the works and most importantly suggests possible improvements of the model and of musculoskeletal modeling in general as well as future possible implementation within clinical rehabilitation protocols.

2 Upper limb numerical model

2.1 Musculoskeletal modeling

As we stated before 1.1.2, the CNS regulates the movement of the human body by generating neural commands to activate muscles, which in turn generates forces. Combining these to the inertia and to the external forces acting on the body, a movement, or motion occurs. A musculoskeletal model should capture both the dynamics of the muscle force production and the skeletal system's movements [101].

We mentioned in section 1.1.1 for the upper limb, the bones considered (as rigid body) connected to each other via the joints, this ensemble forms a multibody system in which motion is influenced by forces (from the muscles, the environment and gravity) and the overall constraints imposed by the articulations. In order to apply a muscular force to the skeleton, however, the muscle path needs to be computed, from its origin to its insertion. [76, 145, 177]

From their origin until their insertion, muscles may encounter anatomical obstacles, such as bones, other muscles, or tissues, which they must wrap around. Because of this, muscles cannot be modeled as straight lines from their origin to their insertions. In the literature, different wrapping techniques were explored. Although finite element approaches give the maximum degree of detail because of their use of muscle deformations and accurate bone geometry for wrapping, they are computationally costly and hence not optimal for musculoskeletal modeling [47, 99]. The majority of musculoskeletal models, however, employ a different wrapping technique, which consists of modeling bones and tissue obstacles using geometric elements in order to approximate the muscle path around them [38, 51, 54, 145] or if only the muscle length and moment arm was needed they were approximated with polynomial regression or [112] multidimensionnal B-splines methods [151].

Once the skeletal geometries and articulation and the muscle paths are modeled, the muscle actuation should be considered. The feasible force produced by a muscle depends on several parameters including its lengths, contraction velocity as well as its activation. Hill-Type muscle models [71] are commonly used to describe muscle behaviour from a mechanical point of view. These muscle models are crucial for understanding the neural control of movement.

2.2 Musculokeletal geometry

Here we will present the musculoskeletal model used [75, 107, 145] that was validated with *in vivo* measurements to provide estimations of the glenohumeral joint reaction forces with an inverse dynamics method. MRI scans were used on a healthy male subject (29 years, 186 cm, 85.5 kg) to model the 3d bony structures of the shoulder and arm. Six rigid bodies are considered including the thorax, clavicle, scapula, humerus, ulna, and radius. A rigid hand was modeled and rigidly fixed to the radius mostly for muscle and tendon insertions, but no motion was permitted yet, (future development could include a carpal joint). As mentioned before, 1.1.1, eleven degrees of freedom are considered, three ball and sockets joints for the sternoclavicular, acromioclavicular, and glenohumeral joints and two hinge joints for the forearm flexion/extension and pronation/supination to replicate the anatomical joints including the humeroulnar, the radioulnar proximal and distal, and the humeroradial joints. The model also incorporates two holonomic constraints that prevent the scapula from moving anywhere else but along the rib cage. The skeletal geometry and the joints associated are presented in the following figure 2.1

For each segment and their articulations, the ISB recommendations [174] were respected to define the joints' fixed frames and their associated index defined as followed:

- 0. Thorax frame:
 - Center: IJ
 - \vec{x}_T : normal to the plan defined by IJ, C7, $\frac{1}{2}(T8 + P X)$ -IJ, pointing to the right
 - \vec{y}_T : normal to the x and z axis pointing forward
 - \vec{z}_T : parallel to the line between the points $P1 = \frac{1}{2}(P X + C7)$ and $P2 = \frac{1}{2}(T8 + IJ)$
- 1. Clavicular frame:
 - Center: SC
 - \vec{x}_C : parallel to the line defined by SC and AC, pointing to the right
 - \vec{y}_C : normal to the plane defined by \vec{x}_C and \vec{z}_T , pointing forwards

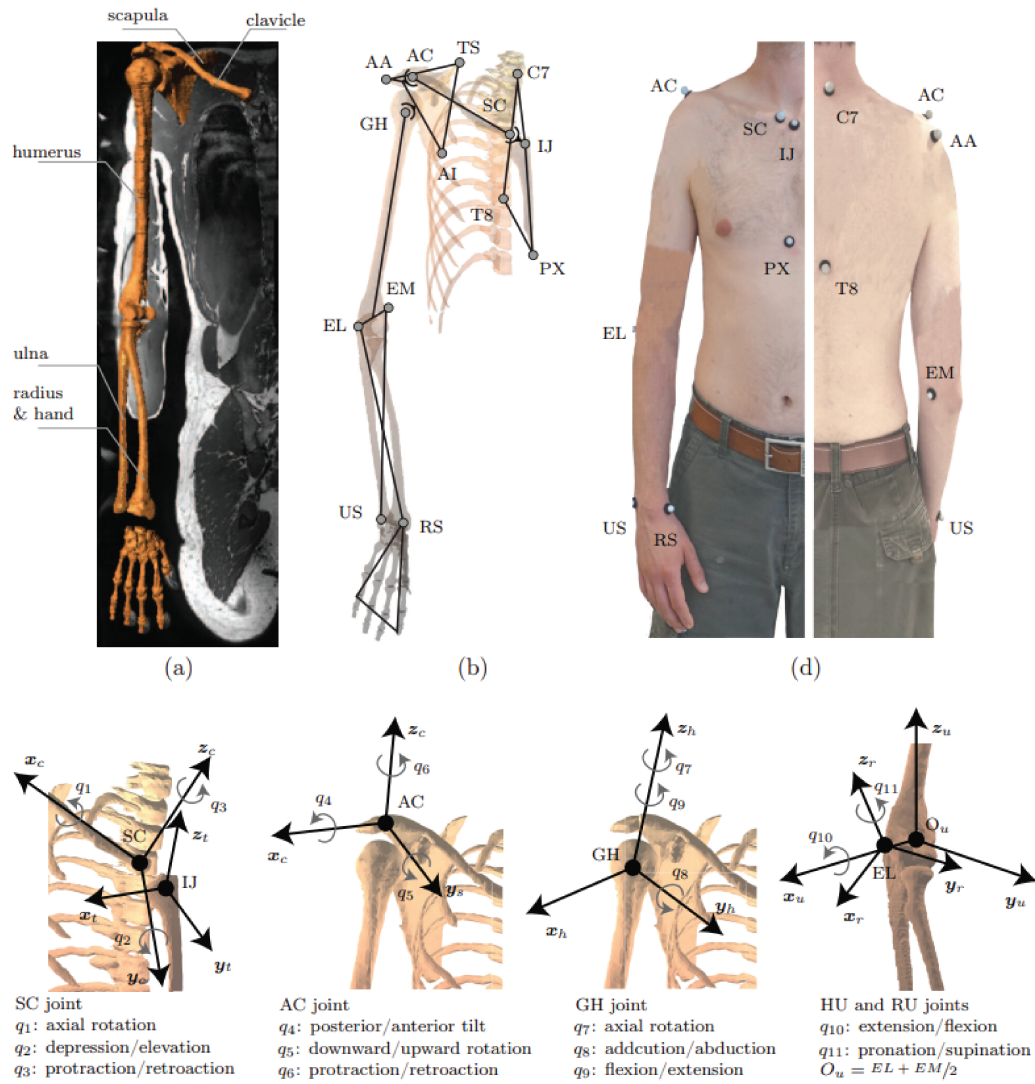


Figure 2.1: (a) The MRI scan used for the geometric reconstruction of the bony structures, with the 6 rigid bodies modeled. (b) The bony landmarks considered for modeling the orientations and structures of the articulations. With at least three landmarks per bone segment, except for the clavicle. (c) the 11 joint angles of SC, AC, GH, HU, and RU joints, $q = [q_1 \dots q_{11}]$. (d) The Bony landmark used for VICON videogrammetry systems and needed for kinematic reconstruction from [145] These figures are modified from [145] with Dr. Sarshari's consent

– \vec{z}_C : normal to the x and y axes, pointing upwards

• 2. Scapular frame:

– Center: AC

– \vec{x}_S : parallel to the line defined by TS and AA, pointing externally

– \vec{y}_S : normal to the plane defined by the x and the AI-TS axes, pointing forward

- \vec{z}_S : normal to the x and y axes, pointing upwards
- 3. Humeral frame:
 - Center: GH
 - \vec{x}_H : normal to the y and z axes, pointing externally
 - \vec{y}_H : normal to the plane defined by GH, EL and EM, pointing forwards
 - \vec{z}_H : parallel to the line between the points $O_u = \frac{1}{2}(EL + EM)$ and GH
- 4. Ulnar frame:
 - Center: O_u
 - \vec{x}_U parallel to the line between O_u and EL, pointing to EL
 - \vec{y}_U normal to the plane defined by US, EL, EM, pointing forward
 - \vec{z}_U normal to the x and y axes, pointing upwards
- 5: Radius frame
 - Center: EL
 - \vec{x}_R normal to the y and z axes, pointing externally
 - \vec{y}_R normal to the plane defined by EL, RS and US, pointing forward
 - \vec{z}_R parallel to the line between EL and US, pointing to the top.

In a mathematical standpoint, the Euclidean displacements that transforms a point \vec{p}_i in a bone's reference frame \mathcal{R}_γ into a point $\vec{p}_{0,i}$ defined in the thorax reference frame \mathcal{R}_γ , are defined by:

$$P_{0,1} : \vec{p}_{0,1} = \vec{d}_{0,1} + \mathbf{R}_{1,0}\vec{p}_1 \quad (2.1)$$

$$P_{0,2} : \vec{p}_{0,2} = \vec{d}_{0,2} + \mathbf{R}_{2,0}\vec{x}_2 = \vec{d}_{0,1} + \mathbf{R}_{1,0}\vec{z}_1 + \mathbf{R}_{2,0}\vec{p}_2 \quad (2.2)$$

...

$$P_{0,5} : \vec{p}_{0,5} = \vec{d}_{0,5} + \mathbf{R}_{5,0}\vec{x}_5 = \vec{d}_{0,1} + \sum \mathbf{R}_{i,0}\vec{z}_i + \mathbf{R}_{5,0}\vec{p}_5 \quad (2.3)$$

The different vectors $\vec{d}_{0,i}$ correspond to the vectors between the different centers of the joints in the thorax reference frame, for instance, $\vec{d}_{0,1}$ is the vector from IJ to SC in \mathcal{R}_γ . The vectors \vec{z}_i between the centers within the bone's reference frame, for instance: \vec{z}_1 is the vector from SC to AC in \mathcal{R}_∞ .

The rotation matrices are defined by:

$$\text{Clavicle : } \mathbf{R}_{1,0} = \mathbf{R}_{z,1} \mathbf{R}_{y,1}^T \mathbf{R}_{x,1}, \quad (2.4)$$

$$\mathbf{R}_{x,1} = \begin{pmatrix} 1 & 0 & 0 \\ 0 & \cos(q_1) & -\sin(q_1) \\ 0 & \sin(q_1) & \cos(q_1) \end{pmatrix}, \quad \mathbf{R}_{y,1} = \begin{pmatrix} \cos(q_2) & 0 & -\sin(q_2) \\ 0 & 1 & 0 \\ \sin(q_2) & 0 & \cos(q_2) \end{pmatrix}, \quad \mathbf{R}_{z,1} = \begin{pmatrix} \cos(q_3) & -\sin(q_3) & 0 \\ \sin(q_3) & \cos(q_3) & 0 \\ 0 & 0 & 1 \end{pmatrix}$$

$$\text{Scapula : } \mathbf{R}_{2,0} = \mathbf{R}_{z,2} \mathbf{R}_{y,2}^T \mathbf{R}_{x,2}, \quad (2.5)$$

$$\mathbf{R}_{x,2} = \begin{pmatrix} 1 & 0 & 0 \\ 0 & \cos(q_4) & -\sin(q_4) \\ 0 & \sin(q_4) & \cos(q_4) \end{pmatrix}, \quad \mathbf{R}_{y,2} = \begin{pmatrix} \cos(q_5) & 0 & -\sin(q_5) \\ 0 & 1 & 0 \\ \sin(q_5) & 0 & \cos(q_5) \end{pmatrix}, \quad \mathbf{R}_{z,2} = \begin{pmatrix} \cos(q_6) & -\sin(q_6) & 0 \\ \sin(q_6) & \cos(q_6) & 0 \\ 0 & 0 & 1 \end{pmatrix}$$

$$\text{Humerus : } \mathbf{R}_{3,0} = \mathbf{R}_{z',2} \mathbf{R}_{y,3}^T \mathbf{R}_{z,3}, \quad (2.6)$$

$$\mathbf{R}_{x,3} = \begin{pmatrix} \cos(q_7) & -\sin(q_7) & 0 \\ \sin(q_7) & \cos(q_7) & 0 \\ 0 & 0 & 1 \end{pmatrix}, \quad \mathbf{R}_{y,3} = \begin{pmatrix} \cos(q_8) & 0 & -\sin(q_8) \\ 0 & 1 & 0 \\ \sin(q_8) & 0 & \cos(q_8) \end{pmatrix}, \quad \mathbf{R}_{z',3} = \begin{pmatrix} \cos(q_9) & -\sin(q_9) & 0 \\ \sin(q_9) & \cos(q_9) & 0 \\ 0 & 0 & 1 \end{pmatrix}$$

Regarding the elbow, the rotation matrices defining the flexion/extension and pronation/supination from the generalized coordinates q_{10} and q_{11} are the following:

$$\text{Ulna : } \mathbf{R}_{4,0} = \mathbf{R}_{x,4},$$

$$\mathbf{R}_{x,4} = \begin{pmatrix} 1 & 0 & 0 \\ 0 & \cos(q_{10}) & -\sin(q_{10}) \\ 0 & \sin(q_{10}) & \cos(q_{10}) \end{pmatrix} \quad (2.7)$$

$$\text{Radius : } \mathbf{R}_{5,0} = \mathbf{R}_{z,5},$$

$$\mathbf{R}_{z,5} = \begin{pmatrix} \cos(q_{11}) & -\sin(q_{11}) & 0 \\ \sin(q_{11}) & \cos(q_{11}) & 0 \\ 0 & 0 & 1 \end{pmatrix} \quad (2.8)$$

2.2.1 Equations of movement

The rotations and the positions of the point with respect to the overall joints' configuration from the generalized coordinates $\vec{q} = (q_1, q_2, q_3, q_4, q_5, q_6, q_7, q_8, q_9, q_{10}, q_{11})$ corresponding to the 11 rotation angles from the model are now defined. Their center of mass can be then obtained and the mass and inertial properties are attributed to the bone segments according to [53].

The upper extremity equations of motion are derived from analytical mechanics using Euler-Lagrange's equations (Eq. 2.9)

$$\frac{d}{dt} \left(\frac{\partial \mathcal{L}}{\partial \dot{\mathbf{q}}} \right) - \frac{\partial \mathcal{L}}{\partial \mathbf{q}} = \mathbf{t}_0 = \frac{\partial \Omega}{\partial \dot{\mathbf{q}}} \mathbf{M} = \frac{\partial \Omega}{\partial \dot{\mathbf{q}}} \mathbf{W} \mathbf{f} \quad (2.9)$$

Where, $\frac{\partial \Omega}{\partial \dot{q}}$ M corresponds to the generalized force vector with Ω the horizontal matrix including the angular velocities of all the bony segments. M , the vertical matrix, including the resultant moments around each articulation. This corresponds to the generalized torques t_0 in the thorax frame resulting from each muscle on each bone. M can be rewritten as Wf , with W , the moment arm matrix, and f a vector of all the muscle force magnitudes.

The moment arm is computed using its geometric definition alongside the tendon excursion method. ([75, 76, 145]) Where the muscle paths are modeled as massless elastic strings approximated using the obstacle set method from [54]. The origins/insertions, via points, and wrapping objects of 42 muscles spanning the upper extremity joints are defined from the MRI scans. Each of the muscles can be represented with up to 20 cables. The 42 muscles modeled are: subclavius, serratus anterior upper, middle and lower parts, trapezius C1-C6/C7/T1/T2-T7, elevator scapulae, rhomboid minor, rhomboid major T1-T2 and T3-T4, pectoralis minor, pectoralis major clavicular sternal and ribs, latissimus dorsi thoracic, lumbar and iliac, deltoid clavicular, acromial and scapular, supraspinatus, infraspinatus, subscapularis, teres minor and major, coracobrachialis, triceps brachii long, medial and lateral, biceps brachii short and long, brachialis, brachioradialis, supinator, pronator Teres, flexor carpi radialis and ulnaris, extensor carpi radialis long and brevis, and extensor carpi ulnaris.

On the left hand side of equ 2.9, the acceleration and conservative forces including Coriolis forces and gravity are included. The Lagrangian \mathcal{L} , is the sum of all the bone segments Lagrangian including \mathcal{L}_{scap} obtained from the two scapulothoracic constraints ([75, 145]).

$$\mathcal{L} = \mathcal{L}_1 + \mathcal{L}_2 + \mathcal{L}_3 + \mathcal{L}_4 + \mathcal{L}_5 + \mathcal{L}_{scap} \quad (2.10)$$

The Lagrangian from each bone is defined by its kinetic and potential energies. The general expression for the Lagrangian is given by:

$$\mathcal{L}_i = \frac{1}{2} \{ m_i \dot{\vec{x}}_{0,i}^T \dot{\vec{x}}_{0,i} + \vec{\omega}_i^T \mathcal{I}_i \vec{\omega}_i \} - m_i g \begin{pmatrix} 0 & 0 & 1 \end{pmatrix} \cdot \vec{x}_{0,i}, \quad i = 1 : 5 \quad (2.11)$$

\vec{x}_i , is the position of the center of gravity of the bone i in the thorax (or global) reference frame. The vector $\dot{\vec{x}}_{0,i}$ corresponds to its translational velocity in the thorax reference frame. $\vec{\omega}_{0,i}$ is the instantaneous rotational velocity vector in the bone's reference frame. m_i is the mass of the bone i and \mathcal{I}_i , the inertia tensor, defined in the bone's reference frame from its longitudinal and transverse inertia such as defined below:

$$\mathcal{I}_i = \begin{pmatrix} I_{1,1} & 0 & 0 \\ 0 & I_{2,2} & 0 \\ 0 & 0 & I_{3,3} \end{pmatrix} \quad (2.12)$$

Where for the clavicle and the scapula, $I_{1,1}$ is the longitudinal inertia and $I_{2,2} = I_{3,3}$ the transverse inertia, whereas for the humerus, ulna, and radius, $I_{3,3}$ is the longitudinal inertia and $I_{1,1} = I_{2,2}$ the transverse inertia.

2.3 Musculotendon dynamics

As mentioned in previous section the upper-limb musculoskeletal model uses 42 muscles as cables, which paths approximated using the obstacle-set method [54] using the origins and insertions defined with MRI scans ([75, 145]). Moreover, their associated wrapping objects are set by modifying recommendations of [53] for the type, center, axis, and radius of the objects to best fit the MRI scans. Figure 2.2

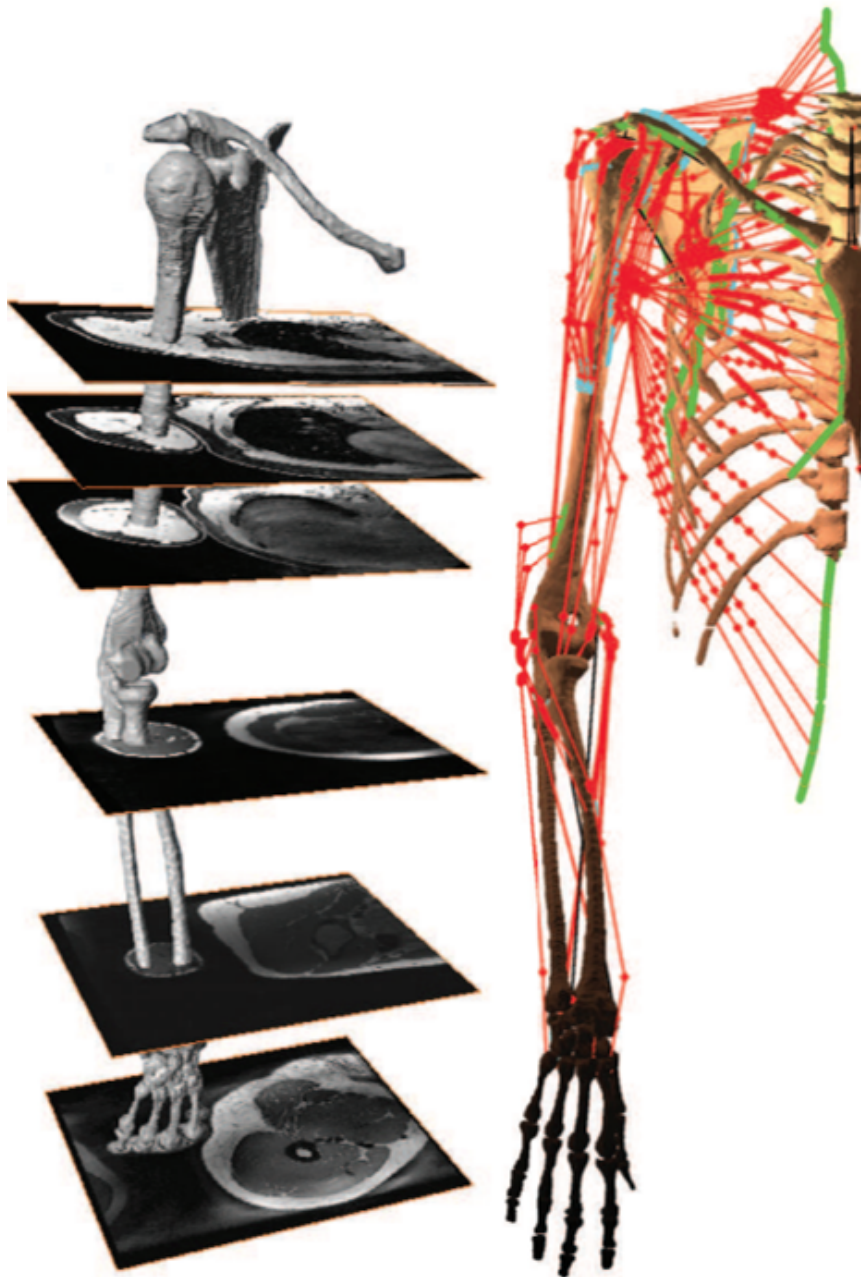


Figure 2.2: The musculoskeletal model: On the left, MRI scans of a healthy male subject from which the bone morphologies, muscles origins and insertions, and wrapping objects are obtained. On the right, the musculoskeletal model, and the 42 muscles as cables, with their insertions in blue and origins in green. The muscles are represented with 3 massless elastic strings in the figure but can be represented by up to 20. Modified from [145] with the author's consent.

we saw in eq: 2.9 the impact of the muscle forces in the dynamics in the model's equa-

tion; the different muscles will apply on the skeletal structure forces in the direction given by the cables representing them. All the forces applied by a single cable on the same bone are reduced to a single force magnitude and a moment of force at that point and thus apply a moment of force around each joint. For a model with N_p muscle segments the force and moment of force at each joint in the inertial frame \mathcal{R}_l is defined by:

$$\mathbf{f}_{0,i} = \sum_{k=1}^{N_p} \mathbf{f}_{0,i,k} \quad i = 1 : 5 \quad (2.13)$$

$$\mathbf{t}_{0,i} = \sum_{k=1}^{N_p} \mathbf{y}_{0,i,k} \times \mathbf{f}_{0,i,k} = \sum_{k=1}^{N_p} (\mathbf{y}_{0,i,k} \times \mathbf{b}_{0,i,k}) f_k = \sum_{k=1}^{N_p} \mathbf{c}_{0,i,k} f_k = \mathbf{C}_{0,i} \mathbf{f} \quad (2.14)$$

With, $\mathbf{f}_{0,i,k}$ the resulting force of muscle k applied to body \mathcal{B}_i in \mathcal{R}_l , $\mathbf{y}_{0,i,k}$ the resultant of force vector in the system for muscle k in the body \mathcal{B}_i in \mathcal{R}_0 , $\mathbf{b}_{0,i,k}$ the force direction vector. Their cross product form the moment arm: $\mathbf{c}_{0,i,k}$.

The importance of the moment arm is mostly for numerical considerations, in classical mechanics the forces \mathbf{f}_k of magnitude f_k , are applied on a rigid body \mathcal{B}_i at a certain point, this creates a moment of force at any other point of the body. The moment of force is defined as the cross product between the vector from those two points, the lever arm, and the vector of the force with its direction. The associated moment-arm $\mathbf{c}_{0,i,k}$ is defined by the same cross product but with a normalized force vector \mathbf{b} . In our equations: $\mathbf{b}_{0,i,k} f_k = \mathbf{f}_{0,i,k}$. Therefore, the moment-arm is purely geometric quantity depending on the direction of the force and its point of application. This allows the separation between the geometric quantities of the forces and applications on joint i in \mathcal{R}_0 with the moment-arm matrix $\mathbf{C}_{0,i}$ of the system and the vector of the muscle force magnitudes \mathbf{f}

The muscles can only contract from their initial position, thus they can only pull the skeletal structure leading to a muscle force constraint, to be only positive or zero. Depending on the musculoskeletal application, the vector of muscle force magnitudes calculation will differ. For an inverse dynamics simulation, these are unknown and a solution must be found to satisfy the equation of motion. In forward dynamics simulation, those will be obtained directly from their geometry and their activation with the Hill-type muscle model [71], a musculotendon actuation model describing the input-output behaviors of the musculotendon system and its phenomenological properties.

2.3.1 Musculotendon contraction dynamics

The Hill-Type models correspond to a mechanical representation of the muscle-tendon complex [71, 172, 177]. They are extensively used in the literature for coordinated movements and representation of the muscle force from an activation signal[100, 123, 148] They provide a single first-order ordinary differential equation representing the contraction dynamics of the musculotendon. It associates the muscle fiber velocity to a function of the muscle fiber length, musculotendon length and activation.

2.3.2 Activation dynamics

The activation of the muscle corresponds the active state of the musculotendon apparatus, it corresponds to the physiological relative amount of calcium released in the muscle fiber as mentioned in 1.1.2. During muscle activation, calcium ions concentration increases in the sarcoplasmic reticulum, while muscle deactivation involves the removal of calcium. However, as mentioned in 1.1.4, the physiological signals measured, electromyographic signals, correspond to the sum of the electric fields generated by the depolarization of the outer muscle fiber membrane. Therefore, there is a need to model the dynamics associating from a neural excitation $u(t)$ a muscle activation $a(t)$, this is done via the activation dynamics equations.

This was described previously [176, 177] and later adapted [145] to the following equation:

$$\dot{a} = \frac{u - a}{\tau}, \quad \begin{cases} \frac{\tau_{act}}{0.5 + 1.5a} & u < a, \text{ activation} \\ \frac{\tau_{deact}}{0.5 + 1.5a} & u \geq a, \text{ deactivation} \end{cases} \quad (2.15)$$

Where a is the activation, u the excitation u (both between 0 and 1), and τ_{act}, τ_{deact} , the activation and deactivation time constants. The entry point excitation $u(t)$ corresponds to the filtered EMG signals. There is no consensus in the literature about a systematic filtering and transformation of the EMG signals to u [74], However, there is a common ground and a standard procedure for the processing of the EMG signals which should be adapted for the study specificities. For their use in this thesis and our specifics, with EMG signals recorded at 1.5kHz, the processing is done offline with MATLAB, following the methods in [27, 83, 130, 131]. EMG signals were detrended, band-pass filtered first at 50-500Hz with a 7th order Butterworth filter, rectified, then low-pass filtered with a 7th order Butterworth filter with a 10Hz cut-off frequency to obtain the envelope. We further normalized the signals by the median across all the computed movements per subject in order to ensure a wide amplitude of signals fed to the musculotendon contraction dynamics of the model favoring expected signals and avoiding high-amplitude spikes caused by noises. As mentioned before, for the Hill-

Type contraction dynamics and its underlying activation dynamics, the input signal activation should be between 0 and 1 which is then ensured with the normalization of the EMG by the similarly filtered maximum voluntary contraction recorded for each muscle.

2.3.3 Contraction dynamics

the Hill-type model, gives a simplified mechanical representation of the musculotendon contraction [71, 172, 177]. For musculoskeletal modeling, they are key components when the muscular activation is involved [100, 123, 148] They provide a single first-order ordinary differential equation representing the contraction dynamics of the musculotendon. It associates the muscle fiber velocity to a function of the muscle fiber length, musculotendon length and activation. Fig 2.3 The musculotendon actuator is represented as a mechanical system involving a contractile element (CE), a parallel elastic element (PEE) and a serial elastic element (SEE) to replicate respectively the active force production of the fiber, the passive force generated by the muscle fibers during their elongation and the passive force replicating tendon elongation resistance.

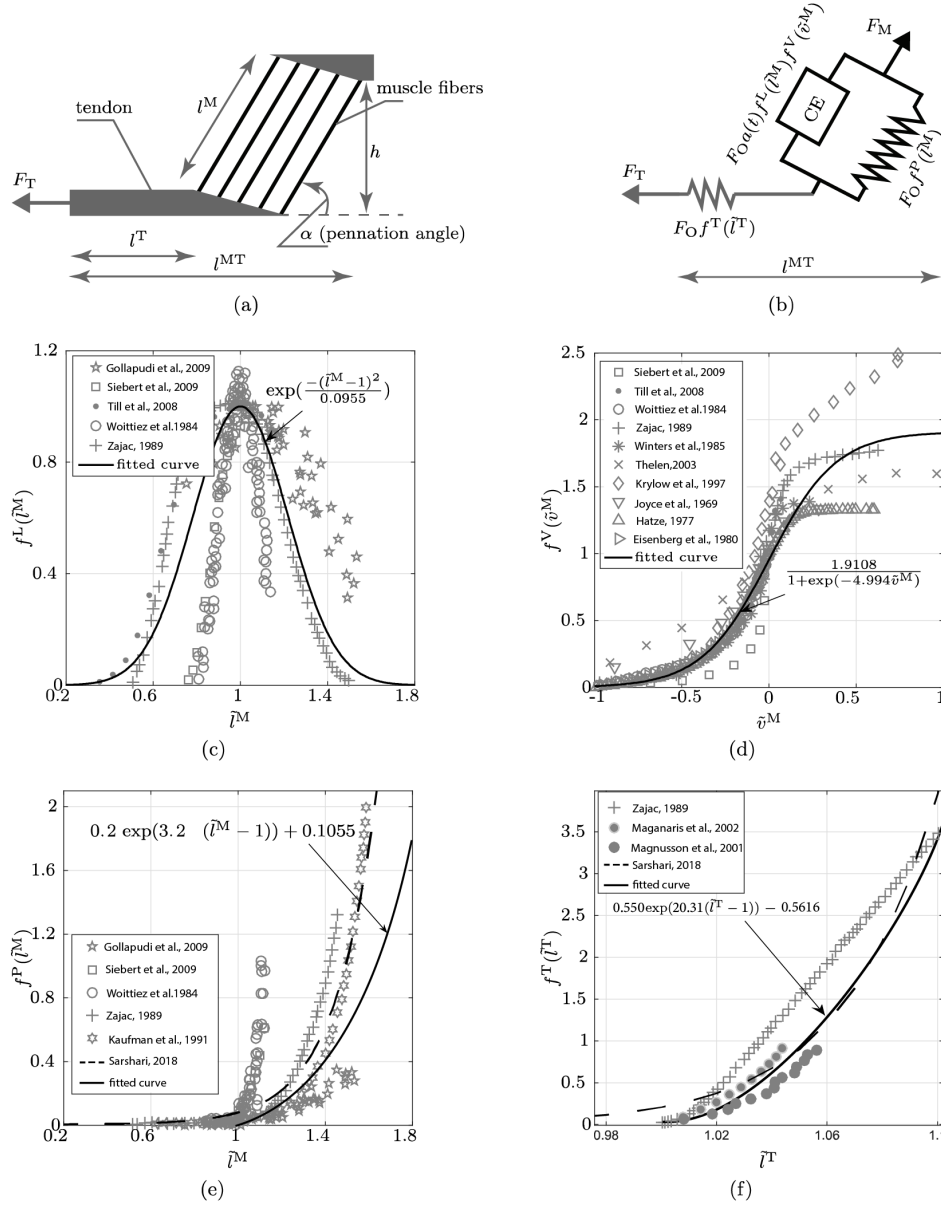


Figure 2.3: The Hill-type model used: (a) the physiological representation of the modeled elements in the Hill-type model. The fiber lengths are approximated by a set of straight parallel muscle fibers with equal lengths l^M deviated with a pennation angle α , from the axis of force production (in the direction of the muscle tendon) (b) The corresponding mechanical representation, including the contractile element (CE), the parallel passive elastic element (PEE) and the tendon, the serial elastic element (SEE). The force produced by the muscle F_M is the resultant of the force generated by the CE ($F_{Oe(t)}f^L(\tilde{l}^M)f^V(\tilde{v}^M)$), PEE ($F_O f^P(\tilde{l}^M)$) and SEE ($F_O f^T(\tilde{l}^T)$). The normalized functions f^P , f^L , f^V and f^T were obtained in [145], with a curve fitting of the experimental data from [45, 58, 66, 79, 81, 88, 105, 106, 157, 163, 164, 172, 173, 177]. In this present work, the curves fitted of f^P and f^T were adapted to better reflect the curves behaviours and avoid numerical errors. Modified from [145] with the author's consent.

The Hill-type approximates the different fibers of various lengths and physical properties included in a musculotendon unit to a single scaled-up version of normalized fiber. Indeed, the multiple fibers are assumed to be parallel and of the same lengths, with their orientation deviated from the muscle force direction with the pennation angle. In order to describe the musculotendon actuation as a black box to be used for each of the muscles, the muscle fiber length, velocity, tendon length and force quantities are normalized with respect to their so-called optimum values. With these considerations, the forces produced by the CE, PEE and SEE are defined with dimensionless functions with the muscle force-length f^L , muscle force-velocity f^V , passive muscle force f^P and tendon force-length f^T relationships. These were obtained by curve-fitting the experimental data reported in the literature [45, 58, 66, 79, 81, 88, 105, 106, 157, 163, 164, 172, 173, 177]. The expressions resulting from these are shown below (equations 2.16 2.17 2.18 2.19);

$$f^L(\tilde{l}^M) = \exp\left(\frac{-(\tilde{l}^M - 1)^2}{0.0955}\right) \quad (2.16)$$

$$f^V(\tilde{v}^M) = \frac{1.9108}{1 + \exp(-4.994\tilde{v}^M)} \quad (2.17)$$

$$f^P(\tilde{l}^M) = 0.2 \exp(3.2(\tilde{l}^M - 1) + 0.1055) \quad (2.18)$$

$$f^T(\tilde{l}^T) = 0.550 \exp(20.31(\tilde{l}^T - 1) + 0.5616) \quad (2.19)$$

For these forces to be scaled to a variety of human and animal muscles their values are normalized relative to the maximum force (F_0) at the optimal fiber length (l_0^M). Additionally, the normalized muscle fiber length \tilde{l}^M is defined as

$$\tilde{l}^M = \frac{l^M}{l_0^M} \quad (2.20)$$

The normalized muscle fiber velocity as

$$\tilde{v}^M = \frac{v^M}{v_0^M} \quad (2.21)$$

The normalized tendon lengths as

$$\tilde{l}^T = \frac{l^T}{l_S^T} \quad (2.22)$$

With the fiber lengths l^M , velocities v^M and tendon lengths l^T , the optimal fiber lengths l_0^M , velocities v_0^M and tendon slack lengths l_S^T respectively. These parameters are highly important in a Hill-type model and are different for each muscle modeled. The optimal fiber length of a muscle corresponds to its length where the fiber can produce the maximal force. At the optimal contraction velocity is obtained where the force in the

force-velocity relationship is zero.

Given the mechanical representation of the Hill-type model (see Fig 2.3 (b)), the force equilibrium between the tendon and fiber leads to the following equations if the tendon is assumed to be elastic. Of note, for a rigid tendon model, only 2.25 is valid, since the force is directly transmitted to the insertion point.

$$F^{MT} = F_{SEE} = (F_{CE} + F_{PEE}) \cos \alpha \quad (2.23)$$

$$= F_0 f^T(\tilde{l}^T) \quad (2.24)$$

$$= F_0 [a(t) f^L(\tilde{l}^M) f^V(\tilde{v}^M) + f^P(\tilde{l}^M)] \cos \alpha \quad (2.25)$$

Leading to

$$F_0 [a(t) f^L(\tilde{l}^M) f^V(\tilde{v}^M) + f^P(\tilde{l}^M)] \cos \alpha - F_0 f^T(\tilde{l}^T) = 0 \quad (2.26)$$

Where α is the pennation angle, the deviation angle between the fiber elements and the muscle tendon such as $l^M \sin \alpha = l^{MT} - l^M$, with l^{MT} the musculotendon complex length that is obtained with the muscle path in the model. The height h of the fibers in fig 2.3 (a), remains constant as the muscle shortens [18, 52, 114] which leads to

$$l^M \sin \alpha = l_0^M \sin \alpha_0 \quad (2.27)$$

We can therefore obtain the following ordinary differential equation in terms of $\dot{\tilde{l}}^M$

$$\left[a(t) f^L(\tilde{l}^M) f^V \left(\frac{l_0^M}{v_0^M} \dot{\tilde{l}}^M \right) + f^P(\tilde{l}^M) \right] \sqrt{1 - \left(\frac{\sin \alpha_0}{\tilde{l}^M} \right)^2} = f^T \left(\frac{l^{MT} - l_0^M \sqrt{\tilde{l}^{M^2} - \sin^2 \alpha_0}}{l_S^T} \right) \quad (2.28)$$

Equation 2.26 or equation 2.28 alone cannot be used to estimate the force given the length, velocity and activation of the muscle since multiple combinations of these values can satisfy the equation. However, a unique solution can be found by solving the equation 2.26 for the normalized muscle velocity \tilde{v}^M this can be done either implicitly on equation 2.28 [15] or explicitly with the following ordinary differential equation including the inverse of the force-velocity curve f_{inv}^V

$$\tilde{v}^M = f_{inv}^V \left(\frac{\frac{f^T(\tilde{l}^T)}{\cos \alpha} - f^P(\tilde{l}^M)}{a f^L(\tilde{l}^M)} \right) \quad (2.29)$$

Which can be rewritten similarly to equation 2.28 in terms of $\dot{\tilde{l}}^M$ as

$$\frac{l_0^M}{v_0^M} \dot{\tilde{l}}^M = f_{inv}^V \left(\frac{1}{af^L(\tilde{l}^M)} \left[\frac{f^T \left(\frac{l^{MT} - l_0^M \sqrt{\tilde{l}^{M^2} - \sin^2 \alpha_0}}{l_S^T} \right)}{\sqrt{1 - \left(\frac{\sin \alpha_0}{\tilde{l}^M} \right)^2}} - f^P(\tilde{l}^M) \right] \right) \quad (2.30)$$

If the equation 2.28 does not present any numerical singularities, the introduction of the formulation with equation 2.30 presents four: $a \rightarrow 0$, $f^L(\tilde{l}^M) \rightarrow 0$, $\tilde{l}^M \rightarrow \sin \alpha_0$ and as $\frac{\partial f^V(\tilde{v}^M)}{\partial \tilde{v}^M} \rightarrow 0$.

In both cases, the normalized muscle fiber is able to reach unrealistic short lengths and cannot be simulated when fully deactivated, therefore, a unilateral constraint is included on the candidate value obtained from: Eq. 2.28 or Eq. 2.30

$$\dot{\tilde{l}}^M = \begin{cases} 0 & \dot{\tilde{l}}^M < 0 \text{ and } \tilde{l}^M < \max(f_{inv}^L(0), \sin \alpha_0) \\ \tilde{l}^M & \text{otherwise} \end{cases} \quad (2.31)$$

With f_{inv}^L the inverse function of the active force-length curve. These constraints are highly important in the numerical approaches since they can ensure a realistic lower bound for the muscle fiber length, avoiding numerically stiff equations.

2.3.4 Rigid-tendon model

With a rigid tendon assumption, it is possible to determine the muscle length l^M and velocity v^M directly from the musculotendon length l^{MT} and velocity v^{MT} as the tendon is inextensible, its length l^T remains l_S^T giving:

$$l^{MT} = l^T - l^M \cos \alpha \quad (2.32)$$

Which differentiates with respect to time to

$$v^{MT} = v^T + v^M \cos \alpha - l^M \dot{\alpha} \sin \alpha \quad (2.33)$$

or v^T with a rigid tendon and

$$h = l^M \sin \alpha = l_0^M \sin \alpha_0 \quad (2.34)$$

With h being constant, this previous equation differentiates with respect to time to obtain:

$$\dot{\alpha} = -\frac{v^M \sin \alpha}{l^M \cos \alpha} \quad (2.35)$$

Given the known values of l^T , l^{MT} and v^{MT} and the system of equations 2.35 and 2.33 we can obtain v^M and l^M from 2.32 and 2.34.

It greatly reduces the system complexity since it transforms the contraction dynamics into an algebraic relationship that needs no integration. Indeed, Eq. 2.25 directly gives the output force.

However, if this assumption is appealing for a great numerical cost reduction, for muscle with a high tendon slack length to optimal fiber length ratio is far from unity it is not recommended as an alteration in the tendon length will most likely occur and thus the force computation can be greatly affected [117].

2.4 Inverse dynamics formulation

The musculoskeletal model presents 11 degrees of freedom, and 42 muscle actuators spanning them which is more than the technically required from a mechanical standpoint, which means that, in theory, an endless variety of force configurations are feasible. This issue is often referred to as the redundancy problem [36] or force-sharing problem [44]. In the formulation of the inverse dynamics, the kinematic of the model is known, thus the musculotendon lengths, joint angles, velocities, and accelerations can be obtained. Together with the Euler-Lagrange equations 2.9 the equations of motions can be formulated in the following way:

$$MDYN\ddot{q} = RHS + \frac{\partial \Omega}{\partial \dot{q}}M + constraints \quad (2.36)$$

To compute numerically the MDYN (corresponding to the "mass" matrix) and RHS (the right-hand side of Lagrange's equation) in the Matlab environment using the symbolic toolbox. The following methods are applied to the previously computed Lagrangians from Eq. 2.11 in a symbolic formulation as functions of the generalized coordinates q and \dot{q}

$$MDYN(q) = \frac{\partial^2 \mathcal{L}}{\partial \dot{q}^2} \quad (2.37)$$

$$\text{RHS}(\mathbf{q}, \dot{\mathbf{q}}) = \frac{\partial \mathcal{L}}{\partial \mathbf{q}} - \frac{\partial^2 \mathcal{L}}{\partial \mathbf{q} \partial \dot{\mathbf{q}}} \dot{\mathbf{q}} \quad (2.38)$$

These functions of the generalized coordinates are subject to the inertial properties of the system, including the masses of the bones, the inertial tensors, the gravitational constant, and initial bony lengths. However, their numerical computations are costly as they must be obtained at every step in the simulation (including within the optimization procedures). For a scaled model, these must be symbolically computed after the scaling procedure. For a simulation based on the generic model, Matlab functions to numerically compute these functions are precomputed in C and developed as Matlab Mex files to speed up their computations.

With this, the inverse dynamics formulation intends to obtain the muscle forces and their underlying activations satisfying the following equation:

$$\text{MDYN}(\mathbf{q})\ddot{\mathbf{q}} - \text{RHS}(\mathbf{q}, \dot{\mathbf{q}}) = \left[\frac{\partial \Omega}{\partial \dot{\mathbf{q}}} W(\mathbf{q}) M_c(\mathbf{q}) \right] \tilde{\mathbf{f}} = J_{\text{torque}} \quad (2.39)$$

Where M_c accounts for the generalized moment arms of the scapulo-thorax constraints [75, 145], and $\tilde{\mathbf{f}}$ the augmented force vector including the forces \mathbf{f}_c associated to these constraints $\tilde{\mathbf{f}} = [\mathbf{f} \ \mathbf{f}_c]$. J_{torque} corresponds to the resulting torques acting on the joints

Of note, M_c is obtained from the definition of the Lagrangian in Eq. 2.11 as explained in [75, 145] in details.

From Eq. 2.39 we now have defined the dynamics of the system that the forces need to satisfy. From Eq. 2.26 we also have the constraints on the possible force produced by a muscle given its fiber length, velocity and activation with the lower and upper boundaries with a minimum value of activation of 0 and a maximal activation of 1 as $f_{MT}^{\text{low}}(a_0, l_{MT}, v_{MT})$ and $f_{MT}^{\text{up}}(a_1, l_{MT}, v_{MT})$ respectively. However, these constraints would still not be sufficient to define the forces and a unique set of activations needed to satisfy the system of equation. In the inverse dynamics proposed in this thesis, we want to minimize the cost function corresponding to the squared sum of muscle stresses. First presented in [31], its aim is to reduce overall muscle fatigue and is frequently used in musculoskeletal models as a standard load-sharing scheme.[46, 53, 70, 123, 137, 156, 162]. The muscle stresses are obtained using the physiological cross-section areas of the muscles, assuming the stress is evenly distributed over the entire cross-section it is obtained as the following for a single muscle.

$$\sigma_i = \frac{f_i}{PCSA_i} \quad (2.40)$$

The cost function to minimize thus is:

$$C_s = \sum \sigma^2 = \mathbf{f}^T P \mathbf{f} \quad (2.41)$$

With P, the diagonal matrix contains the inverse squared of muscle physiological cross-section areas. Those values are obtained from [52].

The natural corresponding optimization problem becomes the following:

$$\begin{aligned} \min_{\mathbf{f}} \quad & \tilde{\mathbf{f}}^T P \tilde{\mathbf{f}} \\ \text{s.t.} \quad & \mathbf{f}_{MT}^{low}(a_0, l_{MT}, v_{MT}) \leq \tilde{\mathbf{f}} \leq \mathbf{f}_{MT}^{up}(a_1, l_{MT}, v_{MT}) \\ & MDYN(\mathbf{q})\ddot{\mathbf{q}} - RHS(\mathbf{q}, \dot{\mathbf{q}}) = \left[\frac{\partial \Omega}{\partial \dot{\mathbf{q}}} W(\mathbf{q}) M_c(\mathbf{q}) \right] \tilde{\mathbf{f}} \\ & \mathbf{C}_{mat} \cdot \mathbf{JRF} \leq 0 \end{aligned} \quad (2.42)$$

Finally, a glenoid stability cone constraint was included; the glenoid fossa was approximated by a cone and to keep the joint reaction forces (JRF) inside the glenoid and to have them facing the opposite direction of the normal vectors of the glenoid fossa cone basis \mathbf{C}_{mat} , their scalar product should be negative. Its implementation and description can be found in both [75] and [145].

When solving this quadratic programming optimization problem using quadprog in Matlab a solution is rarely obtained within the shown constraints. This is in contrast to what was shown in [145] in which the force boundaries criterion was less stringent and, more importantly, less physiologically realistic [91].

Indeed, the force boundaries presented there were defined between 0 and a value f_{max} which was defined as $f_{max_k} = K \cdot PCSA_k$, with K, the Fick constant equal to $33.011 Nm^{-2}$ [31]. The problem arises from ignoring the passive forces of the muscles, which is not null for elongated muscles, and the total musculotendon parameters. Indeed, as presented before the contraction dynamics and the resulting forces are highly dependent of the musculotendon properties. In fact, their primary objective was to assess the forces operating on the upper limb. However, the muscle activations are the emphasis of this thesis, with the calculated forces only serving as a means of obtaining these activations. Another reason for the lack of possible solution within the boundaries lies in the obtained dynamics. Indeed the movements recorded studied in [145] were well-defined movements of the shoulder joint which would lead to relatively smooth accelerations and dynamics in general. One goal of this thesis is to estimate and study the activations of healthy subjects and impaired neurological patients while performing 3d reaching tasks as it will be presented in chapters 3 and 4, therefore the movements are expected to be unpredictable and noisy.

The modified optimization problem, therefore, includes a possible error from the inverse dynamics obtained torque at the joints J_{torque} (in Eq.2.39) so that a physiologically possible solution is obtained within the force boundaries, this accounts for the possible miscalculations of the kinematics and possible robotic interactions within the assessments (see chapters 3 and 4). Similarly to the "hybrid EMG-informed" developed in [148] for the lower limb the joint torque is minimized alongside the absolute difference between experimental activations and the estimated ones (in our case, for the available ones). However, here, the sum of muscle activations is not minimized but the previously described stress of the induced force is, which is in line with the recent comparison between cost function [104] and their performances

The cost function becomes:

$$A_{cf} = \sum |W_m \tilde{\mathbf{f}} - J_{torque}| + \alpha \sum |a_{rec} - \tilde{a}| + \beta \tilde{\mathbf{f}}^T P \tilde{\mathbf{f}} \quad (2.43)$$

$$A_{cf} = \hat{E}_J + \alpha \hat{E}_{a_{EMG}} + \beta C_s \quad (2.44)$$

The α and β are positive weighting coefficients obtained experimentally ensuring $\hat{E}_J \leq \hat{E}_{a_{EMG}} \leq 1e^{-2}$. The activations minimizing the cost function are obtained with the *fmincon* algorithm in Matlab.

Of note, the joint reaction force constraint was not implemented in this new formulation. Therefore the use of the inverse dynamics method choice should be adapted to the study itself, if the goal is to evaluate the forces and their stability at the joints and the tasks and movements recorded are simple the optimization chosen should be the one described in Eq. 2.42. Otherwise, the one from Eq.2.43 should be preferred.

Additionally, it is strongly advised to use the rigid tendon formulation with the Eq.2.43 since at each step of the optimization process the forces are computed. This is done via a precomputation of the possible force values given the musculotendon state $(l_{ti}^{MT}, v_{ti}^{MT})$ as a function of the activation at each time step t_i before the activation optimization is solved.

$$\mathbf{f}_{ti}(a) = \mathbf{f}_{MT_{ti}}(a, \mathbf{l}_{MT_{ti}}, \mathbf{v}_{MT_{ti}}) \quad (2.45)$$

Where \mathbf{f}_{ti} is simply interpolated from computed forces with activations ranging from 0 to 1. To speed up the computation process the contraction dynamics to obtain the force could be precomputed in C and used as a Matlab mex file.

2.5 Forward dynamics formulation

In forward dynamics, the inputs of the system are the forces or the associated muscle activations leading to a motion. Here the Euler-Lagrange equations 2.9 can be

formulated to obtain the joint angles accelerations to be integrated.

$$\ddot{\mathbf{q}} = MDYN(\mathbf{q})^{-1} [RHS(\mathbf{q}, \dot{\mathbf{q}}) + Control(\mathbf{q}, \dot{\mathbf{q}})] \quad (2.46)$$

Where *Control* is the input of the forward dynamics formulation. For a torque-based formulation:

$$Control = J_{torque} \quad (2.47)$$

For a force-based formulation:

$$Control(\mathbf{q}) = MA(\mathbf{q})\tilde{\mathbf{f}} \quad (2.48)$$

With MA the augmented Moment arm matrix including the partial velocity matrix $MA = \left[\frac{\partial \Omega}{\partial \dot{\mathbf{q}}} W(\mathbf{q}) M_c(\mathbf{q}) \right]$ In an activation-based formulation, the input are the activations that will be fed in the contraction dynamics leading to forces.

This system with only the forces as input is considered the feedforward controller. The associated solution from the inverse dynamics formulation if it exists is always a candidate for the feedforward design [Slotine1991, 146].

The formulation from Eq. 2.46 is written as an ordinary differential equation in the following way to be solved numerically with the Runge-Kutta Fehlber fourth and fifth order method [41, 146].

$$\mathbf{u} = \begin{pmatrix} \mathbf{q} \\ \dot{\mathbf{q}} \end{pmatrix}, \quad \dot{\mathbf{u}} = \begin{pmatrix} \dot{\mathbf{q}} \\ \ddot{\mathbf{q}} \end{pmatrix}, \quad (2.49)$$

The open loop formulation, however, deviates fast from the trajectory used in the inverse dynamics to define the control, this is due to the accumulation of successive errors in the numerical integration and is well known in the literature [38, 61] which happens even on reduced model of a single joint with three degrees of freedom [146].

2.6 GUI visualization and reduced model

The existing model architecture is rather complex, consisting of an excessive number of files and functions, which may be intimidating and not really efficient when working with. If there exists a graphical user interface (GUI), it does not support most recent versions of Matlab and most importantly is mostly adapted to previous functions and to force evaluations. With the newly developed inverse dynamics and forward dynamics based on activation a new toolbox was required. This one is tailored to

facilitate muscle analysis and activation comparisons rather than the study of forces acting on the joints during a single movement from kinematic data. It allows for multiple movement studies to run in parallel using the parallel computing Matlab toolbox, which greatly reduces the computational time required for a study involving multiple repetitions. Finally, this toolbox can be callable from the current GUI and can open some of the available existing toolboxes making it perfectly adaptable.

In this GUI, the user has the possibility to tune selected parameters directly, or choose the tendon model, rigid or flexible, if the kinematics should be scaled to the generic model, if no ENG data is loaded, the model will run a static-optimization to obtain the overall forces and activations leading to the measured kinematics. Otherwise, the latter will be included in the EMG-assisted model. In the multiple simulations tab of the inverse dynamics mode, the user can select the subjects of study, the assessments, and the targets reached and the simulation will run over the repetitions across these choices in parallel (In our recorded data, there are around 5 repetitions per subject and targets). In the forward dynamics tab, the inputs can be either, the muscles' activations, their forces, or the torques at the joints. Initial configuration can be set for the feedforward simulation and for the closed loop one, the kinematics. Damping at the joints and user-specific functions can be directly set within the GUI to have those changes simpler for the user and to avoid accessing Matlab function. In all cases, extra parameters or simple functions can be written in a script (text file opened with the extra parameters pushbutton and directly linked to the used functions) for fast and efficient interactions within the inner Matlab functions.

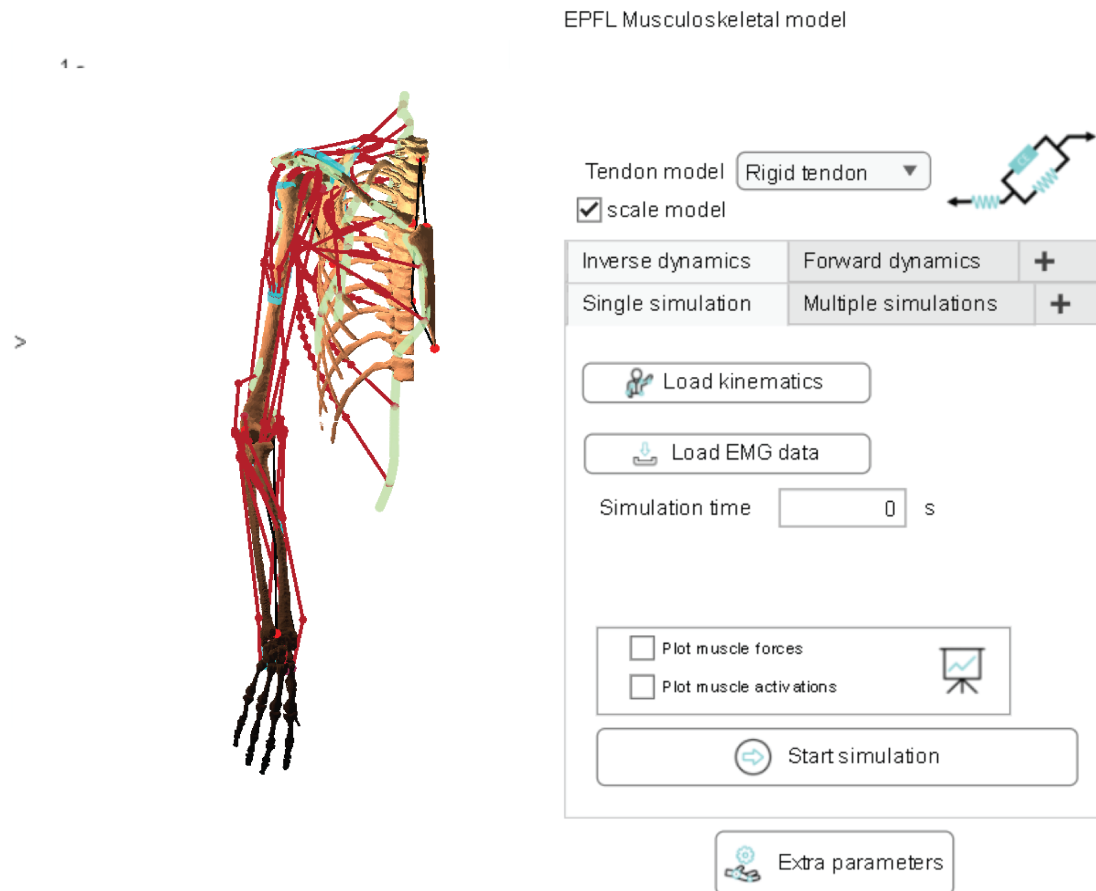


Figure 2.4: Graphical user interface for inverse dynamics of a single movement the choice of the tendon model can be made, and its scaling will open the existing scaling toolbox of the model

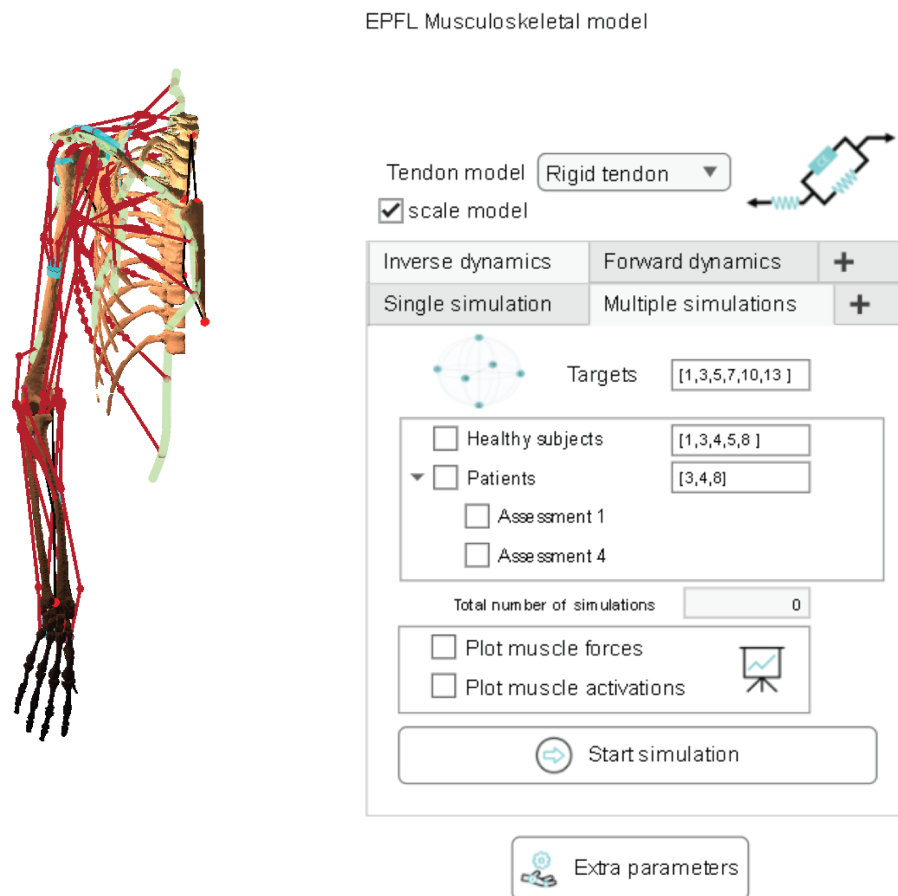


Figure 2.5: Graphical user interface for inverse dynamics of a multiple movements. The user can select the tasks and subjects to study and the repetitions of those movements will be computed in parallel

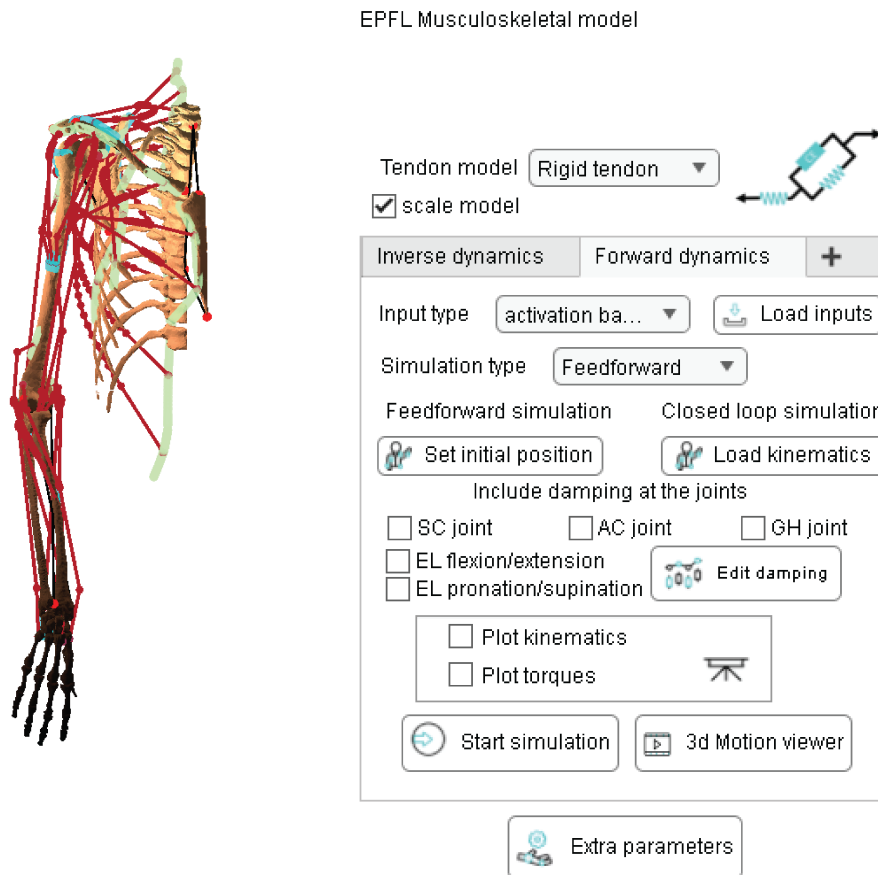


Figure 2.6: Graphical user interface for forward dynamics: closed loop or feedward simulations can be selected with choices for possible custom-made dampings at the joints

2.7 Future possibilities

The model can still be developed and improved. I could reduce the computational cost during simulations by using precomputed functions in C and developed as Matlab Mex files to speed up their computations. But other means could achieve great performances. Indeed the moment arm and muscles lengths computations as functions of joint angles for instance could be obtained via regression models, drastically reducing the computation time, however, building models like this would totally block the model scaling features if the latter ones are not included. Unfortunately, this would take a long computational time to obtain.

Future development of the model should take the forward dynamics methods and directly couple it with the cost function from the inverse dynamics method. The

forward dynamics computation is not only faster, it could compensate on its own for the variations from the desired torque. Indeed in the cost function proposed, the activation estimation should minimize also the difference in the measured torque at the joints and the produced torque from the musculotendon actuation. This would be similar to the methods proposed in [72, 148] and to more recently [2]. The current drawbacks of the forward dynamics model would be then discarded as it would act as a closed-loop in this mode. Moreover, given the already computed function and methods as "black box", this should be relatively fast achieved.

With overall activations estimated from the inverse dynamics across different directions at multiple speeds and corresponding EMG recorded. It could be possible to develop a machine learning model for simple movements leading to the overall activations from recorded EMG. This however would require a large dataset of EMG and movements since the model is composed of 11 degrees of freedom but could provide a good insight of muscular impairments and variations in movement from recorded EMG only.

Finally, the hand as a single bone and the wrist joint are already available in the model, and most of the muscles spanning the wrist joint are already modeled. With the current state, movement of the wrist is maintained fixed which overlooks activation from muscles spanning this joint.

I would suggest future development starting from the mex precomputation of more functions used in the model, and possibly even developing the model and the graphical user interface as an application for easier use by a wider range of population, including clinicians. This would also limit the access of most of the functions, and their behavior could be rather simply modified by tuning a limited number of parameters as I did for the graphical user interface and the tuning of the activation cost functions. Furthermore, the existing architecture is rather cumbersome, consisting of an excessive number of files and functions, which may be intimidating for the new user.

3 Biomechanical model and healthy subjects muscle activation assessment

During this thesis we presented the development of the upper-limb model as well as the inverse dynamics methods and potential use. In this chapter, the aim is to validate the model, stating that with the reconstructed kinematic from the exoskeleton and with the integration of a limited number of EMG recorded we can improve the activation estimation.

Manuscript under revision

The content of this chapter is adapted from a manuscript currently under revision. Preprint available at Research Square:

Tristan Barjavel, Tommaso Proietti, Camilla Pierella and Silvestro Micera, "*A realistic upper-limb musculoskeletal model for overall muscle activation estimation*", 17 May 2023, available at Research Square <https://doi.org/10.21203/rs.3.rs-2802018/v1>

Personal contributions as first author: Implemented the model, adapted the kinematics and EMG recordings, analyzed the results, created the figures, and wrote the manuscript.

A realistic upper-limb musculoskeletal model for muscle activation estimation

Tristan Barjavel^{*1}, Tommaso Proietti², Camilla Pierella^{3,4}, Silvestro Micera^{1,2}

¹ Ecole Polytechnique Federale de Lausanne (EPFL), Bertarelli Foundation Chair in Translational Neuroengineering, Center for Neuroprosthetics and School of Engineering, Geneva, 1202, Switzerland

² Scuola Superiore Sant'Anna, Biorobotics Institute and Department of Excellence in Robotics & AI, Pisa, 56025, Italy

³ University of Genoa, Department of Neurosciences, Rehabilitation, Ophthalmology, Genetics, and Maternal and Children's Sciences (DINOEMI), Genoa, 16126, Italy

⁴ University of Genoa, Department Informatics, Bioengineering, Robotics and Systems Engineering (DIBRIS), Genoa, 16126, Italy

3.1 Abstract

The human upper limb can perform complex tasks thanks to the ability of the central nervous system (CNS) to control and modulate the activation of more than 40 muscles. A deeper understanding of the strategies implemented by the CNS to perform these movements could help develop more effective rehabilitation protocols. Unfortunately, given the number of muscles acting on the shoulder and arm and their positions with respect to each other, a complete upper-limb's muscles electromyographic (EMG) recording is not feasible in practice. Numerical musculoskeletal model could represent a very useful alternative approach to gather this kind of information. Here, we develop a new realistic upper-limb biomechanical model which uses a combination of few recorded EMG data (up to max $N=16$) and an inverse dynamics model reducing the muscle stress to predict the overall upper-limb muscle activations ($N=42$). The predictions from this model (EMG-assisted) were compared to 1) a full set of 16 arm muscles EMG data of healthy subjects performing 3D upper-limb movements, 2) a model using none of the these recorded EMG data (static-optimization). If, predicted signals from the EMG-assisted and static-optimization led to a 3.4% and 2.3% error respectively in the resulting moment of joint when fed into the movement dynamics, the EMG-assisted method presented a more physiological sharing of the muscle activations and errors with respect to the activations from EMG signals for non used muscles in a comparison leave-one-out method. These promising results open up to adopting this musculoskeletal model as a tool to evaluate healthy motion data, with the potential of applying in the future the same analysis to impaired individuals motions and to compare inter-subject activation behaviours.

3.2 Introduction

Human healthy individuals can easily control their upper-limb movements despite a complex and redundant musculoskeletal system. In 1967, Nikolai Bernstein [11] hypothesized that the central nervous system (CNS) activates groups of muscles as muscle synergies instead of activating them independently, with each synergy specifying a particular balance of activation across a set of muscles. More recently, this hypothesis has been tested and confirmed by other groups [12, 33, 120]. Understanding how the CNS manages to perform complex tasks requires a deep comprehension of how the different muscles activate. Because of the often-overlapping physical location and the large number, simultaneous direct measurement of multiple muscles (e.g. the ones in the upper-limb) via electromyography (EMG) is generally not feasible at a large scale, in particular in a clinical environment. However, EMG is still largely considered the gold standard for assessing muscle activity, being a non-intrusive method with fast setup time. It is important to notice that EMG recordings are able to show the activity of the muscles but do not provide their contribution to the general movement, underestimating the muscles passive forces derived from their sole elongation [118]. Musculoskeletal numerical models could represent an interesting alternative approach to directly probing the muscles [152]. Existing models mainly focus on estimating the force produced by the different muscles, often neglecting the dynamics of muscle activation. Forces are usually computed by optimization of physiological cost-functions and constraints, applied to equations of moment equilibrium at each joint. Most of these optimization criteria are based on muscle-related properties, for instance, muscle stress [28], muscle forces [81], and muscle's energy consumed [63], or the so-called min/max criterion [138, 161]. In a few studies, EMG signals were incorporated into lower-limb musculoskeletal models [100, 148] and upper-limb musculoskeletal models [7, 50, 82, 123, 147], resulting in more accurate estimates of muscle co-contraction estimations.

In this study, we propose an overall fast muscle activation estimator (42 muscles in total) as a comparative and evaluation tool, that improves muscle co-contraction estimations with the use of a reduced number of recorded EMG signals (up to $N=16$). The estimator works together with a numerical upper-limb musculoskeletal model that uses a combination of approaches: 1) minimization of the sum of squared muscle stresses, setting an evenly distributed load over the muscles; 2) constraining muscle forces to keep a glenoid stability and to keep their values within their physiological boundaries; 3) minimization of the squared differences in the obtained and experimental joint moments. Physiological boundaries are defined by the contraction dynamics with feasible activations as well as available recorded EMGs. The minimization criteria is different from previous models where authors mostly minimized the overall muscle activations for non-recorded muscles while keeping a low predicted error between joint moments and measured activations in forward dynamics for lower limb [72, 148],

with CEINMS toolbox on OpenSim [132]. In our previous previous upper-limb model [147], the minimization was done on the forces, using the null space from the underlying matrix of the muscle moment arms; however, using this strategy a solution could not always be met. Another difference with the state of the art is that the provided cost function to minimize is not subject-specific as it was previously proposed [72, 148]. This important feature aims at improving the ability of the model to perform subject comparisons with the future goal of analyzing intra-subject activation evolution to optimize and guide subject-specific rehabilitation therapy.

Despite the different minimization criteria, the model we present is also an improved version of our previous upper-limb models [75, 145, 147] in terms of computational quickness and efficiency regarding inner processes, such as musculotendon parameters estimations, rigid tendon modelling, signal treatments, and the methods to perform inverse dynamics. The model was tested and validated by processing data from five healthy subjects performing 3D reaching movements using ALE_x RS [98], an upper-limb exoskeleton. In particular, we used our model to predict the activities of the upper-limb muscles during the reaching movements and compared them with available EMG signals recorded during the experiments. The general overview of the work is shown in Fig. 3.1.

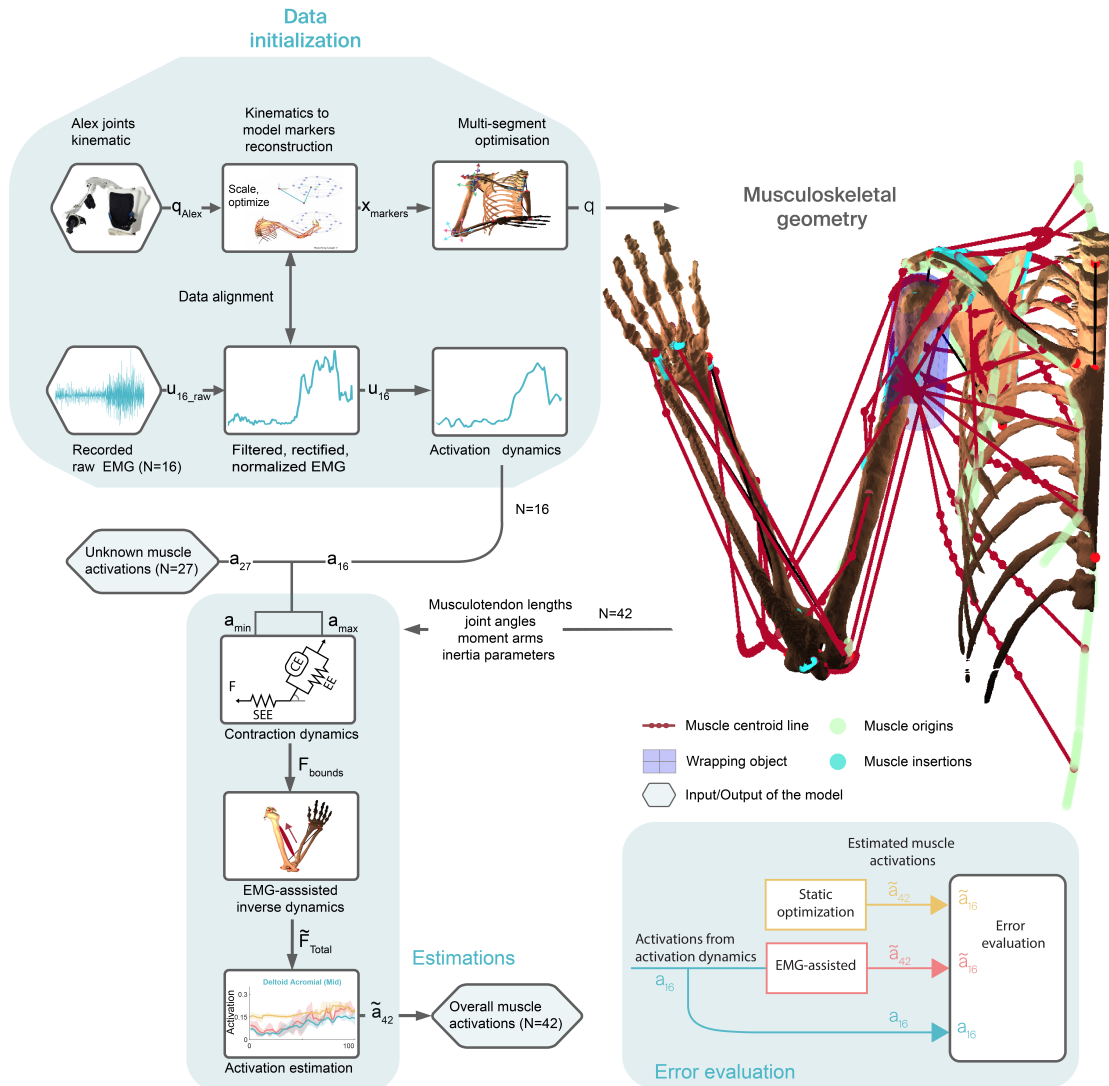


Figure 3.1: General overview of the presented estimation model. During data initialization, the recorded kinematics q_{ALEx} and EMG signals u_{raw} are used to compute the joint angles q and muscle activations a_{16} . These are in turn inputs to the numerical model and the estimation framework to obtain the overall muscle activations \tilde{a}_{42} , where the tilde denotes an estimated value. To quantify the errors from the model (error evaluation, *i.e.* cross-correlation and RMSE), the estimated 16 muscles activations are compared to the ones directly obtained from EMG measurement and to a static optimization using no EMG data. In the musculoskeletal model representation, the red strings represent the 42 muscles originally considered, from their origin (light green) to their insertion (cyan) with one wrapping object represented around the glenohumeral joint as an example. The modelled muscles are: subclavius, serratus anterior upper, middle and lower parts, trapezius C1-C6/C7/T1/T2-T7, elevator scapulae, rhomboid minor, rhomboid major T1-T2 and T3-T4, pectoralis minor, pectoralis major clavicular sternal and ribs, latissimus dorsi thoracic, lumbar and iliac, deltoid clavicular, acromial and scapular, supraspinatus, infraspinatus, subscapularis, teres minor and major, coracobrachialis, triceps brachii long, medial and lateral, biceps brachii short and long, brachialis, brachioradialis, supinator, pronator Teres, flexor carpi radialis and ulnaris, extensor carpi radialis long and brevis, and extensor carpi ulnaris.

3.3 Methods

3.3.1 Numerical model

In this work we present a model derived from an existing validated shoulder musculoskeletal model [75, 145, 147] that was initially developed for both the muscle and joint reaction forces prediction. The numerical musculoskeletal model, developed in MATLAB (MathWorks, USA), is based on anthropometric cadaveric data but allows for scaling parameters to match the dimensions of each specific subject. Tunable parameters are the bone inertial properties, the skeletal morphologies as well as the muscle architectures, all features that could benefit a proper inter-subject, healthy/impaired muscle activation evaluation in the future [145]. However, subject-specific models require complex modeling workflows [32, 115] and well-defined methods, especially for musculotendon parameters estimation. For our study, given the nature of the recorded kinematics and the collected information about the subjects (see following section), a generic model to which only the recorded data would be scaled was needed so that all subject would have a common basis for the model outputs evaluations, based on their movement and their EMG recorded [116]. In the original model, 42 muscle bundles are considered, spanning 11 degrees of freedom (sternoclavicular, acromioclavicular, glenohumeral modeled as ball and sockets joint as well as the elbow flexion-extension and pronation-supination) between the thorax, clavicle, scapula, humerus ulna and radius according to the ISB recommendations [174]. The muscles are represented with their centroid lines, from their origin to their insertions, and they lie on defined wrapping objects (Fig. 3.1). With the movement represented by the model's angular rotations at the joint levels, the different musculotendon lengths, their directions, their moment arms [76], and all inertia parameters can be obtained.

3.3.2 Experimental set-up and recorded data

To validate the model, we used the EMG and kinematic recordings of five healthy subjects (4 females, 1 male, 60 ± 12 yo, 65 ± 11 kg, 167 ± 9 cm) performing reaching tasks while assisted by an upper-limb exoskeleton (Arm Light Exoskeleton Rehab Station, ALEx RS from [98, 131]). The full experimental set-up and the description of the subjects are available elsewhere [130]. The robotic assessment consisted in performing center-out 3D reaching movements toward 18 points equally distributed on a sphere (with a 19cm radius). Subjects executed these movements with the right arm while seated, wearing ALEx RS, 5 times and were always returning to a starting position placed in the center of the target sphere. A monitor in front of the subject displayed the end-effector position, the different targets of the sphere, and the specific target to reach. The center of the spherical workspace position was defined to be aligned with the right acromion of the subject and equidistant between the monitor and the acromion (Fig. 3.2).

To test the model, the targets considered were the 6 points positioned along the 3 main directional axes from the center of the sphere, corresponding to reaching upwards (target 1), downwards (target 5), to the left (target 7) to the right (target 3), frontwards (target 13) and rearwards (target 10). The robot did not provide any assistance to the subject while performing the tasks and only supported the weight of its components to be as transparent as possible for the user [131]. During the robotic assessment, the EMG signals of 16 muscles of the upper limb were recorded: deltoid clavicular, acromial and scapular, trapezius C1/C7, pectoralis major clavicular, latissimus dorsi thoracic, infraspinatus, triceps brachii long and lateral, biceps brachii short and long, brachialis, brachioradialis and pronator teres. The EMGs were recorded at 1.5kHz using AgCl Kendall surface EMG electrodes with a Desktop DTS wireless system (Noraxon, USA). The electrode placement followed the European recommendations for surface electromyography for non-invasive assessment of muscles (SENIAM) and anatomical guidelines [69, 128]. Regarding the kinematic data, the robotic joint angles (shoulder abduction, rotation, flexion elbow flexion, prono-supination), as well as the end-effector position and velocities, were acquired at a 1kHz. The kinematic data acquisition was synchronized with the EMG signals recordings via trigger signals sent from ALEx RS when the movement started and stopped.

3.3.3 Data initialization

Matching ALEx joints kinematics to the model markers

Given that the acquired kinematics from ALEx RS does not correspond to the musculoskeletal model markers requirements [75, 145], assumptions had to be made so that the model matches the subject's movement. First, the position of the glenohumeral joint was considered fixed in the workspace: the arm and thorax were attached to the robotic exoskeleton leaving a reduced possibility for the rotations and translations of the shoulder complex. Moreover, the design of the shoulder rotation mechanism [98] uses a remote center of rotation, which corresponds to the glenohumeral joint center, allowing the exoskeleton kinematics to be similar to the one of the subjects. Second, the position of the subject's arm with respect to the robotic exoskeleton was also fixed, thanks to the rigid anchoring that does not allow for translation during the motion. Although we know that these assumptions reduce the accuracy of the activation predictions for a single trial, they would still ensure that all the possible movements performed by each subject during the different movement directions and repetitions could be similarly numerically reconstructed.

The robot kinematics (joint angles and end-effector position), together with robot arm lengths, allowed to obtain the skeletal positions with respect to the initial acromion position. In particular, we reconstructed a wireframe including estimated positions of the glenohumeral (GH) point, set as fixed, anatomical landmarks radial styloid (RS),

ulnar styloid (US) and lateral and medial elbow (EL, EM). The GH joint is modelled as a ball and socket joint corresponding to three shoulder rotations: abduction, rotation, and flexion around the robotic joint axes 1, 2, and 3 corresponding to the X, Y, and Z axes respectively, following the Cardan angle convention and the length of the robotic upper arm. The robotic elbow could be obtained, derived from it and based on the generic model distance between the EM and EL, the latter position could be estimated. With the elbow flexion/extension as a pin around the joint number 4 (Z-Axis) and the length of the forearm, the wrist position was obtained (corresponding to the joint number 5, Y-axis) and the US point, assumed to be close to the rotational wrist axis, could be derived. The pronation/supination of the elbow was also considered as a pin joint and together with its rotation and the wrist length in the generic model, the position of the RS point could be obtained from the US point.

The robotic exoskeleton was reconstructed numerically as a verification tool for the overall point and segment positions obtained with respect to the model skeletal ones (Fig. 3.2). Moreover, the resulting markers' positions and their corresponding skeletal representations were linearly scaled so that the recordings would match the skeletal numerical model. As the result of the markers position estimations and the hypothesis of a fixed GH point, the remaining needed markers of the numerical model could be derived from both the original skeletal positions and the fixed distances between the different remaining markers of the model. This procedure works only with the hypothesis of a fixed GH point; the evaluations of the internal dynamics in the shoulder girdle limits the model to a general overview, as the scapula dynamic is underestimated.

Once all the bony landmarks were defined and the kinematics of the robot matched the one of the model, the joint angles of the numerical model could be computed with the multi-segment optimization as previously reported[75, 145]. These optimization algorithms use the minimization of the distance between measured markers and their associated bony landmark. The output of the kinematic data initialization is the collection of musculoskeletal joints angles, velocities, and accelerations.

3.3.4 EMG signals preprocessing and activation dynamics

The EMG signals recorded at 1.5kHz were processed offline with MATLAB, following standard literature [130, 131]. EMG signals were detrended, band-pass filtered first at 50-500Hz with a 7th order Butterworth filter, rectified, then low-pass filtered with a 7th order Butterworth filter with a 10Hz cut-off frequency to obtain the envelope. To ensure a wide amplitude of signals fed to the musculotendon contraction dynamics of the model, the envelope was first normalized by the median computed across all the executed movements, favoring expected signals and avoiding high-amplitude spikes caused by noises. For the Hill-Type contraction dynamics described later, the input signal activation should be between 0 and 1 which is then ensured with the normalization

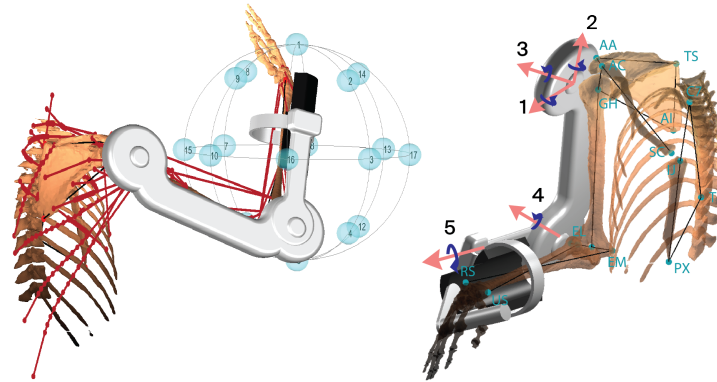


Figure 3.2: Illustrations representing ALEx RS exoskeleton and musculoskeletal model performing a task in the virtual environment. The blue spheres in the left panel are the different available targets, the red lines are the muscle represented in the model. The different skeletal markers used in the model, right panel, are shown in blue. The numbered robotic joint axes and their rotations are shown in pink.

of the EMG by the similarly filtered maximum voluntary contraction recorded for each muscle [131, 177]. For this study and for computational complexity cost reasons, the kinematic and EMG recorded were interpolated to a timestep of 0.01 second. Adapted from [177] and presented in previous work on this model [145], the activation dynamics associates the filtered EMG signal, or neural excitation u , to the muscle activation. In other words, it corresponds, if activated, to the increase of calcium concentration by the sarcoplasmic reticulum in the muscle fiber, or if deactivated, its removal. The activation dynamics are described in 3.1 with the activation a , the excitation u (both between 0 and 1) and τ_{act}, τ_{deact} , the activation and deactivation time constants.

$$\dot{a} = \frac{u - a}{\tau}, \quad \begin{cases} \frac{\tau_{act}}{0.5 + 1.5a} & u < a, \text{ activation} \\ \frac{\tau_{deact}}{0.5 + 1.5a} & u \geq a, \text{ deactivation} \end{cases} \quad (3.1)$$

3.3.5 Activation estimation

To obtain the activations of the muscle with no recorded EMG, the following estimation method is proposed. It is based on an inverse dynamics solver to compute the magnitudes of the forces needed to generate the torques at each joint that would explain the subject recorded movement. Given the over-actuated musculoskeletal model, (42 muscle bundles for 11 degrees of freedom), the estimation of the forces involves the optimization of net joint moments among muscles via load-sharing schemes (SLS) [70, 162]. However, antagonistic muscles are counterproductive in the net joint moment and SLS overlooks muscle co-contraction [7, 28, 30, 50, 123, 147]. The presented musculoskeletal model solves the indeterminacy problem by minimizing the sum of squared muscle stress and constraining the forces within physiological limits [162] which are

derived from the available EMG recording [147] and musculotendon parameters (i.e max isometric forces, minimum tendon force from the musculotendon actuation). The overall activation estimation step will be presented in the following order: first, the contraction dynamics and the estimation of the musculotendon parameters will be presented. The EMG-based inverse dynamics will be then explained with the resulting activation computed.

Contraction dynamics

The constitutive law derived from the Hill type model, the equations of motions and the performance criteria in the optimization procedure can be adapted and expressed in terms of the muscle activations instead of the muscle forces. Leading to some advantages, with the variables now being limited between 0 and 1.

The musculotendon actuation links the muscle state and its activation to a produced force. A hill-type model is used to describe the contraction dynamics [5, 71, 147, 177] and consists of three different elements replicating the force production function of the musculotendon system: the contractile element (CE), the passive elastic element (PEE), and serial elastic element (SEE). Each of these elements produces a force defined with normalized functions depending on the muscle intrinsic parameters as presented in the original model [145]. This results in the ordinary differential equation for each muscle 3.2.

$$F_{CE}(l_{CE}, v_{CE}, a) + F_{PEE}(l_{CE}) = F_{SEE}(l_{CE}, l_{MTC}) \quad (3.2)$$

The inputs of the model are the musculotendon length l_{MTC} and activations a together with the fiber lengths and velocities, respectively l_{CE} and v_{CE} . Moreover, although the musculoskeletal model has an elastic tendon model feature incorporated, to allow a wider range of possible solutions for the overall muscle forces, a rigid tendon model was used. This would limit the errors and avoid not feasible solutions from the inverse dynamics as well as considerably reduce the simulation time, which is a critical element for a model developed for an extended study of muscle activations across a big dataset. In a rigid tendon model, the muscle fiber length l_{CE} can be directly obtained from the musculotendon length l_{MTC} without an extra optimization. In addition to the computational cost reduction, an elastic tendon model increases the importance of perfectly scaled physiological musculotendon parameters. However, obtaining those would require the knowledge of the subject's physiological muscle and skeletal lengths or we would need to use, as it is currently done in recent literature, an optimization on those parameters from the output desired torques to fit a trained model [7, 100, 148, 150]. However, given the purpose of the proposed model to analyze improvement after rehabilitation, such an optimization would lead to different outcomes if performed at the early stages or at the end of rehabilitation. More importantly, if performed for each

of the assessments such an optimization would lead to different muscle parameters values which would not be possible in real life, the muscle fiber and tendon lengths should not be altered before and after rehabilitation for instance.

With Eq. 3.2 and the rigid tendon modelization, the muscle fiber and its contraction velocity could be directly obtained from the musculotendon lengths and velocities, leading to the following equation for the musculotendon force produced:

$$f_{MT}(a, \tilde{l}^M, \tilde{v}^M) = F_0 [a f^L(\tilde{l}^M) f^V(\tilde{v}^M) + f^P(\tilde{l}^M)] \cos \alpha \quad (3.3)$$

With \tilde{l}^M and \tilde{v}^M the fiber length and velocity normalized by the muscle optimal fiber length and maximal contraction velocity respectively. F_0 the muscle maximal force at optimal fiber length and f^L , f^V and f^P the normalized function derived from the force-length, force velocity and passive forces relationships as defined in chapter 2 and shown in figure 2.3. These were obtained by curve fitting of experimental data and are reported in Chapter 2 and in [145].

The contraction dynamics model gives the boundary values for the physiological muscle forces produced in the EMG-assisted inverse dynamics. The minimal force F_{MT}^{low} produced should correspond to the maximum between the force obtained with an activation of 0 and the passive elastic one, and its maximal F_{MT}^{up} should correspond to the solution with a fully activated contractile element. The lower activation was set to $1e-5$ for later mathematical purposes and to avoid numerical discrepancies. In previous work [147], the muscle forces without using EMG data have boundaries between 0 and a Fick constant $k = 33 N m^{-2}$ times the muscle physiological cross-sectional area (PCSA) which does not take into consideration the muscular dynamics over the movement. In this study, however, they are defined based on the contraction dynamics, which significantly affects their values, particularly due to the previously neglected passive elastic component.

The musculotendon parameters such as the maximum isometric force, optimal fiber length, pennation angle, maximum velocity contraction, and tendon slack length are adapted from the musculoskeletal model of Garner and Pandy[53] as the muscular architecture from our original model is the same. Using the reported methods[52, 62, 177], it was then possible to obtain those parameters adapted for the range of muscle lengths across all the possible joint rotations in our model so that a solution always exists for the musculotendon actuation. More precisely, we aimed at keeping the same operating range predicted for each muscle as the ones presented in another study[52], this means that we kept the same ratios of the normalized minimum and maximum length over the muscle optimal fiber length. This ensures a solution for all possible motions of the musculoskeletal model and thus, with the given scaling of the recordings to the generic model, a possible comparison between the different subjects

is possible.

EMG-assisted inverse dynamics

As mentioned before, the musculoskeletal system is defined with redundant muscles acting on the same degrees of freedom, this means that in the equations of motions, there are more unknowns than number of degrees of freedom. To estimate the muscle forces of the over-actuated musculoskeletal model, optimizations among muscles via static-optimization (SO) are usually performed. However, given the presence of antagonistic muscles, co-contraction among them can be overlooked in static-optimization as their net joint moment would compensate each other. The aim for the model would be to simulate the central nervous system criteria on muscle recruitment when performing a movement.

The presented musculoskeletal model solves the indeterminacy of the load-sharing problem thanks to the following optimizations. The main optimization criterion is the reduction of the muscle fatigue that is represented as the reduction of the overall muscle stresses squared $\sum \sigma^2$ [31, 53] as it was shown to give the best estimation of the muscle activations [104].

The cost function to minimize thus is:

$$C_s = \sum \sigma^2 = \mathbf{f}^T \mathbf{P} \mathbf{f} \quad (3.4)$$

With σ the muscle stresses, \mathbf{P} , the diagonal matrix of inverse squared PCSA, and \mathbf{f} , the muscle forces magnitudes.

However, the model needs to account for constraints such as the maximal and minimal force that the musculotendon can produce given its actual state. These boundaries values are obtained via the contraction dynamics as mentioned before (Eq. 3.2) For the 16 muscles with recorded EMG, their derived activations a_{16rec} were obtained via the activation dynamics [145, 177] as presented in the supplementary material. Because of inter-variability of the EMG recordings [74], the preprocessing steps and the multiple treatments of the EMG signals and their normalization, the estimated activations from those signals \tilde{a}_{16} were not strictly set. Thus an error was made possible but had to be minimized, with a cost function corresponding to:

$$\hat{E}_{a_{EMG}} = \sum |a_{16rec} - \tilde{a}_{16}| \quad (3.5)$$

This choice was made to maximize the feasible solutions from the inverse dynamics while keeping a constant process for intra-subject, muscle and movement comparisons. This can not only compensate for possible inaccuracies from EMG signals but also adapt the solution to the overall feasible activities defined by the movement. It

ensures a limited deviation from the activation obtained from the activation dynamics for the recorded muscles. Given the complexity of the movement recorded with the unconstrained 3D reaching task, some flexibility was permitted regarding the dynamics of the model. Indeed, a feasible solution within the force bounds satisfying the dynamics of the movement could not always be found. This flexibility was also introduced since there might be some inaccuracies in the computed joint angles around the scapulothoracic and acromioclavicular joints given the limited set of obtained positions from the exoskeleton.

The cost corresponding function becomes:

$$\hat{E}_J = \sum |W_m \mathbf{f} - \mathbf{J}_{torque}| \quad (3.6)$$

With \mathbf{J}_{torque} the torque at the joint satisfying the equations of movement, W_m , the moment arm matrix, corresponding to the cross product between the lever arms and the force direction vectors. The Moment arm matrix, is of size (11x44) defined in the inertial frame and its product with the vector of the 44 force magnitudes \mathbf{f} gives the resulting torque from the forces to the joint. Indeed, although there are 42 muscles studied, these elements are augmented with the scapulothoracic contact constraints ($[W_{m_{TS}} \ W_{m_{AI}}][\lambda_{TS} \ \lambda_{AI}]^T$) ensuring the gliding of the scapula over the ribcage as defined for the model in previous work [75, 145, 147].

Finally the overall cost function to minimize with the estimated activations becomes:

$$A_{cf} = \hat{E}_J + \alpha \hat{E}_{a_{EMG}} + \beta C_s \quad (3.7)$$

$$= \sum |W_m \mathbf{f} - \mathbf{J}_{torque}| + \alpha \sum |a_{rec} - \tilde{a}| + \beta \mathbf{f}^T P \mathbf{f} \quad (3.8)$$

The α and β are positive weighting coefficients obtained experimentally ensuring similar order weights for $\hat{E}_J \hat{E}_{a_{EMG}}$. The activations minimizing the cost function are obtained with the *fmincon* algorithm in MATLAB. Of note, the parameters α and β were kept constant for all the simulations as we did not want to introduce a supplementary source of differences between the subjects and the different repetitions. For a faster implementation, the forces from contraction dynamics were precomputed at each time step to be functions of the activations only, greatly reducing the computational cost in the *fmincon* algorithm.

3.3.6 Model results validation

In general, three main methodologies are compared to evaluate the model's outputs, see Fig. 3.1. The first one – *static-optimization* – used no EMG data in the computation of the muscle boundaries for the inverse dynamics, which are therefore obtained with

a 0 or 1 muscle activation in the musculotendon actuation (low and upper bound respectively). The second one – *EMG-assisted* – used for the recorded muscles their activations obtained from the activation dynamics to compute the musculotendon actuation. For muscle without available EMG, the boundaries are obtained with a 0 or 1 muscle activation (16 muscle activations used to estimate the overall 42 muscle bundles activations). Finally, for the third one – *from-activation-dynamics* – the activations were directly obtained via the activation dynamics from the recordings and represent the ground truth. This last method is however only available for the 16 muscles with recorded EMG, thus in the following results when those 16 muscles are evaluated, only their corresponding 16 estimations from the static-optimization and EMG-assisted methods were used.

A leave one-out signal comparison (including 15 out of the 16 EMG data) was performed to further validate the estimation process and to have an overview of its robustness. To validate the signal outputs of the model and to have a quantified metric of the similarity between estimated signals and the ones considered as ground truth, a correlation analysis was also performed. For sake of readability, only a selection of the most informative figures representing the results of the simulation and of the comparison is displayed; for a full set of simulations and results, please refer to the supplementary material.

3.4 Results

3.4.1 Raw comparison of activations for a specific target

Fig. 3.3 shows for a specific reaching target (13), the raw comparison between the means across the repetitions of activations obtained via the static-optimization, the EMG-assisted method, and the activations directly derived from the recorded EMG. The duration of each repetition has been normalized so that the activations are displayed as a function of the percentage of movement duration. Ideally, we would expect the static optimization model to be different from the EMG-assisted method as a demonstration that EMG data are needed to build a good estimation, to show the central nervous system strategy to perform a movement by reducing the overall stress and activations given movement specificity. The first element that can be observed is that the levels of activations over time for all muscles are similar and consistent between all estimated activations; it is important to note also that there is more variation in the muscles activation estimations from the EMG-assisted method than from the static-optimization for non-recorded muscles suggesting a better representation of co-contractions and dynamics within a movement.

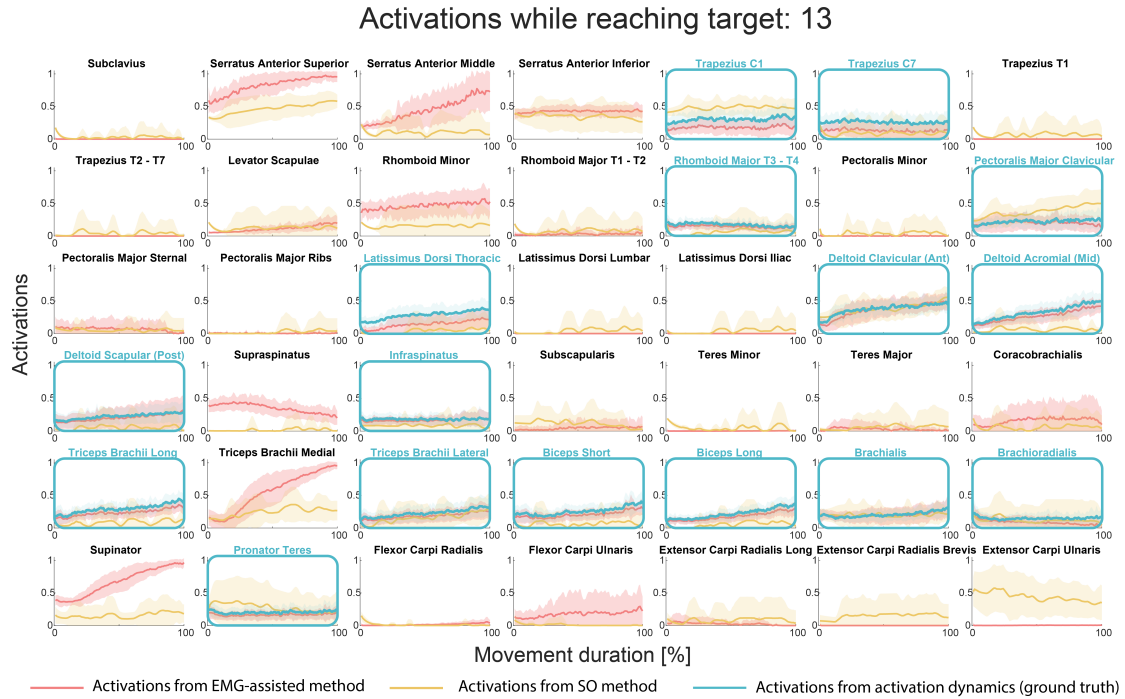


Figure 3.3: Means of the estimated muscles activations across the 5 repetitions for all 5 subjects while reaching target 13 with respect to the percentage of movement. The blue lines correspond to the activation obtained directly via the activation dynamics for muscles with available recorded EMG (their name in blue). The red lines correspond to the ones obtained from the presented method including the EMG available. The yellow lines are the activations obtained from the method without using the recorded EMG, setting the boundaries in the optimization only using the musculotendon actuation with an activation of 0 and 1 for lower bound and upper bound respectively. The thick lines represent the means of those activations across the 5 repetitions. The shaded areas represent their standard deviations.

3.4.2 Error evaluation in joint moments and activations estimations

To further illustrate the overall consistency of the estimations, the mean value of the coefficient of determination R^2 between the static-optimization method and the activations from the EMG-assisted model ones over the whole set of activations obtained is 0.27 ± 0.28 which shows a weak with high variability, statistically significant correlation ($p < 0.01$ for the 5 subjects, 6 targets, 5 repetitions each target, and the 42 muscles spanning the shoulder, humerus, ulna, and radius). Table 3.1 shows per target reached, the mean values of the root mean squared error (RMSE) and the R^2 between the estimated activations and the recorded ones ($N=16$) with respect to the method used. The overall RMSE for the EMG-estimated method is as expected lower than the one from SO with an overall mean of 0.03 ± 0.01 against 0.22 ± 0.04 ($p < 0.01$). The same trend is observable with the coefficient of determination R^2 reported with a weak, but significant correlation with the SO (mean of 0.21 ± 0.2 and p always < 0.01). Its large standard deviation

indicates that the correlation coefficients have high variabilities, suggesting that some data points are well correlated while others no. With the EMG-assisted method, we can observe strongly correlated signals with an overall mean of 0.91 ± 0.21 and median value of 0.99. To be noticed, the results while reaching target 5 show a better fit in the static optimization method for the RMSE but a lower one for the R2 with respect to the other targets reached. It corresponds to the reaching downwards and this could be explained by the reduced muscle forces needed to perform the movement due to the exoskeleton's resistive action and its gravity compensation for transparency, as well as the lower activation levels of the static-optimization method. In other words, fewer differences in low activation values but more differences in their shapes, which especially shows the importance of the introduction of EMG data in the estimations. The presented values are also reported with respect to each of the muscles activations in the supplementary materials. Additionally the error from the recomputed moment of force at the joints and the one satisfying the equations of movement corresponding to the cost function minimization of eq. 3.6 is shown. Here, values are represented as a percentage of their maximum measured joint moment from the equations of movement for each of the targets and repetition to have a clear and comparable understanding. These for both methods were kept low with a mean of $3.39\% \pm 2.13$ for the EMG-assisted and $2.33\% \pm 1.56$. We can notice that this value is lower for the SO ($p < 0.01$) as expected since there are fewer constraints on each of the muscles' forces from the contraction dynamics. Figures showing the estimated moments with respect to the ones from equations of movement can be found in the supplementary materials.

| Target reached | 1 | 3 | 5 | 7 | 10 | 13 | total |
|--------------------------------------|-------------------|-------------------|-------------------|-------------------|-------------------|-------------------|-------------------|
| NRMSE Moment EMG-assisted | $2.70\% \pm 1.25$ | $2.30\% \pm 0.06$ | $4.01\% \pm 3.05$ | $2.95\% \pm 1.05$ | $4.77\% \pm 2.86$ | $3.58\% \pm 1.82$ | $3.39\% \pm 2.13$ |
| NRMSE Moment static-optimization | $1.64\% \pm 0.42$ | $1.89\% \pm 0.45$ | $2.77\% \pm 2.21$ | $1.97\% \pm 0.52$ | $3.94\% \pm 2.31$ | $1.79\% \pm 0.42$ | $2.33\% \pm 1.56$ |
| RMSE activations EMG-assisted | 0.04 ± 0.01 | 0.02 ± 0.01 | 0.03 ± 0.01 | 0.03 ± 0.01 | 0.03 ± 0.01 | 0.04 ± 0.02 | 0.03 ± 0.01 |
| RMSE activations static-optimization | 0.28 ± 0.07 | 0.25 ± 0.03 | 0.25 ± 0.05 | 0.29 ± 0.03 | 0.27 ± 0.07 | 0.28 ± 0.06 | 0.27 ± 0.05 |
| R2 EMG-assisted | 0.82 ± 0.35 | 0.80 ± 0.33 | 0.68 ± 0.38 | 0.82 ± 0.23 | 0.88 ± 0.24 | 0.83 ± 0.29 | 0.89 ± 0.20 |
| R2 static-optimization | 0.25 ± 0.24 | 0.16 ± 0.19 | 0.11 ± 0.15 | 0.19 ± 0.19 | 0.20 ± 0.20 | 0.32 ± 0.25 | 0.21 ± 0.22 |

Table 3.1: Table representing for each of the 6 targets reached the overall errors from estimations and recorded data. First, the error from the computed moments and the ones needed to satisfy the equations of movement, in both the static-optimization and EMG-assisted cases. Values are normalized by the maximum moment from the equations of movement for each of the target and repetition. We can notice that this value is lower for the SO ($p < 0.001$). Then the RMS and coefficient of determination R2 between the activations resulting from the recorded EMG and their estimations via the EMG-assisted and SO methods are reported for each of the targets. As expected, the EMG-assisted method presents a better fit ($p < 0.001$ in both cases). We can see the low means of R2 in static-optimization showing a weak correlation, the large standard deviation indicates that the correlation coefficients have high variability, which suggests that the estimated signals may be somewhat correlated with the recorded signals for some data points, but not for others. To be noticed, the Targets 5 shows a reduced fit in both methods with respect to the other targets reached.

3.4.3 Mean activation for all targets

Another way to validate the obtained activation signals is to compare their levels of activation for specific movements. Fig. 3.4(a) shows these different levels of activations for two muscles with respect to the reached target. From the figure, one can observe that on the one hand, there is a good estimated activation level for some muscles in the static-optimization. On the other hand, this shows its limits, overlooking co-contractions and therefore underestimating values of activations for most muscles. Indeed, the activation levels obtained from the static-optimization were almost always below the ones of the EMG-assisted or the activation dynamics. In any case, the EMG-assisted method provides consistent results with respect to the activations obtained directly from the activation dynamics, and the difference among those values is explained by the fact that the EMG-assisted estimations take the geometrical model state and the contraction dynamics during the motion, and therefore depends on the muscle parameters in addition to the needs from the equations of movement. Regarding the values of the estimated activations, it is clear that there is a good correlation between the expected activation levels and the obtained ones (mean $R^2 = 0.89 \pm 0.20$ and median $R^2 = 0.99$) as presented in Table 3.1. In the presented Fig. 3.4(a), expected higher activation levels were met for brachialis for reaching targets 10 (involving an elbow flexion) for all cases and a lower one for reaching target 5 (elbow extension). It was however less evident for the biceps short which was more used for the upper sagittal plane targets (1,10 and 13). For the static optimization, the biceps short activations were underestimated and not physiologically expected. It seems that the combination of all the synergistic muscle forces produced still induced a torque leading to the correct movement.

Leave-one-out cross validation

Fig. 3.4(b) represents a spider map showing for each recorded muscle that was removed successively in the leave-one-out cross-validation, the root mean square errors between the activation directly obtained from the activation dynamics and the method using all muscle EMG signals ($N=16$ in the EMG-assisted method), using all EMG available excluding the specific muscle shown ($N=15$ in the EMG-assisted method) and without any. The mean RMSE for the EMG-assisted method was 0.03 ± 0.01 , for the leave-one-out of 0.17 ± 0.02 and for the static-optimization 0.22 ± 0.08 . This shows a slight improvement using the EMG-assisted method for the activation estimations for non-recorded muscles ($p=0.03$), but most importantly, it seems to ensure a physiological sharing of the load, and to give more information about the muscle's behavior providing a better insight of the actual co-contractions with lower variations in specific estimated activations within same movements, being particularly noticeable with the brachialis with the biceps and the deltoids.

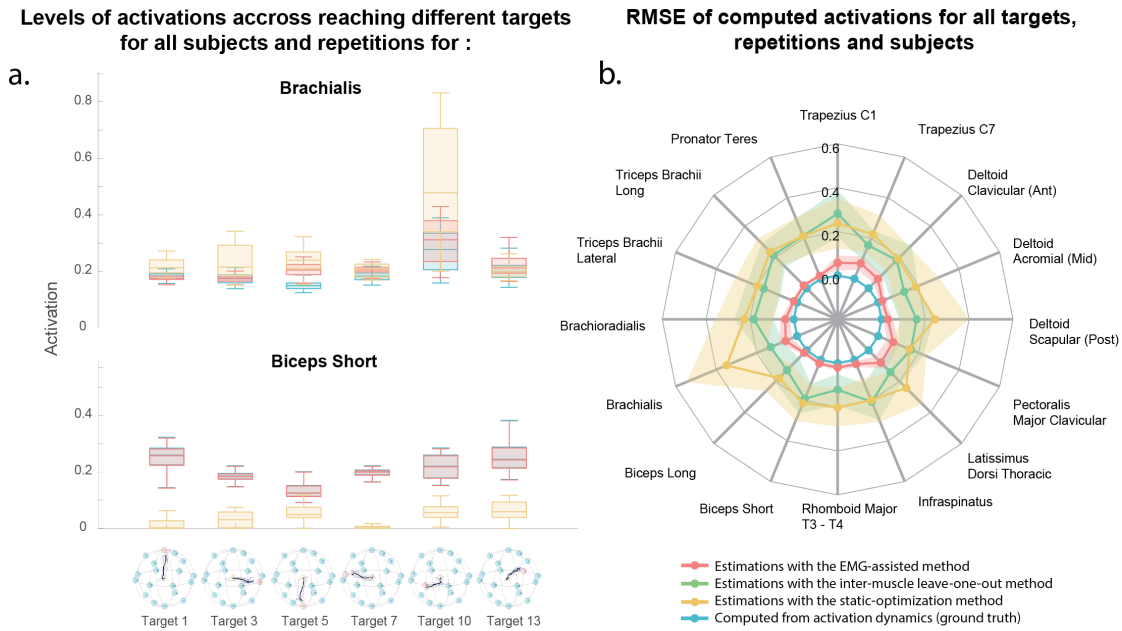


Figure 3.4: **(a)** Comparisons between the ranges of activations directly obtained from activation dynamics (blue boxplot), the estimated ones with the model including the recorded EMG (red boxplot) and the one from the model without using the recorded EMG (yellow boxplot) with respect to the reached target. The first comparison is for the brachialis and below for the biceps (Short head). The different reached targets are represented, in the bottom, as red spheres and in yellow is shown the starting position, corresponding to the center of the reachable globe. The black line is the means trajectory of the end effector and the thinner blue lines are the 5 repetitions recorded. **(b)** Spider map of the root mean square errors of the computed estimation of the muscle activation through all targets reached and repetitions of subject 2. The figure shows for each muscle with recorded EMG the errors between the activation directly obtained from the activation dynamics and, in red, the method using all the available muscle EMG signals in the EMG-assisted model (16 muscles out of 16). In green, using all EMG available excluding the specific muscle in the EMG-assisted model (15 muscles used out of 16), and without any EMG (in yellow) corresponding to the static-optimization.

3.5 Discussion

This work aimed at developing a tool for an overall muscle activation estimation using a limited amount of recorded EMG data. Knowing the inter-subject muscle parameter differences as well as the variability in EMG signal recordings from the same motion, the goal is not to provide an exact estimation of each specific muscle activation, but to infer the scheme of overall muscles activation during a specific task, with the overall values highlighted in Fig. 3.3 and Fig. 3.4. We first accurately reproduced with a generic numerical model the trajectory performed by the subjects with the ALEX RS exoskeleton. Then we showed that the EMG-assisted estimation process allowed us

to have a clearer insight into the overall activation patterns. This was mostly done by inducing restrictions using recorded EMG signals to the possible forces produced in the contraction dynamics of the model, which resulted in a finer range of solutions to the load sharing problem as it was highlighted also in another EMG-assisted model [72]. As noticeable in Fig. 3.3, the outcome is a thorough estimation of possible activations when using the EMG-assisted method. Despite the static-optimization model computed activations, with no recorded EMG used in the estimation process, has a similar root mean square error with a mean RMSE of 0.22 ± 0.08 (Fig. 3.4(b)), the EMG-assisted model, illustrated with the leave-one-out validation, is still more accurate in providing a general overview about the typical activations with a mean RMSE of 0.17 ± 0.02 for the remaining muscles. More importantly, we can observe less variability in the estimations, showing that its consistency is better and that it is less prone to random fluctuations. This further validates the use of recorded signals in our estimation process. Although the improvement of activation signal estimates using EMG-assisted methods has been demonstrated previously, to the authors' knowledge this has never been performed outside of the OpenSim environment and with a complex shoulder model including 11 DOF and 42 distinct muscles. Moreover, the tasks and movements presented here do not constrain the range of motion and the plane of action, as it was done previously while studying upper limb activations [6] or to a 3 DOF study [7]

The ground truth used in the comparisons is the activation dynamics from recorded EMG [72]. Even though the experimental muscle activations are used in the EMG-assisted model, giving this method an advantage over the static-optimization one in the evaluations, the result of the leave-one-out cross-validation (Fig. 3.4(b)) indicates that the EMG-assisted model still performs better in estimating muscle activation without any EMG-related information.

While we could obtain estimated muscle activations with reasonable values for all muscles during the reaching task, it is important to emphasize that the contraction dynamics equations for the numerical estimates of forces from excitations are derived from a rigid tendon model. One could argue that with a compliant tendon model for the contraction dynamics we would obtain a more accurate activation. Despite true, this would lead to a supplementary optimization process to obtain at each iteration the muscles' fiber lengths and their tendon lengths [145], not something that can be easily assessed experimentally or without a computational costly optimization [114]. Another possibility would be to use a different tendon model depending on the ratio of the tendon slack length to the optimal fiber length as suggested in another study [117], but for a validation process, we wanted to be consistent within the muscle model used. Finally, the resulting nRMSE between the torques needed for the GH, EL and PS joints in the equations of movement and the ones resulting from both optimisation process were kept low (with means of 3.4% and 2.3% for the EMG-assisted and static-optimization respectively). Even though we could reconstruct the motion of

the clavicular and scapular, these were constrained by our initial assumptions, and thus potential motions would be overlooked, reducing the activations estimation relevance. On a general note, the EMG-assisted model predicted more accurate activations for the muscles involved in the movement, with greater co-contractions. Apart from the mean of comparison, using the experimental muscle activations that were used by the EMG-assisted model, this could be explained as the SO method is solely based on the minimization of the inverse squared of muscles' physiological cross-section areas criteria, disregarding possible unique activations patterns between subjects [19]. With a full scaling of all musculotendon parameters and inertia based on subjects' data, which is permitted by the model [145] we could expect even better-tracked activations.

In this study, we gathered motion data from healthy individuals and the resulting model is a promising first step toward a general understanding of the CNS strategy to control the upper-limb. In a future application, we will apply the same methodology to trajectory data from individuals with physical disability (e.g. Parkinson, stroke). Being able to understand patterns of activation, maybe even compare pre- vs post-intervention data in a rehabilitation scenario could be of great interest for the community and open up new possibilities in designing optimized therapy for the patients [149] or lower dimensional controllers for the upper-limb, as it was done with reduced models for the frog hindlimb [10] or human lower limbs [121]. The knowledge of a generalized activations estimation could also be used to further improve motor intention decoding for prosthetic-end users [111] as well as improve personalized prosthesis myoelectric control [152]. In the future, this methodology and model could also potentially be an open tool for everyone to use.

3.6 Conclusion

This work presents the development and validation of a musculo-skeletal model usable to increase our basic understanding of upper-limb motor control. It presents a protocol with ALEx RS exoskeleton to assess the overall muscle activity while performing reaching tasks. We first reconstructed the upper-limb motion, then, with the combined recorded EMG signals while reaching tasks, we showed how our model can estimate the overall muscle activation with an EMG-assisted load sharing optimization method. This protocol and the activations estimation represent a tool to evaluate inter-subject muscle activation behavior, possible interactions and synergies. This was applied to healthy motion data but in the future, we will target neurological diseases patient's motion data. Potentially, this could help with the development of novel neurorehabilitation strategies, lower dimensional controllers for the upper-limb, improve motor intention decoding for prosthetic-end users as well as improve personalized prosthesis myoelectric control.

Author contributions statement

T.B conceived the work on the numerical model, its development, the initial draft and the figures. T.P provided critical insights and contributed to the final paper. C.P designed the experimental protocol and conducted the experiments. S.M directed the study. All authors reviewed the manuscript.

Competing interests

The authors declare no competing interests.

4 Impairment and improvement of muscle assessments through activation modeling

Future publication possible

This chapter is written in a hybrid thesis chapter/journal paper for future possible publication. The accent is not set on the muscle activation estimation and the experimental protocol as it would be redundant with the previous chapter.

Personal contributions: I participated in some of the experiments recordings. I processed the data, performed the simulations and the data analysis. I prepared the figures and wrote the manuscript.

During this thesis, we presented the stroke neurological disease affecting the reaching and grasping abilities (and movement in general) of patients. The severity of the impairments, as well as how they contribute to mobility and function, helps medical practitioners in the process of creating rehabilitation objectives, thus, the evaluation and functional diagnosis of stroke patients are key elements of their rehabilitation procedure. We also presented in the previous chapter the possibility to obtain the overall muscular activation of subjects performing reaching tasks while assisted with an exoskeleton.

In this chapter, we will discuss the potential applications and benefits of a numerical model for assessing the muscle activation and impairments of stroke patients during rehabilitation. In order to accomplish this, the previously discussed activation estimator is applied to recorded kinematic and EMG data from stroke patients during their initial and follow-up assessments of their personalized robotic-assisted rehabilitation procedures, as described in previous studies [130] and [56].

The experimental setup and output of kinematic and EMG data are identical to those used in the previous chapter with healthy participants. This chapter begins with the validation of quantitative estimates of impairments based on estimated activations

and the upper-limb Fugl-Meyer score of the associated patient with the introduction of a novel metric. Following is an evaluation and investigation of antagonistic muscle co-contraction during reaching tasks. For a more scientific observation and comprehension of the rehabilitation process, the muscle synergies during reaching activities of healthy subjects and stroke patients are investigated during their initial and final assessments.

A numerical method to improve quantitative impairment assessment of the upperlimb muscles

Tristan Barjavel^{*1}, Tommaso Proietti², Camilla Pierella^{3,4}, Silvestro Micera^{1,2}

¹ Ecole Polytechnique Federale de Lausanne (EPFL), Bertarelli Foundation Chair in Translational Neuroengineering, Center for Neuroprosthetics and School of Engineering, Geneva, 1202, Switzerland

² Scuola Superiore Sant'Anna, Biorobotics Institute and Department of Excellence in Robotics & AI, Pisa, 56025, Italy

³ University of Genoa, Department of Neurosciences, Rehabilitation, Ophthalmology, Genetics, and Maternal and Children's Sciences (DINOEMI), Genoa, 16126, Italy

⁴ University of Genoa, Department Informatics, Bioengineering, Robotics and Systems Engineering (DIBRIS), Genoa, 16126, Italy

4.1 Abstract

Evaluation and functional diagnosis of stroke patients are essential parts of their rehabilitation process. However, present assessment techniques do not sufficiently evaluate the overall muscular behavior of the upper limb during reaching tasks. Here, we hypothesized that the incorporation of a numerical upper limb model into an exoskeleton-based rehabilitation protocol may not only precisely measure the upper limb impairment but also provide additional information for establishing personalized rehabilitation objectives and designing physical therapy strategies. We use a numerical upper-limb model in addition to a robotic exoskeleton and 16 electromyography recordings to estimate the overall muscles involved in the reaching tasks of stroke patients. We first demonstrate the applicability of our numerical model for a precise estimation of the patient's disability by comparing the differences between patients and healthy groups and see if there is a correlation between these and their Fugl-Meyer Score. Then, we show that it may offer additional information on muscle co-contraction and, therefore, therapy enhancements. Finally, we demonstrate that it has the potential to provide a deeper understanding of the muscle synergies and their reorganization after a stroke and after rehabilitation.

Keywords Biomechanics, Electromyography (EMG), Muscle activations, Musculoskeletal model, Upper-limb, Stroke

4.2 Introduction

Stroke is one of the main causes of long-term disability in adults [170]. An impairment of the upper-limb is experienced by 70 to 80% of survivors. [136] and nearly one third of all stroke survivors will have significant long term disability. The evaluation and

functional diagnosis of stroke patients are key elements in their rehabilitation procedure. The severity of the impairments as well as how they contribute to mobility and function loss helps medical practitioners in the process of creating rehabilitation objectives and developing physical therapy plans. The current state of the art to estimate the patient's impairment is mostly done via a qualitative evaluation of ranges of motion, smoothness of movement, and muscle spasticity with therapists, evaluation of forces and kinematics with robot-assisted therapies or with surface electromyography (EMG) recordings with a selected number of muscles. [39, 94, 110] Clinical scales are often used to assess therapy effectiveness, however, these measurements may not be sensitive enough to accurately depict the actual improvements produced. [124, 153]. Among the clinical-scales is the Fugl-Meyer Assessment (FMA), which is intended particularly to assess stroke survivors' impairment. It evaluates the patient's upper-limb mobility and assigns a score depending on the level of impairment of the stroke survivor. The FMA also assesses muscle tone, reflexes, and coordination [49]. It has been extensively evaluated in the stroke population and is acknowledged as a tool for assessing changes in motor impairment after stroke [57]. The reliability of clinical tests is also limited by the clinicians' inter-observer and intra-observer reliability [16, 64, 87] and floor and ceiling effects [93, 96, 119]. Of note, these clinical tests can also take a considerable amount of time and fatigue for the clinicians. Using recorded EMG signals would help clinicians quantify muscle activity, track recovery, and inform rehabilitation, which could aid the development of new recovery techniques for stroke survivors [125, 158]. Moreover, a synergy analysis can be performed out of those signals, indeed, the number and structure of synergies has been associated with motor function impairments and their analysis may provide physiotherapists and clinicians further insight about changes occurring at the CNS and muscular level. [1, 26, 29, 139, 169] More importantly, although muscle coordination has been extensively studied using muscle synergies [8, 12, 21, 77, 142, 155], it was not done to our knowledge using a full set of muscular activation of the upper limb.

Here we present a tool to provide more monitoring options regarding the stroke survivor's impairment including the overall muscle activity signals, their impairment assessment, their co-contractions evaluations and synergy analysis. We will discuss the potential use and advantages of a numerical model to assess the muscle activation and impairments of stroke survivors during their rehabilitation. To this end, a numerical muscle activation estimator is used with recorded kinematic and EMG data from stroke survivors during their first and follow-up assessments of their personalized robotic-aided rehabilitation procedures as described in the previous work [56, 130]. Indeed, the experimental setup is identical to the one used in the previous chapter with healthy participants and the kinematic and EMG data output is similar.

The first element covered is the validation of the quantitative assessment of impairments based on the estimated activations and the FMA score of the associated stroke survivor. The assessment and investigation of antagonistic muscle co-contraction

during reaching tasks follow. Lastly, muscle synergies during reaching activities are investigated for healthy subjects and stroke survivors at their first and final assessments.

4.3 Material and methods

4.3.1 Subjects

The study included a small group of 3 subjects who had all experienced a stroke. These individuals were recruited 2 to 6 weeks after their stroke occurred, and all had right-side paralysis and some residual motion in their shoulder and elbow joints. The participants were chosen from a larger group detailed in [130] based on their rehabilitation outcome measured by the evolution of the upper-limb section of their Fugl-Meyer (FM) score. These subjects were chosen to respectively represent no significant improvement (FM-score from 7 to 14), moderate improvement (FM-score from 17 to 34), large improvement after the rehabilitation (FM-score from 17 to 52), characterized in table 4.1. This study does not focus on showing the subject demographic reasons for an increased improvement but rather to understand the changes occurring within muscular coordination. The study also included 5 healthy individuals who were also right-handed (4 females, 60 year old ± 12). These healthy volunteers had normal ranges of motion and muscular strength, as well as no known skeletal or neurological disorders. This is the healthy group used to analyze variations in patient impairment and improvement.

| Subject | Age | Gender | Time after stroke | UL FM score A1 | UL FM score A4 | Classification |
|---------|-----|--------|-------------------|----------------|----------------|----------------------------|
| 1 | 34 | female | 2 weeks | 17 | 52 | large improvement |
| 2 | 86 | male | 3 weeks | 17 | 34 | moderate improvement |
| 3 | 84 | male | 6 weeks | 7 | 14 | no significant improvement |

Table 4.1: Demographics of the stroke population recruited in the study.

The original research project was conducted at two facilities, in the Neurorehabilitation Unit of the University Hospital of Geneva (HUG), Switzerland and in the one of the University Hospital of Pisa (Cisanello hospital), Italy. It was approved by the Commission Cantonale d’Ethique de la Recherche (CCER) de Genève, Switzerland, and by the Comitato Etico Area Vasta Nord Ovest (CEAVNO) in Pisa. The recordings were conducted in accordance with the guidelines of the Declaration of Helsinki and Good Clinical Practice. The trial’s registration number in ClinicalTrials.gov is NCT02770300. All participants were given an in-depth explanation of the study’s purpose, methods, and potential risks, and all consented to having their data collected during the study published in scientific journals before they agreed to take part.

4.3.2 Experimental protocol

The experimental set-up corresponds to the one presented in the previous chapter 3.3.2 with the addition of recorded data from three stroke patients during their first and last assessments (before and after the 4 weeks of training) as they performed a reaching task with the upper-limb exoskeleton (ALEX RS, presented in [98, 131]). These subjects could not always manage to reach the targets and were assisted by the exoskeleton after a period of inactivity, or a certain amount of time. For healthy subjects however, the robot did not provide any assistance to the subject while performing the tasks. Due to the fatigue, the patients could not always do more than one repetition of some targets. The exoskeleton is supposed to be transparent for the user, supporting its own weight. [131].

The targets considered in this study were the 6 points positioned along the 3 main directional axes from the center of the sphere, corresponding to reaching upwards (target 1), downwards (target 5), to the left (target 7) to the right (target 3), frontwards (target 13) and rearwards (target 10).

During the robotic assessment, the EMG signals of 16 muscles of the upper limb were recorded: deltoid clavicular/acromial/scapular, trapezius C1/C7, pectoralis major clavicular, latissimus dorsi thoracic, infraspinatus, triceps brachii long/lateral, biceps brachii short/long, brachialis, brachioradialis and pronator teres. The EMGs were recorded at 1.5kHz using AgCl Kendall surface EMG electrodes with a Desktop DTS wireless system (Noraxon, USA). The electrode placement followed the European recommendations for surface electromyography for non-invasive assessment of muscles (SENIAM) and anatomical guidelines [69, 128]. Regarding the kinematic data, the robotic joint angles (shoulder abduction, rotation, flexion elbow flexion, pronosupination), as well as the end-effector position and velocities, were acquired at a 1kHz. The kinematic data was synchronized with the recorded EMG signals via triggers obtained from the exoskeleton ALEX RS, stating when the movement began and ended. A schematic representation of the study is shown in figure 4.1.

4.3.3 Muscle activations estimations

To estimate the muscular activations, we use a musculoskeletal model presented in Chapter 2 and 3, with eleven degrees of freedom including nine for the overall shoulder complex (sternoclavicular, acromioclavicular glenohumeral joints modeled as ball and sockets joints) and 2 for the elbow flexion/extension and pronation/supination. The 42 muscle actuators spanning these joints are: subclavius, serratus anterior upper, middle and lower parts, trapezius C1-C6/C7/T1/T2-T7, elevator scapulae, rhomboid minor, rhomboid major T1-T2 and T3-T4, pectoralis minor, pectoralis major clavicular sternal and ribs, latissimus dorsi thoracic, lumbar and iliac, deltoid clavicular, acromial

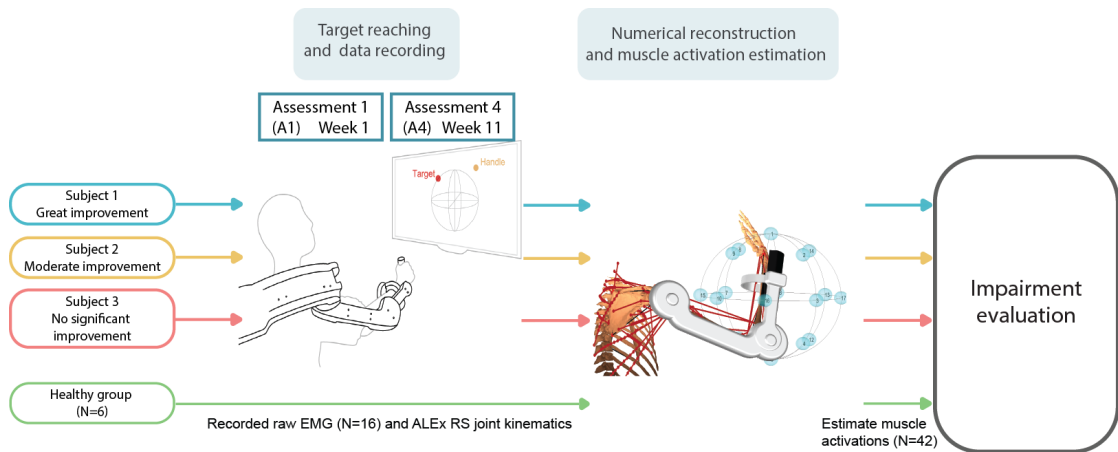


Figure 4.1: General overview of the presented study to evaluate subject's impairment. Three representative stroke survivors (large, moderate, and no significant improvement in cyan, yellow and red respectively) and their muscular assessment are evaluated with respect to the healthy population (in green). First, these subjects perform the reaching tasks with the exoskeleton with their kinematics as well as 16 muscle EMG recorded. Then these data are fed into the numerical model to estimate their corresponding overall muscle activation for each assessment. These activations at the first and follow up assessment for each subject are then compared with each other and with the average healthy population assessment while performing these tasks.

and scapular, supraspinatus, infraspinatus, subscapularis, teres minor and major, coracobrachialis, triceps brachii long, medial and lateral, biceps brachii short and long, brachialis, brachioradialis, supinator, pronator Teres, flexor carpi radialis and ulnaris, extensor carpi radialis long and brevis, and extensor carpi ulnaris.

As mentioned in chapter 3, the musculoskeletal model was not scaled to the subjects it was the recorded kinematics from ALEx that were scaled to the generic model. Although this overlooks the subjects' inter-specificities, this allowed for a possible comparison based on the kinematics, the EMG recorded and estimated solely without induced differences. With further information about the subjects' weights, heights, and force assessments the estimations would be potentially more accurate per subject. However, for a comparison between subjects without the muscle physiological cross-section areas (PCSA) or maximum forces, a wrongly estimated scaling method could lead to false results and could induce differences between subjects that are not reflecting real measures [104, 116]. More importantly, using a scaling method for the muscle parameters such as the ones presented in [148, 150] including the maximal force at optimal fiber length F_0 , optimal fiber length l_0^M , pennation angle α and tendon slack length T_S^L would lead to different values of these parameters even for a same patient from the first assessment to the final one, although this would have no physiological meaning since those are physical parameters. Thus it would alter the variations in the estimated signals from the different assessments and modify the outcome results.

The kinematics obtained from ALEx exoskeleton correspond to the robotic joint angles (shoulder abduction, rotation, flexion, elbow flexion, prono-supination). Given the subject's attachment to the exoskeleton, it was possible to reconstruct the model bony landmarks which could therefore be used in the multi-segment optimization as reported in Chapter 3 and [75, 145]. In other words, the induced constraints imposed by the robotic exoskeleton attachments were used to reconstruct the user's kinematics. The output of the kinematic data reconstruction is the collection of musculoskeletal joints angles, velocities, and accelerations. A representation of the model ALEx RS exoskeleton, its associated rotation angles as well as the attached musculoskeletal model and its bony landmarks used is shown in figure 3.2 from chapter 3. The red lines correspond to the 42 muscles modeled and the blue spheres to the targets to reach. With the reconstructed musculoskeletal joint angles, the dynamics of the model can be computed and information about the muscles states are available at each iteration step, including the moment arms, muscle lengths, and velocities.

Due to the redundancy of the musculoskeletal system: the muscle activations are estimated via inverse dynamics as presented in chapter 2 and 3. The main optimization criterion is the reduction of the muscle fatigue that is represented as the reduction of the overall muscle stresses squared $\sum \sigma^2$ [31, 53] as it was shown to give the best estimation of the muscle activations [104]. The parameters' choices and flexibility within the reconstructed torques were kept as before as this present study was already considered.

4.3.4 Impairment estimation

Having obtained estimated the overall muscle activations from patients and from healthy subjects their evaluation can be performed. In order to estimate the patient's impairment, we first have to define what are the main rotations occurring while reaching the different targets and the muscles associated with these rotations for a better representation of the impairment impact.

The table A.1 allows us to estimate the rotations occurring at the joints of the model while reaching the different targets. The reported data correspond to the rotational joint angle ranges from the beginning to the completion of the movements. The addition of the standard deviations indicated if there is a high degree of variation in the rotations that are observed during multiple repetitions of a movement, it suggests that those rotations may not be necessary for achieving the desired target. Instead, they could be considered unintended or accidental movements that are occurring occasionally. The analysis of the table allows us to report in table 4.2 the dominant rotations in reaching a specific target. The ones that are happening less frequently or are less relevant for reaching a target are discarded. The actual rotations and their

positive and negative values are described in Fig. 4.2.

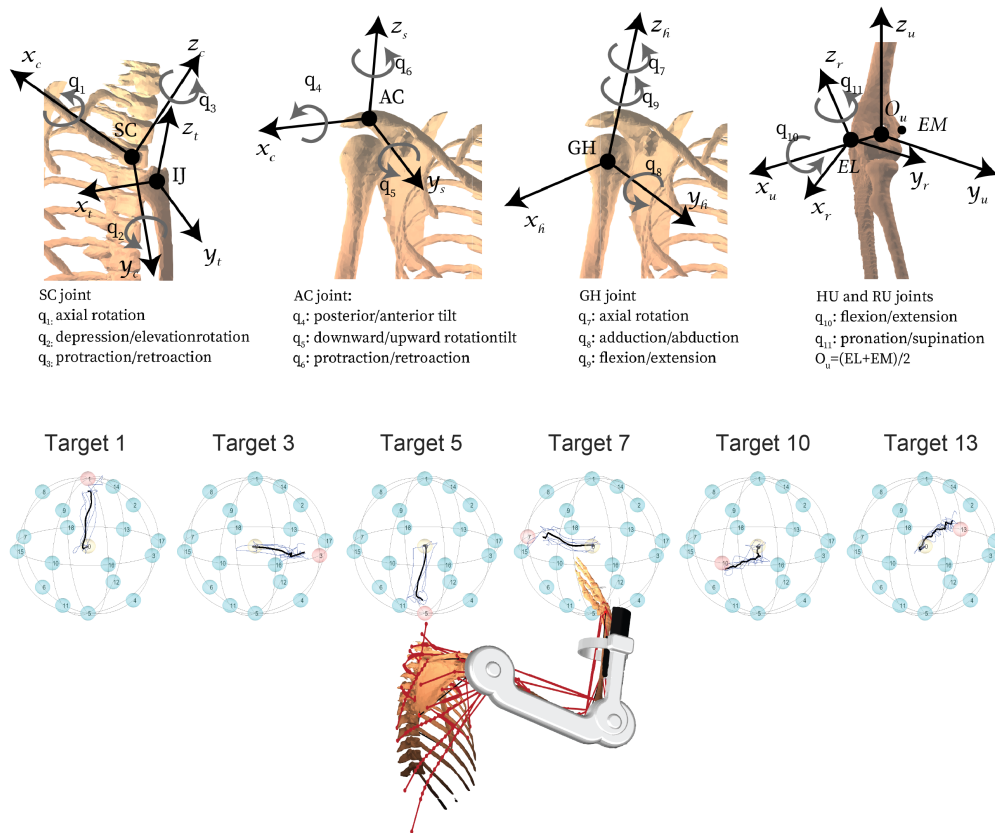


Figure 4.2: Top: Illustrations representing the musculoskeletal joints and the associated rotations. Bottom: The different targets to reach considered, the initial position of the end-effector is on the yellow sphere, and the goal is to reach the red one. The black lines correspond the mean trajectory for healthy subjects (blues ones are the for each repetition). The shoulder model and the exoskeleton are modeled on the model to show the subject's position

As a comprehensive examination of the effects of each muscle on the different joints would be too difficult to illustrate, particularly, given the occurrence of unintentional movements, such an evaluation is not realistic. Therefore, we focus the study to examine selected "Agonist muscles" and "Antagonist muscles." This selection is accomplished by building the moment arm matrix at each simulation iteration. The latter refers to the distance from the line of action of a muscle force to the joint's rotation center. Each element of the matrix represents the moment arm of a particular muscle at a particular joint. It defines the relationship between muscle forces and joint moments or the extent to which the magnitude of the force impacts the joint torque and its rotation. Table 4.2 reports the primary joint rotations and the main agonistic and antagonistic muscles affecting the moment at the joint for each target, it is important to note that we organize them by target since the muscle moment arm

Table 4.2: Main agonist and antagonist muscle per target reached in a geometrical point of view, the agonist muscle listed are the ones that will produce the highest impact on the rotation for the same force magnitude.

| Reaching task | Main rotation(s) | Agonist muscles | Antagonist muscles |
|----------------------|--|---|--|
| Target 1 | GH abduction | Deltoid Clavicular (Ant) Deltoid Acromial (Mid) Triceps Brachii Lateral Coracobrachialis Brachioradialis | Pectoralis Major Clavicular Pectoralis Major Sternal Latissimus Dorsi Thoracic Teres Minor Teres Major |
| Target 3 | GH extension | Deltoid Scapular (Post) Infraspinatus Triceps Brachii Long Pronator Teres | Pectoralis Major Clavicular Pectoralis Major Sternal Deltoid Clavicular (Ant) Brachioradialis |
| Target 5 | GH adduction | Pectoralis Major Sternal Latissimus Dorsi Thoracic Latissimus Dorsi Iliac Teres Minor Teres Major | Deltoid Clavicular (Ant) Deltoid Acromial (Mid) Supraspinatus Coracobrachialis Brachioradialis |
| Target 7 | GH flexion | Pectoralis Major Clavicular Pectoralis Major Sternal Deltoid Clavicular (Ant) Latissimus Dorsi Thoracic | Deltoid Acromial (Mid) Deltoid Scapular (Post) Supraspinatus Infraspinatus |
| Target 10 | GH axial rotation (+) HU flexion RU supination | Subscapularis Biceps short Biceps Long Brachialis Supinator | Infraspinatus Triceps Brachii Long Triceps Brachii Lateral Triceps Brachii Medial Pronator Teres |
| Target 13 | GH abduction HU extension | Deltoid Clavicular (Ant) Deltoid Acromial (Mid) Triceps Brachii Medial Triceps Brachii Lateral Extensor Carpi Radialis Brevis | Latissimus Dorsi Thoracic Biceps Short Biceps Long Brachialis Supinator |

changes with the joint angles.

In other words, even if the primary rotation of the joint is in the same direction, the agonistic and antagonistic muscles that are involved in reaching different targets may differ since the muscle moment arm changes with the different joint angles. Therefore it explains the difference in the primary agonistic and antagonistic muscles involved in targets 1 and 5 for instance although the joint rotation is the opposite.

To evaluate impairments, the metrics discussed in the next section 4.3.4 will be evaluated on the main muscles acting on the joints of interest as these muscles have the most significant impact on the studied movement.

Metrics for quantification

A combination of two metrics is used to quantify the subjects motor impairments. The root mean squared error (RMSE) is a gold standard for evaluating the difference in between signals. It however does not account for differences in timings. For instance if two signals are delayed the RMSE will be significant but the "amount of activation" during the movement might be similar. In our case, for instance, it depends on the patient's strategy. To reach the target 13, he might first extend the elbow and then lift the humerus or do the inverse, therefore a quantitative metric for the amount of activation of a muscle is needed, it is all the more important as some muscle might be less activated after a neurological disease. Such a quantity can be obtained by computing the cumulative sum of the signals over the movement duration (in percentage) and to apply the Pearson's correlation formula between these obtained signals. This was obtained using the *corrcoeff* Matlab function. This cumulative sum's Pearson's correlation coefficient (CSR) metric is even more important as the alignment of the movement was not always perfect from the robotics, a smooth start was sometimes observed or motion was starting directly. Moreover, after qualitative evaluation of the signals, the cumulative sum was still able to capture a similitude in activation despite variations of speed in the recorded movements.

Figure 4.3 shows, as an example for simplified signals, the differences in the metrics used and why the use of CSR computation in addition to RMSE is important for a good evaluation of the similarity on the overall level of activation. Of note, given the nature of the potential signals and their cumulative sum computed, the Pearson's coefficient between these will always have a positive value. It presents the advantages of combining the shape of the curve and the levels of activation which is not achievable by using the area under the curve metrics and the most widely used one for muscle signals similitude estimations, the coefficient of determination only.

4.3.5 Muscle co-contractions evaluations

One topic of interest within the literature, is the alteration of muscle co-contraction after a neurological impairment [23, 24, 155]. We, therefore, want to evaluate the muscle co-contraction with the full activation available via the numerical model. The idea is to compare if, from the larger set of activation estimated, we can observe variations with respect to using the limited EMG signals recorded. To evaluate the muscle co-contractions, the muscles of interest from the table 4.2 are evaluated together. The co-contraction index (CCI) is used to describe co-contraction occurring while performing a task [85, 141]. The adapted CCI is defined as follow:

$$CCI = \frac{\sum a_{antagonist}}{\sum a_{agonist}} * (\sum a_{antagonist} + \sum a_{agonist}) \quad (4.1)$$

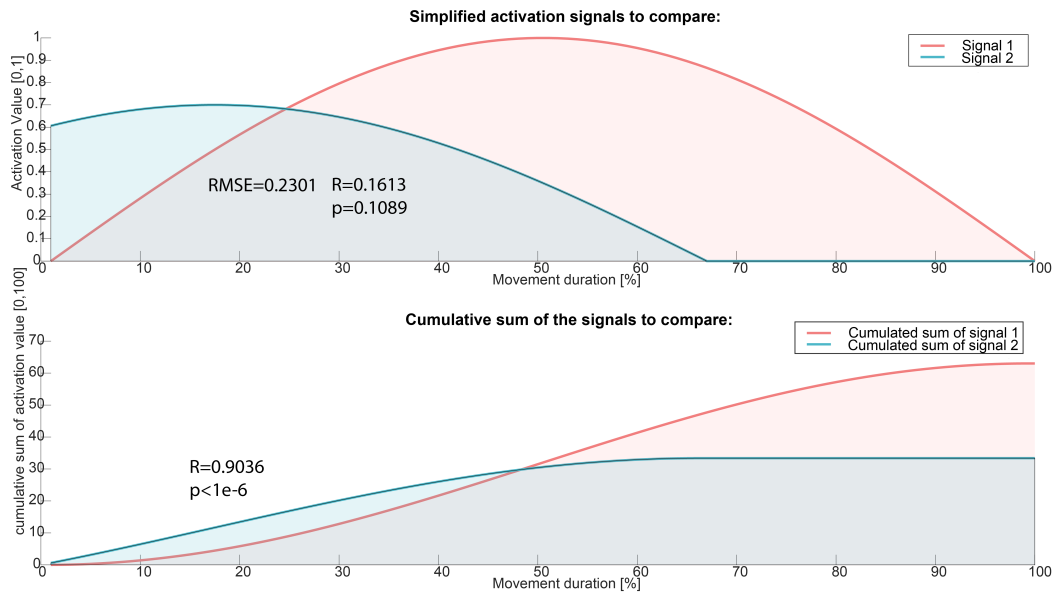


Figure 4.3: Illustrations presenting the importance of having metrics for the level of activations. On the top, two sinusoids are generated with one delayed and scaled up, this aims at showing two signals that should not be considered as completely dissimilar. However, they present a RMSE and a Pearson's coefficient R very low. With the introduction of the cumulative sum of the signals on the bottom, the levels of activations are considered and a Pearson's coefficient is more representative of this level of activation.

4.3.6 Muscle synergies evaluation

We used the non negative matrix factorization (NNMF) algorithm to extract muscle synergies from activation signals. [27, 33, 95, 96]. We concatenated for each subjects, target, and assessment the estimated muscle activations in a matrix with 42 rows for the muscles. The NNMF algorithm extracts from the EMG envelopes a matrix of weights W , accounting for each of the muscle its participation in each synergy. A matrix C of activation coefficients representing the timing of activity of each muscle synergy is associated.

The synergy number was extracted using two methods; 1) the inspection of the R^2 , the fraction of total variation accounted for (VAF) [9, 35], the minimum number of muscle synergies explaining a $R^2 > 95\%$ and 2) the detection of the change in the slope of the R^2 curve or VAF curves, finding the elbow point[80]. When the number of synergies from the two methods did not match, the larger one was picked. [127] Fig 4.4 shows for the healthy population the VAF curves and the corresponding position of the number of synergies.

A set of reference muscle synergies was created in order to compare the different ones

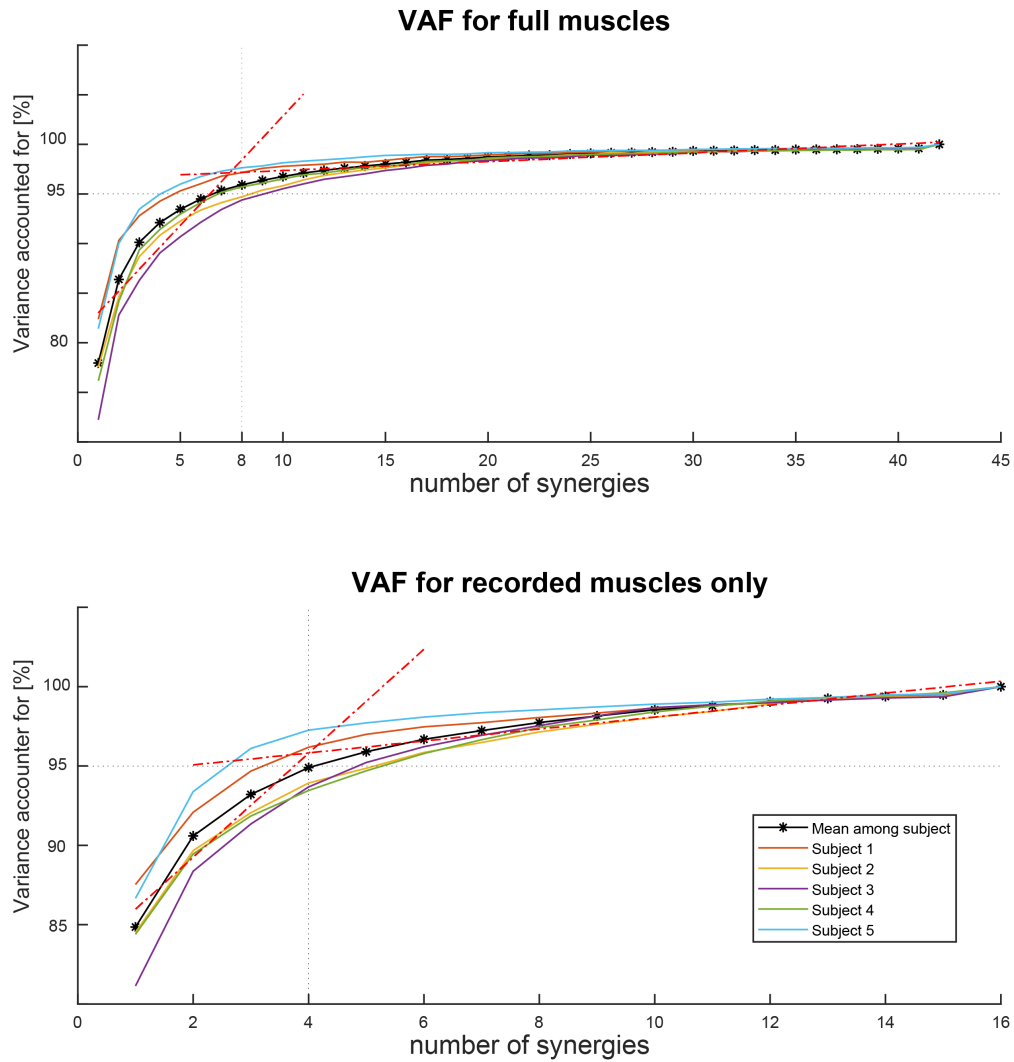


Figure 4.4: Variance accounted for with the reconstructed signal from synergies, the number of synergy selected correspond to the highest between the position of the knee point of the curves and the one where VAF was higher than 95%

from the subjects, tasks, and groups [26, 127, 131]. This was achieved by employing a hierarchical clustering approach based on the minimization of the Minkowski distance between weighting coefficient vectors to classify the muscle synergies of healthy people [27]. The muscles synergies obtained from healthy as well as from patients performing the different tasks from the first and final assessments could then be compared with the reference one by using the scalar product between the weights (\dot{dot}_H for healthy subjects and \dot{dot}_{S_i} for stroke patients.). The overall comparison procedure followed the recommendation from a previous study [130] as a mean for results comparability.

4.4 Results

4.4.1 Validation of the impairment assessment

The reported RMSE between estimated muscle activation signals from healthy population and the patients during their first and final assessments are reported per target reached for all the muscles in the appendices in tables A.2 to A.7. The Pearson's correlations of the cumulative sums (CSR) of the muscles activations are reported in tables A.8 to A.13. The same metrics are reported for the activations directly derived from the recorded EMG signals via the activation dynamics, with for CSR, table A.14 for targets 1,3 and 5 and table A.15 for targets 7,10 and 13. For the RMSE, tables A.16 and A.17 and show their values.

A summary representing means of the RMSE per target is presented in table 4.3. Table 4.4 shows the corresponding average CSR of activations.

| | Healthy | S1 | | S2 | | S3 | |
|--|----------------|-----------|---------------|---------------|---------------|---------------|---------------|
| | | A1 | A4 | A1 | A4 | A1 | A4 |
| From EMG recorded (N=16) | | | | | | | |
| Target 1 | 0,105 ± 0,037 | 0,11 ± 0 | 0,099 ± 0,015 | 0,133 ± 0,026 | 0,158 ± 0,064 | 0,176 ± 0,008 | 0,191 ± 0,019 |
| Target 3 | 0,097 ± 0,042 | 0,149 ± 0 | 0,093 ± 0,014 | 0,148 ± 0,034 | 0,122 ± 0,016 | 0,143 ± 0,028 | 0,184 ± 0,004 |
| Target 5 | 0,076 ± 0,034 | 0,062 ± 0 | 0,069 ± 0,011 | 0,106 ± 0 | 0,106 ± 0,016 | 0,099 ± 0,008 | 0,116 ± 0,008 |
| Target 7 | 0,091 ± 0,037 | 0,112 ± 0 | 0,079 ± 0,011 | 0,125 ± 0 | 0,13 ± 0,046 | 0,129 ± 0,015 | 0,136 ± 0,006 |
| Target 10 | 0,11 ± 0,04 | 0,15 ± 0 | 0,101 ± 0,022 | 0,14 ± 0 | 0,142 ± 0,021 | 0,147 ± 0,018 | 0,153 ± 0,009 |
| Target 13 | 0,102 ± 0,037 | 0,183 ± 0 | 0,11 ± 0,023 | 0,114 ± 0 | 0,132 ± 0,03 | 0,182 ± 0,009 | 0,181 ± 0,005 |
| Mean ± std | 0,097 ± 0,038 | 0,128 ± 0 | 0,092 ± 0,016 | 0,128 ± 0,01 | 0,132 ± 0,032 | 0,146 ± 0,014 | 0,160 ± 0,009 |
| From overall computed activations (N=42) | | | | | | | |
| Target 1 | 0,179 ± 0,069 | 0,185 ± 0 | 0,196 ± 0,040 | 0,218 ± 0,033 | 0,199 ± 0,039 | 0,161 ± 0,011 | 0,190 ± 0,015 |
| Target 3 | 0,1970 ± 0,076 | 0,253 ± 0 | 0,182 ± 0,027 | 0,221 ± 0,042 | 0,183 ± 0,015 | 0,183 ± 0,047 | 0,211 ± 0,036 |
| Target 5 | 0,172 ± 0,088 | 0,170 ± 0 | 0,152 ± 0,021 | 0,206 ± 0 | 0,163 ± 0,011 | 0,130 ± 0,025 | 0,173 ± 0,018 |
| Target 7 | 0,157 ± 0,073 | 0,180 ± 0 | 0,157 ± 0,022 | 0,198 ± 0 | 0,187 ± 0,057 | 0,134 ± 0,020 | 0,145 ± 0,015 |
| Target 10 | 0,203 ± 0,067 | 0,203 ± 0 | 0,197 ± 0,037 | 0,193 ± 0 | 0,206 ± 0,023 | 0,180 ± 0,034 | 0,198 ± 0,019 |
| Target 13 | 0,166 ± 0,041 | 0,196 ± 0 | 0,175 ± 0,033 | 0,176 ± 0 | 0,184 ± 0,036 | 0,166 ± 0,020 | 0,198 ± 0,013 |
| Mean ± std | 0,179 ± 0,072 | 0,198 ± 0 | 0,177 ± 0,030 | 0,202 ± 0,013 | 0,187 ± 0,030 | 0,159 ± 0,026 | 0,186 ± 0,019 |

Table 4.3: Root mean squared errors between the means of healthy activations and the subject's ones. The top part includes only the RMSE corresponding to the recorded EMG, between the 16 recorded activations directly derived from the activation dynamics. The bottom part includes the overall activations estimated (from the 42 muscles). The means are reported based on the target reached, and the overall mean is also reported. The RMSE reported for the healthy population corresponds to the mean of the RMSE of all healthy subject with respect to the means of activations of the overall healthy means. A1 corresponds to the first assessment, A4 to the follow up.

| | Healthy | S1 | | S2 | | S3 | |
|--|---------------|-----------|---------------|---------------|---------------|---------------|---------------|
| | | A1 | A4 | A1 | A4 | A1 | A4 |
| From EMG recorded (N=16) | | | | | | | |
| Target 1 | 0.994 ± 0.004 | 0.996 ± 0 | 0.996 ± 0.003 | 0.989 ± 0.009 | 0.959 ± 0.045 | 0.992 ± 0.006 | 0.995 ± 0.003 |
| Target 3 | 0.997 ± 0.002 | 0.928 ± 0 | 0.993 ± 0.005 | 0.976 ± 0.006 | 0.991 ± 0.004 | 0.996 ± 0.003 | 0.979 ± 0.009 |
| Target 5 | 0.995 ± 0.003 | 0.997 ± 0 | 0.995 ± 0.003 | 0.985 ± 0 | 0.99 ± 0.005 | 0.996 ± 0.004 | 0.979 ± 0.015 |
| Target 7 | 0.995 ± 0.003 | 0.997 ± 0 | 0.997 ± 0.002 | 0.985 ± 0 | 0.993 ± 0.004 | 0.998 ± 0.002 | 0.989 ± 0.005 |
| Target 10 | 0.992 ± 0.003 | 0.917 ± 0 | 0.996 ± 0.003 | 0.934 ± 0 | 0.975 ± 0.012 | 0.994 ± 0.003 | 0.983 ± 0.011 |
| Target 13 | 0.997 ± 0.002 | 0.979 ± 0 | 0.992 ± 0.004 | 0.987 ± 0 | 0.993 ± 0.004 | 0.996 ± 0.002 | 0.987 ± 0.005 |
| Mean ± std | 0.995 ± 0.003 | 0.969 ± 0 | 0.995 ± 0.003 | 0.976 ± 0.003 | 0.984 ± 0.012 | 0.995 ± 0.003 | 0.985 ± 0.008 |
| From overall computed activations (N=42) | | | | | | | |
| Target 1 | 0.969 ± 0.017 | 0.967 ± 0 | 0.959 ± 0.023 | 0.968 ± 0.017 | 0.955 ± 0.024 | 0.974 ± 0.014 | 0.958 ± 0.026 |
| Target 3 | 0.965 ± 0.019 | 0.905 ± 0 | 0.961 ± 0.021 | 0.958 ± 0.02 | 0.969 ± 0.018 | 0.977 ± 0.019 | 0.953 ± 0.044 |
| Target 5 | 0.97 ± 0.017 | 0.979 ± 0 | 0.972 ± 0.021 | 0.945 ± 0 | 0.971 ± 0.019 | 0.977 ± 0.019 | 0.969 ± 0.017 |
| Target 7 | 0.965 ± 0.019 | 0.966 ± 0 | 0.973 ± 0.013 | 0.966 ± 0 | 0.971 ± 0.018 | 0.983 ± 0.01 | 0.979 ± 0.009 |
| Target 10 | 0.959 ± 0.022 | 0.935 ± 0 | 0.965 ± 0.028 | 0.945 ± 0 | 0.966 ± 0.016 | 0.963 ± 0.036 | 0.954 ± 0.028 |
| Target 13 | 0.972 ± 0.014 | 0.947 ± 0 | 0.975 ± 0.014 | 0.976 ± 0 | 0.971 ± 0.019 | 0.958 ± 0.026 | 0.954 ± 0.012 |
| Mean ± std | 0.967 ± 0.018 | 0.95 ± 0 | 0.968 ± 0.02 | 0.96 ± 0.006 | 0.967 ± 0.019 | 0.972 ± 0.021 | 0.961 ± 0.023 |

Table 4.4: Pearson's correlation coefficient errors between the means of cumulative sums of healthy activations and the subject's ones. The top part includes only the ones obtained from 16 recorded muscle EMG, that have been directly derived from the activation dynamics. The bottom part includes the overall activations estimated (from the 42 muscles). The means are reported based on the target reached, and the overall mean is also reported. A1 corresponds to the first assessment, A4 to the follow up.

From the result tables 4.3 and 4.4 the variations of the RMSE and CSR with respect to the healthy population gives us details about the improvement of the subject between the first and final assessment. Indeed, if we consider the reported error and its standard deviation between the healthy group as a threshold for a healthy behaviour. From EMG recorded and for the full estimated model, we observe have an improvement of S1 (28% and 10% less mean error respectively from first to final assessment) For this other subjects on the opposite, it seems to have more error after the final assessment, but the interesting element is that from the EMG only, for the subject 2 we would have observe a augmentation of 3% of the error, however when using all muscles this becomes a reduction of the error (8%). Regarding S3, both metrics showed an augmentation of error . If the significance of these result is to be discussed, this still shows that including an overall muscle activation, not only we observe expected improvement or decrease of the performances but these are actually corresponding to the measured one, (subject 2 had moderate improvement from FM score). A similar pattern can be observed when viewing the CSR values, this time, S2 improved its CSR sets of evaluated muscles, whereas this time, S3 even decreased this value in both cases. With reported values such as the presented ones, we can target specific muscles leading to an overall error. For instance, the Target 3 appeared to present more difficulties to subject 3 and no improvement at all was observed with the help of table A.3 and table A.9, Flexor Carpi Radialis Long and Extensor Carpi Radialis present both low CSR2 and high RMSE, meaning that there might be an issue with these muscles and their interaction might need to be investigated.

4.4.2 Muscle co-contraction between healthy and patients groups

While studying the CCI during reaching tasks of the subjects in figure 4.5. We can observe the limits of using recorded EMG signals only to evaluate muscle co-contractions. Indeed, the major muscles acting on joint rotations are not necessarily recorded, nor are they necessarily the ones expected at first glance from the literature, since with the model we have an estimate of these muscles and their potential action on the joint that is defined within the combination of joint motions, which is essential in 3D reaching tasks and especially for a part of the body as complex as the shoulder. We can observe from the figure a total diminution of the CCI for target 5, this is mostly caused by the absence of most of the main agonist muscles recorded (Latissimus dorsi Iliac and Teres minor/major). We can also observe low co-contractions for subject 3 while reaching target 13 with no improvement between assessments, on the opposite, subject 1 presented a low co-contraction at the first assessment , and reached at the assessment 4 values similar to the healthy ones displaying a improvement in that area.

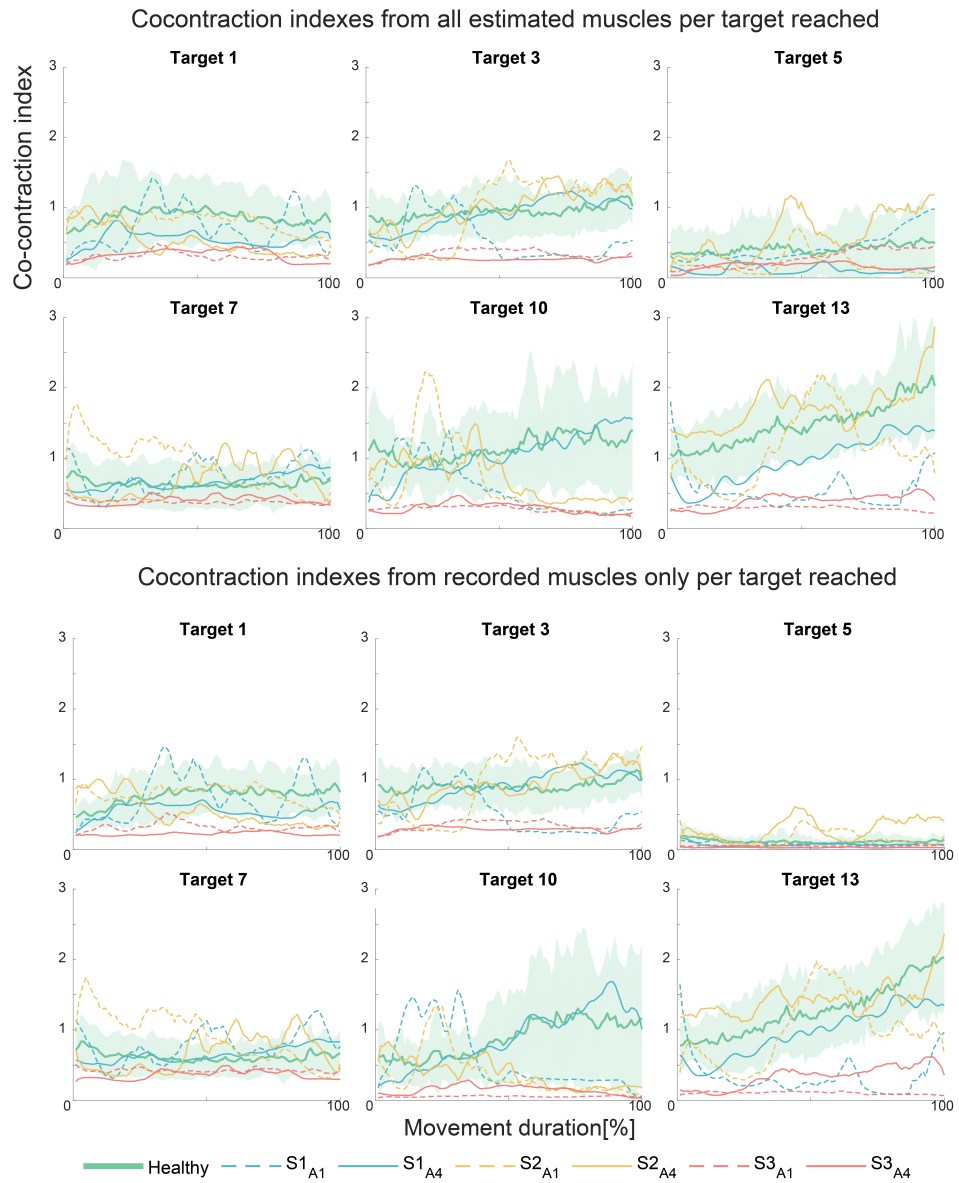


Figure 4.5: Figures showing the Co-contraction index while performing the reaching movements, dotted lines correspond to the first assessment signals and plain lines to the last one. In green, and with the shaded area, the healthy subjects signals and their standard deviation are represented

4.4.3 Muscle synergy analysis

The figure 4.6, represent the computed dot product per subject, assessment and Target reached. We can observe variations with these values before and after the rehabilitation treatment and more importantly, these variations are not necessarily the one expected from the literature. We would expect a reorganization of the muscle synergies towards the reference cluster obtained from the healthy group. It seems, however, that although a reorganization occurs and changes can be observed, the synergy weight dot product, showing the similarity with the reference, is not necessarily increasing, even for the subject S1, presenting the higher improvement and with a FM score of 52 (out of 66 for upper-limb). Given the reduced number of stroke survivors studied in this work, an extended analysis of the underlying activation changes would not be significant enough to suggest a specific hypothesis. However, the figure 4.6 shows us that the results differ when studying the full estimated muscles activations or the EMG recorded only. Although only recorded muscles are considered when studying muscle synergies in the literature, this result highly suggests that researchers and clinicians should include the larger set of activations from the model for increased significance and understanding of the physiology behind this reorganization.

These previous results should lead us to understand more about what is happening within this reorganization. For instance, when observing in detail the synergies and their weights for all muscles available as it is done in figure 4.7, we could observe large variations in terms of similarity between the subject and the reference cluster before and after the therapy for some muscle groups, however, for some of them, no alteration is observed. Moreover, an improvement with respect to the healthy group is not observed (with the similarity between the reference cluster and the subject from the dot product at 0.81 for the first assessment to 0.79 for the last one). This, once again, suggests considering the overall muscles activations in the synergy study, since information regarding the reorganization might not be captured otherwise. For the sake of readability, and since we argued that an extensive study of the reorganization is beyond the scope of this thesis, only a representative figure of the result for the first target for the subject with moderate improvement is displayed in figure 4.7. The full set of figures for all subjects and all targets reached is available upon request.

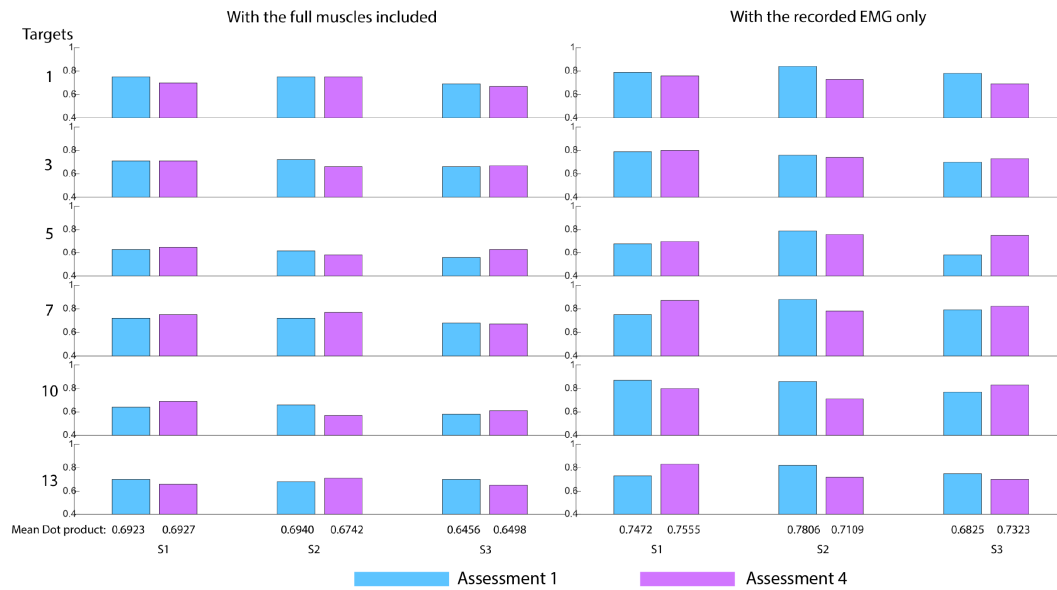
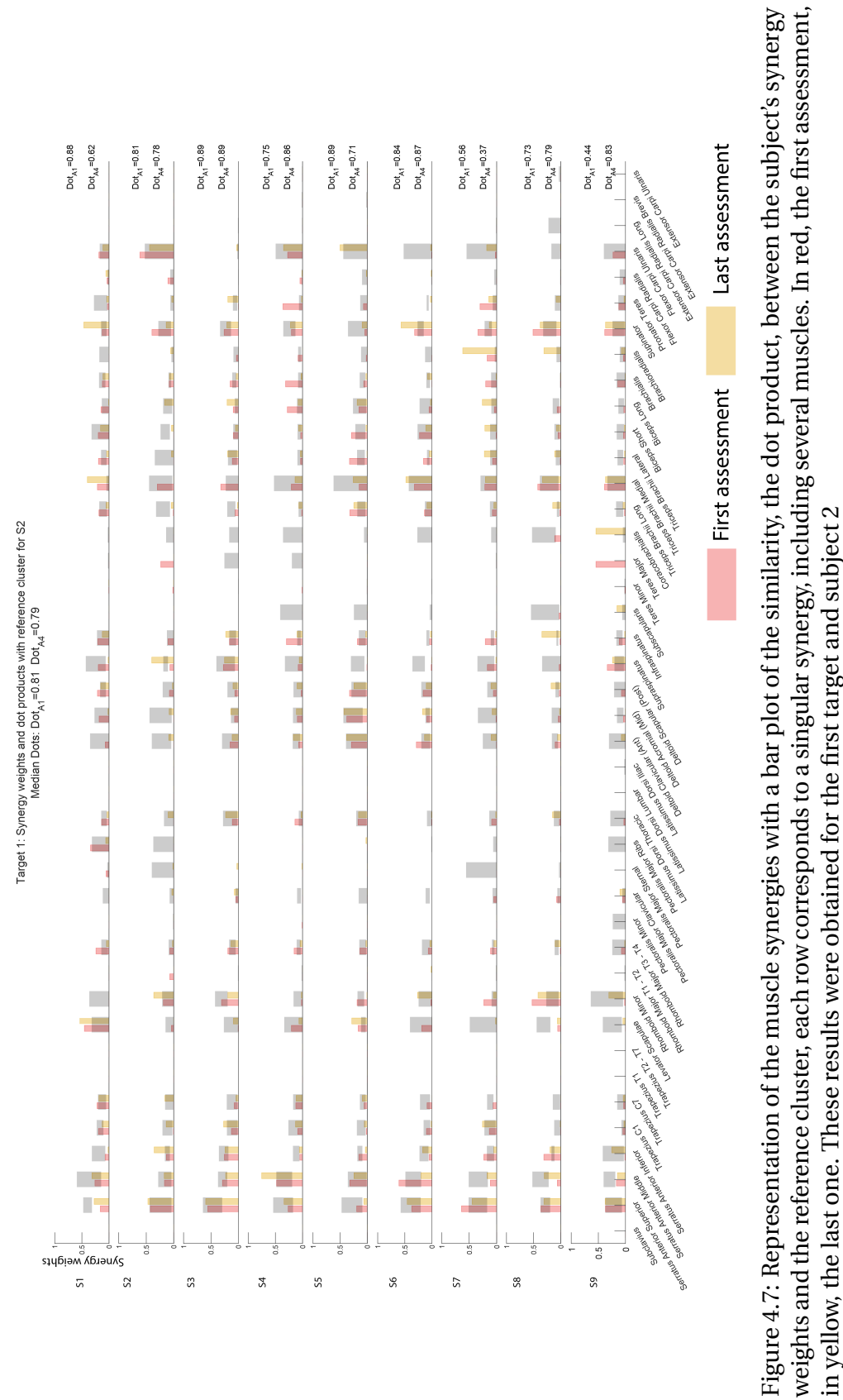


Figure 4.6: Bar plots of dot products from reference cluster based on the target reached. Each row corresponds to the result for a target reached, and the bar to the mean of the dot product between reference cluster weights and the subject's synergy weights. On the left, these are computed from all the estimated muscles activations. On the right, only the recorded EMG are used in the analysis. The bottom dot product, corresponds to the overall mean of the dot product, per subject and assessments. First assessment is represented in blue, the last one corresponding to the follow up is represented in magenta.



4.5 Discussion

Including an in-depth examination of overall muscle activation in the shoulder and arm, the current study, despite its limited applicability, holds significant promise in the field of rehabilitation. By incorporating a broader view of the muscles involved in the rehabilitation process, we could observe promising results. The ability to quantitatively evaluate muscle impairment by comparing specific metrics of impaired muscles to those of a healthy control group is one of the key elements of this study. Indeed, including the cumulative sum's Pearson's coefficient of the activations with the traditional root mean squared error provides us with a greater source of information regarding the level of activation of a muscle while performing a movement, when traditionally, only the coefficient of determination or the Pearson's coefficient are evaluated to show a similarity. This method enables a more precise evaluation of muscle function and variation with respect to the healthy group, thereby providing clinicians with valuable information, particularly regarding muscles that are difficult to access due to ethical considerations or discomfort for stroke survivors.

In addition, our research reveals limitations in existing studies on co-contraction, which tend to present a limited view of muscle actions. The majority of research has been conducted in two-dimensional plane, ignoring the potential interaction between muscles and joint rotation and most importantly the variations of a muscle's influence while performing a movement. With our reevaluation of the muscle's importance during a motion based on the moment arm dynamics, we could potentially obtain new information including the muscle dynamics with respect to existing methods.

In addition, despite the fact that numerous studies have investigated muscle synergies, we present a preliminary illustration of the discrepancies that can arise when considering the entire set of muscles involved in upper-limb movement with respect to using the reduced number of recorded EMG. Current research focuses only on the EMG to perform synergy analysis, neglecting additional muscles that might have been included in the subject's muscular reorganization after the therapy. This supports the importance of employing a musculoskeletal model to estimate the activation of the remaining muscles. This model provides a more complete view, taking into account aspects that might otherwise be overlooked.

Nonetheless, it is essential to recognize the limitations of our study. First, the ability of the model to replicate muscle activation is not yet error-free, as certain hypotheses and estimates were required when reconstructing upper-limb motion. Furthermore, the model is based on the minimization of the overall muscle stress, which might not be the main central nervous system strategy to perform a movement. In addition, the model was not scaled to each subject individually, which greatly diminished the physiological relevance of the predicted activations although it allowed us to observe variations in the muscular activations during a therapy without inducing a bias via

optimization protocols to scale the muscle parameters. Lastly, the musculoskeletal model employs rigid tendons, which, despite allowing for a faster and more extensive use of the model, may result in a loss of precision in comparison to models with flexible tendons.

It is essential to emphasize that the application of such a model holds great promise for enhancing our understanding of rehabilitation processes. Nonetheless, it should be viewed as a tool that provides a comprehensive overview of the involved mechanical aspects to clinicians and researchers while studying rehabilitation. Estimations of output activation should not be regarded as absolute truth, but rather serve as valuable insights to guide and enhance rehabilitation strategies.

4.6 Conclusion

In conclusion, our study highlights the potential of examining overall muscle activation in the shoulder and arm for rehabilitation. Using a limited number of three stroke survivors representing rehabilitation outcomes with large, moderate and no significant improvement in their upper-limb Fugl Meyer scores before and after their therapy we could provide a quantitative evaluation from the overall muscles reflective the subject's FM score. Quantitative evaluation involves the inclusion of a new metric, the cumulative sum's Pearson's coefficient of the muscle activations with the traditional root mean squared error. It provides us additional information than the standard evaluations of similarity using only the coefficient of determination or Pearson's coefficient, and hence more insight into the degree to which a muscle is activated during a movement.

Additionally, the inclusion of the joint rotation and the muscles dynamics and the underlying modifications in the muscle moment arms while performing a movement in this research exposed limitations in current co-contraction studies where muscles considered highly influential in the motion were not included.

Employing a musculoskeletal model enhances our understanding of overlooked aspects. However, limitations still exist in this research with the estimation the overall muscle activations which is not error-free due to assumptions and estimates made during the upper-limb motion reconstruction and its constraints. Additionally the model's focus on minimizing overall muscle stress may not align with the central nervous system's primary strategy for movement although it was considered the most reliable. Individual subject scaling was not implemented, reducing the physiological relevance of predicted activations but allowing for unbiased observation of therapy-induced muscular activation variations. The use of rigid tendons in the musculoskeletal model compromises precision compared to models with flexible tendons but allows it to be faster and more widely useable.

This research greatly emphasizes on the importance of the inclusion of numerical models to evaluate and provide advanced information to researchers and clinicians regarding rehabilitation strategies.

Author contributions statement

T.B conceived the work on the numerical model, its development, metrics assessment, co-contraction evaluation, synergy study, the initial draft and the figures. T.P provided critical insights. C.P designed the experimental protocol and conducted the experiments. S.M directed the study.

Competing interests

The authors declare no competing interests.

5 Conclusion and perspectives

The thesis was motivated by the need for a better understanding of the human motor control and impairments after a neurological disease in order to improve rehabilitation treatments. Recent research towards this goal propose an approach including combined bio markers during the rehabilitation [17, 55, 84, 129, 130]. However, regarding the muscles, their impairment, co-contractions and synergies, their study were based on the low number of recorded EMG signals. Among the musculoskeletal subsystems of the human body, the shoulder presents unique challenges due to its singular kinematics, including combined joints, and a high number of muscles acting in coordination to control their movements. Therefore each of these muscles may greatly introduce a reorganization and an impairment, and thus, need to be studied. A recording of all of these is however infeasible in practice due to their overlapping and positions as well as the complexity of the recording set-up required for this large number of muscles. The use of a musculoskeletal model could therefore greatly help with the overall muscles activations estimations and their study during rehabilitation. While the knee and the hip have both been widely addressed in the literature, the shoulder is less understood and existing musculoskeletal models are mostly based on the study of contact forces, require an extensive number of measurement points or a computational time not suitable for the study of large sets of data. [126, 133, 145]. The main drawback of currently existing models is that they are not usable for a rehabilitation improvement assessment. Indeed, this requires no optimization of the muscle parameters per subject between assessments to avoid an induced non-physiological bias after the therapy. I first wanted to solely rely on the minimization of the overall muscle stress, and not the overall muscle activation that could potentially hinder co-contraction from occurring without necessarily being physiologically relevant. Additionally, I wanted to include all the muscles involved in the upper limb motions (42 muscles), and no existing model was satisfying these conditions. Lastly, I wanted to have a fast and reliable model, that could be usable by a wider range of

researchers and also clinicians for understanding muscle coordination and developing rehabilitation plans.

In this thesis I therefore presented an improvement of a validated upper-limb musculoskeletal model, the latter had been then tailored for the possible study of overall muscular activation signals while performing complex tasks using an exoskeleton. While discussions and limitations are available in each of the chapters, I will summarize and discuss them more broadly, and present future research directions here.

5.1 Summary

In chapter 1, we presented the upper-limb anatomy and the background of the overall needs and goals to understand the next parts of the thesis. In chapter 2, we showed the upper-limb musculoskeletal model and its development. It corresponds to 11 degrees of freedom model, with the sternoclavicular, acromioclavicular and glenohumeral joints modeled as ball and sockets and ulna flexion/extension and radius pro-supination as hinges following the ISB recommendations [174]. 42 muscle segments are represented, in the model each of these can be divided up to 20 parts. The basis for a forward dynamics formulation has been developed as well as an improved (and less prone to errors) inverse dynamics method, including the possible use of EMG recordings for better estimates and a modified load-sharing optimization protocol. Given the complexity of the model, the codes, and the extensive amount of files and functions needed to run it, a graphical user interface had been developed to reduce the understanding burden of the user. Finally, a number of functions were precomputed and developed in C to be used as Matlab Mex files, greatly reducing the computational time required for a simulation. A clear comparison of the time required was not feasible since the previous model was not usable for recent Matlab versions, but it could be approximated with a time reduction of two orders of magnitude enabling the study of a large number of movements, and therefore activation comparisons.

In chapter 3, we showed that using this model and with the introduction of a limited number of recorded EMG signals we could estimate physiological muscle activations of 42 muscles from subject performing complex 3D reaching tasks using an upper limb exoskeleton. We compared the physiological static-optimization method (with no EMG signals included) and the EMG-assisted one (using recorded muscles). It showed that we can better estimate the activations with EMG-assisted while keeping a low error in the reconstructed torques at the joints. If the estimates are not perfect, they show a better representation of the levels of activation than with static-optimization only as it was shown with a leave-one-out cross-validation method on the recorded muscles. It would therefore be suitable for a comparison of muscle levels of activation signals between subjects paving the way for the next study.

In chapter 4 the same methodology was applied to 3 stroke patients for two assessments, before and after their rehabilitation procedure. The subjects and their data were selected among available others from a previous study [130] to represent 3 levels of rehabilitation outcomes. 1) Subject with a great improvement after rehabilitation, 2) subject with a moderate improvement and 3) subject with a poor improvement based on the evolution of their upper-limb Fugl Meyer score between the first assessment and the follow-up after the therapy. Here the goal was to show that indeed, including the overall muscle activations estimated, we could provide more information on singular muscles to the clinicians to improve the rehabilitation process. The metrics presented were directly correlated with the Fugl-Meyer score of the patients, showing that when comparing the overall muscle activations with healthy subjects only, we could obtain a deeper understanding of the patient's impairment. It included a novel metric for similarity evaluation with the healthy group; the Pearson's coefficient of the cumulative sum of the muscle activation, that took into consideration, the timing of activation but also the activation level. We showed a dynamics representation of the main muscles acting on a specific movement, with the inclusion of the dynamics moment arms while performing movement, this presented variations in terms of muscle influence with respect to existing literature. We also shown the importance of having the overall muscle activation estimated in the co-contraction study, shedding light on existing studies' limitations that might overlook main muscles influencing the movement. Finally, we showed that outcomes from synergy analysis may differ when using the overall muscle activation with respect to only the recorded ones. This highly suggests the use of musculoskeletal numerical models when performing synergy analysis, as the reorganization of muscle coordination might include non-recorded muscles.

5.2 Limitations and future developments

The model can still be developed and improved. I could reduce the computational cost during simulations by using precomputed functions in C and developed as Matlab Mex files to speed up their computations. But other means could achieve great performances. Indeed the moment arm and muscles lengths computations as functions of joint angles for instance could be obtained via regression models, drastically reducing the computation time, however, building models like this would totally block the model scaling features if the latter ones are not included. Unfortunately, this would take a long computational time to obtain.

Future development of the model should take the forward dynamics methods and directly couple it with the cost function from the inverse dynamics method. The forward dynamics computation is not only faster, it could compensate on its own for the variations from the desired torque. Indeed in the cost function proposed, the activation estimation should minimize also the difference in the measured torque at the joints and the produced torque from the musculotendon actuation. This would

be similar to the methods proposed in [72, 148] and to more recently [2]. The current drawbacks of the forward dynamics model would be then discarded as it would act as a closed-loop in this mode. Moreover, given the already computed function and methods as "black box", this should be relatively fast achieved.

With overall activations estimated from the inverse dynamics across different directions at multiple speed and corresponding EMG recorded. It could be possible to develop a machine learning model for simple movements leading to the overall activations from recorded EMG. This however would require a large dataset of EMG and movements since the model is composed of 11 degrees of freedom but could provide a good insight of muscular impairments and variations in movement from recorded EMG only.

Another possibility would be to apply reinforcement learning methods to provide a physiological controller, as it was done previously [78]. With this the activations are learned from current and desired joint positions and velocities given sets of predefined rewards. Such a method would be particularly interesting for the evaluation of strategies involved right after an impairment or surgery occurs.

Finally, the hand as a single bone and the wrist joint are already available in the model, and most of the muscles spanning the wrist joint are already modeled. With the current state, movement of the wrist is maintained fixed which overlooks activation from muscles spanning this joint. Consequently, the inclusion of such a joint would significantly enhance and expand the applicability of this model with minimum further development.

I would suggest future development starting from the mex precomputation of more functions used in the model, and possibly even developing the model and the graphical user interface as an application for easier use by a wider range of population, including clinicians. This would also limit the access of most of the functions, and their behaviour could be rather simply modified by tuning a limited number of parameters as I did for the graphical user interface and the tuning of the activation cost functions. Furthermore, the existing architecture is rather cumbersome, consisting of an excessive number of files and functions, which may be intimidating for the new user.

Regarding the use of the musculoskeletal model as a tool for a better understanding of muscular control and impairment, although it showed really promising preliminary results, the model's ability to replicate muscle activation is still not perfect, due to several assumptions made to tailor it for comparison goals. However, if long simulations are permitted and more detailed kinematics are available, especially for the scapula movements, it could really provide clinicians and scientists with a powerful tool, enabling a complete study of the overall muscles acting on the shoulder, their co-contractions and, as widely studied from the past decades, the muscle synergies

but with the addition of all muscles.

Because it has the potential to be interesting for clinicians and researchers and help them in the process of understanding and developing more tailored rehabilitation protocols, improving the graphical user interface, simplifying its use, and developing potential studies using it for larger sets of results and significance should be the key goal for the future of this model.

A Appendix

A.1 Appendix chapter 3

A.1.1 Joint moment reconstruction and error

An error is introduced by the cost function 3.6 between the moment of joints of equations of movement \mathbf{J}_{torque} (Eq. 2.9) from the measured kinematics and the ones reconstructed after the EMG-assisted and static-optimization. After the optimization, the augmented obtained activations signals $\tilde{\mathbf{a}}$ were fed into the contraction dynamics. to obtain the augmented forces for each time steps $\tilde{\mathbf{f}}$. From these, it was possible to recompute the corresponding joint moment, using the moment arm matrix \mathbf{W}_m .

$$\tilde{\mathbf{J}} = \mathbf{W}_m \tilde{\mathbf{f}} \quad (\text{A.1})$$

Fig. A.1 shows the corresponding estimated torques of the unconstrained joints from EMG-assisted and static-optimization obtained signals. This demonstrates a minimal difference between the estimated ones and the measured ones. It seemed however that the recomputed moments at the Radius pronation/supination and the humerus axial rotations were less steady than the measured one for both optimization process.

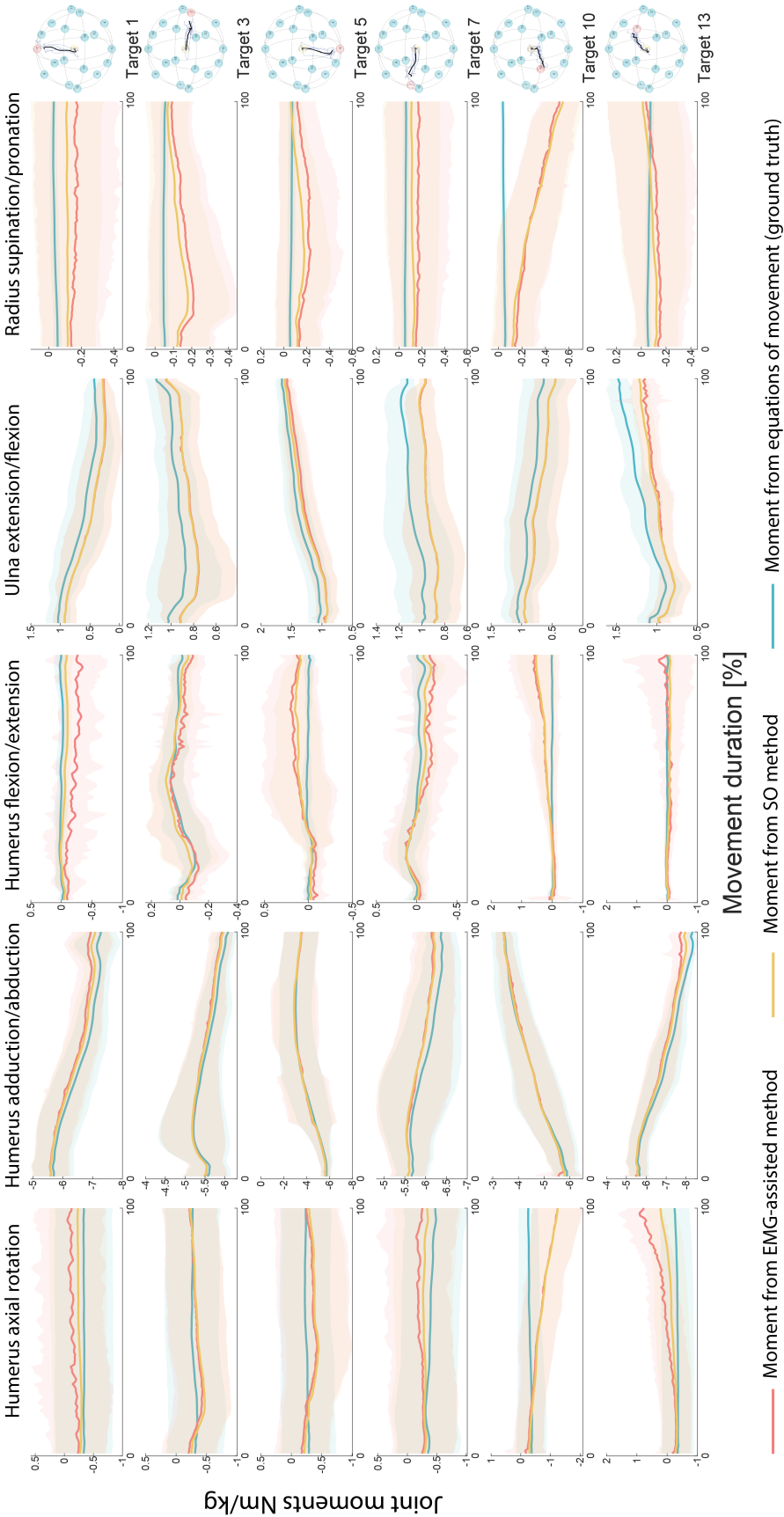


Figure A.1: Measured and recomputed joint moments with the EMG-assisted and static-optimization methods for the different tasks and joints. The lines correspond to the means across subjects and repetitions and the shaded areas to their standard deviation

A.1.2 Means of activation computed per target reached

Below are the figures of the estimated activations from the EMG-assisted, static-optimization and the ones from activation dynamics. These figures took the means from all subjects and repetitions for sake of clarity within the figures and to reduce the overall number of total figures. The figures of means of activations per subject and target are available upon request.

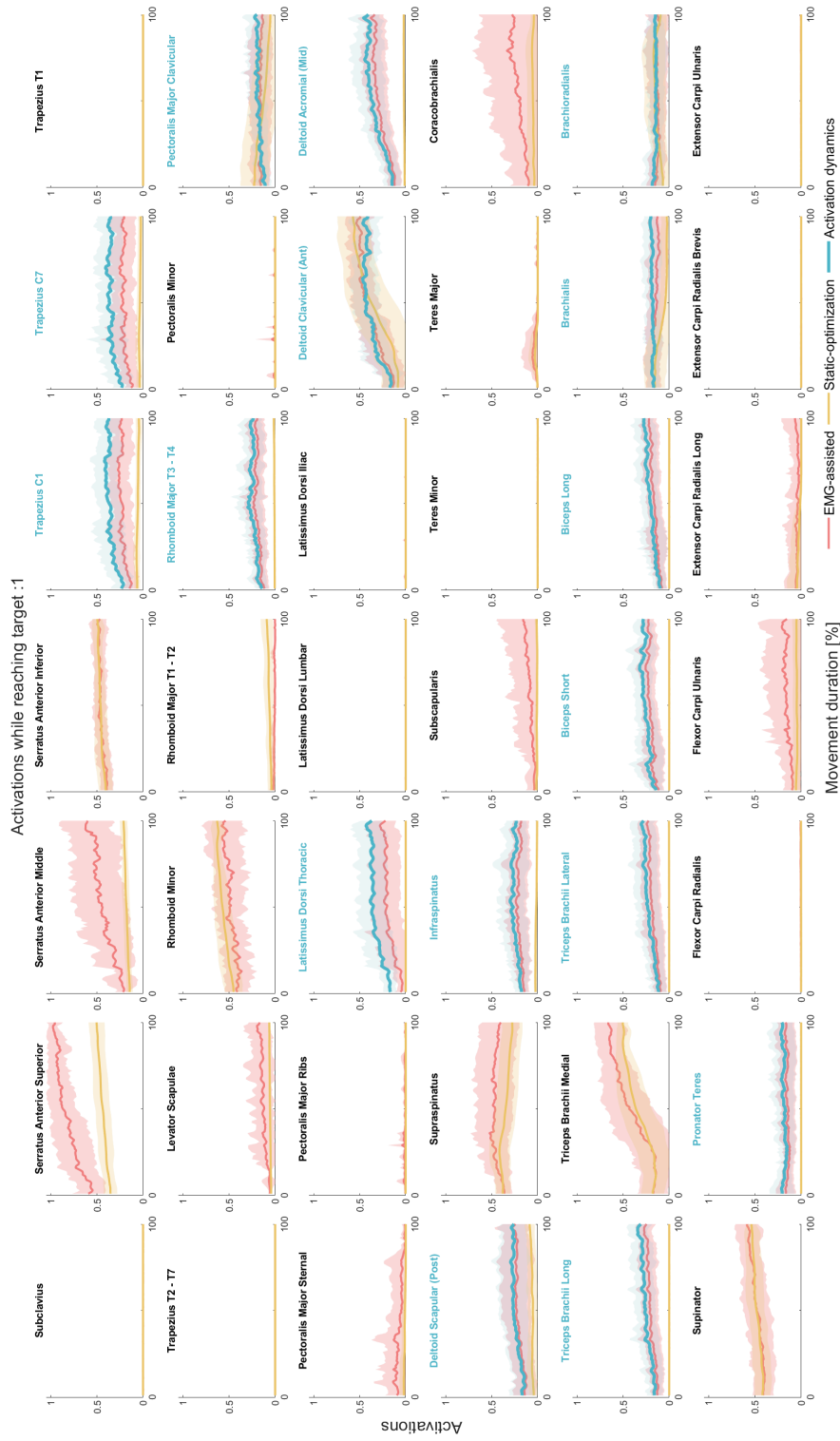


Figure A.2: Means of the estimated muscle activations across the 5 repetitions for all 5 subjects while reaching target: 1 with respect to the percentage of movement. The blue lines correspond to the activation obtained directly via the activation dynamics for muscles with available recorded EMG (their name in blue). The red lines correspond to the ones obtained from the presented method including the EMG available. The yellow lines are the activations obtained from the method without using the recorded EMG, setting the boundaries in the optimization only using the musculotendon activation with an activation of 0 and 1 for lower bound and upper bound respectively. The thick lines represent the means of those activations across the 5 subjects and repetitions. The shaded areas represent their standard deviations.

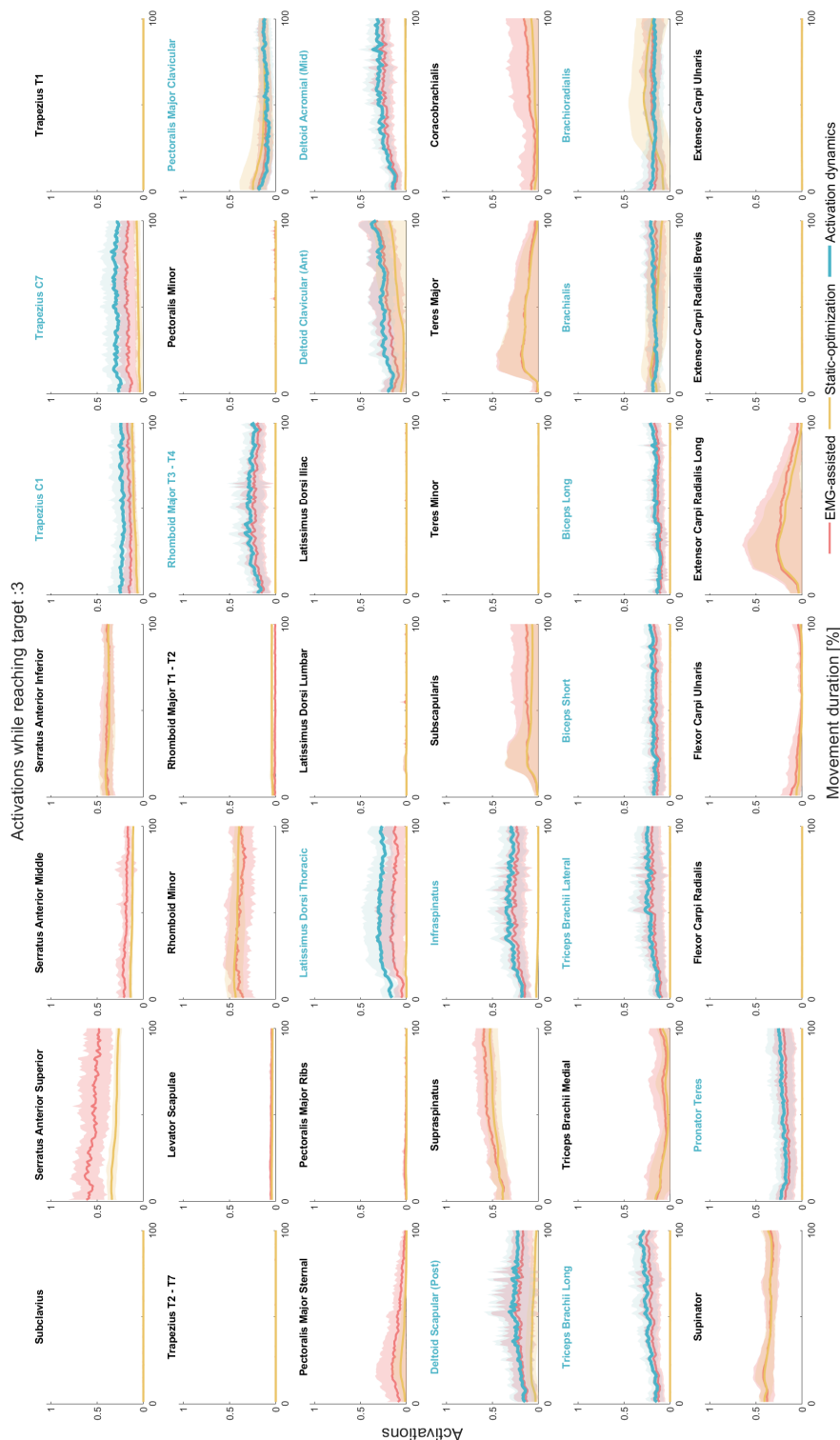


Figure A.3: Means of the estimated muscles activations across the 5 repetitions for all 5 subjects while reaching target: 3 with respect to the percentage of movement. The blue lines correspond to the activation obtained directly via the activation dynamics for muscles with available recorded EMG (their name in blue). The red lines correspond to the ones obtained from the presented method including the EMG available. The yellow lines are the activations obtained from the method without using the recorded EMG, setting the boundaries in the optimization only using the musculotendon activation with an activation of 0 and 1 for lower bound and upper bound respectively. The thick lines represent the means of those activations across the 5 subjects and repetitions. The shaded areas represent their standard deviations.

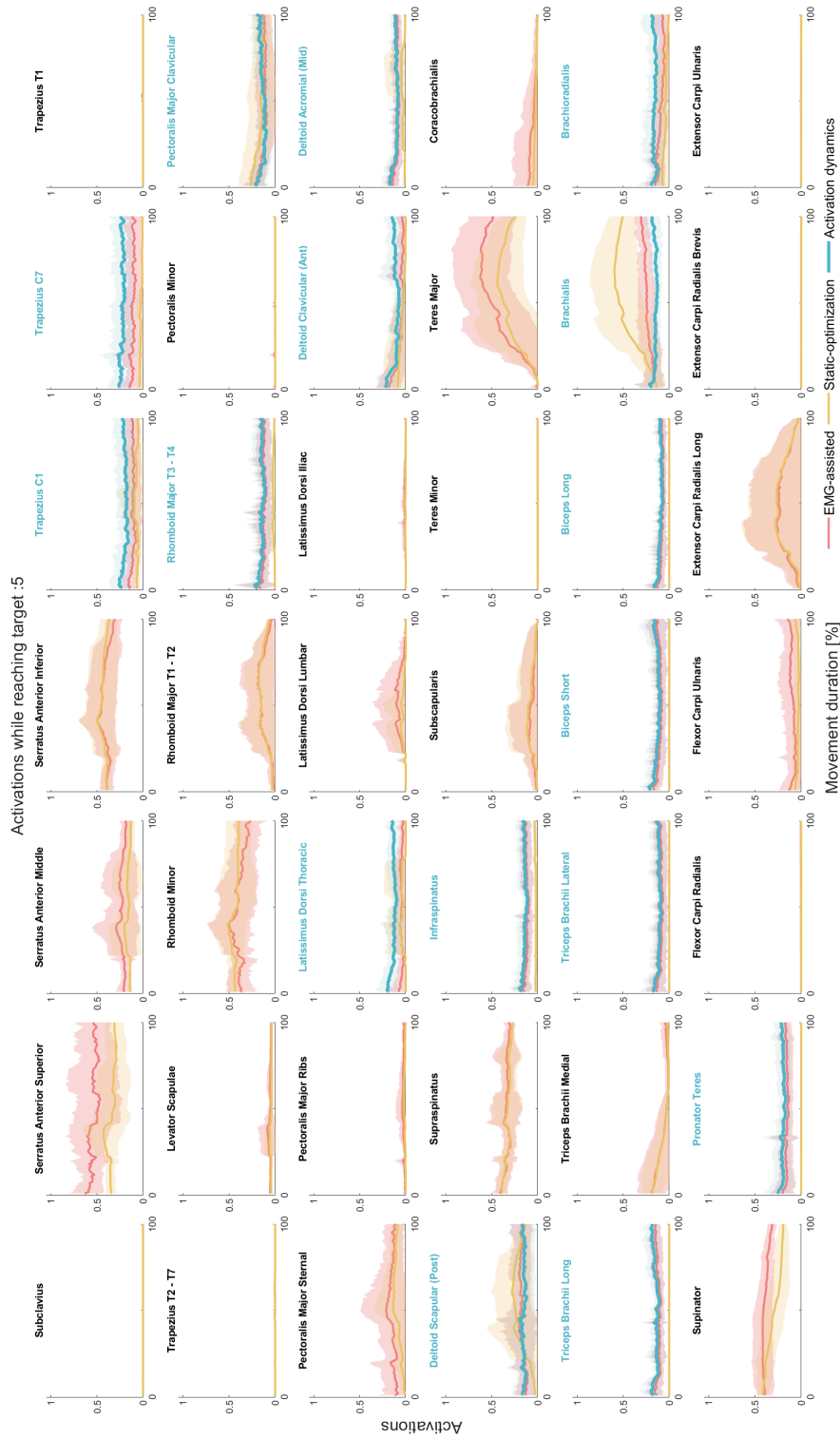


Figure A.4: Means of the estimated muscles activations across the 5 repetitions for all 5 subjects while reaching target: 5 with respect to the percentage of movement. The blue lines correspond to the activation obtained directly via the activation dynamics for muscles with available recorded EMG (their name in blue). The red lines correspond to the ones obtained from the presented method including the EMG available. The yellow lines are the activations obtained from the method without using the recorded EMG, setting the boundaries in the optimization only using the musculotendon activation with an activation of 0 and 1 for lower bound and upper bound respectively. The thick lines represent the means of those activations across the 5 subjects and repetitions. The shaded areas represent their standard deviations.

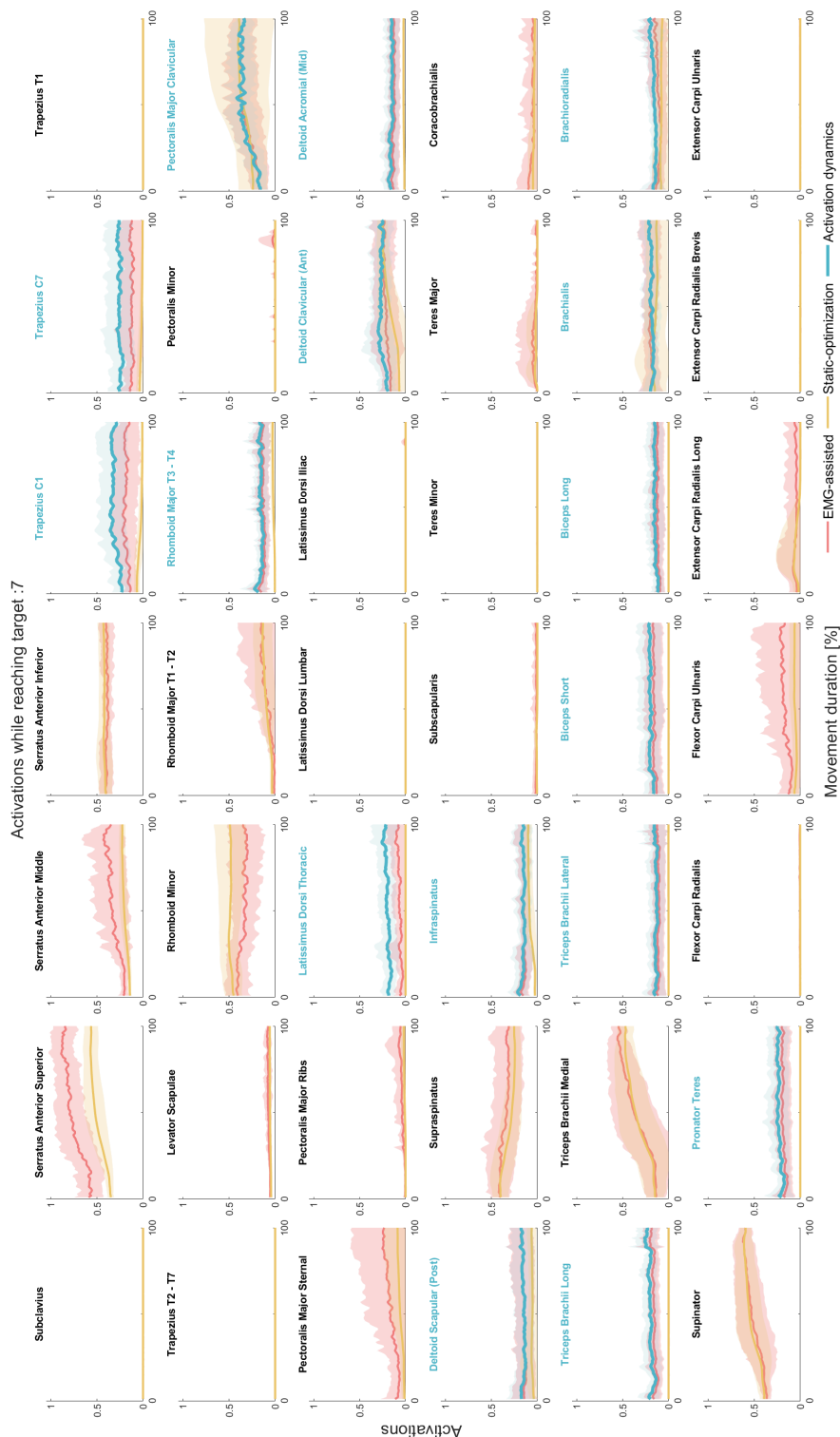


Figure A.5: Means of the estimated muscles activations across the 5 repetitions for all 5 subjects while reaching target: 7 with respect to the percentage of movement. The blue lines correspond to the activation obtained directly via the activation dynamics for muscles with available recorded EMG (their name in blue). The red lines correspond to the ones obtained from the presented method including the EMG available. The yellow lines are the activations obtained from the method without using the recorded EMG, setting the boundaries in the optimization only using the musculotendon actuation with an activation of 0 and 1 for lower bound and upper bound respectively. The thick lines represent the means of those activations across the 5 subjects and repetitions. The shaded areas represent their standard deviations.

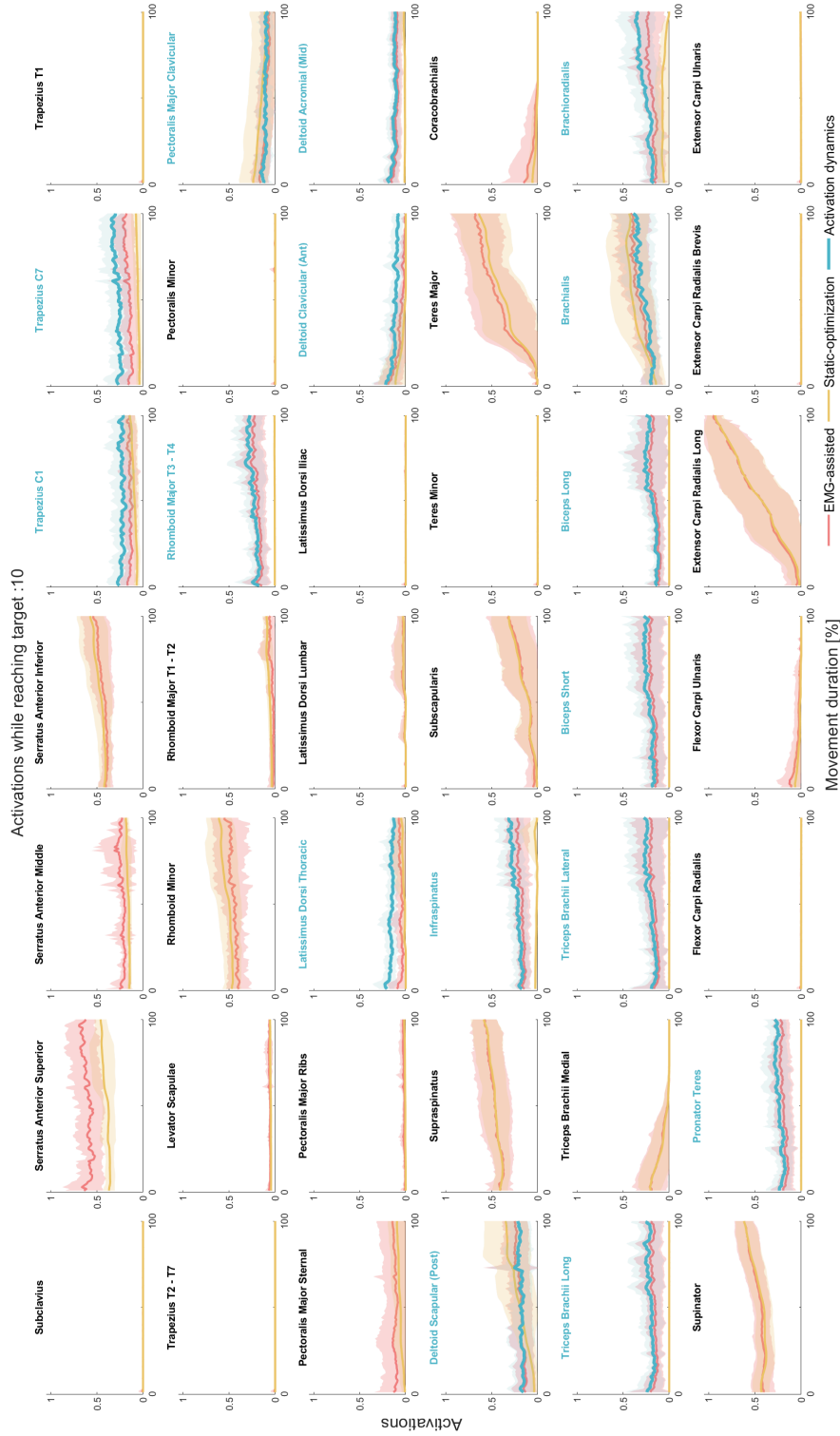


Figure A.6: Means of the estimated muscles activations across the 5 repetitions for all 5 subjects while reaching target: 10 with respect to the percentage of movement. The blue lines correspond to the activation obtained directly via the activation dynamics for muscles with available recorded EMG (their name in blue). The red lines correspond to the ones obtained from the presented method including the EMG available. The yellow lines are the activations obtained from the method without using the recorded EMG, setting the boundaries in the optimization only using the musculotendon actuation with an activation of 0 and 1 for lower bound and upper bound respectively. The thick lines represent the means of those activations across the 5 subjects and repetitions. The shaded areas represent their standard deviations.

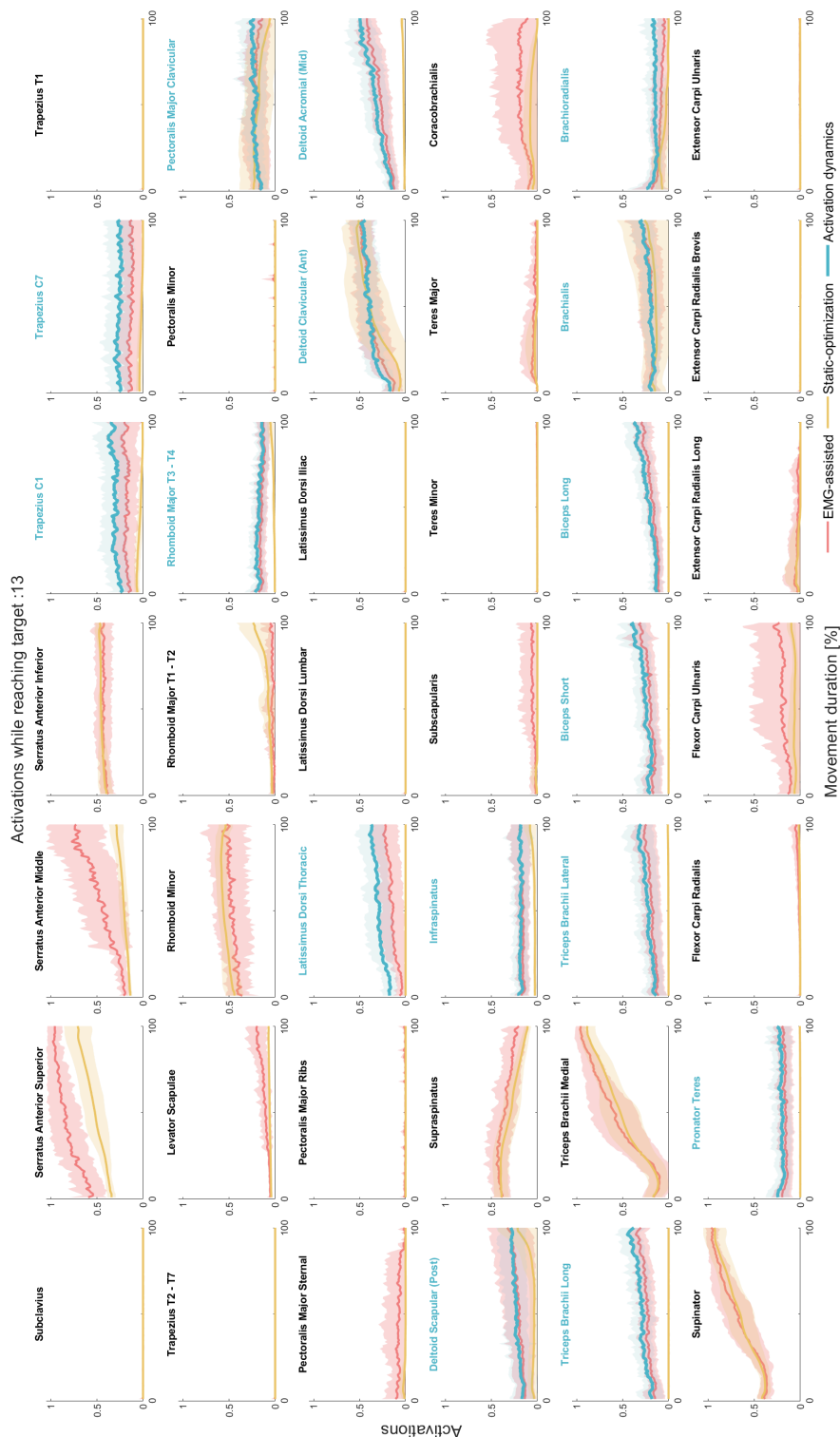


Figure A.7: Means of the estimated muscles activations across the 5 repetitions for all 5 subjects while reaching target: 13 with respect to the percentage of movement. The blue lines correspond to the activation obtained directly via the activation dynamics for muscles with available recorded EMG (their name in blue). The red lines correspond to the ones obtained from the presented method including the EMG available. The yellow lines are the activations obtained from the method without using the recorded EMG, setting the boundaries in the optimization only using the musculotendon actuation with an activation of 0 and 1 for lower bound and upper bound respectively. The thick lines represent the means of those activations across the 5 subjects and repetitions. The shaded areas represent their standard deviations.

A.1.3 Levels of activation computed per muscle and target reached**A.1.4 Leave-one-out cross-validation for all subjects**

A.2 Appendix chapter 4

A.2.1 Rotations observed per target reached

Table A.1: Table of the rotated joint angles per target reached: The positive and negative angles follow the described rotations from Fig. 4.2 when the standard deviation shown is at 0, it means that there were only one repetition of the recorded movement. A1 correspond to the first assessment, before the rehabilitation and A4 correspond to the final one.

| Target and Joint | Healthy | S1 A1 | S2 A1 | S3 A1 | S1 A4 | S2 A4 | S3 A4 |
|------------------|----------------|---------------|----------------|----------------|----------------|----------------|----------------|
| T1 J7 | -7.70 ± 6.20 | -11.70 ± 0.00 | -17.00 ± 2.80 | -18.20 ± -1.60 | -22.80 ± 1.70 | -14.90 ± -7.10 | -13.40 ± -5.00 |
| T1 J8 | -27.40 ± -3.70 | -27.90 ± 0.00 | -31.10 ± 2.60 | -26.30 ± -0.50 | -22.20 ± -0.50 | -26.70 ± -4.30 | -25.80 ± -2.40 |
| T1 J9 | 3.40 ± -4.50 | 7.90 ± 0.00 | 9.80 ± 4.10 | 12.20 ± -0.80 | 13.00 ± 2.60 | 7.30 ± -3.30 | 6.70 ± -1.20 |
| T1 J10 | -9.90 ± -1.70 | -6.00 ± 0.00 | -16.20 ± 0.20 | -11.70 ± 0.00 | -7.40 ± 1.80 | -7.90 ± 3.10 | -6.80 ± 1.00 |
| T1 J11 | -13.70 ± 32.40 | -9.20 ± 0.00 | -5.60 ± -5.10 | -4.20 ± 1.70 | -8.30 ± -2.70 | -5.30 ± 2.30 | -5.90 ± 0.60 |
| T3 J7 | -3.70 ± -2.20 | 6.80 ± 0.00 | -2.20 ± 9.50 | -4.40 ± 7.70 | 2.40 ± 0.80 | 2.50 ± 3.60 | 1.30 ± 2.70 |
| T3 J8 | -2.10 ± -1.50 | -4.30 ± 0.00 | -7.70 ± -1.20 | -4.60 ± 0.20 | -7.10 ± -1.90 | -4.40 ± 3.70 | -4.90 ± 2.40 |
| T3 J9 | -23.50 ± -2.40 | -30.70 ± 0.00 | -24.20 ± 4.80 | -22.60 ± 4.60 | -27.10 ± 0.70 | -27.20 ± 3.50 | -25.30 ± 2.50 |
| T3 J10 | -7.70 ± -4.00 | -8.20 ± 0.00 | -12.70 ± 2.60 | -11.90 ± 5.50 | -11.10 ± -0.50 | -7.90 ± 2.20 | -8.00 ± 0.50 |
| T3 J11 | -33.70 ± 52.20 | -7.50 ± 0.00 | -12.20 ± -4.10 | -11.00 ± 7.40 | -4.80 ± 0.30 | -4.00 ± 2.10 | 12.60 ± -5.20 |
| T5 J7 | 22.80 ± 32.00 | -3.10 ± 0.00 | 18.70 ± 0.00 | 15.50 ± -3.50 | 23.60 ± 1.50 | 11.00 ± 9.70 | 17.70 ± 1.30 |
| T5 J8 | 22.30 ± 6.60 | 14.60 ± 0.00 | 17.80 ± 0.00 | 20.20 ± 3.10 | 16.80 ± -0.40 | 18.00 ± 3.50 | 15.20 ± -0.20 |
| T5 J9 | -21.90 ± 34.90 | 0.10 ± 0.00 | -20.50 ± 0.00 | -15.50 ± -2.60 | -20.10 ± 2.60 | -9.90 ± 7.30 | -14.50 ± 1.90 |
| T5 J10 | -7.50 ± -2.90 | -10.20 ± 0.00 | -13.50 ± 0.00 | -10.00 ± 2.20 | -9.00 ± 4.40 | -9.70 ± 4.60 | -13.40 ± 3.70 |
| T5 J11 | -13.50 ± 32.40 | -3.80 ± 0.00 | -5.00 ± 0.00 | -1.20 ± -1.00 | -2.10 ± 3.00 | -3.40 ± 0.70 | 2.70 ± 0.90 |
| T7 J7 | 0.00 ± -1.70 | -1.40 ± 0.00 | -5.80 ± 0.00 | -7.00 ± -3.60 | -0.00 ± -1.30 | 1.70 ± -3.80 | 4.40 ± -6.90 |
| T7 J8 | -5.10 ± -1.30 | -5.40 ± 0.00 | -4.40 ± 0.00 | -2.20 ± -0.80 | -4.50 ± -1.50 | -3.60 ± 0.20 | -5.90 ± -3.10 |
| T7 J9 | 23.80 ± -2.70 | 22.40 ± 0.00 | 28.60 ± 0.00 | 28.90 ± -2.90 | 26.60 ± -0.80 | 23.40 ± -4.90 | 22.60 ± -5.90 |
| T7 J10 | -11.70 ± -0.70 | -10.80 ± 0.00 | -14.70 ± 0.00 | -7.60 ± -0.40 | -9.50 ± 3.20 | -10.10 ± 1.00 | -10.60 ± 0.30 |
| T7 J11 | -13.20 ± 45.70 | -3.90 ± 0.00 | -4.90 ± 0.00 | -1.00 ± 1.30 | -3.40 ± 1.60 | -3.10 ± -0.40 | -5.30 ± -2.10 |
| T10 J7 | 49.20 ± 12.70 | 53.80 ± 0.00 | 66.10 ± 0.00 | 31.30 ± 11.60 | 46.50 ± -12.10 | 39.40 ± 6.30 | 46.20 ± -8.00 |
| T10 J8 | 14.80 ± 3.10 | 15.70 ± 0.00 | 6.70 ± 0.00 | 17.10 ± 0.60 | 7.90 ± 1.70 | 12.80 ± 4.40 | 11.50 ± 2.90 |
| T10 J9 | -12.40 ± 13.30 | -31.00 ± 0.00 | -42.00 ± 0.00 | -14.30 ± 12.80 | -33.50 ± -8.50 | -22.60 ± 13.20 | -30.90 ± -1.60 |
| T10 J10 | 46.10 ± -1.90 | 43.30 ± 0.00 | 43.20 ± 0.00 | 42.80 ± 0.50 | 42.90 ± 3.20 | 41.10 ± 1.60 | 41.90 ± 1.90 |
| T10 J11 | -52.70 ± 20.70 | 33.90 ± 0.00 | 31.10 ± 0.00 | 4.50 ± -3.40 | 32.70 ± 0.90 | 25.40 ± -9.60 | 30.00 ± -0.60 |
| T13 J7 | -13.00 ± -5.10 | -0.10 ± 0.00 | -16.30 ± 0.00 | -15.70 ± -0.40 | -10.20 ± 5.70 | -5.40 ± 7.30 | -8.60 ± 10.50 |
| T13 J8 | -23.40 ± -2.80 | -24.80 ± 0.00 | -20.60 ± 0.00 | -23.50 ± -1.30 | -22.20 ± 0.70 | -27.20 ± -0.90 | -23.30 ± 1.80 |
| T13 J9 | 8.70 ± -9.30 | 8.30 ± 0.00 | 16.10 ± 0.00 | 13.50 ± -1.70 | 16.20 ± -0.80 | 8.10 ± -3.70 | 14.00 ± 2.80 |
| T13 J10 | -53.80 ± -2.70 | -51.90 ± 0.00 | -55.30 ± 0.00 | -52.90 ± 0.60 | -56.80 ± 2.80 | -57.00 ± 5.50 | -54.60 ± 2.90 |
| T13 J11 | -1.70 ± 4.50 | -0.70 ± 0.00 | -18.00 ± 0.00 | -13.40 ± 4.80 | -12.50 ± 3.50 | -16.30 ± -0.70 | -16.60 ± -0.10 |

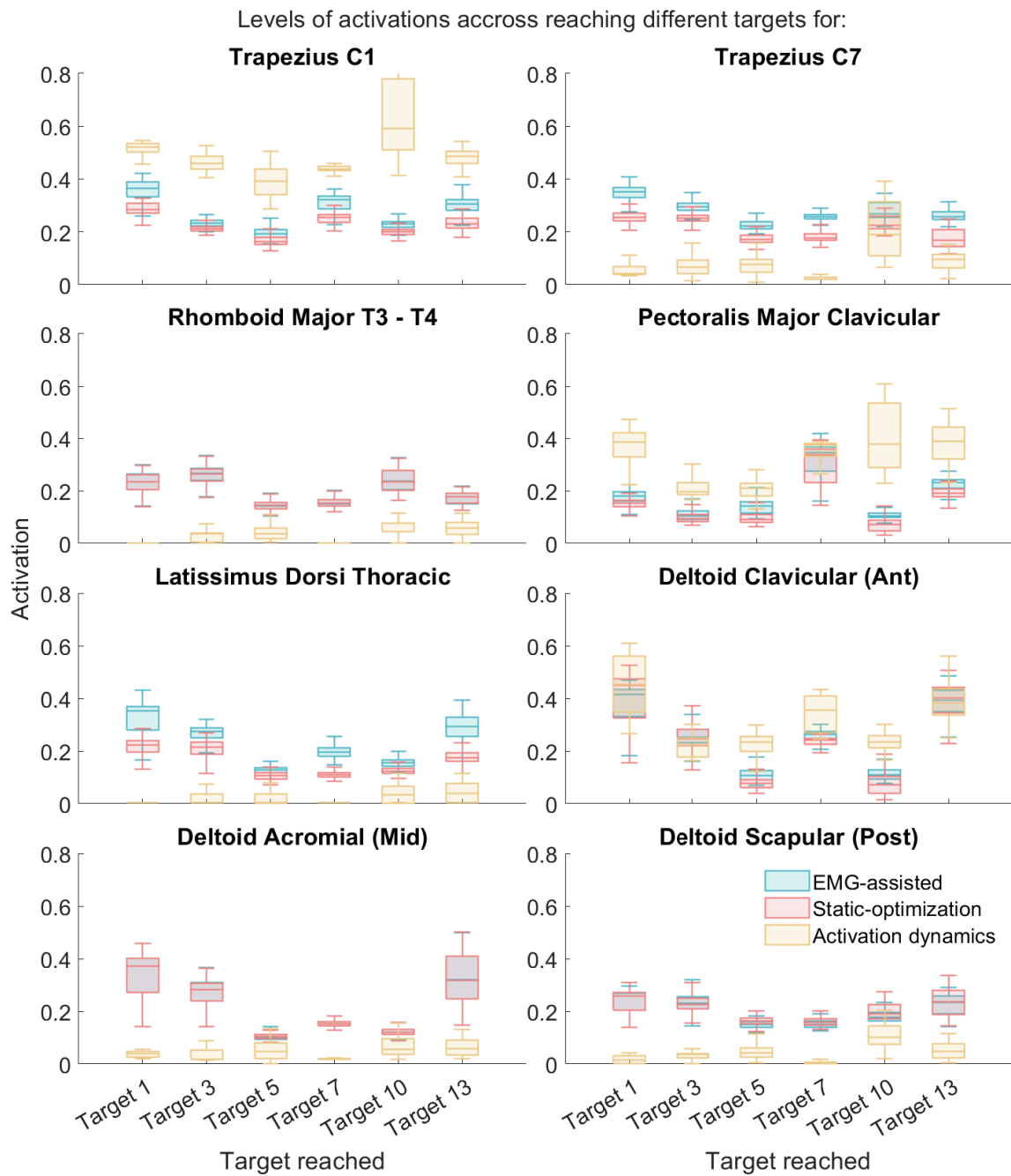


Figure A.8: Comparisons between the ranges of activations directly obtained from activation dynamics (blue boxplot), the estimated ones with the model including the recorded EMG (red boxplot) and the one from the model without using the recorded EMG (yellow boxplot) with respect to the reached target.

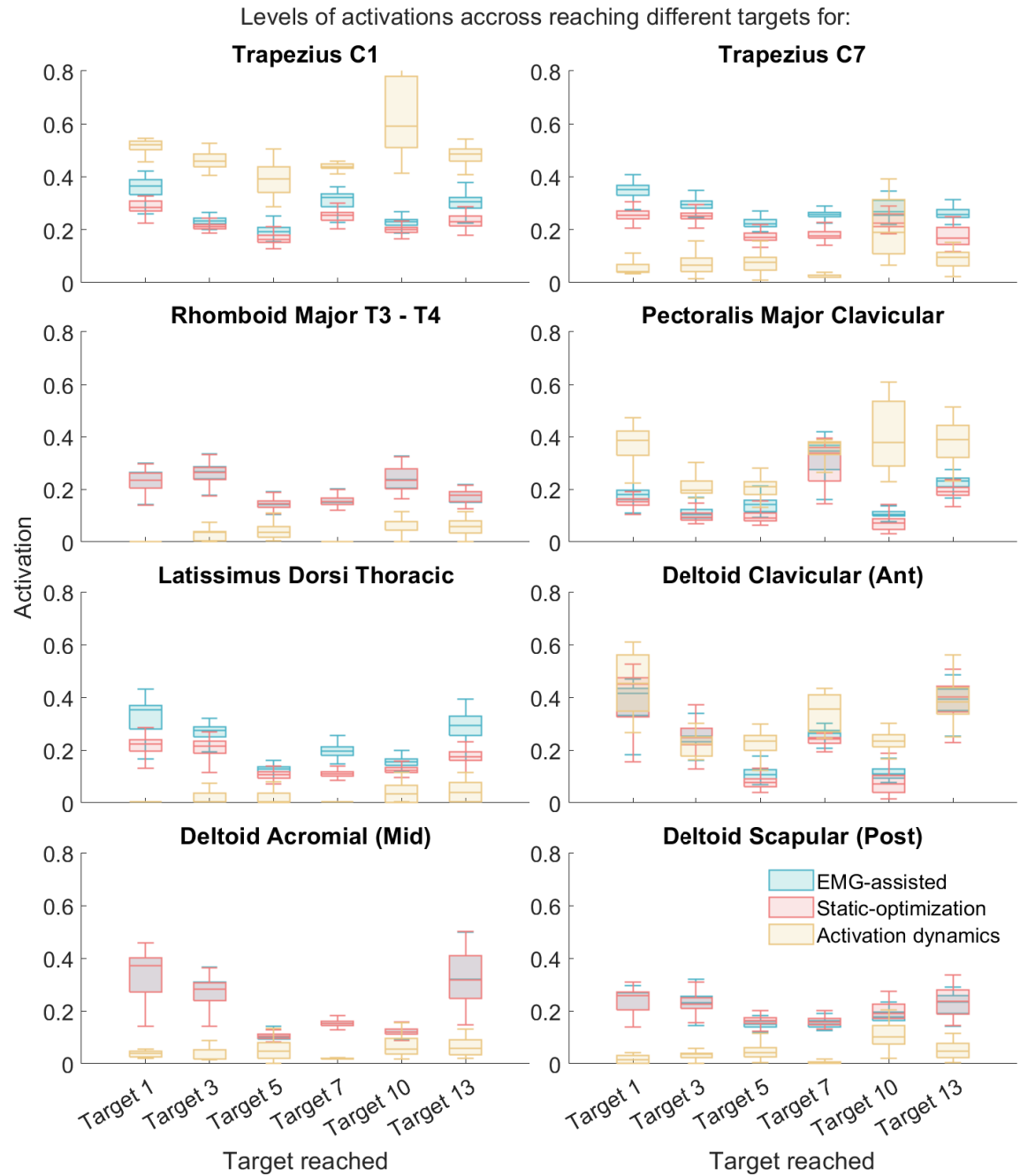
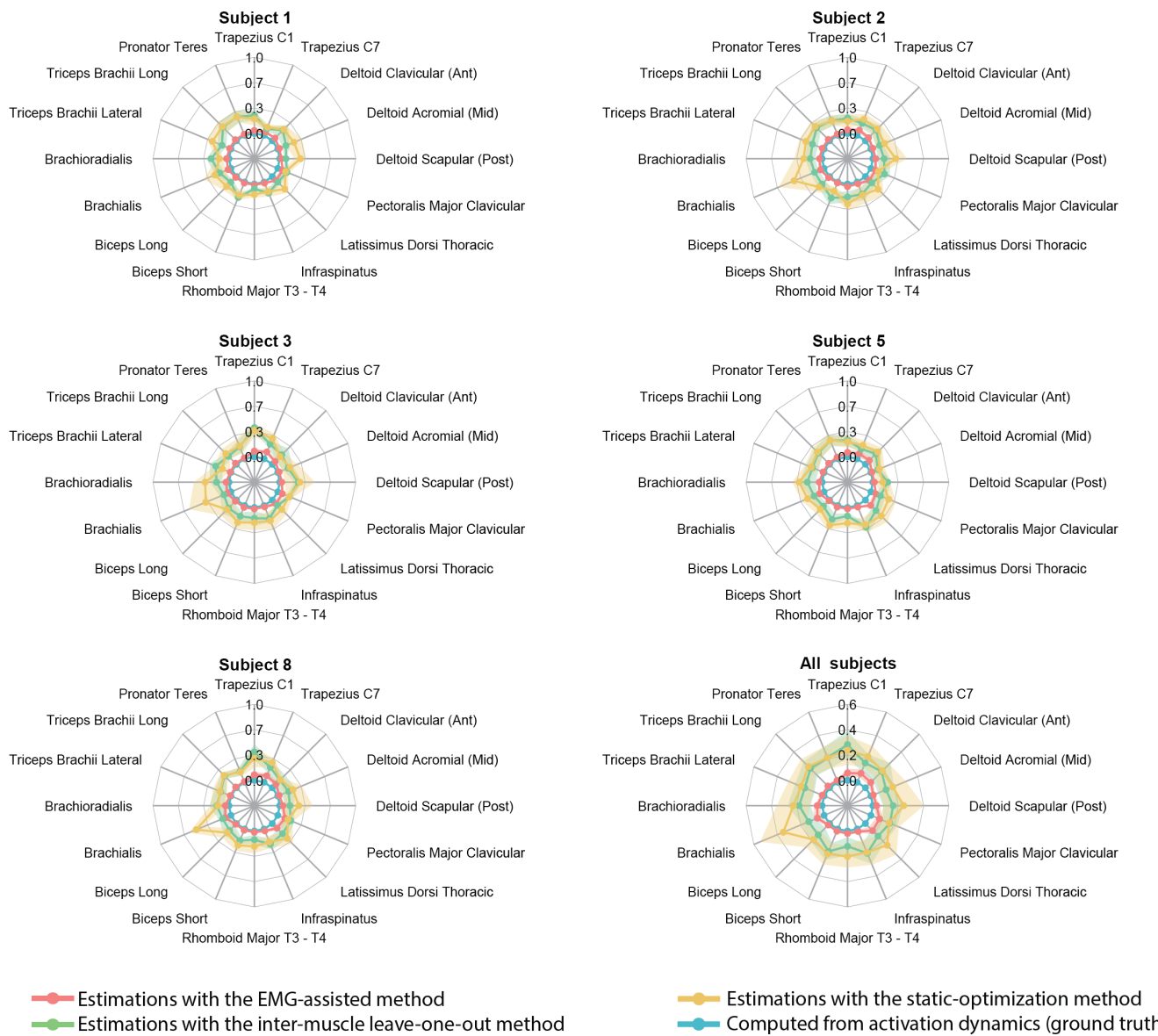


Figure A.9: Comparisons between the ranges of activations directly obtained from activation dynamics (blue boxplot), the estimated ones with the model including the recorded EMG (red boxplot) and the one from the model without using the recorded EMG (yellow boxplot) with respect to the reached target.



| | Subject 1 | Subject 2 | Subject 3 | Subject 5 | Subject 8 | All subjects |
|-------------------------------|-------------|-------------|-------------|-------------|-------------|--------------|
| Mean RMSE EMG-Assisted | 0.02 ± 0.00 | 0.02 ± 0.01 | 0.03 ± 0.00 | 0.03 ± 0.01 | 0.03 ± 0.01 | 0.03 ± 0.01 |
| Mean RMSE static-optimization | 0.19 ± 0.04 | 0.23 ± 0.07 | 0.23 ± 0.05 | 0.21 ± 0.05 | 0.22 ± 0.03 | 0.22 ± 0.08 |
| Mean RMSE leave-one-out | 0.15 ± 0.03 | 0.17 ± 0.04 | 0.18 ± 0.04 | 0.17 ± 0.05 | 0.17 ± 0.03 | 0.17 ± 0.02 |

Figure A.10: Spider maps of the root mean square errors of the computed estimation of the muscle activation through all targets reached and repetitions of all subjects (with the last one being the mean accross subjects). The figures show for each muscle with recorded EMG the errors between the activation directly obtained from the activation dynamics and, in red, the method using all the available muscle EMG signals in the EMG-assisted model (16 muscles out of 16). In green, using all EMG available excluding the specific muscle in the EMG-assisted model (15 muscles used out of 16), and without any EMG (in yellow) corresponding to the static-optimization.

A.2.2 Tables of RMSE between healthy and patients activations while reaching targets

Table A.2: Root mean squared errors between the means of healthy activations and the computed activations while reaching target 1 for each subjects. The RMSE reported for the healthy population corresponds to the mean of the RMSE of all healthy subject with respect to the means of activations of the overall healthy. A1 corresponds to the first assessment, A4 to the final one.

| Activations RMSE and standard deviations while reaching target 1 | | | | | | | |
|--|----------------|---------------|---------------|---------------|---------------|----------------|---------------|
| Target 1 | Healthy | S1 | | S2 | | S3 | |
| | | A1 | A4 | A1 | A4 | A1 | A4 |
| Subclavius | 0.031 ± 0.013 | 0.022 ± 0 | 0.041 ± 0.013 | 0.032 ± 0.011 | 0.035 ± 0.006 | 0.024 ± 0.001 | 0.035 ± 0.028 |
| Serratus Anterior Superior | 0.192 ± 0.08 | 0.126 ± 0 | 0.48 ± 0.158 | 0.142 ± 0.013 | 0.135 ± 0.001 | 0.134 ± 0.003 | 0.132 ± 0.005 |
| Serratus Anterior Middle | 0.271 ± 0.112 | 0.352 ± 0 | 0.148 ± 0.017 | 0.405 ± 0.036 | 0.315 ± 0.084 | 0.252 ± 0.003 | 0.259 ± 0.019 |
| Serratus Anterior Inferior | 0.182 ± 0.042 | 0.2 ± 0 | 0.124 ± 0.054 | 0.199 ± 0.041 | 0.202 ± 0.059 | 0.115 ± 0.006 | 0.259 ± 0.007 |
| Trapezius C1 | 0.125 ± 0.043 | 0.12 ± 0 | 0.114 ± 0.026 | 0.119 ± 0.04 | 0.175 ± 0.023 | 0.186 ± 0.001 | 0.184 ± 0.034 |
| Trapezius C7 | 0.152 ± 0.051 | 0.141 ± 0 | 0.093 ± 0.023 | 0.156 ± 0.024 | 0.184 ± 0.057 | 0.206 ± 0.011 | 0.16 ± 0.001 |
| Trapezius T1 | 0.24 ± 0.054 | 0.274 ± 0 | 0.158 ± 0.057 | 0.324 ± 0.048 | 0.23 ± 0.105 | 0.194 ± 0.028 | 0.194 ± 0.003 |
| Trapezius T2 - T7 | 0.138 ± 0.036 | 0.11 ± 0 | 0.159 ± 0.048 | 0.117 ± 0.017 | 0.133 ± 0.004 | 0.118 ± 0.011 | 0.072 ± 0.03 |
| Levator Scapulae | 0.167 ± 0.046 | 0.135 ± 0 | 0.086 ± 0.016 | 0.159 ± 0.05 | 0.144 ± 0.031 | 0.129 ± 0.008 | 0.165 ± 0.001 |
| Rhomboid Minor | 0.225 ± 0.052 | 0.243 ± 0 | 0.159 ± 0.064 | 0.22 ± 0.004 | 0.236 ± 0.016 | 0.196 ± 0.003 | 0.306 ± 0.01 |
| Rhomboid Major T1 - T2 | 0.317 ± 0.072 | 0.382 ± 0 | 0.299 ± 0.035 | 0.405 ± 0.028 | 0.332 ± 0.078 | 0.291 ± 0.006 | 0.214 ± 0.015 |
| Rhomboid Major T3 - T4 | 0.108 ± 0.038 | 0.144 ± 0 | 0.056 ± 0.001 | 0.117 ± 0.058 | 0.098 ± 0 | 0.1 ± 0 | 0.151 ± 0.01 |
| Pectoralis Minor | 0.056 ± 0.054 | 0.026 ± 0 | 0.049 ± 0.024 | 0.026 ± 0 | 0.026 ± 0 | 0.039 ± 0.003 | 0.029 ± 0.004 |
| Pectoralis Major Clavicular | 0.085 ± 0.027 | 0.109 ± 0 | 0.071 ± 0.002 | 0.071 ± 0.021 | 0.082 ± 0.025 | 0.068 ± 0.002 | 0.085 ± 0.001 |
| Pectoralis Major Sternal | 0.145 ± 0.052 | 0.128 ± 0 | 0.107 ± 0.004 | 0.169 ± 0.048 | 0.146 ± 0.068 | 0.115 ± 0.008 | 0.085 ± 0.03 |
| Pectoralis Major Ribs | 0.077 ± 0.07 | 0.033 ± 0 | 0.041 ± 0.005 | 0.034 ± 0 | 0.041 ± 0.01 | 0.055 ± 0.01 | 0.041 ± 0.001 |
| Latissimus Dorsi Thoracic | 0.141 ± 0.05 | 0.123 ± 0 | 0.067 ± 0.017 | 0.125 ± 0.029 | 0.159 ± 0.036 | 0.167 ± 0.008 | 0.17 ± 0.009 |
| Latissimus Dorsi Lumbar | 0.163 ± 0.077 | 0.127 ± 0 | 0.199 ± 0.089 | 0.079 ± 0.002 | 0.078 ± 0.001 | 0.079 ± 0 | 0.079 ± 0.002 |
| Latissimus Dorsi Iliac | 0.054 ± 0.042 | 0.034 ± 0 | 0.145 ± 0.127 | 0.026 ± 0.001 | 0.026 ± 0 | 0.026 ± 0 | 0.026 ± 0 |
| Deltoid Clavicular (Ant) | 0.131 ± 0.033 | 0.136 ± 0 | 0.12 ± 0.023 | 0.143 ± 0.012 | 0.176 ± 0.025 | 0.188 ± 0.007 | 0.212 ± 0.02 |
| Deltoid Acromial (Mid) | 0.101 ± 0.035 | 0.11 ± 0 | 0.072 ± 0.013 | 0.093 ± 0.001 | 0.151 ± 0.046 | 0.083 ± 0.008 | 0.172 ± 0.011 |
| Deltoid Scapular (Post) | 0.109 ± 0.056 | 0.069 ± 0 | 0.117 ± 0.018 | 0.153 ± 0.045 | 0.125 ± 0.025 | 0.127 ± 0.015 | 0.147 ± 0.029 |
| Supraspinatus | 0.24 ± 0.155 | 0.229 ± 0 | 0.592 ± 0.145 | 0.298 ± 0.079 | 0.36 ± 0.227 | 0.149 ± 0.007 | 0.372 ± 0.006 |
| Infraspinatus | 0.106 ± 0.032 | 0.107 ± 0 | 0.194 ± 0.048 | 0.136 ± 0.055 | 0.132 ± 0.046 | 0.168 ± 0.013 | 0.109 ± 0 |
| Subscapularis | 0.212 ± 0.166 | 0.145 ± 0 | 0.152 ± 0.006 | 0.225 ± 0.073 | 0.206 ± 0.002 | 0.149 ± 0.007 | 0.157 ± 0.007 |
| Teres Minor | 0.244 ± 0.105 | 0.192 ± 0 | 0.298 ± 0.177 | 0.25 ± 0.063 | 0.228 ± 0.074 | 0.166 ± 0 | 0.16 ± 0.001 |
| Teres Major | 0.405 ± 0.068 | 0.408 ± 0 | 0.396 ± 0.017 | 0.392 ± 0.02 | 0.375 ± 0.015 | 0.311 ± 0.016 | 0.381 ± 0.013 |
| Coracobrachialis | 0.268 ± 0.131 | 0.277 ± 0 | 0.262 ± 0.082 | 0.465 ± 0.099 | 0.477 ± 0.006 | 0.135 ± 0.007 | 0.16 ± 0.001 |
| Triceps Brachii Long | 0.182 ± 0.123 | 0.116 ± 0 | 0.107 ± 0.017 | 0.17 ± 0.019 | 0.149 ± 0.1 | 0.208 ± 0.011 | 0.237 ± 0.009 |
| Triceps Brachii Medial | 0.355 ± 0.05 | 0.351 ± 0 | 0.405 ± 0.043 | 0.426 ± 0.011 | 0.42 ± 0 | 0.386 ± 0.002 | 0.386 ± 0.002 |
| Triceps Brachii Lateral | 0.097 ± 0.049 | 0.157 ± 0 | 0.051 ± 0.009 | 0.268 ± 0.015 | 0.091 ± 0.046 | 0.064 ± 0.005 | 0.069 ± 0.003 |
| Biceps Short | 0.11 ± 0.043 | 0.086 ± 0 | 0.069 ± 0.012 | 0.175 ± 0.007 | 0.106 ± 0.029 | 0.148 ± 0.005 | 0.08 ± 0.004 |
| Biceps Long | 0.093 ± 0.034 | 0.155 ± 0 | 0.151 ± 0.012 | 0.145 ± 0.001 | 0.118 ± 0.02 | 0.117 ± 0.003 | 0.06 ± 0.001 |
| Brachialis | 0.121 ± 0.097 | 0.063 ± 0 | 0.109 ± 0.007 | 0.102 ± 0.055 | 0.13 ± 0.018 | 0.136 ± 0.007 | 0.142 ± 0.004 |
| Brachioradialis | 0.122 ± 0.073 | 0.056 ± 0 | 0.145 ± 0.025 | 0.11 ± 0.004 | 0.143 ± 0.085 | 0.135 ± 0.002 | 0.107 ± 0.018 |
| Supinator | 0.242 ± 0.068 | 0.201 ± 0 | 0.218 ± 0.018 | 0.311 ± 0.126 | 0.209 ± 0.001 | 0.257 ± 0.118 | 0.506 ± 0.014 |
| Pronator Teres | 0.1 ± 0.044 | 0.065 ± 0 | 0.101 ± 0.023 | 0.119 ± 0.01 | 0.086 ± 0.019 | 0.053 ± 0 | 0.115 ± 0.042 |
| Flexor Carpi Radialis | 0.136 ± 0.078 | 0.456 ± 0 | 0.1 ± 0.008 | 0.297 ± 0.026 | 0.555 ± 0.111 | 0.176 ± 0.01 | 0.094 ± 0.001 |
| Flexor Carpi Ulnaris | 0.357 ± 0.072 | 0.528 ± 0 | 0.466 ± 0.061 | 0.546 ± 0.03 | 0.489 ± 0.067 | 0.446 ± 0.046 | 0.46 ± 0.156 |
| Extensor Carpi Radialis Long | 0.35 ± 0.153 | 0.289 ± 0 | 0.449 ± 0.068 | 0.43 ± 0.096 | 0.284 ± 0.008 | 0.271 ± 0.004 | 0.398 ± 0.059 |
| Extensor Carpi Radialis Brevis | 0.379 ± 0.085 | 0.505 ± 0 | 0.549 ± 0.002 | 0.532 ± 0.012 | 0.445 ± 0.014 | 0.335 ± 0.036 | 0.55 ± 0.003 |
| Extensor Carpi Ulnaris | 0.201 ± 0.123 | 0.256 ± 0 | 0.511 ± 0.061 | 0.457 ± 0.057 | 0.143 ± 0.045 | 0.085 ± 0.001 | 0.253 ± 0.021 |
| Total | 0.179 ± 0.0957 | 0.185 ± 0.131 | 0.196 ± 0.155 | 0.218 ± 0.145 | 0.199 ± 0.133 | 0.161 ± 0.0947 | 0.19 ± 0.132 |

Table A.3: Root mean squared errors between the means of healthy activations and the computed activations while reaching target 3 for each subjects. The RMSE reported for the healthy population corresponds to the mean of the RMSE of all healthy subject with respect to the means of activations of the overall healthy. A1 corresponds to the first assessment, A4 to the final one.

Activations RMSE and standard deviations while reaching target 3

| Target 3 | Healthy | S1 | | S2 | | S3 | |
|--------------------------------|----------------------|----------------------|----------------------|---------------------|----------------------|----------------------|----------------------|
| | | A1 | A4 | A1 | A4 | A1 | A4 |
| Subclavius | 0.037 ± 0.016 | 0.039 ± 0 | 0.073 ± 0.01 | 0.078 ± 0.053 | 0.06 ± 0.011 | 0.033 ± 0.01 | 0.029 ± 0.006 |
| Serratus Anterior Superior | 0.325 ± 0.078 | 0.486 ± 0 | 0.406 ± 0.044 | 0.29 ± 0.018 | 0.225 ± 0.031 | 0.294 ± 0.008 | 0.319 ± 0 |
| Serratus Anterior Middle | 0.3 ± 0.126 | 0.379 ± 0 | 0.18 ± 0.046 | 0.259 ± 0.031 | 0.202 ± 0.003 | 0.248 ± 0.068 | 0.312 ± 0.008 |
| Serratus Anterior Inferior | 0.191 ± 0.045 | 0.256 ± 0 | 0.146 ± 0.027 | 0.182 ± 0.032 | 0.127 ± 0.004 | 0.218 ± 0.107 | 0.293 ± 0.088 |
| Trapezius C1 | 0.125 ± 0.071 | 0.177 ± 0 | 0.092 ± 0.015 | 0.109 ± 0.028 | 0.135 ± 0.022 | 0.135 ± 0.067 | 0.176 ± 0.008 |
| Trapezius C7 | 0.174 ± 0.095 | 0.178 ± 0 | 0.111 ± 0.016 | 0.11 ± 0.021 | 0.133 ± 0.017 | 0.149 ± 0.05 | 0.201 ± 0.034 |
| Trapezius T1 | 0.217 ± 0.053 | 0.26 ± 0 | 0.232 ± 0.012 | 0.217 ± 0.078 | 0.265 ± 0.022 | 0.227 ± 0.024 | 0.242 ± 0.044 |
| Trapezius T2 - T7 | 0.194 ± 0.08 | 0.319 ± 0 | 0.217 ± 0.003 | 0.166 ± 0.026 | 0.198 ± 0.015 | 0.138 ± 0.025 | 0.163 ± 0.067 |
| Levator Scapulae | 0.143 ± 0.056 | 0.219 ± 0 | 0.124 ± 0.048 | 0.094 ± 0.003 | 0.088 ± 0.005 | 0.077 ± 0.039 | 0.107 ± 0.001 |
| Rhomboid Minor | 0.199 ± 0.045 | 0.337 ± 0 | 0.16 ± 0.04 | 0.258 ± 0.017 | 0.206 ± 0.011 | 0.226 ± 0.129 | 0.348 ± 0.01 |
| Rhomboid Major T1 - T2 | 0.341 ± 0.091 | 0.278 ± 0 | 0.306 ± 0.039 | 0.368 ± 0.1 | 0.211 ± 0.043 | 0.241 ± 0.067 | 0.181 ± 0.081 |
| Rhomboid Major T3 - T4 | 0.117 ± 0.057 | 0.101 ± 0 | 0.073 ± 0.016 | 0.144 ± 0.096 | 0.08 ± 0.006 | 0.074 ± 0.032 | 0.15 ± 0.003 |
| Pectoralis Minor | 0.152 ± 0.137 | 0.321 ± 0 | 0.17 ± 0.085 | 0.088 ± 0.005 | 0.088 ± 0.002 | 0.084 ± 0.008 | 0.085 ± 0.002 |
| Pectoralis Major Clavicular | 0.055 ± 0.021 | 0.046 ± 0 | 0.054 ± 0.007 | 0.092 ± 0.036 | 0.048 ± 0.004 | 0.037 ± 0 | 0.035 ± 0.007 |
| Pectoralis Major Sternal | 0.112 ± 0.072 | 0.064 ± 0 | 0.067 ± 0.005 | 0.1 ± 0.009 | 0.109 ± 0.01 | 0.068 ± 0.016 | 0.071 ± 0.013 |
| Pectoralis Major Ribs | 0.04 ± 0.041 | 0.016 ± 0 | 0.029 ± 0.016 | 0.029 ± 0.008 | 0.037 ± 0.009 | 0.017 ± 0.002 | 0.036 ± 0.026 |
| Latissimus Dorsi Thoracic | 0.126 ± 0.043 | 0.111 ± 0 | 0.091 ± 0.006 | 0.117 ± 0.012 | 0.195 ± 0.005 | 0.136 ± 0.072 | 0.188 ± 0.002 |
| Latissimus Dorsi Lumbar | 0.371 ± 0.079 | 0.513 ± 0 | 0.376 ± 0.061 | 0.312 ± 0.007 | 0.299 ± 0.001 | 0.392 ± 0.146 | 0.296 ± 0.006 |
| Latissimus Dorsi Iliac | 0.206 ± 0.102 | 0.285 ± 0 | 0.259 ± 0.087 | 0.142 ± 0.006 | 0.144 ± 0.002 | 0.153 ± 0.016 | 0.144 ± 0.001 |
| Deltoid Clavicular (Ant) | 0.111 ± 0.041 | 0.141 ± 0 | 0.1 ± 0.021 | 0.145 ± 0.008 | 0.101 ± 0.02 | 0.117 ± 0.02 | 0.149 ± 0.002 |
| Deltoid Acromial (Mid) | 0.099 ± 0.037 | 0.187 ± 0 | 0.077 ± 0.016 | 0.091 ± 0.013 | 0.085 ± 0.014 | 0.086 ± 0.045 | 0.188 ± 0.02 |
| Deltoid Scapular (Post) | 0.168 ± 0.078 | 0.226 ± 0 | 0.062 ± 0.004 | 0.134 ± 0.01 | 0.084 ± 0.011 | 0.191 ± 0.109 | 0.253 ± 0.008 |
| Supraspinatus | 0.34 ± 0.086 | 0.459 ± 0 | 0.375 ± 0.016 | 0.294 ± 0.04 | 0.349 ± 0.049 | 0.336 ± 0.06 | 0.321 ± 0.022 |
| Infraspinatus | 0.127 ± 0.054 | 0.211 ± 0 | 0.091 ± 0.018 | 0.133 ± 0.017 | 0.108 ± 0.007 | 0.145 ± 0.069 | 0.21 ± 0.058 |
| Subscapularis | 0.306 ± 0.19 | 0.247 ± 0 | 0.234 ± 0.014 | 0.215 ± 0.016 | 0.207 ± 0.038 | 0.235 ± 0 | 0.184 ± 0.076 |
| Teres Minor | 0.248 ± 0.095 | 0.434 ± 0 | 0.223 ± 0.038 | 0.189 ± 0.021 | 0.191 ± 0.009 | 0.144 ± 0 | 0.185 ± 0.027 |
| Teres Major | 0.418 ± 0.057 | 0.41 ± 0 | 0.41 ± 0.038 | 0.515 ± 0.08 | 0.507 ± 0.033 | 0.341 ± 0.101 | 0.416 ± 0.066 |
| Coracobrachialis | 0.177 ± 0.112 | 0.101 ± 0 | 0.102 ± 0.006 | 0.268 ± 0.082 | 0.34 ± 0.009 | 0.094 ± 0.019 | 0.097 ± 0.015 |
| Triceps Brachii Long | 0.181 ± 0.114 | 0.172 ± 0 | 0.112 ± 0.006 | 0.138 ± 0.015 | 0.088 ± 0.015 | 0.202 ± 0.011 | 0.233 ± 0.003 |
| Triceps Brachii Medial | 0.261 ± 0.096 | 0.397 ± 0 | 0.355 ± 0.137 | 0.574 ± 0.129 | 0.22 ± 0.004 | 0.422 ± 0.126 | 0.557 ± 0.107 |
| Triceps Brachii Lateral | 0.11 ± 0.059 | 0.144 ± 0 | 0.064 ± 0.006 | 0.203 ± 0.01 | 0.092 ± 0.01 | 0.092 ± 0.005 | 0.065 ± 0.033 |
| Biceps Short | 0.086 ± 0.033 | 0.069 ± 0 | 0.067 ± 0.004 | 0.174 ± 0.059 | 0.09 ± 0.016 | 0.094 ± 0.006 | 0.085 ± 0.027 |
| Biceps Long | 0.098 ± 0.043 | 0.117 ± 0 | 0.128 ± 0.013 | 0.221 ± 0.081 | 0.185 ± 0.048 | 0.079 ± 0.036 | 0.058 ± 0.008 |
| Brachialis | 0.093 ± 0.092 | 0.124 ± 0 | 0.119 ± 0.006 | 0.18 ± 0.082 | 0.114 ± 0.004 | 0.125 ± 0.002 | 0.139 ± 0.009 |
| Brachioradialis | 0.141 ± 0.117 | 0.119 ± 0 | 0.091 ± 0.019 | 0.131 ± 0.034 | 0.076 ± 0.002 | 0.166 ± 0.026 | 0.131 ± 0.036 |
| Supinator | 0.265 ± 0.102 | 0.569 ± 0 | 0.216 ± 0.02 | 0.426 ± 0.005 | 0.224 ± 0 | 0.301 ± 0.075 | 0.391 ± 0.206 |
| Pronator Teres | 0.107 ± 0.054 | 0.103 ± 0 | 0.097 ± 0.01 | 0.182 ± 0.053 | 0.103 ± 0.012 | 0.042 ± 0.012 | 0.081 ± 0.052 |
| Flexor Carpi Radialis | 0.065 ± 0.037 | 0.172 ± 0 | 0.046 ± 0.016 | 0.142 ± 0.156 | 0.065 ± 0.003 | 0.066 ± 0.051 | 0.091 ± 0.069 |
| Flexor Carpi Ulnaris | 0.278 ± 0.124 | 0.691 ± 0 | 0.261 ± 0.066 | 0.663 ± 0.099 | 0.27 ± 0.04 | 0.421 ± 0.233 | 0.498 ± 0.173 |
| Extensor Carpi Radialis Long | 0.408 ± 0.084 | 0.366 ± 0 | 0.495 ± 0.022 | 0.398 ± 0.088 | 0.399 ± 0.061 | 0.42 ± 0.027 | 0.483 ± 0.073 |
| Extensor Carpi Radialis Brevis | 0.387 ± 0.095 | 0.374 ± 0 | 0.352 ± 0.004 | 0.341 ± 0.012 | 0.603 ± 0.013 | 0.355 ± 0.05 | 0.349 ± 0.001 |
| Extensor Carpi Ulnaris | 0.379 ± 0.069 | 0.39 ± 0 | 0.422 ± 0.037 | 0.383 ± 0.075 | 0.334 ± 0.002 | 0.252 ± 0.017 | 0.329 ± 0.005 |
| Total | 0.197 ± 0.109 | 0.253 ± 0.158 | 0.182 ± 0.126 | 0.221 ± 0.14 | 0.183 ± 0.124 | 0.183 ± 0.116 | 0.211 ± 0.133 |

Table A.4: Root mean squared errors between the means of healthy activations and the computed activations while reaching target 5 for each subjects. The RMSE reported for the healthy population corresponds to the mean of the RMSE of all healthy subject with respect to the means of activations of the overall healthy. A1 corresponds to the first assessment, A4 to the final one.

| Activations RMSE and standard deviations while reaching target 5 | | | | | | | |
|--|-----------------------|---------------------|----------------------|----------------------|----------------------|----------------------|---------------------|
| Target 5 | Healthy | S1 | | S2 | | S3 | |
| | | A1 | A4 | A1 | A4 | A1 | A4 |
| Subclavius | 0.067 ± 0.05 | 0.042 ± 0 | 0.073 ± 0.029 | 0.166 ± 0 | 0.118 ± 0.004 | 0.035 ± 0.005 | 0.045 ± 0.011 |
| Serratus Anterior Superior | 0.152 ± 0.105 | 0.101 ± 0 | 0.18 ± 0.055 | 0.161 ± 0 | 0.092 ± 0.001 | 0.092 ± 0.007 | 0.095 ± 0.001 |
| Serratus Anterior Middle | 0.152 ± 0.124 | 0.112 ± 0 | 0.073 ± 0.013 | 0.08 ± 0 | 0.062 ± 0.007 | 0.085 ± 0.02 | 0.113 ± 0.006 |
| Serratus Anterior Inferior | 0.177 ± 0.084 | 0.143 ± 0 | 0.112 ± 0.019 | 0.136 ± 0 | 0.112 ± 0.008 | 0.129 ± 0.027 | 0.101 ± 0.013 |
| Trapezius C1 | 0.079 ± 0.034 | 0.088 ± 0 | 0.053 ± 0.01 | 0.063 ± 0 | 0.06 ± 0.005 | 0.094 ± 0.013 | 0.116 ± 0.009 |
| Trapezius C7 | 0.122 ± 0.054 | 0.088 ± 0 | 0.067 ± 0.011 | 0.055 ± 0 | 0.081 ± 0.001 | 0.065 ± 0.025 | 0.062 ± 0.005 |
| Trapezius T1 | 0.203 ± 0.082 | 0.089 ± 0 | 0.144 ± 0.021 | 0.154 ± 0 | 0.186 ± 0.009 | 0.127 ± 0.05 | 0.153 ± 0.009 |
| Trapezius T2 - T7 | 0.159 ± 0.1 | 0.129 ± 0 | 0.088 ± 0.016 | 0.075 ± 0 | 0.111 ± 0.004 | 0.07 ± 0.033 | 0.07 ± 0.013 |
| Levator Scapulae | 0.119 ± 0.074 | 0.078 ± 0 | 0.077 ± 0.03 | 0.062 ± 0 | 0.059 ± 0.001 | 0.06 ± 0.007 | 0.076 ± 0.017 |
| Rhomboid Minor | 0.194 ± 0.101 | 0.176 ± 0 | 0.083 ± 0.015 | 0.095 ± 0 | 0.124 ± 0.002 | 0.116 ± 0.022 | 0.093 ± 0.007 |
| Rhomboid Major T1 - T2 | 0.269 ± 0.063 | 0.192 ± 0 | 0.156 ± 0.045 | 0.18 ± 0 | 0.227 ± 0.002 | 0.208 ± 0.014 | 0.361 ± 0.021 |
| Rhomboid Major T3 - T4 | 0.087 ± 0.044 | 0.038 ± 0 | 0.054 ± 0.01 | 0.139 ± 0 | 0.108 ± 0.001 | 0.059 ± 0.018 | 0.099 ± 0.016 |
| Pectoralis Minor | 0.085 ± 0.075 | 0.041 ± 0 | 0.047 ± 0.002 | 0.044 ± 0 | 0.04 ± 0.002 | 0.041 ± 0.001 | 0.04 ± 0 |
| Pectoralis Major Clavicular | 0.067 ± 0.028 | 0.026 ± 0 | 0.075 ± 0.024 | 0.171 ± 0 | 0.116 ± 0.008 | 0.045 ± 0.003 | 0.045 ± 0.003 |
| Pectoralis Major Sternal | 0.145 ± 0.089 | 0.074 ± 0 | 0.122 ± 0.006 | 0.107 ± 0 | 0.09 ± 0.008 | 0.079 ± 0.008 | 0.075 ± 0.027 |
| Pectoralis Major Ribs | 0.167 ± 0.18 | 0.096 ± 0 | 0.104 ± 0.01 | 0.101 ± 0 | 0.098 ± 0.004 | 0.092 ± 0.005 | 0.111 ± 0.009 |
| Latissimus Dorsi Thoracic | 0.084 ± 0.032 | 0.095 ± 0 | 0.083 ± 0.019 | 0.078 ± 0 | 0.169 ± 0.017 | 0.076 ± 0.007 | 0.11 ± 0 |
| Latissimus Dorsi Lumbar | 0.366 ± 0.08 | 0.403 ± 0 | 0.383 ± 0.053 | 0.396 ± 0 | 0.44 ± 0.015 | 0.35 ± 0.019 | 0.404 ± 0.004 |
| Latissimus Dorsi Iliac | 0.278 ± 0.131 | 0.235 ± 0 | 0.288 ± 0.099 | 0.233 ± 0 | 0.295 ± 0.014 | 0.2 ± 0.007 | 0.237 ± 0.001 |
| Deltoid Clavicular (Ant) | 0.076 ± 0.029 | 0.032 ± 0 | 0.043 ± 0.009 | 0.072 ± 0 | 0.064 ± 0.004 | 0.038 ± 0.006 | 0.076 ± 0.005 |
| Deltoid Acromial (Mid) | 0.067 ± 0.021 | 0.053 ± 0 | 0.101 ± 0.012 | 0.086 ± 0 | 0.074 ± 0.009 | 0.038 ± 0.002 | 0.042 ± 0 |
| Deltoid Scapular (Post) | 0.11 ± 0.085 | 0.094 ± 0 | 0.053 ± 0.009 | 0.087 ± 0 | 0.047 ± 0.004 | 0.108 ± 0.013 | 0.125 ± 0.004 |
| Supraspinatus | 0.191 ± 0.173 | 0.14 ± 0 | 0.166 ± 0.025 | 0.452 ± 0 | 0.134 ± 0.004 | 0.135 ± 0.003 | 0.132 ± 0.025 |
| Infraspinatus | 0.09 ± 0.021 | 0.054 ± 0 | 0.051 ± 0.004 | 0.069 ± 0 | 0.125 ± 0.012 | 0.052 ± 0.016 | 0.023 ± 0.004 |
| Subscapularis | 0.28 ± 0.13 | 0.291 ± 0 | 0.267 ± 0.009 | 0.263 ± 0 | 0.199 ± 0.043 | 0.233 ± 0.035 | 0.298 ± 0.001 |
| Teres Minor | 0.194 ± 0.088 | 0.128 ± 0 | 0.113 ± 0.02 | 0.139 ± 0 | 0.15 ± 0.002 | 0.089 ± 0.017 | 0.107 ± 0.011 |
| Teres Major | 0.353 ± 0.107 | 0.626 ± 0 | 0.362 ± 0.068 | 0.615 ± 0 | 0.404 ± 0.075 | 0.317 ± 0.056 | 0.612 ± 0.02 |
| Coracobrachialis | 0.148 ± 0.097 | 0.175 ± 0 | 0.095 ± 0.004 | 0.416 ± 0 | 0.136 ± 0.04 | 0.068 ± 0.026 | 0.068 ± 0.005 |
| Triceps Brachii Long | 0.164 ± 0.123 | 0.1 ± 0 | 0.081 ± 0.01 | 0.126 ± 0 | 0.063 ± 0.002 | 0.105 ± 0.031 | 0.147 ± 0.006 |
| Triceps Brachii Medial | 0.27 ± 0.1 | 0.331 ± 0 | 0.22 ± 0.037 | 0.52 ± 0 | 0.32 ± 0.007 | 0.259 ± 0.13 | 0.439 ± 0.041 |
| Triceps Brachii Lateral | 0.059 ± 0.037 | 0.068 ± 0 | 0.04 ± 0.01 | 0.094 ± 0 | 0.154 ± 0.038 | 0.049 ± 0.009 | 0.036 ± 0.015 |
| Biceps Short | 0.108 ± 0.092 | 0.053 ± 0 | 0.079 ± 0.009 | 0.051 ± 0 | 0.095 ± 0.001 | 0.13 ± 0.004 | 0.091 ± 0.008 |
| Biceps Long | 0.074 ± 0.04 | 0.118 ± 0 | 0.089 ± 0.022 | 0.15 ± 0 | 0.089 ± 0.014 | 0.074 ± 0.01 | 0.032 ± 0.005 |
| Brachialis | 0.177 ± 0.14 | 0.133 ± 0 | 0.174 ± 0.008 | 0.133 ± 0 | 0.149 ± 0.003 | 0.195 ± 0.002 | 0.197 ± 0.005 |
| Brachioradialis | 0.097 ± 0.063 | 0.034 ± 0 | 0.052 ± 0.018 | 0.148 ± 0 | 0.119 ± 0.038 | 0.128 ± 0.005 | 0.104 ± 0.015 |
| Supinator | 0.243 ± 0.108 | 0.2 ± 0 | 0.265 ± 0.057 | 0.488 ± 0 | 0.288 ± 0 | 0.267 ± 0.206 | 0.432 ± 0.036 |
| Pronator Teres | 0.106 ± 0.041 | 0.063 ± 0 | 0.129 ± 0.02 | 0.143 ± 0 | 0.052 ± 0.009 | 0.063 ± 0.01 | 0.089 ± 0.061 |
| Flexor Carpi Radialis | 0.152 ± 0.13 | 0.092 ± 0 | 0.094 ± 0.002 | 0.094 ± 0 | 0.09 ± 0.001 | 0.081 ± 0.01 | 0.095 ± 0 |
| Flexor Carpi Ulnaris | 0.325 ± 0.13 | 0.663 ± 0 | 0.236 ± 0.021 | 0.671 ± 0 | 0.314 ± 0.006 | 0.334 ± 0.089 | 0.514 ± 0.199 |
| Extensor Carpi Radialis Long | 0.367 ± 0.154 | 0.649 ± 0 | 0.631 ± 0.009 | 0.571 ± 0 | 0.551 ± 0.026 | 0.258 ± 0.034 | 0.437 ± 0.114 |
| Extensor Carpi Radialis Brevis | 0.367 ± 0.109 | 0.577 ± 0 | 0.571 ± 0.004 | 0.578 ± 0 | 0.443 ± 0.007 | 0.301 ± 0.03 | 0.576 ± 0.003 |
| Extensor Carpi Ulnaris | 0.25 ± 0.155 | 0.201 ± 0 | 0.21 ± 0.03 | 0.204 ± 0 | 0.198 ± 0.002 | 0.111 ± 0.029 | 0.192 ± 0.004 |
| Total | 0.172 ± 0.0929 | 0.17 ± 0.171 | 0.152 ± 0.133 | 0.206 ± 0.179 | 0.163 ± 0.122 | 0.13 ± 0.0901 | 0.173 ± 0.16 |

Table A.5: Root mean squared errors between the means of healthy activations and the computed activations while reaching target 7 for each subjects. The RMSE reported for the healthy population corresponds to the mean of the RMSE of all healthy subject with respect to the means of activations of the overall healthy. A1 corresponds to the first assessment, A4 to the final one.

| Activations RMSE and standard deviations while reaching target 7 | | | | | | | |
|--|-----------------------|---------------------|----------------------|----------------------|----------------------|----------------------|----------------------|
| Target 7 | Healthy | S1 | | S2 | | S3 | |
| | | A1 | A4 | A1 | A4 | A1 | A4 |
| Subclavius | 0.061 ± 0.018 | 0.088 ± 0 | 0.104 ± 0.017 | 0.075 ± 0 | 0.089 ± 0.014 | 0.033 ± 0.004 | 0.04 ± 0 |
| Serratus Anterior Superior | 0.148 ± 0.072 | 0.096 ± 0 | 0.166 ± 0.036 | 0.108 ± 0 | 0.105 ± 0.007 | 0.1 ± 0.013 | 0.102 ± 0.004 |
| Serratus Anterior Middle | 0.177 ± 0.123 | 0.097 ± 0 | 0.109 ± 0.013 | 0.169 ± 0 | 0.223 ± 0.167 | 0.125 ± 0.011 | 0.137 ± 0.01 |
| Serratus Anterior Inferior | 0.202 ± 0.094 | 0.221 ± 0 | 0.147 ± 0.026 | 0.304 ± 0 | 0.232 ± 0.113 | 0.157 ± 0.007 | 0.07 ± 0.02 |
| Trapezius C1 | 0.091 ± 0.034 | 0.15 ± 0 | 0.079 ± 0.006 | 0.097 ± 0 | 0.077 ± 0.008 | 0.126 ± 0.024 | 0.128 ± 0.004 |
| Trapezius C7 | 0.134 ± 0.053 | 0.11 ± 0 | 0.079 ± 0.012 | 0.092 ± 0 | 0.102 ± 0.034 | 0.077 ± 0 | 0.059 ± 0.005 |
| Trapezius T1 | 0.218 ± 0.108 | 0.178 ± 0 | 0.146 ± 0.031 | 0.289 ± 0 | 0.263 ± 0.187 | 0.12 ± 0.012 | 0.187 ± 0.023 |
| Trapezius T2 - T7 | 0.109 ± 0.03 | 0.083 ± 0 | 0.104 ± 0.022 | 0.106 ± 0 | 0.131 ± 0.037 | 0.073 ± 0.023 | 0.093 ± 0.018 |
| Levator Scapulae | 0.139 ± 0.075 | 0.094 ± 0 | 0.084 ± 0.006 | 0.118 ± 0 | 0.173 ± 0.1 | 0.087 ± 0.005 | 0.083 ± 0.003 |
| Rhomboid Minor | 0.211 ± 0.091 | 0.174 ± 0 | 0.135 ± 0.03 | 0.204 ± 0 | 0.267 ± 0.154 | 0.138 ± 0.015 | 0.095 ± 0.011 |
| Rhomboid Major T1 - T2 | 0.311 ± 0.071 | 0.423 ± 0 | 0.244 ± 0.029 | 0.434 ± 0 | 0.331 ± 0.042 | 0.256 ± 0.009 | 0.267 ± 0.033 |
| Rhomboid Major T3 - T4 | 0.092 ± 0.047 | 0.173 ± 0 | 0.043 ± 0.006 | 0.116 ± 0 | 0.064 ± 0.036 | 0.063 ± 0.034 | 0.116 ± 0.008 |
| Pectoralis Minor | 0.06 ± 0.052 | 0.029 ± 0 | 0.038 ± 0.01 | 0.029 ± 0 | 0.034 ± 0.004 | 0.028 ± 0.001 | 0.029 ± 0 |
| Pectoralis Major Clavicular | 0.122 ± 0.039 | 0.141 ± 0 | 0.092 ± 0.006 | 0.132 ± 0 | 0.154 ± 0.051 | 0.165 ± 0.024 | 0.18 ± 0.001 |
| Pectoralis Major Sternal | 0.157 ± 0.073 | 0.162 ± 0 | 0.139 ± 0.018 | 0.129 ± 0 | 0.159 ± 0.08 | 0.095 ± 0.003 | 0.098 ± 0.028 |
| Pectoralis Major Ribs | 0.125 ± 0.096 | 0.071 ± 0 | 0.068 ± 0.007 | 0.081 ± 0 | 0.077 ± 0.011 | 0.078 ± 0.02 | 0.076 ± 0.009 |
| Latissimus Dorsi Thoracic | 0.088 ± 0.036 | 0.086 ± 0 | 0.065 ± 0.009 | 0.136 ± 0 | 0.136 ± 0.007 | 0.079 ± 0.008 | 0.082 ± 0.004 |
| Latissimus Dorsi Lumbar | 0.126 ± 0.076 | 0.141 ± 0 | 0.335 ± 0.077 | 0.087 ± 0 | 0.096 ± 0.037 | 0.25 ± 0.208 | 0.063 ± 0.002 |
| Latissimus Dorsi Iliac | 0.12 ± 0.165 | 0.07 ± 0 | 0.232 ± 0.082 | 0.068 ± 0 | 0.07 ± 0.006 | 0.066 ± 0.001 | 0.066 ± 0.001 |
| Deltoid Clavicular (Ant) | 0.109 ± 0.056 | 0.144 ± 0 | 0.06 ± 0.009 | 0.134 ± 0 | 0.125 ± 0.048 | 0.107 ± 0 | 0.137 ± 0 |
| Deltoid Acromial (Mid) | 0.086 ± 0.024 | 0.174 ± 0 | 0.06 ± 0.018 | 0.144 ± 0 | 0.129 ± 0.101 | 0.045 ± 0 | 0.034 ± 0.005 |
| Deltoid Scapular (Post) | 0.078 ± 0.035 | 0.054 ± 0 | 0.109 ± 0.016 | 0.137 ± 0 | 0.083 ± 0.051 | 0.051 ± 0.018 | 0.072 ± 0.001 |
| Supraspinatus | 0.232 ± 0.155 | 0.18 ± 0 | 0.209 ± 0.044 | 0.222 ± 0 | 0.172 ± 0.012 | 0.181 ± 0.007 | 0.154 ± 0 |
| Infraspinatus | 0.071 ± 0.033 | 0.105 ± 0 | 0.108 ± 0.019 | 0.154 ± 0 | 0.11 ± 0.084 | 0.056 ± 0.014 | 0.035 ± 0.003 |
| Subscapularis | 0.233 ± 0.132 | 0.194 ± 0 | 0.163 ± 0.018 | 0.301 ± 0 | 0.245 ± 0.005 | 0.164 ± 0.004 | 0.25 ± 0.002 |
| Teres Minor | 0.067 ± 0.029 | 0.042 ± 0 | 0.073 ± 0.025 | 0.038 ± 0 | 0.097 ± 0.074 | 0.058 ± 0.003 | 0.046 ± 0.007 |
| Teres Major | 0.363 ± 0.051 | 0.349 ± 0 | 0.354 ± 0.058 | 0.339 ± 0 | 0.33 ± 0.018 | 0.541 ± 0.028 | 0.32 ± 0.013 |
| Coracobrachialis | 0.219 ± 0.125 | 0.591 ± 0 | 0.215 ± 0.038 | 0.508 ± 0 | 0.386 ± 0.217 | 0.148 ± 0.011 | 0.136 ± 0.019 |
| Triceps Brachii Long | 0.125 ± 0.081 | 0.048 ± 0 | 0.052 ± 0.006 | 0.107 ± 0 | 0.095 ± 0.063 | 0.083 ± 0.024 | 0.122 ± 0.011 |
| Triceps Brachii Medial | 0.307 ± 0.092 | 0.35 ± 0 | 0.302 ± 0.044 | 0.346 ± 0 | 0.436 ± 0.021 | 0.247 ± 0.029 | 0.267 ± 0.024 |
| Triceps Brachii Lateral | 0.071 ± 0.041 | 0.162 ± 0 | 0.04 ± 0.008 | 0.183 ± 0 | 0.168 ± 0.091 | 0.077 ± 0.002 | 0.052 ± 0.007 |
| Biceps Short | 0.097 ± 0.051 | 0.118 ± 0 | 0.062 ± 0.008 | 0.153 ± 0 | 0.087 ± 0.04 | 0.107 ± 0.007 | 0.063 ± 0.01 |
| Biceps Long | 0.068 ± 0.04 | 0.185 ± 0 | 0.104 ± 0.031 | 0.183 ± 0 | 0.222 ± 0.072 | 0.065 ± 0.008 | 0.029 ± 0.003 |
| Brachialis | 0.101 ± 0.059 | 0.054 ± 0 | 0.082 ± 0.006 | 0.11 ± 0 | 0.081 ± 0.01 | 0.093 ± 0.004 | 0.09 ± 0.004 |
| Brachioradialis | 0.106 ± 0.068 | 0.043 ± 0 | 0.067 ± 0.009 | 0.144 ± 0 | 0.178 ± 0.055 | 0.164 ± 0.004 | 0.117 ± 0.018 |
| Supinator | 0.223 ± 0.07 | 0.263 ± 0 | 0.225 ± 0.027 | 0.282 ± 0 | 0.255 ± 0.002 | 0.228 ± 0.124 | 0.508 ± 0.002 |
| Pronator Teres | 0.109 ± 0.034 | 0.063 ± 0 | 0.132 ± 0.02 | 0.146 ± 0 | 0.064 ± 0.001 | 0.057 ± 0.002 | 0.093 ± 0.07 |
| Flexor Carpi Radialis | 0.079 ± 0.054 | 0.09 ± 0 | 0.046 ± 0.004 | 0.072 ± 0 | 0.205 ± 0.223 | 0.044 ± 0.004 | 0.049 ± 0.006 |
| Flexor Carpi Ulnaris | 0.333 ± 0.061 | 0.594 ± 0 | 0.313 ± 0.007 | 0.596 ± 0 | 0.34 ± 0.051 | 0.386 ± 0.011 | 0.442 ± 0.216 |
| Extensor Carpi Radialis Long | 0.238 ± 0.169 | 0.595 ± 0 | 0.783 ± 0.006 | 0.645 ± 0 | 0.483 ± 0.023 | 0.133 ± 0.007 | 0.542 ± 0.022 |
| Extensor Carpi Radialis Brevis | 0.349 ± 0.085 | 0.395 ± 0 | 0.396 ± 0.003 | 0.398 ± 0 | 0.563 ± 0.023 | 0.353 ± 0.088 | 0.396 ± 0.001 |
| Extensor Carpi Ulnaris | 0.241 ± 0.167 | 0.18 ± 0 | 0.243 ± 0.058 | 0.201 ± 0 | 0.202 ± 0.013 | 0.111 ± 0 | 0.185 ± 0.004 |
| Total | 0.157 ± 0.0858 | 0.18 ± 0.149 | 0.157 ± 0.137 | 0.198 ± 0.145 | 0.187 ± 0.122 | 0.134 ± 0.103 | 0.145 ± 0.128 |

Table A.6: Root mean squared errors between the means of healthy activations and the computed activations while reaching target 10 for each subjects. The RMSE reported for the healthy population corresponds to the mean of the RMSE of all healthy subject with respect to the means of activations of the overall healthy. A1 corresponds to the first assessment, A4 to the final one.

| Activations RMSE and standard deviations while reaching target 10 | | | | | | | |
|---|----------------------|----------------------|----------------------|----------------------|----------------------|---------------------|----------------------|
| Target 10 | Healthy | S1 | | S2 | | S3 | |
| | | A1 | A4 | A1 | A4 | A1 | A4 |
| Subclavius | 0.043 ± 0.02 | 0.095 ± 0 | 0.075 ± 0.038 | 0.058 ± 0 | 0.115 ± 0.024 | 0.04 ± 0.026 | 0.021 ± 0.007 |
| Serratus Anterior Superior | 0.145 ± 0.084 | 0.136 ± 0 | 0.247 ± 0.12 | 0.087 ± 0 | 0.119 ± 0.027 | 0.082 ± 0.005 | 0.083 ± 0.005 |
| Serratus Anterior Middle | 0.164 ± 0.082 | 0.096 ± 0 | 0.106 ± 0.052 | 0.091 ± 0 | 0.106 ± 0.007 | 0.096 ± 0.014 | 0.106 ± 0.013 |
| Serratus Anterior Inferior | 0.228 ± 0.048 | 0.138 ± 0 | 0.195 ± 0.09 | 0.201 ± 0 | 0.292 ± 0.006 | 0.228 ± 0.011 | 0.207 ± 0.046 |
| Trapezius C1 | 0.104 ± 0.035 | 0.124 ± 0 | 0.108 ± 0.033 | 0.082 ± 0 | 0.099 ± 0.052 | 0.096 ± 0.041 | 0.095 ± 0.004 |
| Trapezius C7 | 0.131 ± 0.059 | 0.128 ± 0 | 0.088 ± 0.018 | 0.09 ± 0 | 0.157 ± 0.005 | 0.136 ± 0.002 | 0.1 ± 0.008 |
| Trapezius T1 | 0.238 ± 0.044 | 0.134 ± 0 | 0.191 ± 0.076 | 0.275 ± 0 | 0.399 ± 0.043 | 0.221 ± 0.099 | 0.226 ± 0.064 |
| Trapezius T2 - T7 | 0.145 ± 0.069 | 0.136 ± 0 | 0.15 ± 0.044 | 0.108 ± 0 | 0.155 ± 0.001 | 0.131 ± 0.009 | 0.105 ± 0.008 |
| Levator Scapulae | 0.14 ± 0.086 | 0.077 ± 0 | 0.075 ± 0.013 | 0.073 ± 0 | 0.107 ± 0.003 | 0.094 ± 0.004 | 0.089 ± 0.002 |
| Rhomboid Minor | 0.214 ± 0.065 | 0.129 ± 0 | 0.155 ± 0.093 | 0.132 ± 0 | 0.279 ± 0.007 | 0.197 ± 0.007 | 0.165 ± 0.001 |
| Rhomboid Major T1 - T2 | 0.289 ± 0.056 | 0.2 ± 0 | 0.243 ± 0.029 | 0.214 ± 0 | 0.358 ± 0.023 | 0.208 ± 0.071 | 0.229 ± 0.013 |
| Rhomboid Major T3 - T4 | 0.118 ± 0.039 | 0.098 ± 0 | 0.076 ± 0.015 | 0.064 ± 0 | 0.11 ± 0.029 | 0.061 ± 0.017 | 0.142 ± 0.005 |
| Pectoralis Minor | 0.074 ± 0.069 | 0.036 ± 0 | 0.044 ± 0.016 | 0.041 ± 0 | 0.043 ± 0.012 | 0.033 ± 0.002 | 0.034 ± 0.001 |
| Pectoralis Major Clavicular | 0.063 ± 0.023 | 0.055 ± 0 | 0.07 ± 0.014 | 0.058 ± 0 | 0.125 ± 0.032 | 0.036 ± 0.007 | 0.039 ± 0.007 |
| Pectoralis Major Sternal | 0.113 ± 0.042 | 0.118 ± 0 | 0.09 ± 0.002 | 0.11 ± 0 | 0.077 ± 0.002 | 0.082 ± 0.024 | 0.073 ± 0.028 |
| Pectoralis Major Ribs | 0.275 ± 0.133 | 0.202 ± 0 | 0.196 ± 0.002 | 0.195 ± 0 | 0.205 ± 0.02 | 0.188 ± 0.001 | 0.195 ± 0 |
| Latissimus Dorsi Thoracic | 0.097 ± 0.036 | 0.1 ± 0 | 0.087 ± 0.024 | 0.099 ± 0 | 0.099 ± 0.011 | 0.086 ± 0.023 | 0.094 ± 0.011 |
| Latissimus Dorsi Lumbar | 0.391 ± 0.062 | 0.497 ± 0 | 0.525 ± 0.049 | 0.287 ± 0 | 0.416 ± 0.094 | 0.33 ± 0.035 | 0.346 ± 0.025 |
| Latissimus Dorsi Iliac | 0.327 ± 0.119 | 0.44 ± 0 | 0.578 ± 0.053 | 0.227 ± 0 | 0.275 ± 0.032 | 0.2 ± 0.058 | 0.245 ± 0.006 |
| Deltoid Clavicular (Ant) | 0.086 ± 0.024 | 0.106 ± 0 | 0.057 ± 0.012 | 0.105 ± 0 | 0.071 ± 0.008 | 0.047 ± 0.019 | 0.058 ± 0.003 |
| Deltoid Acromial (Mid) | 0.092 ± 0.03 | 0.097 ± 0 | 0.172 ± 0.043 | 0.074 ± 0 | 0.097 ± 0.015 | 0.042 ± 0.003 | 0.038 ± 0.001 |
| Deltoid Scapular (Post) | 0.131 ± 0.054 | 0.123 ± 0 | 0.16 ± 0.057 | 0.102 ± 0 | 0.064 ± 0.001 | 0.088 ± 0.064 | 0.121 ± 0.026 |
| Supraspinatus | 0.395 ± 0.08 | 0.398 ± 0 | 0.403 ± 0.076 | 0.293 ± 0 | 0.395 ± 0.021 | 0.393 ± 0.038 | 0.303 ± 0.044 |
| Infraspinatus | 0.111 ± 0.033 | 0.126 ± 0 | 0.086 ± 0.041 | 0.067 ± 0 | 0.117 ± 0.031 | 0.108 ± 0.002 | 0.069 ± 0.002 |
| Subscapularis | 0.36 ± 0.082 | 0.468 ± 0 | 0.39 ± 0.097 | 0.51 ± 0 | 0.358 ± 0.093 | 0.473 ± 0.021 | 0.512 ± 0.022 |
| Teres Minor | 0.11 ± 0.062 | 0.172 ± 0 | 0.126 ± 0.076 | 0.061 ± 0 | 0.106 ± 0.037 | 0.092 ± 0.042 | 0.06 ± 0.008 |
| Teres Major | 0.427 ± 0.063 | 0.459 ± 0 | 0.457 ± 0.024 | 0.422 ± 0 | 0.406 ± 0.044 | 0.357 ± 0.108 | 0.43 ± 0.079 |
| Coracobrachialis | 0.127 ± 0.077 | 0.079 ± 0 | 0.08 ± 0.01 | 0.33 ± 0 | 0.101 ± 0.029 | 0.065 ± 0.017 | 0.197 ± 0.053 |
| Triceps Brachii Long | 0.179 ± 0.087 | 0.151 ± 0 | 0.087 ± 0.011 | 0.169 ± 0 | 0.129 ± 0.003 | 0.144 ± 0.037 | 0.188 ± 0.01 |
| Triceps Brachii Medial | 0.251 ± 0.069 | 0.23 ± 0 | 0.207 ± 0.037 | 0.411 ± 0 | 0.321 ± 0.015 | 0.306 ± 0.253 | 0.454 ± 0.109 |
| Triceps Brachii Lateral | 0.14 ± 0.051 | 0.138 ± 0 | 0.078 ± 0.025 | 0.148 ± 0 | 0.16 ± 0.025 | 0.127 ± 0.009 | 0.114 ± 0.014 |
| Biceps Short | 0.161 ± 0.06 | 0.15 ± 0 | 0.08 ± 0.01 | 0.16 ± 0 | 0.182 ± 0.003 | 0.203 ± 0.003 | 0.158 ± 0.012 |
| Biceps Long | 0.147 ± 0.068 | 0.181 ± 0 | 0.116 ± 0.042 | 0.14 ± 0 | 0.126 ± 0.019 | 0.163 ± 0.019 | 0.118 ± 0.014 |
| Brachialis | 0.192 ± 0.08 | 0.285 ± 0 | 0.255 ± 0.011 | 0.271 ± 0 | 0.3 ± 0.001 | 0.314 ± 0.001 | 0.311 ± 0.004 |
| Brachioradialis | 0.181 ± 0.058 | 0.197 ± 0 | 0.189 ± 0.032 | 0.246 ± 0 | 0.182 ± 0.019 | 0.243 ± 0.015 | 0.228 ± 0.016 |
| Supinator | 0.192 ± 0.078 | 0.136 ± 0 | 0.166 ± 0.026 | 0.29 ± 0 | 0.171 ± 0.028 | 0.153 ± 0.069 | 0.518 ± 0.068 |
| Pronator Teres | 0.128 ± 0.057 | 0.061 ± 0 | 0.077 ± 0.011 | 0.148 ± 0 | 0.06 ± 0.003 | 0.086 ± 0.047 | 0.08 ± 0.004 |
| Flexor Carpi Radialis | 0.221 ± 0.158 | 0.124 ± 0 | 0.137 ± 0.003 | 0.134 ± 0 | 0.133 ± 0.011 | 0.12 ± 0.008 | 0.135 ± 0.006 |
| Flexor Carpi Ulnaris | 0.386 ± 0.086 | 0.572 ± 0 | 0.352 ± 0.019 | 0.508 ± 0 | 0.357 ± 0.026 | 0.363 ± 0.122 | 0.577 ± 0.018 |
| Extensor Carpi Radialis Long | 0.399 ± 0.116 | 0.397 ± 0 | 0.401 ± 0.01 | 0.334 ± 0 | 0.442 ± 0.03 | 0.517 ± 0.004 | 0.269 ± 0.011 |
| Extensor Carpi Radialis Brevis | 0.407 ± 0.077 | 0.449 ± 0 | 0.404 ± 0.03 | 0.376 ± 0 | 0.475 ± 0.066 | 0.313 ± 0.046 | 0.432 ± 0.015 |
| Extensor Carpi Ulnaris | 0.414 ± 0.09 | 0.476 ± 0 | 0.501 ± 0.057 | 0.323 ± 0 | 0.347 ± 0.002 | 0.278 ± 0.03 | 0.375 ± 0.003 |
| Total | 0.203 ± 0.113 | 0.203 ± 0.146 | 0.197 ± 0.145 | 0.193 ± 0.128 | 0.206 ± 0.127 | 0.18 ± 0.123 | 0.198 ± 0.148 |

Table A.7: Root mean squared errors between the means of healthy activations and the computed activations while reaching target 13 for each subjects. The RMSE reported for the healthy population corresponds to the mean of the RMSE of all healthy subject with respect to the means of activations of the overall healthy. A1 corresponds to the first assessment, A4 to the final one.

| Activations RMSE and standard deviations while reaching target 13 | | | | | | | |
|---|-----------------------|----------------------|----------------------|---------------------|----------------------|----------------------|----------------------|
| Target 13 | Healthy | S1 | | S2 | | S3 | |
| | | A1 | A4 | A1 | A4 | A1 | A4 |
| Subclavius | 0.039 ± 0.015 | 0.066 ± 0 | 0.063 ± 0.013 | 0.052 ± 0 | 0.05 ± 0.011 | 0.032 ± 0.015 | 0.045 ± 0.001 |
| Serratus Anterior Superior | 0.168 ± 0.095 | 0.142 ± 0 | 0.168 ± 0.034 | 0.117 ± 0 | 0.134 ± 0.021 | 0.11 ± 0.006 | 0.114 ± 0 |
| Serratus Anterior Middle | 0.259 ± 0.087 | 0.262 ± 0 | 0.188 ± 0.047 | 0.207 ± 0 | 0.309 ± 0.097 | 0.254 ± 0.004 | 0.236 ± 0.022 |
| Serratus Anterior Inferior | 0.186 ± 0.039 | 0.173 ± 0 | 0.145 ± 0.022 | 0.158 ± 0 | 0.177 ± 0.031 | 0.308 ± 0.021 | 0.142 ± 0.008 |
| Trapezius C1 | 0.107 ± 0.021 | 0.175 ± 0 | 0.111 ± 0.025 | 0.083 ± 0 | 0.1 ± 0.024 | 0.19 ± 0.004 | 0.161 ± 0.002 |
| Trapezius C7 | 0.123 ± 0.041 | 0.127 ± 0 | 0.128 ± 0.01 | 0.069 ± 0 | 0.154 ± 0.066 | 0.119 ± 0.001 | 0.129 ± 0.005 |
| Trapezius T1 | 0.246 ± 0.062 | 0.188 ± 0 | 0.206 ± 0.054 | 0.248 ± 0 | 0.282 ± 0.067 | 0.183 ± 0.027 | 0.202 ± 0.032 |
| Trapezius T2 - T7 | 0.124 ± 0.031 | 0.094 ± 0 | 0.128 ± 0.025 | 0.107 ± 0 | 0.179 ± 0.002 | 0.077 ± 0.003 | 0.1 ± 0.009 |
| Levator Scapulae | 0.173 ± 0.075 | 0.127 ± 0 | 0.119 ± 0.019 | 0.12 ± 0 | 0.193 ± 0.026 | 0.142 ± 0.005 | 0.134 ± 0.022 |
| Rhomboid Minor | 0.23 ± 0.06 | 0.202 ± 0 | 0.154 ± 0.02 | 0.158 ± 0 | 0.239 ± 0.065 | 0.28 ± 0.014 | 0.183 ± 0.003 |
| Rhomboid Major T1 - T2 | 0.319 ± 0.059 | 0.294 ± 0 | 0.263 ± 0.05 | 0.331 ± 0 | 0.315 ± 0.065 | 0.325 ± 0.025 | 0.295 ± 0.01 |
| Rhomboid Major T3 - T4 | 0.096 ± 0.029 | 0.092 ± 0 | 0.058 ± 0.006 | 0.063 ± 0 | 0.082 ± 0.002 | 0.052 ± 0.013 | 0.122 ± 0.003 |
| Pectoralis Minor | 0.06 ± 0.058 | 0.034 ± 0 | 0.029 ± 0.002 | 0.029 ± 0 | 0.029 ± 0.001 | 0.029 ± 0.001 | 0.029 ± 0 |
| Pectoralis Major Clavicular | 0.107 ± 0.03 | 0.144 ± 0 | 0.081 ± 0.02 | 0.066 ± 0 | 0.087 ± 0.002 | 0.102 ± 0.003 | 0.118 ± 0.015 |
| Pectoralis Major Sternal | 0.147 ± 0.052 | 0.121 ± 0 | 0.164 ± 0.039 | 0.172 ± 0 | 0.246 ± 0.011 | 0.114 ± 0.001 | 0.118 ± 0.008 |
| Pectoralis Major Ribs | 0.038 ± 0.022 | 0.042 ± 0 | 0.045 ± 0.012 | 0.049 ± 0 | 0.022 ± 0.006 | 0.035 ± 0.004 | 0.04 ± 0.01 |
| Latissimus Dorsi Thoracic | 0.135 ± 0.044 | 0.16 ± 0 | 0.061 ± 0.009 | 0.084 ± 0 | 0.094 ± 0.017 | 0.16 ± 0.001 | 0.15 ± 0.001 |
| Latissimus Dorsi Lumbar | 0.127 ± 0.063 | 0.131 ± 0 | 0.237 ± 0.132 | 0.072 ± 0 | 0.075 ± 0.002 | 0.218 ± 0.103 | 0.072 ± 0 |
| Latissimus Dorsi Iliac | 0.039 ± 0.02 | 0.092 ± 0 | 0.148 ± 0.126 | 0.021 ± 0 | 0.021 ± 0.001 | 0.037 ± 0.015 | 0.021 ± 0 |
| Deltoid Clavicular (Ant) | 0.116 ± 0.041 | 0.232 ± 0 | 0.089 ± 0.018 | 0.123 ± 0 | 0.127 ± 0.008 | 0.257 ± 0.011 | 0.224 ± 0.002 |
| Deltoid Acromial (Mid) | 0.093 ± 0.029 | 0.165 ± 0 | 0.065 ± 0.019 | 0.07 ± 0 | 0.125 ± 0.028 | 0.146 ± 0.009 | 0.154 ± 0.003 |
| Deltoid Scapular (Post) | 0.115 ± 0.055 | 0.102 ± 0 | 0.131 ± 0.009 | 0.102 ± 0 | 0.121 ± 0.008 | 0.101 ± 0.026 | 0.119 ± 0 |
| Supraspinatus | 0.161 ± 0.055 | 0.635 ± 0 | 0.171 ± 0.037 | 0.261 ± 0 | 0.131 ± 0.009 | 0.116 ± 0.01 | 0.61 ± 0.021 |
| Infraspinatus | 0.083 ± 0.024 | 0.078 ± 0 | 0.158 ± 0.048 | 0.1 ± 0 | 0.136 ± 0.076 | 0.105 ± 0.006 | 0.068 ± 0.011 |
| Subscapularis | 0.116 ± 0.041 | 0.158 ± 0 | 0.256 ± 0.054 | 0.204 ± 0 | 0.148 ± 0.102 | 0.064 ± 0.014 | 0.234 ± 0.047 |
| Teres Minor | 0.174 ± 0.076 | 0.116 ± 0 | 0.146 ± 0.016 | 0.116 ± 0 | 0.163 ± 0.014 | 0.112 ± 0.002 | 0.113 ± 0.001 |
| Teres Major | 0.356 ± 0.091 | 0.224 ± 0 | 0.339 ± 0.078 | 0.316 ± 0 | 0.305 ± 0.005 | 0.524 ± 0.016 | 0.324 ± 0.005 |
| Coracobrachialis | 0.304 ± 0.091 | 0.209 ± 0 | 0.303 ± 0.047 | 0.311 ± 0 | 0.392 ± 0.054 | 0.309 ± 0.08 | 0.281 ± 0.039 |
| Triceps Brachii Long | 0.137 ± 0.065 | 0.15 ± 0 | 0.126 ± 0.031 | 0.106 ± 0 | 0.129 ± 0.029 | 0.136 ± 0.039 | 0.183 ± 0.002 |
| Triceps Brachii Medial | 0.315 ± 0.072 | 0.241 ± 0 | 0.255 ± 0.018 | 0.296 ± 0 | 0.433 ± 0.126 | 0.271 ± 0.013 | 0.287 ± 0.019 |
| Triceps Brachii Lateral | 0.111 ± 0.046 | 0.143 ± 0 | 0.158 ± 0.043 | 0.098 ± 0 | 0.111 ± 0.016 | 0.186 ± 0.026 | 0.137 ± 0.008 |
| Biceps Short | 0.108 ± 0.043 | 0.081 ± 0 | 0.084 ± 0.012 | 0.093 ± 0 | 0.096 ± 0.043 | 0.14 ± 0 | 0.105 ± 0.002 |
| Biceps Long | 0.087 ± 0.035 | 0.069 ± 0 | 0.165 ± 0.03 | 0.141 ± 0 | 0.301 ± 0.002 | 0.102 ± 0.004 | 0.103 ± 0.005 |
| Brachialis | 0.089 ± 0.053 | 0.104 ± 0 | 0.078 ± 0.009 | 0.098 ± 0 | 0.112 ± 0.019 | 0.104 ± 0.002 | 0.118 ± 0.01 |
| Brachioradialis | 0.121 ± 0.079 | 0.062 ± 0 | 0.154 ± 0.035 | 0.13 ± 0 | 0.128 ± 0.026 | 0.143 ± 0.009 | 0.121 ± 0.001 |
| Supinator | 0.292 ± 0.075 | 0.398 ± 0 | 0.245 ± 0.008 | 0.383 ± 0 | 0.32 ± 0.001 | 0.256 ± 0.164 | 0.393 ± 0.019 |
| Pronator Teres | 0.094 ± 0.027 | 0.066 ± 0 | 0.109 ± 0.017 | 0.117 ± 0 | 0.058 ± 0.003 | 0.061 ± 0.006 | 0.078 ± 0.015 |
| Flexor Carpi Radialis | 0.177 ± 0.108 | 0.295 ± 0 | 0.133 ± 0.003 | 0.132 ± 0 | 0.391 ± 0.303 | 0.117 ± 0.029 | 0.406 ± 0.078 |
| Flexor Carpi Ulnaris | 0.354 ± 0.118 | 0.639 ± 0 | 0.313 ± 0.059 | 0.653 ± 0 | 0.414 ± 0.133 | 0.423 ± 0.053 | 0.653 ± 0 |
| Extensor Carpi Radialis Long | 0.242 ± 0.118 | 0.506 ± 0 | 0.454 ± 0.086 | 0.483 ± 0 | 0.298 ± 0.001 | 0.157 ± 0.012 | 0.353 ± 0.099 |
| Extensor Carpi Radialis Brevis | 0.337 ± 0.121 | 0.68 ± 0 | 0.675 ± 0.004 | 0.678 ± 0 | 0.336 ± 0.003 | 0.247 ± 0.022 | 0.675 ± 0.003 |
| Extensor Carpi Ulnaris | 0.251 ± 0.111 | 0.208 ± 0 | 0.228 ± 0.022 | 0.166 ± 0 | 0.181 ± 0.002 | 0.118 ± 0.006 | 0.182 ± 0.007 |
| Total | 0.166 ± 0.0908 | 0.196 ± 0.158 | 0.175 ± 0.118 | 0.176 ± 0.15 | 0.184 ± 0.114 | 0.166 ± 0.107 | 0.198 ± 0.157 |

Table A.8: Pearson's correlation coefficient from cumulated activations between healthy and patients' ones for each muscle while reaching the target 1. For healthy subjects, this shows the intervariability within the healthy population. A1 corresponds to the first assessment, A4 to the final one. The final row correspond to the overall mean of these values.

| Pearson's correlation coefficient from cumulated sum of the signals activations while reaching target 1 | | | | | | | |
|---|-----------------------|-----------------------|-----------------------|-----------------------|-----------------------|-----------------------|-----------------------|
| Target 1 | Healthy | S1 | | S2 | | S3 | |
| | | A1 | A4 | A1 | A4 | A1 | A4 |
| Subclavius | 0.961 ± 0.016 | 0.948 ± 0 | 0.987 ± 0.007 | 0.97 ± 0.004 | 0.975 ± 0.008 | 0.981 ± 0.005 | 0.977 ± 0.007 |
| Serratus Anterior Superior | 0.96 ± 0.022 | 0.994 ± 0 | 0.989 ± 0.008 | 0.952 ± 0.028 | 0.921 ± 0.025 | 0.969 ± 0.027 | 0.823 ± 0.204 |
| Serratus Anterior Middle | 0.982 ± 0.01 | 0.978 ± 0 | 0.99 ± 0.006 | 0.971 ± 0.002 | 0.98 ± 0.017 | 0.983 ± 0.013 | 0.972 ± 0.017 |
| Serratus Anterior Inferior | 0.999 ± 0.001 | 0.998 ± 0 | 0.999 ± 0.001 | 0.999 ± 0 | 0.999 ± 0 | 0.999 ± 0.001 | 0.997 ± 0 |
| Trapezius C1 | 0.997 ± 0.002 | 0.998 ± 0 | 1 ± 0 | 0.996 ± 0.004 | 0.985 ± 0.015 | 0.995 ± 0.006 | 0.999 ± 0.001 |
| Trapezius C7 | 0.994 ± 0.003 | 0.994 ± 0 | 0.998 ± 0.002 | 0.985 ± 0.006 | 0.992 ± 0.003 | 0.995 ± 0.001 | 0.998 ± 0.001 |
| Trapezius T1 | 0.995 ± 0.003 | 0.998 ± 0 | 0.999 ± 0.001 | 0.999 ± 0.001 | 0.999 ± 0.001 | 0.999 ± 0.001 | 0.994 ± 0.001 |
| Trapezius T2 - T7 | 0.986 ± 0.007 | 0.997 ± 0 | 0.997 ± 0.002 | 0.977 ± 0.004 | 0.985 ± 0.008 | 0.991 ± 0.006 | 0.999 ± 0.001 |
| Levator Scapulae | 0.987 ± 0.007 | 0.994 ± 0 | 0.998 ± 0.002 | 0.961 ± 0.045 | 0.997 ± 0.001 | 0.996 ± 0.003 | 0.985 ± 0.003 |
| Rhomboid Minor | 0.997 ± 0.002 | 0.994 ± 0 | 0.998 ± 0.002 | 0.994 ± 0.006 | 0.999 ± 0.001 | 0.997 ± 0.003 | 0.992 ± 0.001 |
| Rhomboid Major T1 - T2 | 0.981 ± 0.017 | 0.958 ± 0 | 0.997 ± 0.002 | 0.926 ± 0.024 | 0.984 ± 0.01 | 1 ± 0 | 0.998 ± 0.002 |
| Rhomboid Major T3 - T4 | 0.992 ± 0.004 | 0.996 ± 0 | 0.998 ± 0.001 | 0.996 ± 0.005 | 0.985 ± 0.016 | 0.994 ± 0.007 | 0.997 ± 0 |
| Pectoralis Minor | 0.91 ± 0.039 | 0.864 ± 0 | 0.904 ± 0.067 | 0.901 ± 0.031 | 0.94 ± 0.011 | 0.837 ± 0.066 | 0.768 ± 0.227 |
| Pectoralis Major Clavicular | 0.99 ± 0.004 | 0.988 ± 0 | 0.987 ± 0.007 | 0.995 ± 0.001 | 0.946 ± 0.062 | 0.996 ± 0.003 | 0.986 ± 0.002 |
| Pectoralis Major Sternal | 0.958 ± 0.019 | 0.984 ± 0 | 0.795 ± 0.119 | 0.953 ± 0.008 | 0.943 ± 0.028 | 0.981 ± 0 | 0.989 ± 0 |
| Pectoralis Major Ribs | 0.933 ± 0.023 | 0.925 ± 0 | 0.901 ± 0.029 | 0.902 ± 0.093 | 0.94 ± 0.004 | 0.824 ± 0.097 | 0.923 ± 0.011 |
| Latissimus Dorsi Thoracic | 0.982 ± 0.008 | 0.993 ± 0 | 0.995 ± 0.003 | 0.992 ± 0.005 | 0.792 ± 0.278 | 0.959 ± 0.045 | 0.968 ± 0.023 |
| Latissimus Dorsi Lumbar | 0.918 ± 0.031 | 0.822 ± 0 | 0.844 ± 0.038 | 0.912 ± 0.037 | 0.954 ± 0.039 | 0.944 ± 0.026 | 0.951 ± 0.026 |
| Latissimus Dorsi Iliac | 0.914 ± 0.027 | 0.856 ± 0 | 0.853 ± 0.03 | 0.928 ± 0.009 | 0.925 ± 0 | 0.887 ± 0.034 | 0.924 ± 0.032 |
| Deltoid Clavicular (Ant) | 0.988 ± 0.007 | 0.99 ± 0 | 0.998 ± 0.001 | 0.991 ± 0.011 | 0.988 ± 0.004 | 0.992 ± 0.007 | 0.997 ± 0.002 |
| Deltoid Acromial (Mid) | 0.995 ± 0.003 | 0.996 ± 0 | 0.996 ± 0.002 | 0.996 ± 0.002 | 0.989 ± 0.003 | 0.996 ± 0.001 | 0.993 ± 0.003 |
| Deltoid Scapular (Post) | 0.992 ± 0.007 | 0.998 ± 0 | 1 ± 0 | 0.99 ± 0.011 | 0.981 ± 0.025 | 0.999 ± 0.001 | 0.987 ± 0.01 |
| Supraspinatus | 0.975 ± 0.008 | 0.952 ± 0 | 0.989 ± 0.007 | 0.963 ± 0.023 | 0.919 ± 0.015 | 0.996 ± 0.001 | 0.98 ± 0.007 |
| Infraspinatus | 0.995 ± 0.002 | 0.994 ± 0 | 0.999 ± 0.002 | 0.991 ± 0.006 | 0.964 ± 0.049 | 0.995 ± 0 | 0.994 ± 0.001 |
| Subscapularis | 0.935 ± 0.032 | 0.874 ± 0 | 0.881 ± 0.072 | 0.928 ± 0.053 | 0.894 ± 0.009 | 0.984 ± 0.014 | 0.902 ± 0.118 |
| Teres Minor | 0.905 ± 0.053 | 0.927 ± 0 | 0.9 ± 0.102 | 0.963 ± 0.003 | 0.838 ± 0.012 | 0.925 ± 0.06 | 0.946 ± 0.008 |
| Teres Major | 0.952 ± 0.031 | 0.871 ± 0 | 0.773 ± 0.096 | 0.931 ± 0.012 | 0.917 ± 0.013 | 0.956 ± 0.01 | 0.946 ± 0.062 |
| Coracobrachialis | 0.942 ± 0.038 | 0.944 ± 0 | 0.946 ± 0.054 | 0.981 ± 0.005 | 0.994 ± 0.003 | 0.991 ± 0.002 | 0.992 ± 0.003 |
| Triceps Brachii Long | 0.99 ± 0.005 | 0.991 ± 0 | 0.997 ± 0.001 | 0.984 ± 0.01 | 0.951 ± 0.064 | 0.992 ± 0.002 | 0.986 ± 0.003 |
| Triceps Brachii Medial | 0.954 ± 0.034 | 0.996 ± 0 | 0.982 ± 0.011 | 0.999 ± 0 | 0.99 ± 0.009 | 1 ± 0 | 1 ± 0 |
| Triceps Brachii Lateral | 0.98 ± 0.016 | 0.987 ± 0 | 0.997 ± 0.003 | 0.992 ± 0.006 | 0.994 ± 0.003 | 0.998 ± 0.001 | 0.997 ± 0.001 |
| Biceps Short | 0.98 ± 0.013 | 0.994 ± 0 | 0.994 ± 0.003 | 0.989 ± 0.009 | 0.971 ± 0.027 | 0.97 ± 0.022 | 0.993 ± 0.003 |
| Biceps Long | 0.978 ± 0.014 | 0.992 ± 0 | 0.997 ± 0.002 | 0.992 ± 0.001 | 0.957 ± 0.034 | 0.931 ± 0.036 | 0.993 ± 0 |
| Brachialis | 0.989 ± 0.008 | 0.998 ± 0 | 0.99 ± 0.001 | 0.982 ± 0.024 | 0.992 ± 0.009 | 0.998 ± 0.001 | 0.996 ± 0 |
| Brachioradialis | 0.99 ± 0.008 | 0.999 ± 0 | 0.974 ± 0.017 | 0.993 ± 0 | 0.976 ± 0.024 | 0.977 ± 0.02 | 0.993 ± 0.008 |
| Supinator | 0.998 ± 0.001 | 0.999 ± 0 | 0.999 ± 0 | 0.979 ± 0.025 | 1 ± 0 | 0.998 ± 0.001 | 0.955 ± 0 |
| Pronator Teres | 0.967 ± 0.038 | 0.999 ± 0 | 0.974 ± 0.02 | 0.979 ± 0.002 | 0.989 ± 0.015 | 0.997 ± 0.002 | 0.975 ± 0.026 |
| Flexor Carpi Radialis | 0.929 ± 0.053 | 0.995 ± 0 | 0.928 ± 0.059 | 0.889 ± 0.108 | 0.984 ± 0.011 | 0.981 ± 0.015 | 0.782 ± 0.178 |
| Flexor Carpi Ulnaris | 0.95 ± 0.04 | 0.995 ± 0 | 0.955 ± 0.028 | 0.997 ± 0.004 | 0.98 ± 0.025 | 0.999 ± 0 | 0.994 ± 0.008 |
| Extensor Carpi Radialis Long | 0.961 ± 0.015 | 0.936 ± 0 | 0.879 ± 0.082 | 0.939 ± 0.023 | 0.639 ± 0.069 | 0.921 ± 0.021 | 0.996 ± 0.003 |
| Extensor Carpi Radialis Brevis | 0.973 ± 0.011 | 0.982 ± 0 | 0.991 ± 0 | 0.993 ± 0 | 0.974 ± 0.023 | 0.968 ± 0.04 | 0.992 ± 0 |
| Extensor Carpi Ulnaris | 0.948 ± 0.03 | 0.933 ± 0 | 0.907 ± 0.085 | 0.909 ± 0.052 | 0.971 ± 0.032 | 0.995 ± 0.002 | 0.624 ± 0.099 |
| Total | 0.969 ± 0.0271 | 0.967 ± 0.0467 | 0.959 ± 0.0601 | 0.968 ± 0.0324 | 0.955 ± 0.0657 | 0.974 ± 0.0413 | 0.958 ± 0.0761 |

Table A.9: Pearson's correlation coefficient from cumulated activations between healthy and patients' ones for each muscle while reaching the target 3. For healthy subjects, this shows the intervariability within the healthy population. A1 corresponds to the first assessment, A4 to the final one. The final row correspond to the overall mean of these values.

Pearson's correlation coefficient from cumulated sum of the signals activations while reaching target 3

| Target 3 | Healthy | S1 | | S2 | | S3 | |
|--------------------------------|-----------------------|----------------------|-----------------------|-----------------------|-----------------------|-----------------------|---------------------|
| | | A1 | A4 | A1 | A4 | A1 | A4 |
| Subclavius | 0.964 ± 0.019 | 0.959 ± 0 | 0.965 ± 0.009 | 0.95 ± 0.064 | 0.947 ± 0.006 | 0.979 ± 0.017 | 0.99 ± 0.003 |
| Serratus Anterior Superior | 0.959 ± 0.035 | 0.806 ± 0 | 0.999 ± 0.001 | 0.886 ± 0.048 | 0.972 ± 0.027 | 0.959 ± 0.054 | 0.819 ± 0.136 |
| Serratus Anterior Middle | 0.988 ± 0.008 | 0.85 ± 0 | 0.983 ± 0.02 | 0.951 ± 0.015 | 0.996 ± 0.001 | 0.989 ± 0.014 | 0.97 ± 0.028 |
| Serratus Anterior Inferior | 0.999 ± 0.001 | 0.987 ± 0 | 0.996 ± 0.003 | 0.995 ± 0.001 | 1 ± 0 | 1 ± 0 | 0.997 ± 0.001 |
| Trapezius C1 | 0.994 ± 0.004 | 0.956 ± 0 | 0.999 ± 0.001 | 0.996 ± 0.001 | 1 ± 0 | 0.996 ± 0 | 0.997 ± 0 |
| Trapezius C7 | 0.988 ± 0.008 | 0.951 ± 0 | 0.999 ± 0.001 | 0.992 ± 0.004 | 0.995 ± 0.006 | 0.998 ± 0.003 | 0.997 ± 0.003 |
| Trapezius T1 | 0.998 ± 0.001 | 0.99 ± 0 | 0.996 ± 0.005 | 0.992 ± 0.009 | 0.999 ± 0.001 | 0.999 ± 0.001 | 0.992 ± 0.002 |
| Trapezius T2 - T7 | 0.99 ± 0.004 | 0.952 ± 0 | 0.994 ± 0.004 | 0.976 ± 0.003 | 0.97 ± 0.028 | 0.995 ± 0.004 | 0.978 ± 0.024 |
| Levator Scapulae | 0.959 ± 0.029 | 0.914 ± 0 | 0.981 ± 0.016 | 0.96 ± 0.005 | 0.997 ± 0.001 | 0.995 ± 0.002 | 0.994 ± 0.002 |
| Rhomboid Minor | 0.998 ± 0.001 | 0.962 ± 0 | 0.994 ± 0.004 | 0.976 ± 0.006 | 0.998 ± 0.001 | 0.998 ± 0.001 | 0.994 ± 0.002 |
| Rhomboid Major T1 - T2 | 0.94 ± 0.051 | 0.99 ± 0 | 0.991 ± 0.004 | 0.977 ± 0.009 | 0.996 ± 0.003 | 0.993 ± 0.008 | 0.999 ± 0 |
| Rhomboid Major T3 - T4 | 0.987 ± 0.011 | 0.947 ± 0 | 0.995 ± 0.003 | 0.99 ± 0.008 | 0.99 ± 0.001 | 0.994 ± 0 | 0.993 ± 0.004 |
| Pectoralis Minor | 0.892 ± 0.057 | 0.714 ± 0 | 0.942 ± 0.041 | 0.873 ± 0.113 | 0.912 ± 0.006 | 0.916 ± 0.055 | 0.889 ± 0.021 |
| Pectoralis Major Clavicular | 0.951 ± 0.033 | 0.808 ± 0 | 0.935 ± 0.037 | 0.968 ± 0.038 | 0.955 ± 0.033 | 0.986 ± 0.002 | 0.992 ± 0.001 |
| Pectoralis Major Sternal | 0.92 ± 0.037 | 0.653 ± 0 | 0.816 ± 0.126 | 0.969 ± 0.001 | 0.964 ± 0.017 | 0.867 ± 0.131 | 0.857 ± 0.189 |
| Pectoralis Major Ribs | 0.908 ± 0.037 | 0.884 ± 0 | 0.897 ± 0.039 | 0.863 ± 0.012 | 0.879 ± 0.13 | 0.929 ± 0.04 | 0.922 ± 0.019 |
| Latissimus Dorsi Thoracic | 0.981 ± 0.011 | 0.974 ± 0 | 0.994 ± 0.002 | 0.976 ± 0.01 | 0.998 ± 0.001 | 0.986 ± 0.01 | 0.976 ± 0.009 |
| Latissimus Dorsi Lumbar | 0.942 ± 0.031 | 0.992 ± 0 | 0.944 ± 0.026 | 0.874 ± 0.054 | 0.874 ± 0.083 | 0.99 ± 0.006 | 0.983 ± 0.005 |
| Latissimus Dorsi Iliac | 0.932 ± 0.028 | 0.991 ± 0 | 0.985 ± 0.008 | 0.867 ± 0.056 | 0.858 ± 0.115 | 0.977 ± 0.006 | 0.97 ± 0.01 |
| Deltoid Clavicular (Ant) | 0.982 ± 0.012 | 0.851 ± 0 | 0.99 ± 0.006 | 0.958 ± 0.004 | 0.992 ± 0.002 | 0.98 ± 0.018 | 0.942 ± 0.057 |
| Deltoid Acromial (Mid) | 0.997 ± 0.002 | 0.936 ± 0 | 0.995 ± 0.003 | 0.99 ± 0.002 | 0.996 ± 0.002 | 0.998 ± 0.001 | 0.994 ± 0.004 |
| Deltoid Scapular (Post) | 0.996 ± 0.002 | 0.934 ± 0 | 0.999 ± 0 | 0.98 ± 0.007 | 0.999 ± 0 | 0.997 ± 0 | 0.996 ± 0.005 |
| Supraspinatus | 0.99 ± 0.005 | 0.879 ± 0 | 0.996 ± 0.006 | 0.982 ± 0.01 | 0.948 ± 0.066 | 0.994 ± 0.003 | 0.968 ± 0.024 |
| Infraspinatus | 0.996 ± 0.001 | 0.9 ± 0 | 0.998 ± 0.001 | 0.98 ± 0.005 | 0.998 ± 0.001 | 0.998 ± 0.001 | 0.9 ± 0.136 |
| Subscapularis | 0.933 ± 0.041 | 0.671 ± 0 | 0.932 ± 0.06 | 0.956 ± 0.017 | 0.969 ± 0.017 | 0.868 ± 0.166 | 0.987 ± 0.009 |
| Teres Minor | 0.955 ± 0.029 | 0.774 ± 0 | 0.956 ± 0.014 | 0.929 ± 0.043 | 0.933 ± 0.021 | 0.992 ± 0.008 | 0.971 ± 0.005 |
| Teres Major | 0.968 ± 0.026 | 0.999 ± 0 | 0.991 ± 0.004 | 0.903 ± 0.08 | 0.896 ± 0.041 | 0.997 ± 0.001 | 0.981 ± 0.011 |
| Coracobrachialis | 0.868 ± 0.061 | 0.6 ± 0 | 0.741 ± 0.072 | 0.974 ± 0.003 | 0.985 ± 0.013 | 0.961 ± 0.025 | 0.981 ± 0.014 |
| Triceps Brachii Long | 0.997 ± 0.002 | 0.934 ± 0 | 0.992 ± 0.004 | 0.962 ± 0.01 | 0.997 ± 0.001 | 0.999 ± 0 | 0.995 ± 0.002 |
| Triceps Brachii Medial | 0.949 ± 0.02 | 0.922 ± 0 | 0.949 ± 0.031 | 0.985 ± 0.003 | 0.985 ± 0.006 | 0.958 ± 0.039 | 0.987 ± 0.004 |
| Triceps Brachii Lateral | 0.962 ± 0.024 | 0.839 ± 0 | 0.961 ± 0.026 | 0.985 ± 0 | 0.979 ± 0.017 | 0.915 ± 0.064 | 0.89 ± 0.147 |
| Biceps Short | 0.978 ± 0.02 | 0.997 ± 0 | 0.988 ± 0.006 | 0.982 ± 0.006 | 0.959 ± 0 | 0.995 ± 0.005 | 0.976 ± 0.027 |
| Biceps Long | 0.982 ± 0.009 | 0.961 ± 0 | 0.997 ± 0.001 | 0.993 ± 0.001 | 0.998 ± 0.001 | 0.998 ± 0.001 | 0.997 ± 0.001 |
| Brachialis | 0.998 ± 0.001 | 0.984 ± 0 | 0.998 ± 0.001 | 0.976 ± 0.015 | 0.998 ± 0.001 | 1 ± 0 | 0.999 ± 0.001 |
| Brachioradialis | 0.989 ± 0.008 | 0.996 ± 0 | 0.986 ± 0.01 | 0.994 ± 0.006 | 0.993 ± 0.003 | 0.992 ± 0.007 | 0.995 ± 0.003 |
| Supinator | 0.998 ± 0.001 | 0.899 ± 0 | 0.996 ± 0.003 | 0.967 ± 0.011 | 1 ± 0 | 0.995 ± 0.005 | 0.997 ± 0.003 |
| Pronator Teres | 0.948 ± 0.033 | 0.979 ± 0 | 0.885 ± 0.073 | 0.991 ± 0.006 | 0.999 ± 0 | 0.999 ± 0 | 0.879 ± 0.17 |
| Flexor Carpi Radialis | 0.91 ± 0.026 | 0.951 ± 0 | 0.818 ± 0.052 | 0.899 ± 0.028 | 0.94 ± 0.008 | 0.96 ± 0.008 | 0.69 ± 0.233 |
| Flexor Carpi Ulnaris | 0.902 ± 0.045 | 0.948 ± 0 | 0.876 ± 0.103 | 0.984 ± 0 | 0.968 ± 0.005 | 0.954 ± 0.038 | 0.762 ± 0.311 |
| Extensor Carpi Radialis Long | 0.978 ± 0.011 | 0.987 ± 0 | 0.956 ± 0.019 | 0.981 ± 0.025 | 0.95 ± 0.061 | 0.946 ± 0.048 | 0.853 ± 0.204 |
| Extensor Carpi Radialis Brevis | 0.983 ± 0.012 | 0.999 ± 0 | 1 ± 0 | 1 ± 0 | 0.926 ± 0.028 | 0.985 ± 0.009 | 1 ± 0 |
| Extensor Carpi Ulnaris | 0.962 ± 0.018 | 0.806 ± 0 | 0.958 ± 0.027 | 0.846 ± 0.098 | 0.979 ± 0.005 | 0.989 ± 0.005 | 0.975 ± 0.003 |
| Total | 0.965 ± 0.0337 | 0.905 ± 0.102 | 0.961 ± 0.0579 | 0.958 ± 0.0431 | 0.969 ± 0.0384 | 0.977 ± 0.0333 | 0.953 ± 0.07 |

Table A.10: Pearson's correlation coefficient from cumulated activations between healthy and patients' ones for each muscle while reaching the target 5. For healthy subjects, this shows the intervariability within the healthy population. A1 corresponds to the first assessment, A4 to the final one. The final row correspond to the overall mean of these values.

| Pearson's correlation coefficient from cumulated sum of the signals activations while reaching target 5 | | | | | | | |
|---|----------------------|-----------------------|-----------------------|--------------------|-----------------------|-----------------------|-----------------------|
| Target 5 | Healthy | S1 | | S2 | | S3 | |
| | | A1 | A4 | A1 | A4 | A1 | A4 |
| Subclavius | 0.971 ± 0.016 | 0.984 ± 0 | 0.984 ± 0.014 | 0.995 ± 0 | 0.982 ± 0.003 | 0.981 ± 0.013 | 0.966 ± 0.02 |
| Serratus Anterior Superior | 0.951 ± 0.03 | 0.967 ± 0 | 0.989 ± 0.004 | 0.875 ± 0 | 0.968 ± 0.012 | 0.95 ± 0.003 | 0.909 ± 0.095 |
| Serratus Anterior Middle | 0.986 ± 0.005 | 0.981 ± 0 | 0.996 ± 0.003 | 0.974 ± 0 | 0.994 ± 0.005 | 0.991 ± 0.008 | 0.97 ± 0.027 |
| Serratus Anterior Inferior | 0.997 ± 0.001 | 1 ± 0 | 0.998 ± 0.002 | 0.998 ± 0 | 0.997 ± 0.002 | 1 ± 0 | 1 ± 0 |
| Trapezius C1 | 0.998 ± 0.001 | 1 ± 0 | 1 ± 0 | 0.997 ± 0 | 1 ± 0 | 1 ± 0 | 0.998 ± 0.002 |
| Trapezius C7 | 0.986 ± 0.013 | 0.994 ± 0 | 1 ± 0 | 0.999 ± 0 | 0.998 ± 0.002 | 0.995 ± 0.007 | 1 ± 0 |
| Trapezius T1 | 0.996 ± 0.002 | 0.999 ± 0 | 0.998 ± 0.001 | 0.996 ± 0 | 0.995 ± 0.005 | 0.998 ± 0.001 | 0.999 ± 0 |
| Trapezius T2 - T7 | 0.985 ± 0.009 | 0.976 ± 0 | 0.999 ± 0 | 0.996 ± 0 | 0.996 ± 0.001 | 0.997 ± 0.003 | 0.999 ± 0.001 |
| Levator Scapulae | 0.984 ± 0.007 | 0.991 ± 0 | 0.994 ± 0.004 | 0.993 ± 0 | 0.991 ± 0.003 | 0.998 ± 0.001 | 0.996 ± 0.002 |
| Rhomboid Minor | 0.994 ± 0.003 | 0.994 ± 0 | 0.998 ± 0.002 | 0.998 ± 0 | 0.995 ± 0.001 | 0.997 ± 0.002 | 0.999 ± 0 |
| Rhomboid Major T1 - T2 | 0.988 ± 0.01 | 0.99 ± 0 | 0.995 ± 0.004 | 0.994 ± 0 | 0.995 ± 0.002 | 0.997 ± 0.003 | 0.998 ± 0 |
| Rhomboid Major T3 - T4 | 0.99 ± 0.006 | 0.999 ± 0 | 0.997 ± 0.001 | 0.998 ± 0 | 0.996 ± 0.001 | 0.997 ± 0.003 | 0.962 ± 0.044 |
| Pectoralis Minor | 0.942 ± 0.019 | 0.94 ± 0 | 0.973 ± 0.01 | 0.705 ± 0 | 0.952 ± 0.009 | 0.967 ± 0.042 | 0.91 ± 0.09 |
| Pectoralis Major Clavicular | 0.978 ± 0.015 | 0.996 ± 0 | 0.987 ± 0.011 | 0.998 ± 0 | 0.991 ± 0 | 0.982 ± 0.003 | 0.981 ± 0.025 |
| Pectoralis Major Sternal | 0.954 ± 0.029 | 0.991 ± 0 | 0.871 ± 0.093 | 0.943 ± 0 | 0.971 ± 0.021 | 0.995 ± 0.003 | 0.983 ± 0.022 |
| Pectoralis Major Ribs | 0.935 ± 0.024 | 0.947 ± 0 | 0.852 ± 0.14 | 0.966 ± 0 | 0.948 ± 0.008 | 0.989 ± 0.009 | 0.843 ± 0.004 |
| Latissimus Dorsi Thoracic | 0.986 ± 0.006 | 0.915 ± 0 | 0.961 ± 0.016 | 0.982 ± 0 | 0.997 ± 0.001 | 0.908 ± 0.105 | 0.934 ± 0.079 |
| Latissimus Dorsi Lumbar | 0.963 ± 0.026 | 0.971 ± 0 | 0.951 ± 0.046 | 0.781 ± 0 | 0.98 ± 0.014 | 0.937 ± 0.071 | 0.983 ± 0.007 |
| Latissimus Dorsi Iliac | 0.946 ± 0.035 | 0.906 ± 0 | 0.907 ± 0.094 | 0.715 ± 0 | 0.968 ± 0.027 | 0.885 ± 0.098 | 0.93 ± 0.054 |
| Deltoid Clavicular (Ant) | 0.975 ± 0.012 | 0.998 ± 0 | 0.985 ± 0.011 | 0.965 ± 0 | 0.94 ± 0.05 | 0.992 ± 0.005 | 0.99 ± 0.003 |
| Deltoid Acromial (Mid) | 0.955 ± 0.031 | 0.985 ± 0 | 0.99 ± 0.005 | 0.969 ± 0 | 0.882 ± 0.086 | 0.988 ± 0.005 | 0.975 ± 0.002 |
| Deltoid Scapular (Post) | 0.992 ± 0.004 | 0.997 ± 0 | 0.997 ± 0.003 | 0.984 ± 0 | 0.997 ± 0 | 0.995 ± 0.002 | 0.994 ± 0.004 |
| Supraspinatus | 0.928 ± 0.04 | 0.924 ± 0 | 0.992 ± 0.007 | 0.997 ± 0 | 0.903 ± 0.045 | 0.878 ± 0.08 | 0.992 ± 0.001 |
| Infraspinatus | 0.976 ± 0.012 | 0.995 ± 0 | 0.998 ± 0.001 | 0.993 ± 0 | 0.995 ± 0.003 | 0.977 ± 0.032 | 0.999 ± 0 |
| Subscapularis | 0.978 ± 0.012 | 0.924 ± 0 | 0.967 ± 0.012 | 0.948 ± 0 | 0.988 ± 0 | 0.933 ± 0.088 | 0.943 ± 0.037 |
| Teres Minor | 0.905 ± 0.072 | 0.978 ± 0 | 0.947 ± 0.036 | 0.85 ± 0 | 0.972 ± 0.025 | 0.963 ± 0.027 | 0.983 ± 0.001 |
| Teres Major | 0.965 ± 0.039 | 0.97 ± 0 | 0.975 ± 0.017 | 0.627 ± 0 | 0.987 ± 0.011 | 0.99 ± 0.005 | 0.966 ± 0.029 |
| Coracobrachialis | 0.936 ± 0.024 | 0.975 ± 0 | 0.863 ± 0.114 | 0.978 ± 0 | 0.88 ± 0.091 | 0.969 ± 0.034 | 0.976 ± 0.005 |
| Triceps Brachii Long | 0.989 ± 0.006 | 0.99 ± 0 | 0.997 ± 0.002 | 0.978 ± 0 | 0.998 ± 0.001 | 0.999 ± 0 | 0.999 ± 0 |
| Triceps Brachii Medial | 0.954 ± 0.038 | 0.965 ± 0 | 0.975 ± 0.018 | 0.988 ± 0 | 0.889 ± 0.089 | 0.988 ± 0.003 | 0.987 ± 0.003 |
| Triceps Brachii Lateral | 0.952 ± 0.019 | 0.986 ± 0 | 0.944 ± 0.058 | 0.973 ± 0 | 0.973 ± 0.003 | 0.968 ± 0.017 | 0.987 ± 0.004 |
| Biceps Short | 0.988 ± 0.006 | 0.997 ± 0 | 0.998 ± 0.002 | 0.997 ± 0 | 0.995 ± 0.003 | 0.997 ± 0.003 | 0.995 ± 0.001 |
| Biceps Long | 0.988 ± 0.011 | 0.999 ± 0 | 0.999 ± 0.001 | 0.996 ± 0 | 1 ± 0 | 0.991 ± 0.011 | 0.996 ± 0.001 |
| Brachialis | 0.996 ± 0.002 | 0.999 ± 0 | 0.999 ± 0.001 | 0.997 ± 0 | 0.993 ± 0.006 | 0.999 ± 0 | 0.999 ± 0 |
| Brachioradialis | 0.988 ± 0.01 | 0.998 ± 0 | 0.992 ± 0.009 | 0.99 ± 0 | 0.991 ± 0.003 | 0.992 ± 0.007 | 0.98 ± 0.006 |
| Supinator | 0.996 ± 0.002 | 1 ± 0 | 0.993 ± 0.005 | 0.993 ± 0 | 0.999 ± 0 | 0.995 ± 0.006 | 0.994 ± 0 |
| Pronator Teres | 0.986 ± 0.006 | 1 ± 0 | 0.97 ± 0.023 | 0.998 ± 0 | 0.999 ± 0 | 0.997 ± 0.003 | 0.949 ± 0.069 |
| Flexor Carpi Radialis | 0.909 ± 0.049 | 0.917 ± 0 | 0.878 ± 0.075 | 0.637 ± 0 | 0.97 ± 0.001 | 0.927 ± 0.047 | 0.691 ± 0.043 |
| Flexor Carpi Ulnaris | 0.943 ± 0.034 | 0.988 ± 0 | 0.986 ± 0.009 | 0.988 ± 0 | 0.923 ± 0.055 | 0.982 ± 0 | 0.954 ± 0.049 |
| Extensor Carpi Radialis Long | 0.982 ± 0.009 | 0.999 ± 0 | 0.999 ± 0 | 0.999 ± 0 | 0.992 ± 0.004 | 0.959 ± 0.058 | 0.998 ± 0.001 |
| Extensor Carpi Radialis Brevis | 0.957 ± 0.015 | 0.988 ± 0 | 0.988 ± 0 | 0.988 ± 0 | 0.915 ± 0.058 | 0.984 ± 0.004 | 0.988 ± 0 |
| Extensor Carpi Ulnaris | 0.968 ± 0.016 | 0.987 ± 0 | 0.934 ± 0.042 | 0.961 ± 0 | 0.875 ± 0.14 | 0.994 ± 0.003 | 0.987 ± 0 |
| Total | 0.97 ± 0.0243 | 0.979 ± 0.0267 | 0.972 ± 0.0405 | 0.945 ± 0.1 | 0.971 ± 0.0377 | 0.977 ± 0.0308 | 0.969 ± 0.0543 |

Table A.11: Pearson's correlation coefficient from cumulated activations between healthy and patients' ones for each muscle while reaching the target 7. For healthy subjects, this shows the intervariability within the healthy population. A1 corresponds to the first assessment, A4 to the final one. The final row correspond to the overall mean of these values.

| Pearson's correlation coefficient from cumulated sum of the signals activations while reaching target 7 | | | | | | | |
|---|-----------------------|-----------------------|-----------------------|-----------------------|-----------------------|-----------------------|-----------------------|
| Target 7 | Healthy | S1 | | S2 | | S3 | |
| | | A1 | A4 | A1 | A4 | A1 | A4 |
| Subclavius | 0.962 ± 0.013 | 0.907 ± 0 | 0.98 ± 0.009 | 0.958 ± 0 | 0.96 ± 0.052 | 0.997 ± 0.001 | 0.988 ± 0 |
| Serratus Anterior Superior | 0.945 ± 0.031 | 0.963 ± 0 | 0.978 ± 0.016 | 0.971 ± 0 | 0.95 ± 0.026 | 0.917 ± 0.052 | 0.913 ± 0.015 |
| Serratus Anterior Middle | 0.979 ± 0.01 | 0.997 ± 0 | 0.971 ± 0.013 | 0.981 ± 0 | 0.987 ± 0.012 | 0.991 ± 0.006 | 0.984 ± 0.002 |
| Serratus Anterior Inferior | 0.996 ± 0.003 | 0.996 ± 0 | 0.996 ± 0.004 | 0.998 ± 0 | 0.993 ± 0.002 | 1 ± 0 | 1 ± 0 |
| Trapezius C1 | 0.999 ± 0.001 | 1 ± 0 | 0.997 ± 0.002 | 0.996 ± 0 | 0.999 ± 0 | 0.999 ± 0 | 0.998 ± 0 |
| Trapezius C7 | 0.967 ± 0.029 | 0.996 ± 0 | 0.989 ± 0.005 | 0.993 ± 0 | 0.993 ± 0.009 | 0.998 ± 0.001 | 0.998 ± 0.001 |
| Trapezius T1 | 0.985 ± 0.006 | 0.991 ± 0 | 0.992 ± 0.003 | 0.996 ± 0 | 0.983 ± 0.019 | 0.995 ± 0.003 | 0.998 ± 0 |
| Trapezius T2 - T7 | 0.985 ± 0.004 | 0.993 ± 0 | 0.991 ± 0.007 | 0.996 ± 0 | 0.974 ± 0.028 | 0.991 ± 0.006 | 0.995 ± 0.005 |
| Levator Scapulae | 0.958 ± 0.018 | 0.971 ± 0 | 0.988 ± 0.001 | 0.997 ± 0 | 0.96 ± 0.008 | 0.978 ± 0.004 | 0.978 ± 0.001 |
| Rhomboid Minor | 0.984 ± 0.006 | 0.985 ± 0 | 0.993 ± 0.006 | 0.998 ± 0 | 0.983 ± 0.012 | 0.998 ± 0.002 | 0.999 ± 0.001 |
| Rhomboid Major T1 - T2 | 0.986 ± 0.01 | 0.989 ± 0 | 0.988 ± 0.011 | 0.994 ± 0 | 0.987 ± 0.011 | 0.996 ± 0.002 | 0.996 ± 0.003 |
| Rhomboid Major T3 - T4 | 0.994 ± 0.004 | 0.999 ± 0 | 0.999 ± 0.001 | 0.992 ± 0 | 0.997 ± 0.003 | 0.998 ± 0.002 | 0.995 ± 0.003 |
| Pectoralis Minor | 0.889 ± 0.027 | 0.982 ± 0 | 0.943 ± 0.032 | 0.888 ± 0 | 0.957 ± 0.025 | 0.901 ± 0.097 | 0.875 ± 0.004 |
| Pectoralis Major Clavicular | 0.992 ± 0.003 | 0.99 ± 0 | 0.994 ± 0.003 | 0.986 ± 0 | 0.992 ± 0.009 | 0.996 ± 0.001 | 0.997 ± 0.001 |
| Pectoralis Major Sternal | 0.985 ± 0.005 | 0.997 ± 0 | 0.975 ± 0.011 | 0.986 ± 0 | 0.996 ± 0.002 | 0.997 ± 0.002 | 0.995 ± 0 |
| Pectoralis Major Ribs | 0.921 ± 0.035 | 0.827 ± 0 | 0.975 ± 0.018 | 0.893 ± 0 | 0.94 ± 0.054 | 0.961 ± 0.014 | 0.944 ± 0.038 |
| Latissimus Dorsi Thoracic | 0.951 ± 0.03 | 0.996 ± 0 | 0.988 ± 0.005 | 0.977 ± 0 | 0.992 ± 0.005 | 0.954 ± 0.026 | 0.94 ± 0.027 |
| Latissimus Dorsi Lumbar | 0.925 ± 0.037 | 0.854 ± 0 | 0.938 ± 0.033 | 0.768 ± 0 | 0.919 ± 0.05 | 0.946 ± 0.037 | 0.979 ± 0.002 |
| Latissimus Dorsi Iliac | 0.86 ± 0.052 | 0.636 ± 0 | 0.717 ± 0.083 | 0.839 ± 0 | 0.859 ± 0.114 | 0.913 ± 0.017 | 0.953 ± 0.024 |
| Deltoid Clavicular (Ant) | 0.993 ± 0.002 | 0.999 ± 0 | 0.999 ± 0.001 | 0.991 ± 0 | 0.982 ± 0.006 | 0.998 ± 0.001 | 0.992 ± 0.004 |
| Deltoid Acromial (Mid) | 0.987 ± 0.006 | 0.993 ± 0 | 0.997 ± 0.002 | 0.997 ± 0 | 0.987 ± 0.004 | 1 ± 0 | 0.997 ± 0 |
| Deltoid Scapular (Post) | 0.962 ± 0.031 | 0.996 ± 0 | 0.998 ± 0.001 | 0.98 ± 0 | 0.987 ± 0.006 | 0.992 ± 0.002 | 0.967 ± 0.021 |
| Supraspinatus | 0.967 ± 0.019 | 0.99 ± 0 | 0.957 ± 0.007 | 0.961 ± 0 | 0.975 ± 0.023 | 0.974 ± 0.009 | 0.998 ± 0 |
| Infraspinatus | 0.976 ± 0.009 | 0.973 ± 0 | 0.989 ± 0.009 | 0.989 ± 0 | 0.963 ± 0.034 | 0.984 ± 0.004 | 0.994 ± 0.005 |
| Subscapularis | 0.974 ± 0.013 | 0.976 ± 0 | 0.96 ± 0.018 | 0.886 ± 0 | 0.974 ± 0.01 | 0.983 ± 0.017 | 0.965 ± 0.008 |
| Teres Minor | 0.921 ± 0.042 | 0.909 ± 0 | 0.965 ± 0.013 | 0.924 ± 0 | 0.871 ± 0.087 | 0.938 ± 0.025 | 0.957 ± 0.043 |
| Teres Major | 0.921 ± 0.047 | 0.777 ± 0 | 0.945 ± 0.042 | 0.834 ± 0 | 0.961 ± 0.032 | 0.979 ± 0.016 | 0.961 ± 0.026 |
| Coracobrachialis | 0.965 ± 0.016 | 0.995 ± 0 | 0.939 ± 0.041 | 0.999 ± 0 | 0.992 ± 0.008 | 0.995 ± 0.001 | 0.998 ± 0 |
| Triceps Brachii Long | 0.992 ± 0.003 | 0.998 ± 0 | 0.997 ± 0.002 | 0.995 ± 0 | 0.996 ± 0.004 | 0.999 ± 0 | 0.998 ± 0 |
| Triceps Brachii Medial | 0.97 ± 0.035 | 0.992 ± 0 | 0.985 ± 0.01 | 0.999 ± 0 | 0.951 ± 0.02 | 0.995 ± 0.006 | 1 ± 0 |
| Triceps Brachii Lateral | 0.966 ± 0.034 | 0.997 ± 0 | 0.992 ± 0.006 | 0.991 ± 0 | 0.986 ± 0.016 | 0.965 ± 0.029 | 0.993 ± 0.001 |
| Biceps Short | 0.975 ± 0.018 | 0.992 ± 0 | 0.996 ± 0.004 | 0.992 ± 0 | 0.997 ± 0.003 | 0.998 ± 0.002 | 0.992 ± 0.007 |
| Biceps Long | 0.981 ± 0.017 | 1 ± 0 | 0.996 ± 0.003 | 0.984 ± 0 | 0.998 ± 0.002 | 0.999 ± 0.001 | 0.998 ± 0.001 |
| Brachialis | 0.986 ± 0.012 | 0.998 ± 0 | 0.999 ± 0.001 | 0.997 ± 0 | 0.999 ± 0 | 0.999 ± 0 | 0.998 ± 0 |
| Brachioradialis | 0.989 ± 0.008 | 0.996 ± 0 | 0.995 ± 0.004 | 0.98 ± 0 | 0.998 ± 0.001 | 0.993 ± 0.001 | 0.997 ± 0.003 |
| Supinator | 0.998 ± 0.002 | 0.997 ± 0 | 0.998 ± 0.002 | 0.998 ± 0 | 1 ± 0 | 0.991 ± 0.012 | 0.991 ± 0.003 |
| Pronator Teres | 0.993 ± 0.003 | 0.999 ± 0 | 0.99 ± 0.005 | 0.988 ± 0 | 0.998 ± 0.002 | 0.999 ± 0.001 | 0.959 ± 0.058 |
| Flexor Carpi Radialis | 0.939 ± 0.038 | 0.96 ± 0 | 0.879 ± 0.065 | 0.98 ± 0 | 0.929 ± 0.027 | 0.992 ± 0.001 | 0.856 ± 0.025 |
| Flexor Carpi Ulnaris | 0.96 ± 0.028 | 1 ± 0 | 0.976 ± 0.017 | 1 ± 0 | 0.955 ± 0.005 | 0.999 ± 0.001 | 0.985 ± 0.022 |
| Extensor Carpi Radialis Long | 0.94 ± 0.043 | 0.976 ± 0 | 0.996 ± 0 | 0.999 ± 0 | 0.965 ± 0.005 | 0.99 ± 0.005 | 0.993 ± 0.004 |
| Extensor Carpi Radialis Brevis | 0.968 ± 0.024 | 1 ± 0 | 1 ± 0 | 1 ± 0 | 0.946 ± 0.003 | 0.987 ± 0.007 | 1 ± 0 |
| Extensor Carpi Ulnaris | 0.963 ± 0.016 | 0.99 ± 0 | 0.929 ± 0.044 | 0.907 ± 0 | 0.943 ± 0.025 | 0.997 ± 0.002 | 0.988 ± 0.007 |
| Total | 0.965 ± 0.0303 | 0.966 ± 0.0714 | 0.973 ± 0.0475 | 0.966 ± 0.0537 | 0.971 ± 0.0322 | 0.983 ± 0.0253 | 0.979 ± 0.0324 |

Table A.12: Pearson's correlation coefficient from cumulated activations between healthy and patients' ones for each muscle while reaching the target 10. For healthy subjects, this shows the intervariability within the healthy population. A1 corresponds to the first assessment, A4 to the final one. The final row correspond to the overall mean of these values.

| Pearson's correlation coefficient from cumulated sum of the signals activations while reaching target 10 | | | | | | | |
|--|-----------------------|-----------------------|-----------------------|-----------------------|-----------------------|-----------------------|-----------------------|
| Target 10 | Healthy | S1 | | S2 | | S3 | |
| | | A1 | A4 | A1 | A4 | A1 | A4 |
| Subclavius | 0.977 ± 0.006 | 0.99 ± 0 | 0.977 ± 0.02 | 0.995 ± 0 | 0.991 ± 0.006 | 0.989 ± 0.012 | 0.993 ± 0.001 |
| Serratus Anterior Superior | 0.941 ± 0.033 | 0.953 ± 0 | 0.966 ± 0.024 | 0.927 ± 0 | 0.977 ± 0.019 | 0.934 ± 0.057 | 0.916 ± 0.015 |
| Serratus Anterior Middle | 0.969 ± 0.013 | 0.955 ± 0 | 0.995 ± 0.004 | 0.996 ± 0 | 0.982 ± 0.01 | 0.989 ± 0.003 | 0.983 ± 0.002 |
| Serratus Anterior Inferior | 0.995 ± 0.002 | 0.997 ± 0 | 0.998 ± 0.002 | 0.99 ± 0 | 0.995 ± 0.004 | 0.999 ± 0 | 0.993 ± 0.005 |
| Trapezius C1 | 0.998 ± 0.001 | 0.98 ± 0 | 0.999 ± 0 | 0.995 ± 0 | 0.996 ± 0.004 | 1 ± 0 | 0.998 ± 0.001 |
| Trapezius C7 | 0.991 ± 0.007 | 0.965 ± 0 | 0.998 ± 0.001 | 0.995 ± 0 | 0.969 ± 0.025 | 0.985 ± 0.017 | 0.995 ± 0.001 |
| Trapezius T1 | 0.995 ± 0.002 | 0.999 ± 0 | 0.996 ± 0.004 | 0.976 ± 0 | 0.984 ± 0.007 | 0.996 ± 0.001 | 0.982 ± 0.012 |
| Trapezius T2 - T7 | 0.984 ± 0.01 | 0.989 ± 0 | 0.981 ± 0.013 | 0.995 ± 0 | 0.995 ± 0 | 0.984 ± 0.018 | 0.991 ± 0.003 |
| Levator Scapulae | 0.981 ± 0.008 | 0.997 ± 0 | 0.996 ± 0.004 | 0.997 ± 0 | 0.985 ± 0.017 | 0.992 ± 0.004 | 0.995 ± 0.001 |
| Rhomboid Minor | 0.992 ± 0.002 | 0.996 ± 0 | 0.998 ± 0.003 | 0.996 ± 0 | 0.99 ± 0.01 | 0.999 ± 0 | 0.995 ± 0.002 |
| Rhomboid Major T1 - T2 | 0.992 ± 0.007 | 0.997 ± 0 | 0.997 ± 0.004 | 0.997 ± 0 | 0.994 ± 0.006 | 0.992 ± 0.01 | 0.993 ± 0.006 |
| Rhomboid Major T3 - T4 | 0.991 ± 0.003 | 0.958 ± 0 | 0.997 ± 0.002 | 0.989 ± 0 | 0.985 ± 0.01 | 0.992 ± 0.002 | 0.993 ± 0.001 |
| Pectoralis Minor | 0.931 ± 0.027 | 0.98 ± 0 | 0.917 ± 0.042 | 0.938 ± 0 | 0.975 ± 0.019 | 0.951 ± 0.029 | 0.968 ± 0.022 |
| Pectoralis Major Clavicular | 0.962 ± 0.027 | 0.868 ± 0 | 0.969 ± 0.035 | 0.99 ± 0 | 0.993 ± 0.005 | 0.998 ± 0 | 0.964 ± 0.037 |
| Pectoralis Major Sternal | 0.913 ± 0.07 | 0.767 ± 0 | 0.89 ± 0.123 | 0.843 ± 0 | 0.974 ± 0.02 | 0.909 ± 0.117 | 0.924 ± 0.095 |
| Pectoralis Major Ribs | 0.881 ± 0.065 | 0.811 ± 0 | 0.69 ± 0.179 | 0.851 ± 0 | 0.886 ± 0.042 | 0.96 ± 0.002 | 0.963 ± 0 |
| Latissimus Dorsi Thoracic | 0.981 ± 0.008 | 0.983 ± 0 | 0.993 ± 0.008 | 0.986 ± 0 | 0.98 ± 0.007 | 0.815 ± 0.221 | 0.861 ± 0.142 |
| Latissimus Dorsi Lumbar | 0.915 ± 0.062 | 0.994 ± 0 | 0.951 ± 0.084 | 0.897 ± 0 | 0.962 ± 0.026 | 0.858 ± 0.181 | 0.756 ± 0.125 |
| Latissimus Dorsi Iliac | 0.885 ± 0.083 | 0.995 ± 0 | 0.98 ± 0.026 | 0.926 ± 0 | 0.885 ± 0.006 | 0.838 ± 0.184 | 0.641 ± 0.056 |
| Deltoid Clavicular (Ant) | 0.955 ± 0.019 | 0.817 ± 0 | 0.961 ± 0.032 | 0.901 ± 0 | 0.991 ± 0 | 0.984 ± 0.019 | 0.99 ± 0.001 |
| Deltoid Acromial (Mid) | 0.963 ± 0.023 | 0.976 ± 0 | 0.989 ± 0.009 | 0.985 ± 0 | 0.977 ± 0.001 | 0.995 ± 0.004 | 0.996 ± 0.002 |
| Deltoid Scapular (Post) | 0.976 ± 0.011 | 0.958 ± 0 | 0.998 ± 0.001 | 0.974 ± 0 | 0.99 ± 0.003 | 0.995 ± 0.007 | 0.99 ± 0.008 |
| Supraspinatus | 0.968 ± 0.015 | 0.898 ± 0 | 0.936 ± 0.05 | 0.979 ± 0 | 0.915 ± 0.035 | 0.97 ± 0.014 | 0.942 ± 0.019 |
| Infraspinatus | 0.977 ± 0.009 | 0.92 ± 0 | 0.998 ± 0.002 | 0.992 ± 0 | 0.977 ± 0.003 | 0.986 ± 0.011 | 0.996 ± 0.002 |
| Subscapularis | 0.978 ± 0.013 | 0.848 ± 0 | 0.951 ± 0.064 | 0.78 ± 0 | 0.965 ± 0.017 | 0.866 ± 0.173 | 0.91 ± 0.107 |
| Teres Minor | 0.864 ± 0.053 | 0.932 ± 0 | 0.894 ± 0.118 | 0.909 ± 0 | 0.983 ± 0.006 | 0.895 ± 0.092 | 0.952 ± 0.005 |
| Teres Major | 0.932 ± 0.045 | 0.999 ± 0 | 0.986 ± 0.023 | 0.896 ± 0 | 0.993 ± 0.008 | 0.995 ± 0.006 | 0.792 ± 0.223 |
| Coracobrachialis | 0.913 ± 0.049 | 0.867 ± 0 | 0.929 ± 0.038 | 0.978 ± 0 | 0.975 ± 0.018 | 0.969 ± 0.022 | 0.972 ± 0.028 |
| Triceps Brachii Long | 0.986 ± 0.005 | 0.936 ± 0 | 0.995 ± 0.003 | 0.909 ± 0 | 0.977 ± 0.015 | 0.999 ± 0 | 0.999 ± 0 |
| Triceps Brachii Medial | 0.945 ± 0.029 | 0.877 ± 0 | 0.954 ± 0.022 | 0.993 ± 0 | 0.84 ± 0.107 | 0.976 ± 0.018 | 0.977 ± 0.018 |
| Triceps Brachii Lateral | 0.947 ± 0.022 | 0.691 ± 0 | 0.996 ± 0.002 | 0.797 ± 0 | 0.857 ± 0.043 | 0.922 ± 0.052 | 0.846 ± 0.145 |
| Biceps Short | 0.986 ± 0.005 | 0.946 ± 0 | 0.997 ± 0.002 | 0.925 ± 0 | 0.944 ± 0.023 | 0.99 ± 0.006 | 0.963 ± 0.027 |
| Biceps Long | 0.982 ± 0.013 | 0.916 ± 0 | 0.997 ± 0.001 | 0.936 ± 0 | 0.953 ± 0.024 | 0.991 ± 0.005 | 0.977 ± 0.009 |
| Brachialis | 0.995 ± 0.002 | 0.955 ± 0 | 0.997 ± 0 | 0.959 ± 0 | 0.98 ± 0.005 | 0.99 ± 0 | 0.987 ± 0.003 |
| Brachioradialis | 0.99 ± 0.004 | 0.953 ± 0 | 0.95 ± 0.055 | 0.804 ± 0 | 0.957 ± 0.012 | 0.975 ± 0.028 | 0.967 ± 0.029 |
| Supinator | 0.997 ± 0.002 | 0.999 ± 0 | 1 ± 0 | 0.996 ± 0 | 0.997 ± 0.002 | 1 ± 0 | 0.979 ± 0.007 |
| Pronator Teres | 0.987 ± 0.007 | 0.995 ± 0 | 0.99 ± 0.003 | 0.913 ± 0 | 0.997 ± 0.003 | 0.971 ± 0.037 | 0.988 ± 0 |
| Flexor Carpi Radialis | 0.876 ± 0.049 | 0.869 ± 0 | 0.858 ± 0.098 | 0.882 ± 0 | 0.961 ± 0.028 | 0.916 ± 0.056 | 0.969 ± 0.009 |
| Flexor Carpi Ulnaris | 0.928 ± 0.032 | 0.992 ± 0 | 0.867 ± 0.058 | 0.982 ± 0 | 0.946 ± 0.047 | 0.97 ± 0.03 | 0.995 ± 0.001 |
| Extensor Carpi Radialis Long | 0.986 ± 0.01 | 0.995 ± 0 | 0.995 ± 0 | 0.996 ± 0 | 0.965 ± 0.006 | 0.952 ± 0.048 | 0.998 ± 0.001 |
| Extensor Carpi Radialis Brevis | 0.948 ± 0.04 | 0.987 ± 0 | 0.997 ± 0.001 | 0.999 ± 0 | 0.96 ± 0.013 | 0.995 ± 0.001 | 0.996 ± 0.001 |
| Extensor Carpi Ulnaris | 0.931 ± 0.036 | 0.754 ± 0 | 0.994 ± 0.005 | 0.924 ± 0 | 0.985 ± 0.012 | 0.973 ± 0.025 | 0.979 ± 0.015 |
| Total | 0.959 ± 0.0371 | 0.935 ± 0.0767 | 0.965 ± 0.0576 | 0.945 ± 0.0608 | 0.966 ± 0.0373 | 0.963 ± 0.0474 | 0.954 ± 0.0739 |

Table A.13: Pearson's correlation coefficient from cumulated activations between healthy and patients' ones for each muscle while reaching the target 13. For healthy subjects, this shows the intervariability within the healthy population. A1 corresponds to the first assessment, A4 to the final one. The final row correspond to the overall mean of these values.

Pearson's correlation coefficient from cumulated sum of the signals activations while reaching target 13

| Target 13 | Healthy | S1 | | S2 | | S3 | |
|--------------------------------|-----------------------|-----------------------|-----------------------|-----------------------|-----------------------|-----------------------|-----------------------|
| | | A1 | A4 | A1 | A4 | A1 | A4 |
| Subclavius | 0.974 ± 0.011 | 0.917 ± 0 | 0.965 ± 0.024 | 0.992 ± 0 | 0.92 ± 0.072 | 0.988 ± 0.005 | 0.969 ± 0.001 |
| Serratus Anterior Superior | 0.972 ± 0.011 | 0.888 ± 0 | 0.969 ± 0.012 | 0.965 ± 0 | 0.977 ± 0.001 | 0.963 ± 0.006 | 0.944 ± 0.026 |
| Serratus Anterior Middle | 0.97 ± 0.017 | 0.98 ± 0 | 0.986 ± 0.011 | 0.994 ± 0 | 0.98 ± 0.019 | 0.981 ± 0.008 | 0.988 ± 0.004 |
| Serratus Anterior Inferior | 0.998 ± 0.001 | 0.999 ± 0 | 0.999 ± 0.001 | 0.998 ± 0 | 0.997 ± 0.002 | 0.997 ± 0.001 | 0.999 ± 0.001 |
| Trapezius C1 | 0.998 ± 0.001 | 0.997 ± 0 | 0.999 ± 0 | 0.999 ± 0 | 1 ± 0 | 0.997 ± 0.001 | 0.998 ± 0.001 |
| Trapezius C7 | 0.995 ± 0.003 | 0.989 ± 0 | 0.996 ± 0.002 | 0.998 ± 0 | 0.99 ± 0.013 | 0.994 ± 0.004 | 0.985 ± 0.005 |
| Trapezius T1 | 0.996 ± 0.003 | 0.999 ± 0 | 0.996 ± 0.003 | 0.998 ± 0 | 0.994 ± 0.003 | 0.995 ± 0 | 0.996 ± 0.002 |
| Trapezius T2 - T7 | 0.982 ± 0.01 | 0.989 ± 0 | 0.986 ± 0.007 | 0.979 ± 0 | 0.975 ± 0.018 | 0.993 ± 0.002 | 0.985 ± 0.01 |
| Levator Scapulae | 0.972 ± 0.016 | 0.987 ± 0 | 0.994 ± 0.005 | 0.976 ± 0 | 0.988 ± 0.007 | 0.981 ± 0.011 | 0.973 ± 0.003 |
| Rhomboid Minor | 0.994 ± 0.002 | 0.998 ± 0 | 0.996 ± 0.003 | 0.996 ± 0 | 0.993 ± 0.004 | 0.997 ± 0.002 | 0.999 ± 0.001 |
| Rhomboid Major T1 - T2 | 0.989 ± 0.005 | 0.991 ± 0 | 0.991 ± 0.009 | 0.97 ± 0 | 0.992 ± 0.009 | 0.968 ± 0.017 | 0.995 ± 0.003 |
| Rhomboid Major T3 - T4 | 0.993 ± 0.003 | 0.985 ± 0 | 0.998 ± 0.001 | 0.998 ± 0 | 0.985 ± 0.001 | 0.999 ± 0 | 0.982 ± 0.014 |
| Pectoralis Minor | 0.943 ± 0.023 | 0.732 ± 0 | 0.976 ± 0.009 | 0.909 ± 0 | 0.934 ± 0.052 | 0.9 ± 0.047 | 0.872 ± 0.033 |
| Pectoralis Major Clavicular | 0.993 ± 0.004 | 0.96 ± 0 | 0.996 ± 0.004 | 0.993 ± 0 | 0.989 ± 0.006 | 0.993 ± 0.001 | 0.991 ± 0.005 |
| Pectoralis Major Sternal | 0.953 ± 0.025 | 0.865 ± 0 | 0.968 ± 0.014 | 0.939 ± 0 | 0.973 ± 0.028 | 0.889 ± 0.098 | 0.901 ± 0.025 |
| Pectoralis Major Ribs | 0.928 ± 0.031 | 0.896 ± 0 | 0.91 ± 0.074 | 0.963 ± 0 | 0.907 ± 0.065 | 0.954 ± 0.027 | 0.916 ± 0.023 |
| Latissimus Dorsi Thoracic | 0.967 ± 0.026 | 0.71 ± 0 | 0.995 ± 0.002 | 0.986 ± 0 | 0.992 ± 0.002 | 0.958 ± 0.004 | 0.968 ± 0.025 |
| Latissimus Dorsi Lumbar | 0.93 ± 0.025 | 0.927 ± 0 | 0.948 ± 0.03 | 0.938 ± 0 | 0.93 ± 0.007 | 0.842 ± 0.087 | 0.926 ± 0.002 |
| Latissimus Dorsi Iliac | 0.937 ± 0.023 | 0.945 ± 0 | 0.942 ± 0.039 | 0.905 ± 0 | 0.858 ± 0.131 | 0.766 ± 0.063 | 0.88 ± 0.051 |
| Deltoid Clavicular (Ant) | 0.996 ± 0.002 | 0.992 ± 0 | 0.999 ± 0.001 | 0.988 ± 0 | 0.994 ± 0.007 | 0.993 ± 0.006 | 0.998 ± 0.002 |
| Deltoid Acromial (Mid) | 0.997 ± 0.003 | 0.995 ± 0 | 0.999 ± 0.001 | 0.997 ± 0 | 0.994 ± 0.004 | 0.996 ± 0.002 | 0.99 ± 0.002 |
| Deltoid Scapular (Post) | 0.976 ± 0.017 | 0.988 ± 0 | 0.998 ± 0.001 | 0.981 ± 0 | 0.995 ± 0 | 0.996 ± 0.005 | 0.961 ± 0.007 |
| Supraspinatus | 0.976 ± 0.01 | 0.929 ± 0 | 0.982 ± 0.015 | 0.991 ± 0 | 0.978 ± 0.004 | 0.824 ± 0.228 | 0.903 ± 0.027 |
| Infraspinatus | 0.995 ± 0.002 | 0.983 ± 0 | 0.995 ± 0.006 | 0.984 ± 0 | 0.986 ± 0.014 | 0.989 ± 0.009 | 0.991 ± 0.008 |
| Subscapularis | 0.938 ± 0.021 | 0.844 ± 0 | 0.859 ± 0.055 | 0.916 ± 0 | 0.966 ± 0.008 | 0.956 ± 0.042 | 0.679 ± 0.049 |
| Teres Minor | 0.932 ± 0.032 | 0.721 ± 0 | 0.913 ± 0.048 | 0.91 ± 0 | 0.969 ± 0.014 | 0.916 ± 0.034 | 0.792 ± 0.018 |
| Teres Major | 0.934 ± 0.039 | 0.91 ± 0 | 0.964 ± 0.027 | 0.971 ± 0 | 0.95 ± 0.029 | 0.984 ± 0.005 | 0.899 ± 0.048 |
| Coracobrachialis | 0.968 ± 0.017 | 0.991 ± 0 | 0.98 ± 0.022 | 0.996 ± 0 | 0.983 ± 0.018 | 0.86 ± 0.11 | 0.995 ± 0.004 |
| Triceps Brachii Long | 0.981 ± 0.014 | 0.99 ± 0 | 0.984 ± 0.005 | 0.976 ± 0 | 0.997 ± 0.001 | 0.999 ± 0 | 0.997 ± 0.003 |
| Triceps Brachii Medial | 0.976 ± 0.017 | 0.997 ± 0 | 0.99 ± 0.01 | 0.998 ± 0 | 0.974 ± 0.013 | 0.987 ± 0.001 | 0.998 ± 0.001 |
| Triceps Brachii Lateral | 0.988 ± 0.008 | 0.995 ± 0 | 0.986 ± 0.019 | 0.995 ± 0 | 0.987 ± 0.009 | 0.867 ± 0.142 | 0.997 ± 0.001 |
| Biceps Short | 0.956 ± 0.04 | 0.972 ± 0 | 0.982 ± 0.011 | 0.995 ± 0 | 0.984 ± 0.017 | 0.976 ± 0.014 | 0.976 ± 0.003 |
| Biceps Long | 0.967 ± 0.027 | 0.983 ± 0 | 0.995 ± 0.003 | 0.981 ± 0 | 0.992 ± 0.006 | 0.961 ± 0.016 | 0.881 ± 0.042 |
| Brachialis | 0.995 ± 0.006 | 0.996 ± 0 | 0.996 ± 0.002 | 0.985 ± 0 | 0.99 ± 0.01 | 0.999 ± 0 | 0.996 ± 0.001 |
| Brachioradialis | 0.986 ± 0.01 | 0.998 ± 0 | 0.966 ± 0.008 | 0.987 ± 0 | 0.992 ± 0.001 | 0.989 ± 0.003 | 0.991 ± 0.004 |
| Supinator | 0.996 ± 0.002 | 0.957 ± 0 | 0.997 ± 0.001 | 0.963 ± 0 | 0.999 ± 0 | 0.993 ± 0.009 | 0.953 ± 0.003 |
| Pronator Teres | 0.996 ± 0.002 | 0.997 ± 0 | 0.962 ± 0.013 | 0.996 ± 0 | 0.999 ± 0 | 0.999 ± 0 | 0.99 ± 0.004 |
| Flexor Carpi Radialis | 0.957 ± 0.021 | 0.944 ± 0 | 0.964 ± 0.012 | 0.976 ± 0 | 0.977 ± 0.017 | 0.893 ± 0.016 | 0.874 ± 0.018 |
| Flexor Carpi Ulnaris | 0.957 ± 0.017 | 0.994 ± 0 | 0.953 ± 0.034 | 0.995 ± 0 | 0.909 ± 0.02 | 0.983 ± 0.019 | 0.995 ± 0 |
| Extensor Carpi Radialis Long | 0.945 ± 0.025 | 0.989 ± 0 | 0.978 ± 0.02 | 0.973 ± 0 | 0.898 ± 0.048 | 0.963 ± 0.041 | 0.988 ± 0.004 |
| Extensor Carpi Radialis Brevis | 0.952 ± 0.016 | 0.976 ± 0 | 0.977 ± 0 | 0.978 ± 0 | 0.94 ± 0.051 | 0.974 ± 0.003 | 0.978 ± 0 |
| Extensor Carpi Ulnaris | 0.969 ± 0.013 | 0.882 ± 0 | 0.928 ± 0.026 | 0.974 ± 0 | 0.947 ± 0.064 | 0.985 ± 0.012 | 0.965 ± 0.011 |
| Total | 0.972 ± 0.0223 | 0.947 ± 0.0757 | 0.975 ± 0.0293 | 0.976 ± 0.0262 | 0.971 ± 0.0329 | 0.958 ± 0.0563 | 0.954 ± 0.0648 |

Table A.14: Pearson's correlation coefficient from cumulated activations between healthy and patients' ones for the recorded muscles. For healthy subjects, this shows the inter variability within the healthy population. A1 corresponds to the first assessment, A4 to the final one. These are concatenated by target [1,3,5].

| | Healthy | S1 | | S2 | | S3 | |
|-----------------------------|-----------------|-----------------|-----------------|-----------------|-----------------|-----------------|----------------|
| | | A1 | A4 | A1 | A4 | A1 | A4 |
| Target 1 | | | | | | | |
| Trapezius C1 | 0.997 ± 0.003 | 0.998 ± 0 | 0.999 ± 0 | 0.991 ± 0.01 | 0.962 ± 0.046 | 0.988 ± 0.011 | 0.997 ± 0.003 |
| Trapezius C7 | 0.993 ± 0.004 | 0.996 ± 0 | 0.999 ± 0.001 | 0.987 ± 0.012 | 0.991 ± 0.003 | 0.988 ± 0.012 | 0.996 ± 0.001 |
| Rhomboid Major T3 - T4 | 0.992 ± 0.004 | 0.998 ± 0 | 0.999 ± 0 | 0.995 ± 0.006 | 0.962 ± 0.053 | 0.997 ± 0.003 | 0.999 ± 0.001 |
| Pectoralis Major Clavicular | 0.99 ± 0.004 | 0.998 ± 0 | 0.997 ± 0.001 | 0.99 ± 0.007 | 0.978 ± 0.014 | 0.99 ± 0.013 | 0.998 ± 0 |
| Latissimus Dorsi Thoracic | 0.982 ± 0.008 | 0.995 ± 0 | 0.998 ± 0.002 | 0.996 ± 0.002 | 0.912 ± 0.115 | 0.994 ± 0.007 | 0.998 ± 0 |
| Deltoid Clavicular (Ant) | 0.986 ± 0.009 | 0.995 ± 0 | 0.998 ± 0.001 | 0.993 ± 0.008 | 0.856 ± 0.163 | 0.985 ± 0.013 | 0.993 ± 0.002 |
| Deltoid Acromial (Mid) | 0.995 ± 0.003 | 0.994 ± 0 | 0.991 ± 0.004 | 0.987 ± 0.011 | 0.908 ± 0.097 | 0.992 ± 0 | 0.989 ± 0.002 |
| Deltoid Scapular (Post) | 0.991 ± 0.008 | 0.995 ± 0 | 0.998 ± 0.002 | 0.981 ± 0.02 | 0.977 ± 0.031 | 0.996 ± 0.001 | 0.994 ± 0.002 |
| Infraspinatus | 0.994 ± 0.002 | 0.996 ± 0 | 0.999 ± 0 | 0.994 ± 0.006 | 0.985 ± 0.017 | 0.996 ± 0.002 | 0.997 ± 0 |
| Triceps Brachii Long | 0.99 ± 0.005 | 0.995 ± 0 | 0.997 ± 0.002 | 0.983 ± 0.014 | 0.989 ± 0.008 | 0.989 ± 0.009 | 0.996 ± 0.001 |
| Triceps Brachii Lateral | 0.979 ± 0.016 | 0.994 ± 0 | 0.998 ± 0.001 | 0.986 ± 0.013 | 0.959 ± 0.055 | 0.994 ± 0 | 0.996 ± 0.001 |
| Biceps Short | 0.975 ± 0.018 | 0.994 ± 0 | 0.999 ± 0 | 0.983 ± 0.015 | 0.985 ± 0.02 | 0.98 ± 0.013 | 0.997 ± 0.003 |
| Biceps Long | 0.972 ± 0.019 | 0.991 ± 0 | 0.998 ± 0.001 | 0.992 ± 0.006 | 0.953 ± 0.025 | 0.995 ± 0.005 | 0.997 ± 0.002 |
| Brachialis | 0.985 ± 0.013 | 0.997 ± 0 | 0.987 ± 0.007 | 0.992 ± 0.011 | 0.984 ± 0.02 | 1 ± 0 | 0.989 ± 0.009 |
| Brachioradialis | 0.989 ± 0.008 | 0.999 ± 0 | 0.978 ± 0.017 | 0.993 ± 0.001 | 0.982 ± 0.008 | 0.999 ± 0.001 | 0.983 ± 0.014 |
| Pronator Teres | 0.967 ± 0.037 | 0.999 ± 0 | 0.996 ± 0.002 | 0.986 ± 0.004 | 0.97 ± 0.04 | 0.983 ± 0.009 | 0.998 ± 0.001 |
| Total | 0.986 ± 0.00886 | 0.996 ± 0.00214 | 0.996 ± 0.00594 | 0.989 ± 0.00458 | 0.959 ± 0.0373 | 0.992 ± 0.0057 | 0.995 ± 0.0043 |
| Target 3 | | | | | | | |
| Trapezius C1 | 0.994 ± 0.006 | 0.926 ± 0 | 0.995 ± 0.004 | 0.984 ± 0.002 | 0.999 ± 0 | 0.995 ± 0 | 0.927 ± 0.031 |
| Trapezius C7 | 0.987 ± 0.01 | 0.916 ± 0 | 0.997 ± 0.002 | 0.977 ± 0.001 | 0.998 ± 0 | 0.997 ± 0.003 | 0.985 ± 0 |
| Rhomboid Major T3 - T4 | 0.986 ± 0.012 | 0.98 ± 0 | 0.998 ± 0.001 | 0.974 ± 0.01 | 0.996 ± 0.004 | 1 ± 0 | 0.997 ± 0 |
| Pectoralis Major Clavicular | 0.947 ± 0.036 | 0.941 ± 0 | 0.988 ± 0.008 | 0.98 ± 0.022 | 0.968 ± 0.029 | 0.996 ± 0.002 | 0.999 ± 0 |
| Latissimus Dorsi Thoracic | 0.979 ± 0.011 | 0.929 ± 0 | 0.999 ± 0.001 | 0.982 ± 0.001 | 0.999 ± 0.001 | 0.998 ± 0.002 | 0.991 ± 0.001 |
| Deltoid Clavicular (Ant) | 0.982 ± 0.013 | 0.881 ± 0 | 0.996 ± 0.002 | 0.975 ± 0.011 | 0.984 ± 0.001 | 0.992 ± 0.007 | 0.964 ± 0.023 |
| Deltoid Acromial (Mid) | 0.997 ± 0.002 | 0.861 ± 0 | 0.99 ± 0.003 | 0.965 ± 0.003 | 0.983 ± 0.001 | 0.997 ± 0 | 0.989 ± 0.006 |
| Deltoid Scapular (Post) | 0.995 ± 0.003 | 0.889 ± 0 | 0.997 ± 0.003 | 0.955 ± 0.011 | 0.991 ± 0.002 | 0.998 ± 0.001 | 0.974 ± 0.01 |
| Infraspinatus | 0.996 ± 0.002 | 0.937 ± 0 | 0.999 ± 0.001 | 0.98 ± 0 | 0.996 ± 0 | 0.998 ± 0 | 0.998 ± 0.001 |
| Triceps Brachii Long | 0.997 ± 0.001 | 0.951 ± 0 | 0.991 ± 0.008 | 0.972 ± 0.003 | 0.995 ± 0.002 | 0.997 ± 0.001 | 0.982 ± 0.017 |
| Triceps Brachii Lateral | 0.961 ± 0.024 | 0.9 ± 0 | 0.99 ± 0.005 | 0.966 ± 0.009 | 0.989 ± 0.008 | 0.998 ± 0.001 | 0.995 ± 0 |
| Biceps Short | 0.974 ± 0.024 | 0.916 ± 0 | 0.997 ± 0.002 | 0.969 ± 0 | 0.993 ± 0.001 | 0.992 ± 0.011 | 0.95 ± 0.004 |
| Biceps Long | 0.981 ± 0.01 | 0.887 ± 0 | 0.998 ± 0.001 | 0.977 ± 0.009 | 0.999 ± 0 | 0.99 ± 0.011 | 0.978 ± 0.024 |
| Brachialis | 0.998 ± 0.002 | 0.959 ± 0 | 0.984 ± 0.011 | 0.982 ± 0.008 | 0.983 ± 0.012 | 0.996 ± 0.002 | 0.977 ± 0.007 |
| Brachioradialis | 0.987 ± 0.008 | 0.98 ± 0 | 0.97 ± 0.018 | 0.99 ± 0.001 | 0.993 ± 0.003 | 0.999 ± 0.001 | 0.961 ± 0.014 |
| Pronator Teres | 0.939 ± 0.039 | 0.997 ± 0 | 0.992 ± 0.004 | 0.99 ± 0.009 | 0.993 ± 0.001 | 0.993 ± 0.007 | 0.997 ± 0.002 |
| Total | 0.981 ± 0.018 | 0.928 ± 0.0391 | 0.993 ± 0.00741 | 0.976 ± 0.00929 | 0.991 ± 0.00826 | 0.996 ± 0.00286 | 0.979 ± 0.0201 |
| Target 5 | | | | | | | |
| Trapezius C1 | 0.998 ± 0.001 | 0.999 ± 0 | 0.998 ± 0.001 | 0.993 ± 0 | 0.999 ± 0 | 0.997 ± 0.003 | 0.969 ± 0.035 |
| Trapezius C7 | 0.986 ± 0.012 | 1 ± 0 | 0.998 ± 0.001 | 0.995 ± 0 | 0.998 ± 0.001 | 0.996 ± 0.003 | 0.996 ± 0.001 |
| Rhomboid Major T3 - T4 | 0.99 ± 0.006 | 1 ± 0 | 0.997 ± 0.001 | 0.99 ± 0 | 0.993 ± 0.005 | 0.998 ± 0.001 | 0.995 ± 0.005 |
| Pectoralis Major Clavicular | 0.978 ± 0.015 | 0.994 ± 0 | 0.993 ± 0.003 | 0.998 ± 0 | 0.996 ± 0.002 | 0.995 ± 0.006 | 0.946 ± 0.07 |
| Latissimus Dorsi Thoracic | 0.979 ± 0.007 | 0.998 ± 0 | 0.99 ± 0.003 | 0.986 ± 0 | 0.985 ± 0.005 | 0.999 ± 0 | 0.995 ± 0 |
| Deltoid Clavicular (Ant) | 0.968 ± 0.014 | 0.991 ± 0 | 0.991 ± 0.002 | 0.973 ± 0 | 0.956 ± 0.014 | 0.995 ± 0 | 0.944 ± 0.064 |
| Deltoid Acromial (Mid) | 0.936 ± 0.04 | 0.998 ± 0 | 0.988 ± 0.006 | 0.96 ± 0 | 0.97 ± 0.018 | 0.999 ± 0 | 0.988 ± 0.013 |
| Deltoid Scapular (Post) | 0.991 ± 0.004 | 0.999 ± 0 | 0.999 ± 0.001 | 0.984 ± 0 | 0.993 ± 0.006 | 1 ± 0 | 0.995 ± 0.002 |
| Infraspinatus | 0.976 ± 0.011 | 1 ± 0 | 0.991 ± 0.005 | 0.984 ± 0 | 0.99 ± 0.005 | 0.999 ± 0.001 | 0.993 ± 0.003 |
| Triceps Brachii Long | 0.989 ± 0.006 | 0.995 ± 0 | 0.998 ± 0.001 | 0.992 ± 0 | 0.999 ± 0 | 0.998 ± 0 | 0.997 ± 0.003 |
| Triceps Brachii Lateral | 0.944 ± 0.027 | 0.995 ± 0 | 0.995 ± 0.005 | 0.975 ± 0 | 0.996 ± 0.001 | 0.999 ± 0 | 0.999 ± 0 |
| Biceps Short | 0.987 ± 0.007 | 0.995 ± 0 | 0.997 ± 0.002 | 0.982 ± 0 | 0.996 ± 0.001 | 0.993 ± 0.008 | 0.979 ± 0.004 |
| Biceps Long | 0.982 ± 0.015 | 0.999 ± 0 | 0.993 ± 0.005 | 0.977 ± 0 | 0.986 ± 0.008 | 0.977 ± 0.022 | 0.978 ± 0.003 |
| Brachialis | 0.995 ± 0.004 | 0.998 ± 0 | 0.998 ± 0.001 | 0.982 ± 0 | 0.988 ± 0.004 | 0.999 ± 0.001 | 0.977 ± 0.018 |
| Brachioradialis | 0.986 ± 0.012 | 0.997 ± 0 | 0.989 ± 0.012 | 0.992 ± 0 | 0.997 ± 0.002 | 1 ± 0 | 0.94 ± 0.013 |
| Pronator Teres | 0.986 ± 0.006 | 0.999 ± 0 | 0.996 ± 0.002 | 0.99 ± 0 | 0.997 ± 0.003 | 0.991 ± 0.012 | 0.98 ± 0.001 |
| Total | 0.979 ± 0.0171 | 0.997 ± 0.00246 | 0.995 ± 0.00373 | 0.985 ± 0.00997 | 0.99 ± 0.0118 | 0.996 ± 0.0057 | 0.979 ± 0.02 |

Table A.15: Pearson's correlation coefficient from cumulated activations between healthy and patients' ones for the recorded muscles. For healthy subjects, this shows the inter variability within the healthy population. A1 corresponds to the first assessment, A4 to the final one. These are concatenated by target [7,10,13].

| | Healthy | A1 | S1 A4 | A1 | S2 A4 | A1 | S3 A4 |
|-----------------------------|----------------|-----------------|-----------------|-----------------|-----------------|-----------------|-----------------|
| Target 7 | | | | | | | |
| Trapezius C1 | 0.998 ± 0.001 | 1 ± 0 | 0.996 ± 0.003 | 0.993 ± 0 | 0.995 ± 0.004 | 0.997 ± 0.002 | 0.992 ± 0.004 |
| Trapezius C7 | 0.965 ± 0.031 | 0.998 ± 0 | 0.997 ± 0.002 | 0.99 ± 0 | 0.998 ± 0.002 | 0.998 ± 0.002 | 0.985 ± 0.012 |
| Rhomboid Major T3 - T4 | 0.994 ± 0.004 | 0.998 ± 0 | 0.999 ± 0.001 | 0.982 ± 0 | 0.999 ± 0 | 0.997 ± 0.002 | 0.995 ± 0.002 |
| Pectoralis Major Clavicular | 0.991 ± 0.003 | 0.994 ± 0 | 0.997 ± 0.002 | 0.994 ± 0 | 0.99 ± 0.013 | 0.997 ± 0.001 | 0.99 ± 0.007 |
| Latissimus Dorsi Thoracic | 0.951 ± 0.03 | 0.997 ± 0 | 0.996 ± 0.003 | 0.987 ± 0 | 0.997 ± 0.001 | 0.997 ± 0.003 | 0.99 ± 0.002 |
| Deltoid Clavicular (Ant) | 0.993 ± 0.003 | 0.997 ± 0 | 0.998 ± 0.001 | 0.99 ± 0 | 0.983 ± 0.012 | 0.995 ± 0.006 | 0.991 ± 0.001 |
| Deltoid Acromial (Mid) | 0.986 ± 0.007 | 0.999 ± 0 | 0.996 ± 0.003 | 0.992 ± 0 | 0.975 ± 0.001 | 1 ± 0 | 0.968 ± 0.017 |
| Deltoid Scapular (Post) | 0.954 ± 0.038 | 0.998 ± 0 | 1 ± 0 | 0.991 ± 0 | 0.989 ± 0.01 | 0.999 ± 0 | 0.974 ± 0.001 |
| Infraspinatus | 0.971 ± 0.015 | 0.993 ± 0 | 0.996 ± 0.002 | 0.981 ± 0 | 0.992 ± 0.004 | 0.996 ± 0.002 | 0.981 ± 0.012 |
| Triceps Brachii Long | 0.991 ± 0.003 | 1 ± 0 | 0.998 ± 0.001 | 0.985 ± 0 | 0.996 ± 0.004 | 0.998 ± 0.001 | 0.999 ± 0.001 |
| Triceps Brachii Lateral | 0.968 ± 0.03 | 0.999 ± 0 | 0.998 ± 0.001 | 0.994 ± 0 | 0.995 ± 0.005 | 1 ± 0 | 0.998 ± 0 |
| Biceps Short | 0.972 ± 0.02 | 0.995 ± 0 | 0.999 ± 0.001 | 0.991 ± 0 | 0.999 ± 0.001 | 0.995 ± 0.004 | 0.991 ± 0.005 |
| Biceps Long | 0.981 ± 0.018 | 0.998 ± 0 | 0.998 ± 0.001 | 0.983 ± 0 | 0.996 ± 0.005 | 0.998 ± 0.003 | 0.996 ± 0.002 |
| Brachialis | 0.983 ± 0.015 | 0.993 ± 0 | 0.995 ± 0.003 | 0.975 ± 0 | 0.993 ± 0.006 | 0.999 ± 0.001 | 0.992 ± 0.004 |
| Brachioradialis | 0.987 ± 0.011 | 0.996 ± 0 | 0.99 ± 0.01 | 0.974 ± 0 | 0.999 ± 0.001 | 0.999 ± 0 | 0.986 ± 0.001 |
| Pronator Teres | 0.993 ± 0.003 | 0.999 ± 0 | 0.999 ± 0 | 0.961 ± 0 | 0.998 ± 0.001 | 0.994 ± 0.003 | 0.998 ± 0.001 |
| Total | 0.98 ± 0.0147 | 0.997 ± 0.00223 | 0.997 ± 0.00238 | 0.985 ± 0.00913 | 0.993 ± 0.00669 | 0.998 ± 0.00181 | 0.989 ± 0.00866 |
| Target 10 | | | | | | | |
| Trapezius C1 | 0.998 ± 0.001 | 0.946 ± 0 | 0.999 ± 0.001 | 0.992 ± 0 | 0.99 ± 0.008 | 0.998 ± 0.001 | 0.992 ± 0.004 |
| Trapezius C7 | 0.991 ± 0.007 | 0.928 ± 0 | 0.998 ± 0.002 | 0.993 ± 0 | 0.98 ± 0.02 | 0.991 ± 0.006 | 0.994 ± 0.001 |
| Rhomboid Major T3 - T4 | 0.992 ± 0.002 | 0.978 ± 0 | 0.998 ± 0.001 | 0.98 ± 0 | 0.984 ± 0.011 | 0.995 ± 0.003 | 0.995 ± 0.004 |
| Pectoralis Major Clavicular | 0.962 ± 0.027 | 0.967 ± 0 | 0.993 ± 0.005 | 0.998 ± 0 | 0.998 ± 0.002 | 0.999 ± 0 | 0.993 ± 0.006 |
| Latissimus Dorsi Thoracic | 0.973 ± 0.008 | 0.962 ± 0 | 0.998 ± 0.002 | 0.984 ± 0 | 0.998 ± 0.001 | 0.998 ± 0.001 | 0.996 ± 0.002 |
| Deltoid Clavicular (Ant) | 0.957 ± 0.018 | 0.883 ± 0 | 0.995 ± 0.002 | 0.943 ± 0 | 0.986 ± 0.013 | 0.998 ± 0 | 0.982 ± 0 |
| Deltoid Acromial (Mid) | 0.96 ± 0.024 | 0.859 ± 0 | 0.985 ± 0.015 | 0.9 ± 0 | 0.987 ± 0.012 | 0.999 ± 0 | 0.972 ± 0.017 |
| Deltoid Scapular (Post) | 0.975 ± 0.012 | 0.901 ± 0 | 0.989 ± 0.007 | 0.903 ± 0 | 0.993 ± 0.005 | 0.999 ± 0 | 0.992 ± 0.001 |
| Infraspinatus | 0.973 ± 0.011 | 0.931 ± 0 | 0.999 ± 0.001 | 0.965 ± 0 | 0.98 ± 0.014 | 0.987 ± 0.011 | 0.994 ± 0.006 |
| Triceps Brachii Long | 0.983 ± 0.006 | 0.957 ± 0 | 0.995 ± 0.003 | 0.945 ± 0 | 0.977 ± 0.002 | 0.998 ± 0.001 | 0.994 ± 0.002 |
| Triceps Brachii Lateral | 0.959 ± 0.017 | 0.88 ± 0 | 0.998 ± 0.001 | 0.863 ± 0 | 0.933 ± 0.028 | 0.993 ± 0.002 | 0.993 ± 0.002 |
| Biceps Short | 0.987 ± 0.005 | 0.859 ± 0 | 0.997 ± 0.002 | 0.909 ± 0 | 0.969 ± 0.018 | 0.986 ± 0.003 | 0.977 ± 0.018 |
| Biceps Long | 0.982 ± 0.015 | 0.804 ± 0 | 0.999 ± 0 | 0.914 ± 0 | 0.936 ± 0.009 | 0.991 ± 0.003 | 0.971 ± 0.012 |
| Brachialis | 0.996 ± 0.002 | 0.913 ± 0 | 0.999 ± 0.001 | 0.92 ± 0 | 0.961 ± 0.015 | 0.994 ± 0.001 | 0.955 ± 0.04 |
| Brachioradialis | 0.99 ± 0.004 | 0.92 ± 0 | 0.999 ± 0 | 0.919 ± 0 | 0.963 ± 0.02 | 0.993 ± 0.001 | 0.944 ± 0.042 |
| Pronator Teres | 0.987 ± 0.007 | 0.981 ± 0 | 0.998 ± 0.001 | 0.815 ± 0 | 0.97 ± 0.011 | 0.987 ± 0.014 | 0.982 ± 0.015 |
| Total | 0.979 ± 0.0138 | 0.917 ± 0.05 | 0.996 ± 0.00409 | 0.934 ± 0.0512 | 0.975 ± 0.0194 | 0.994 ± 0.00456 | 0.983 ± 0.0155 |
| Target 13 | | | | | | | |
| Trapezius C1 | 0.997 ± 0.001 | 0.992 ± 0 | 0.998 ± 0.001 | 0.994 ± 0 | 0.998 ± 0.002 | 0.997 ± 0.003 | 0.994 ± 0.002 |
| Trapezius C7 | 0.994 ± 0.003 | 0.978 ± 0 | 0.993 ± 0.003 | 0.986 ± 0 | 0.992 ± 0.009 | 0.999 ± 0 | 0.985 ± 0.001 |
| Rhomboid Major T3 - T4 | 0.994 ± 0.002 | 0.998 ± 0 | 0.984 ± 0.007 | 0.975 ± 0 | 0.999 ± 0.001 | 0.998 ± 0.002 | 0.984 ± 0.005 |
| Pectoralis Major Clavicular | 0.989 ± 0.006 | 0.966 ± 0 | 0.999 ± 0.001 | 0.965 ± 0 | 0.969 ± 0.015 | 0.999 ± 0 | 0.993 ± 0.003 |
| Latissimus Dorsi Thoracic | 0.968 ± 0.023 | 0.989 ± 0 | 0.998 ± 0.003 | 0.995 ± 0 | 0.996 ± 0.001 | 0.995 ± 0.003 | 0.997 ± 0.003 |
| Deltoid Clavicular (Ant) | 0.994 ± 0.004 | 0.946 ± 0 | 0.998 ± 0.001 | 0.989 ± 0 | 0.996 ± 0.004 | 0.995 ± 0 | 0.984 ± 0.002 |
| Deltoid Acromial (Mid) | 0.997 ± 0.002 | 0.91 ± 0 | 0.997 ± 0.001 | 0.991 ± 0 | 0.994 ± 0.007 | 0.993 ± 0 | 0.937 ± 0.017 |
| Deltoid Scapular (Post) | 0.967 ± 0.021 | 0.986 ± 0 | 0.997 ± 0.002 | 0.978 ± 0 | 0.997 ± 0.001 | 0.998 ± 0 | 0.984 ± 0.009 |
| Infraspinatus | 0.995 ± 0.002 | 0.989 ± 0 | 0.99 ± 0.005 | 0.984 ± 0 | 0.994 ± 0.007 | 0.999 ± 0 | 0.99 ± 0 |
| Triceps Brachii Long | 0.977 ± 0.018 | 0.997 ± 0 | 0.985 ± 0.008 | 0.989 ± 0 | 0.994 ± 0.003 | 0.995 ± 0.001 | 0.996 ± 0.001 |
| Triceps Brachii Lateral | 0.979 ± 0.014 | 0.959 ± 0 | 0.991 ± 0.004 | 0.987 ± 0 | 0.989 ± 0.003 | 0.997 ± 0.001 | 0.992 ± 0.008 |
| Biceps Short | 0.946 ± 0.047 | 0.987 ± 0 | 0.996 ± 0.004 | 0.992 ± 0 | 0.997 ± 0.003 | 0.994 ± 0.005 | 0.997 ± 0 |
| Biceps Long | 0.962 ± 0.031 | 0.982 ± 0 | 0.998 ± 0.001 | 0.991 ± 0 | 0.989 ± 0.011 | 0.988 ± 0.005 | 0.999 ± 0 |
| Brachialis | 0.99 ± 0.009 | 0.995 ± 0 | 0.985 ± 0.008 | 0.991 ± 0 | 0.998 ± 0 | 0.995 ± 0.004 | 0.99 ± 0.003 |
| Brachioradialis | 0.981 ± 0.015 | 0.996 ± 0 | 0.978 ± 0.014 | 0.996 ± 0 | 0.999 ± 0.001 | 1 ± 0 | 0.97 ± 0.016 |
| Pronator Teres | 0.995 ± 0.002 | 0.999 ± 0 | 0.99 ± 0.004 | 0.996 ± 0 | 0.996 ± 0.001 | 0.994 ± 0.001 | 0.996 ± 0.002 |
| Total | 0.983 ± 0.0151 | 0.979 ± 0.0238 | 0.992 ± 0.00645 | 0.987 ± 0.00843 | 0.993 ± 0.00731 | 0.996 ± 0.00298 | 0.987 ± 0.0151 |

Table A.16: RMSE values from activations between healthy and patients' ones for the recorded muscles. For healthy subjects, this shows the inter variability within the healthy population. A1 corresponds to the first assessment, A4 to the final one. These are concatenated by target [1,3,5].

| | Healthy | S1 | | S2 | | S3 | |
|-----------------------------|----------------|----------------|----------------|----------------|----------------|----------------|----------------|
| | | A1 | A4 | A1 | A4 | A1 | A4 |
| Target 1 | | | | | | | |
| Trapezius C1 | 0.128 ± 0.038 | 0.1 ± 0 | 0.121 ± 0.023 | 0.125 ± 0.035 | 0.189 ± 0.076 | 0.248 ± 0.001 | 0.246 ± 0.044 |
| Trapezius C7 | 0.128 ± 0.035 | 0.142 ± 0 | 0.105 ± 0.027 | 0.139 ± 0.038 | 0.182 ± 0.051 | 0.247 ± 0.004 | 0.257 ± 0.035 |
| Rhomboid Major T3 - T4 | 0.095 ± 0.038 | 0.164 ± 0 | 0.076 ± 0.014 | 0.134 ± 0.073 | 0.133 ± 0.065 | 0.102 ± 0.008 | 0.15 ± 0.015 |
| Pectoralis Major Clavicular | 0.092 ± 0.025 | 0.071 ± 0 | 0.068 ± 0.006 | 0.073 ± 0 | 0.101 ± 0.003 | 0.101 ± 0.002 | 0.15 ± 0.003 |
| Latissimus Dorsi Thoracic | 0.121 ± 0.048 | 0.13 ± 0 | 0.072 ± 0.012 | 0.11 ± 0.018 | 0.201 ± 0.104 | 0.227 ± 0.014 | 0.233 ± 0.021 |
| Deltoid Clavicular (Ant) | 0.128 ± 0.03 | 0.146 ± 0 | 0.102 ± 0.017 | 0.127 ± 0.02 | 0.275 ± 0.105 | 0.331 ± 0.026 | 0.32 ± 0.026 |
| Deltoid Acromial (Mid) | 0.137 ± 0.034 | 0.139 ± 0 | 0.168 ± 0.032 | 0.147 ± 0.029 | 0.242 ± 0.099 | 0.165 ± 0.005 | 0.303 ± 0.023 |
| Deltoid Scapular (Post) | 0.138 ± 0.04 | 0.107 ± 0 | 0.054 ± 0.013 | 0.151 ± 0.042 | 0.157 ± 0.077 | 0.147 ± 0.002 | 0.214 ± 0.019 |
| Infraspinatus | 0.1 ± 0.053 | 0.091 ± 0 | 0.177 ± 0.029 | 0.168 ± 0.056 | 0.141 ± 0.02 | 0.148 ± 0.016 | 0.145 ± 0.027 |
| Triceps Brachii Long | 0.096 ± 0.035 | 0.129 ± 0 | 0.095 ± 0.01 | 0.152 ± 0.022 | 0.128 ± 0.054 | 0.189 ± 0.016 | 0.199 ± 0.002 |
| Triceps Brachii Lateral | 0.11 ± 0.035 | 0.088 ± 0 | 0.054 ± 0.01 | 0.179 ± 0.011 | 0.115 ± 0.081 | 0.158 ± 0.01 | 0.18 ± 0.012 |
| Biceps Short | 0.097 ± 0.036 | 0.1 ± 0 | 0.066 ± 0.005 | 0.169 ± 0.017 | 0.125 ± 0.08 | 0.209 ± 0.009 | 0.165 ± 0.028 |
| Biceps Long | 0.085 ± 0.046 | 0.174 ± 0 | 0.084 ± 0.012 | 0.129 ± 0.02 | 0.161 ± 0.003 | 0.186 ± 0.002 | 0.177 ± 0.001 |
| Brachialis | 0.067 ± 0.03 | 0.064 ± 0 | 0.099 ± 0.007 | 0.096 ± 0.023 | 0.123 ± 0.003 | 0.145 ± 0.002 | 0.105 ± 0.019 |
| Brachioradialis | 0.067 ± 0.032 | 0.069 ± 0 | 0.187 ± 0.01 | 0.095 ± 0.002 | 0.178 ± 0.154 | 0.088 ± 0.003 | 0.083 ± 0.017 |
| Pronator Teres | 0.09 ± 0.042 | 0.046 ± 0 | 0.055 ± 0.009 | 0.132 ± 0.006 | 0.084 ± 0.047 | 0.129 ± 0.005 | 0.124 ± 0.009 |
| Total | 0.105 ± 0.023 | 0.11 ± 0.0378 | 0.099 ± 0.0437 | 0.133 ± 0.029 | 0.158 ± 0.0511 | 0.176 ± 0.0645 | 0.191 ± 0.0678 |
| Target 3 | | | | | | | |
| Trapezius C1 | 0.095 ± 0.031 | 0.164 ± 0 | 0.115 ± 0.022 | 0.129 ± 0.033 | 0.211 ± 0.027 | 0.141 ± 0.069 | 0.189 ± 0.009 |
| Trapezius C7 | 0.116 ± 0.03 | 0.201 ± 0 | 0.103 ± 0.013 | 0.145 ± 0.005 | 0.076 ± 0.009 | 0.198 ± 0.054 | 0.258 ± 0.008 |
| Rhomboid Major T3 - T4 | 0.111 ± 0.05 | 0.107 ± 0 | 0.129 ± 0.01 | 0.164 ± 0.078 | 0.088 ± 0.004 | 0.122 ± 0.039 | 0.192 ± 0.005 |
| Pectoralis Major Clavicular | 0.069 ± 0.02 | 0.068 ± 0 | 0.068 ± 0.014 | 0.123 ± 0.043 | 0.062 ± 0.013 | 0.057 ± 0.005 | 0.094 ± 0.001 |
| Latissimus Dorsi Thoracic | 0.099 ± 0.053 | 0.16 ± 0 | 0.072 ± 0.007 | 0.134 ± 0.04 | 0.229 ± 0.006 | 0.143 ± 0.062 | 0.2 ± 0.008 |
| Deltoid Clavicular (Ant) | 0.096 ± 0.029 | 0.183 ± 0 | 0.11 ± 0.021 | 0.14 ± 0.011 | 0.108 ± 0.018 | 0.205 ± 0.034 | 0.219 ± 0.003 |
| Deltoid Acromial (Mid) | 0.099 ± 0.035 | 0.229 ± 0 | 0.096 ± 0.006 | 0.141 ± 0.006 | 0.12 ± 0.022 | 0.092 ± 0 | 0.257 ± 0 |
| Deltoid Scapular (Post) | 0.149 ± 0.073 | 0.212 ± 0 | 0.072 ± 0.008 | 0.142 ± 0.001 | 0.082 ± 0.009 | 0.121 ± 0.041 | 0.226 ± 0.003 |
| Infraspinatus | 0.113 ± 0.05 | 0.175 ± 0 | 0.081 ± 0.03 | 0.175 ± 0.069 | 0.159 ± 0.033 | 0.189 ± 0.056 | 0.212 ± 0.006 |
| Triceps Brachii Long | 0.098 ± 0.039 | 0.171 ± 0 | 0.142 ± 0.011 | 0.117 ± 0.003 | 0.104 ± 0.007 | 0.194 ± 0.001 | 0.191 ± 0.006 |
| Triceps Brachii Lateral | 0.123 ± 0.047 | 0.178 ± 0 | 0.07 ± 0.004 | 0.139 ± 0.015 | 0.103 ± 0.022 | 0.149 ± 0.011 | 0.182 ± 0.004 |
| Biceps Short | 0.072 ± 0.03 | 0.119 ± 0 | 0.062 ± 0.013 | 0.106 ± 0.018 | 0.068 ± 0.007 | 0.136 ± 0.036 | 0.14 ± 0.006 |
| Biceps Long | 0.068 ± 0.042 | 0.121 ± 0 | 0.066 ± 0.015 | 0.23 ± 0.059 | 0.255 ± 0.054 | 0.144 ± 0 | 0.136 ± 0.001 |
| Brachialis | 0.073 ± 0.042 | 0.112 ± 0 | 0.119 ± 0.009 | 0.215 ± 0.064 | 0.125 ± 0.005 | 0.136 ± 0.001 | 0.138 ± 0.001 |
| Brachioradialis | 0.079 ± 0.04 | 0.105 ± 0 | 0.089 ± 0.018 | 0.131 ± 0.065 | 0.082 ± 0.015 | 0.113 ± 0.005 | 0.138 ± 0.003 |
| Pronator Teres | 0.099 ± 0.065 | 0.076 ± 0 | 0.097 ± 0.017 | 0.14 ± 0.031 | 0.078 ± 0.003 | 0.153 ± 0.027 | 0.169 ± 0.007 |
| Total | 0.097 ± 0.0221 | 0.149 ± 0.0485 | 0.093 ± 0.0246 | 0.148 ± 0.0332 | 0.122 ± 0.0602 | 0.143 ± 0.0396 | 0.184 ± 0.0462 |
| Target 5 | | | | | | | |
| Trapezius C1 | 0.095 ± 0.034 | 0.092 ± 0 | 0.078 ± 0.01 | 0.076 ± 0 | 0.077 ± 0.024 | 0.141 ± 0.014 | 0.16 ± 0.01 |
| Trapezius C7 | 0.108 ± 0.027 | 0.06 ± 0 | 0.072 ± 0.008 | 0.1 ± 0 | 0.091 ± 0.005 | 0.172 ± 0 | 0.197 ± 0.005 |
| Rhomboid Major T3 - T4 | 0.087 ± 0.049 | 0.077 ± 0 | 0.075 ± 0.008 | 0.079 ± 0 | 0.067 ± 0.001 | 0.053 ± 0.003 | 0.088 ± 0.008 |
| Pectoralis Major Clavicular | 0.075 ± 0.022 | 0.044 ± 0 | 0.101 ± 0.024 | 0.201 ± 0 | 0.14 ± 0.009 | 0.071 ± 0.023 | 0.119 ± 0.018 |
| Latissimus Dorsi Thoracic | 0.063 ± 0.033 | 0.029 ± 0 | 0.054 ± 0.002 | 0.097 ± 0 | 0.179 ± 0.011 | 0.065 ± 0.015 | 0.093 ± 0.007 |
| Deltoid Clavicular (Ant) | 0.073 ± 0.025 | 0.073 ± 0 | 0.065 ± 0.01 | 0.093 ± 0 | 0.089 ± 0.005 | 0.099 ± 0.006 | 0.097 ± 0.002 |
| Deltoid Acromial (Mid) | 0.058 ± 0.019 | 0.039 ± 0 | 0.075 ± 0.021 | 0.083 ± 0 | 0.071 ± 0.004 | 0.085 ± 0.005 | 0.103 ± 0 |
| Deltoid Scapular (Post) | 0.109 ± 0.054 | 0.085 ± 0 | 0.053 ± 0.005 | 0.113 ± 0 | 0.077 ± 0 | 0.06 ± 0.008 | 0.149 ± 0.003 |
| Infraspinatus | 0.064 ± 0.028 | 0.032 ± 0 | 0.056 ± 0.02 | 0.108 ± 0 | 0.131 ± 0.038 | 0.077 ± 0.009 | 0.084 ± 0.008 |
| Triceps Brachii Long | 0.067 ± 0.03 | 0.091 ± 0 | 0.087 ± 0.01 | 0.099 ± 0 | 0.045 ± 0.008 | 0.111 ± 0.003 | 0.108 ± 0.002 |
| Triceps Brachii Lateral | 0.076 ± 0.035 | 0.037 ± 0 | 0.043 ± 0.006 | 0.072 ± 0 | 0.179 ± 0.04 | 0.046 ± 0.031 | 0.088 ± 0.006 |
| Biceps Short | 0.073 ± 0.042 | 0.046 ± 0 | 0.045 ± 0.008 | 0.078 ± 0 | 0.102 ± 0.047 | 0.117 ± 0.001 | 0.096 ± 0.007 |
| Biceps Long | 0.054 ± 0.03 | 0.082 ± 0 | 0.063 ± 0.009 | 0.109 ± 0 | 0.082 ± 0.01 | 0.093 ± 0.001 | 0.084 ± 0.005 |
| Brachialis | 0.062 ± 0.03 | 0.065 ± 0 | 0.102 ± 0.007 | 0.131 ± 0 | 0.103 ± 0.012 | 0.126 ± 0.002 | 0.116 ± 0.01 |
| Brachioradialis | 0.083 ± 0.04 | 0.074 ± 0 | 0.066 ± 0.023 | 0.113 ± 0 | 0.191 ± 0.046 | 0.112 ± 0.001 | 0.126 ± 0.019 |
| Pronator Teres | 0.077 ± 0.043 | 0.059 ± 0 | 0.068 ± 0.011 | 0.146 ± 0 | 0.074 ± 0.002 | 0.159 ± 0.008 | 0.145 ± 0.01 |
| Total | 0.076 ± 0.0165 | 0.062 ± 0.0213 | 0.069 ± 0.0175 | 0.106 ± 0.0324 | 0.106 ± 0.0447 | 0.099 ± 0.0375 | 0.116 ± 0.0322 |

Table A.17: RMSE values from activations between healthy and patients' ones for the recorded muscles. For healthy subjects, this shows the inter variability within the healthy population. A1 corresponds to the first assessment, A4 to the final one. These are concatenated by target [7,10,13].

| | Healthy | S1 | | S2 | | S3 | |
|-----------------------------|----------------|----------------|----------------|----------------|----------------|----------------|----------------|
| | | A1 | A4 | A1 | A4 | A1 | A4 |
| Target 7 | | | | | | | |
| Trapezius C1 | 0.131 ± 0.049 | 0.199 ± 0 | 0.121 ± 0.018 | 0.112 ± 0 | 0.093 ± 0.03 | 0.207 ± 0.03 | 0.204 ± 0.006 |
| Trapezius C7 | 0.129 ± 0.048 | 0.12 ± 0 | 0.079 ± 0.01 | 0.11 ± 0 | 0.084 ± 0.029 | 0.181 ± 0.013 | 0.174 ± 0.013 |
| Rhomboid Major T3 - T4 | 0.075 ± 0.037 | 0.185 ± 0 | 0.063 ± 0.016 | 0.096 ± 0 | 0.064 ± 0.01 | 0.051 ± 0.004 | 0.087 ± 0.002 |
| Pectoralis Major Clavicular | 0.121 ± 0.026 | 0.144 ± 0 | 0.1 ± 0.005 | 0.126 ± 0 | 0.155 ± 0.048 | 0.181 ± 0.051 | 0.251 ± 0.012 |
| Latissimus Dorsi Thoracic | 0.086 ± 0.038 | 0.081 ± 0 | 0.056 ± 0.006 | 0.137 ± 0 | 0.131 ± 0.009 | 0.132 ± 0.013 | 0.123 ± 0.007 |
| Deltoid Clavicular (Ant) | 0.104 ± 0.04 | 0.118 ± 0 | 0.084 ± 0.008 | 0.141 ± 0 | 0.137 ± 0.025 | 0.224 ± 0.01 | 0.198 ± 0.003 |
| Deltoid Acromial (Mid) | 0.075 ± 0.027 | 0.127 ± 0 | 0.06 ± 0.009 | 0.099 ± 0 | 0.139 ± 0.092 | 0.041 ± 0.001 | 0.126 ± 0.003 |
| Deltoid Scapular (Post) | 0.107 ± 0.024 | 0.045 ± 0 | 0.032 ± 0.006 | 0.09 ± 0 | 0.099 ± 0.047 | 0.057 ± 0.008 | 0.133 ± 0 |
| Infraspinatus | 0.065 ± 0.039 | 0.114 ± 0 | 0.11 ± 0.017 | 0.174 ± 0 | 0.107 ± 0.089 | 0.065 ± 0.03 | 0.077 ± 0.001 |
| Triceps Brachii Long | 0.078 ± 0.037 | 0.09 ± 0 | 0.116 ± 0.014 | 0.087 ± 0 | 0.101 ± 0.02 | 0.148 ± 0.005 | 0.147 ± 0 |
| Triceps Brachii Lateral | 0.087 ± 0.03 | 0.053 ± 0 | 0.044 ± 0.006 | 0.128 ± 0 | 0.174 ± 0.058 | 0.058 ± 0.025 | 0.1 ± 0.012 |
| Biceps Short | 0.09 ± 0.044 | 0.119 ± 0 | 0.054 ± 0.011 | 0.094 ± 0 | 0.085 ± 0.072 | 0.145 ± 0.032 | 0.102 ± 0.012 |
| Biceps Long | 0.073 ± 0.04 | 0.228 ± 0 | 0.075 ± 0.017 | 0.126 ± 0 | 0.207 ± 0.128 | 0.132 ± 0.001 | 0.112 ± 0.005 |
| Brachialis | 0.072 ± 0.037 | 0.071 ± 0 | 0.131 ± 0.008 | 0.155 ± 0 | 0.114 ± 0.018 | 0.146 ± 0.004 | 0.099 ± 0 |
| Brachioradialis | 0.071 ± 0.037 | 0.056 ± 0 | 0.069 ± 0.015 | 0.129 ± 0 | 0.304 ± 0.056 | 0.102 ± 0.007 | 0.094 ± 0.012 |
| Pronator Teres | 0.095 ± 0.046 | 0.041 ± 0 | 0.077 ± 0.019 | 0.188 ± 0 | 0.092 ± 0.007 | 0.187 ± 0.005 | 0.155 ± 0.014 |
| Total | 0.091 ± 0.0214 | 0.112 ± 0.0559 | 0.079 ± 0.0291 | 0.125 ± 0.0297 | 0.13 ± 0.0593 | 0.129 ± 0.0596 | 0.136 ± 0.049 |
| Target 10 | | | | | | | |
| Trapezius C1 | 0.102 ± 0.029 | 0.154 ± 0 | 0.094 ± 0.015 | 0.087 ± 0 | 0.151 ± 0.097 | 0.135 ± 0.051 | 0.134 ± 0.008 |
| Trapezius C7 | 0.112 ± 0.036 | 0.186 ± 0 | 0.083 ± 0.006 | 0.117 ± 0 | 0.156 ± 0.016 | 0.198 ± 0.032 | 0.195 ± 0.018 |
| Rhomboid Major T3 - T4 | 0.119 ± 0.036 | 0.101 ± 0 | 0.107 ± 0.014 | 0.115 ± 0 | 0.115 ± 0.028 | 0.14 ± 0.015 | 0.169 ± 0.01 |
| Pectoralis Major Clavicular | 0.065 ± 0.025 | 0.053 ± 0 | 0.09 ± 0.029 | 0.089 ± 0 | 0.166 ± 0.029 | 0.058 ± 0.035 | 0.079 ± 0.006 |
| Latissimus Dorsi Thoracic | 0.065 ± 0.029 | 0.084 ± 0 | 0.06 ± 0.011 | 0.099 ± 0 | 0.1 ± 0.029 | 0.074 ± 0.022 | 0.076 ± 0.013 |
| Deltoid Clavicular (Ant) | 0.08 ± 0.026 | 0.118 ± 0 | 0.063 ± 0.011 | 0.108 ± 0 | 0.092 ± 0.01 | 0.092 ± 0 | 0.079 ± 0.005 |
| Deltoid Acromial (Mid) | 0.063 ± 0.016 | 0.151 ± 0 | 0.131 ± 0.05 | 0.101 ± 0 | 0.093 ± 0.004 | 0.068 ± 0.002 | 0.099 ± 0.011 |
| Deltoid Scapular (Post) | 0.118 ± 0.04 | 0.141 ± 0 | 0.105 ± 0.055 | 0.146 ± 0 | 0.122 ± 0.002 | 0.087 ± 0.008 | 0.157 ± 0.014 |
| Infraspinatus | 0.108 ± 0.033 | 0.16 ± 0 | 0.072 ± 0.019 | 0.131 ± 0 | 0.13 ± 0.05 | 0.158 ± 0.04 | 0.152 ± 0.017 |
| Triceps Brachii Long | 0.121 ± 0.049 | 0.149 ± 0 | 0.096 ± 0.019 | 0.148 ± 0 | 0.134 ± 0 | 0.162 ± 0.007 | 0.161 ± 0.001 |
| Triceps Brachii Lateral | 0.148 ± 0.048 | 0.169 ± 0 | 0.083 ± 0.031 | 0.18 ± 0 | 0.182 ± 0.027 | 0.137 ± 0.035 | 0.179 ± 0.01 |
| Biceps Short | 0.141 ± 0.051 | 0.175 ± 0 | 0.098 ± 0.025 | 0.169 ± 0 | 0.13 ± 0.006 | 0.193 ± 0.012 | 0.166 ± 0.003 |
| Biceps Long | 0.134 ± 0.068 | 0.22 ± 0 | 0.117 ± 0.037 | 0.148 ± 0 | 0.146 ± 0.007 | 0.187 ± 0.001 | 0.175 ± 0 |
| Brachialis | 0.143 ± 0.037 | 0.215 ± 0 | 0.193 ± 0.01 | 0.204 ± 0 | 0.234 ± 0 | 0.251 ± 0.001 | 0.23 ± 0.004 |
| Brachioradialis | 0.137 ± 0.058 | 0.218 ± 0 | 0.159 ± 0.014 | 0.186 ± 0 | 0.154 ± 0.023 | 0.218 ± 0.007 | 0.207 ± 0.022 |
| Pronator Teres | 0.107 ± 0.053 | 0.112 ± 0 | 0.062 ± 0.002 | 0.211 ± 0 | 0.164 ± 0.004 | 0.196 ± 0.011 | 0.19 ± 0.005 |
| Total | 0.11 ± 0.0286 | 0.15 ± 0.0481 | 0.101 ± 0.036 | 0.14 ± 0.0406 | 0.142 ± 0.0362 | 0.147 ± 0.0585 | 0.153 ± 0.0475 |
| Target 13 | | | | | | | |
| Trapezius C1 | 0.133 ± 0.035 | 0.215 ± 0 | 0.136 ± 0.035 | 0.116 ± 0 | 0.112 ± 0.006 | 0.234 ± 0.004 | 0.192 ± 0.006 |
| Trapezius C7 | 0.128 ± 0.038 | 0.206 ± 0 | 0.159 ± 0.021 | 0.099 ± 0 | 0.137 ± 0.061 | 0.207 ± 0.015 | 0.17 ± 0.009 |
| Rhomboid Major T3 - T4 | 0.069 ± 0.027 | 0.052 ± 0 | 0.075 ± 0.013 | 0.102 ± 0 | 0.062 ± 0.026 | 0.081 ± 0.004 | 0.098 ± 0.005 |
| Pectoralis Major Clavicular | 0.108 ± 0.041 | 0.165 ± 0 | 0.077 ± 0.009 | 0.124 ± 0 | 0.122 ± 0.02 | 0.084 ± 0.028 | 0.188 ± 0.004 |
| Latissimus Dorsi Thoracic | 0.118 ± 0.039 | 0.223 ± 0 | 0.081 ± 0.02 | 0.095 ± 0 | 0.093 ± 0.013 | 0.231 ± 0.009 | 0.189 ± 0.005 |
| Deltoid Clavicular (Ant) | 0.116 ± 0.026 | 0.344 ± 0 | 0.101 ± 0.012 | 0.172 ± 0 | 0.13 ± 0.028 | 0.358 ± 0.003 | 0.327 ± 0.007 |
| Deltoid Acromial (Mid) | 0.115 ± 0.039 | 0.301 ± 0 | 0.095 ± 0.011 | 0.185 ± 0 | 0.123 ± 0.006 | 0.164 ± 0.001 | 0.306 ± 0.007 |
| Deltoid Scapular (Post) | 0.123 ± 0.039 | 0.18 ± 0 | 0.051 ± 0.008 | 0.094 ± 0 | 0.094 ± 0.008 | 0.137 ± 0.001 | 0.19 ± 0.003 |
| Infraspinatus | 0.08 ± 0.042 | 0.116 ± 0 | 0.197 ± 0.055 | 0.126 ± 0 | 0.148 ± 0.104 | 0.121 ± 0.018 | 0.09 ± 0.006 |
| Triceps Brachii Long | 0.101 ± 0.045 | 0.242 ± 0 | 0.126 ± 0.035 | 0.123 ± 0 | 0.147 ± 0.059 | 0.254 ± 0.006 | 0.251 ± 0 |
| Triceps Brachii Lateral | 0.116 ± 0.041 | 0.182 ± 0 | 0.128 ± 0.041 | 0.088 ± 0 | 0.1 ± 0.011 | 0.146 ± 0.043 | 0.195 ± 0.002 |
| Biceps Short | 0.101 ± 0.032 | 0.192 ± 0 | 0.074 ± 0.009 | 0.095 ± 0 | 0.101 ± 0.044 | 0.238 ± 0.005 | 0.165 ± 0 |
| Biceps Long | 0.085 ± 0.028 | 0.178 ± 0 | 0.07 ± 0.007 | 0.102 ± 0 | 0.298 ± 0.011 | 0.221 ± 0.001 | 0.204 ± 0.003 |
| Brachialis | 0.083 ± 0.033 | 0.154 ± 0 | 0.099 ± 0.021 | 0.092 ± 0 | 0.151 ± 0.016 | 0.181 ± 0 | 0.103 ± 0.005 |
| Brachioradialis | 0.075 ± 0.045 | 0.095 ± 0 | 0.204 ± 0.049 | 0.108 ± 0 | 0.199 ± 0.069 | 0.1 ± 0.002 | 0.089 ± 0.007 |
| Pronator Teres | 0.089 ± 0.042 | 0.077 ± 0 | 0.086 ± 0.018 | 0.105 ± 0 | 0.093 ± 0.004 | 0.162 ± 0.011 | 0.142 ± 0.006 |
| Total | 0.102 ± 0.0199 | 0.183 ± 0.0767 | 0.11 ± 0.0452 | 0.114 ± 0.028 | 0.132 ± 0.0548 | 0.182 ± 0.0734 | 0.181 ± 0.0703 |

Bibliography

- [1] A. T. Abd et al. “A Perspective on Muscle Synergies and Different Theories Related to Their Adaptation”. In: *Biomechanics 2021, Vol. 1, Pages 253-263* 1 (2021), pp. 253–263.
- [2] D. Ao et al. “EMG-driven musculoskeletal model calibration with estimation of unmeasured muscle excitations via synergy extrapolation”. In: *Frontiers in bioengineering and biotechnology* 10 (2022).
- [3] S. Aoi et al. “Neuromusculoskeletal model that walks and runs across a speed range with a few motor control parameter changes based on the muscle synergy hypothesis”. In: *Scientific Reports* 2019 9:1 9 (1 2019), pp. 1–13.
- [4] S. Arber and R. M. Costa. “Connecting neuronal circuits for movement”. In: *Science* 360 (6396 2018), pp. 1403–1404.
- [5] Y. Z. Arslan et al. “Exoskeletons, Exomusculatures, Exosuits: Dynamic Modeling and Simulation”. In: 2019, pp. 305–331.
- [6] M. F. Ashari, A. Hanafusa, and S. Mohamaddan. “Evaluation of Upper Limb Muscle Activation Using Musculoskeletal Model with Wearable Assistive Device”. In: *Applied Bionics and Biomechanics* 2022 (2022).
- [7] N. Assila et al. “EMG-Assisted Algorithm to Account for Shoulder Muscles Co-Contraction in Overhead Manual Handling”. In: *Applied Sciences* 2020, Vol. 10, Page 3522 10 (10 2020), p. 3522.
- [8] C. L. Banks et al. “Electromyography exposes heterogeneity in muscle co-contraction following stroke”. In: *Frontiers in Neurology* 8 (DEC 2017), p. 699.
- [9] D. J. Berger and A. d’Avella. “Effective force control by muscle synergies”. In: *Frontiers in Computational Neuroscience* 8 (1 APR 2014).
- [10] M. Berniker et al. “Simplified and effective motor control based on muscle synergies to exploit musculoskeletal dynamics”. In: *Proceedings of the National Academy of Sciences of the United States of America* 106 (18 2009), pp. 7601–7606.

- [11] N. Bernstein. *The co-ordination and regulation of movements*. Pergamon Press, 1967.
- [12] E. Bizzi and V. C. Cheung. “The neural origin of muscle synergies”. In: *Frontiers in Computational Neuroscience* 7 (2013), pp. 1–6.
- [13] E. Bizzi, F. A. Mussa-Ivaldi, and S. Giszter. “Computations Underlying the Execution of Movement: A Biological Perspective”. In: *Science* 253 (5017 1991), pp. 287–291.
- [14] D. Blana et al. “A musculoskeletal model of the upper extremity for use in the development of neuroprosthetic systems”. In: *Journal of Biomechanics* 41 (8 2008), pp. 1714–1721.
- [15] A. J. V. D. Bogert, D. Blana, and D. Heinrich. “Implicit methods for efficient musculoskeletal simulation and optimal control”. In: *Procedia IUTAM* 2 (2011), pp. 297–316.
- [16] C. Bosecker et al. “Kinematic robot-based evaluation scales and clinical counterparts to measure upper limb motor performance in patients with chronic stroke”. In: *Neurorehabilitation and neural repair* 24 (1 2010), pp. 62–69.
- [17] L. A. Boyd et al. “Biomarkers of stroke recovery: Consensus-based core recommendations from the Stroke Recovery and Rehabilitation Roundtable”. In: *International journal of stroke : official journal of the International Stroke Society* 12 (5 2017), pp. 480–493.
- [18] E. L. Brainerd and E. Azizi. “Muscle fiber angle, segment bulging and architectural gear ratio in segmented musculature”. In: *The Journal of experimental biology* 208 (Pt 17 2005), pp. 3249–3261.
- [19] T. S. Buchanan and D. A. Shreeve. “An Evaluation of Optimization Techniques for the Prediction of Muscle Activation Patterns During Isometric Tasks”. In: *Journal of Biomechanical Engineering* 118 (4 1996), pp. 565–574.
- [20] F. Buma, G. Kwakkel, and N. Ramsey. “Understanding upper limb recovery after stroke”. In: *Restorative neurology and neuroscience* 31 (6 2013), pp. 707–722.
- [21] G. Cappellini et al. “Motor patterns in human walking and running”. In: *Journal of neurophysiology* 95 (6 2006), pp. 3426–3437.
- [22] E. K. Chadwick et al. “Real-time simulation of three-dimensional shoulder girdle and arm dynamics”. In: *IEEE transactions on bio-medical engineering* 61 (7 2014), pp. 1947–1956.
- [23] J. Chae et al. “Muscle weakness and cocontraction in upper limb hemiparesis: relationship to motor impairment and physical disability”. In: *Neurorehabilitation and neural repair* 16 (3 2002), pp. 241–248.

- [24] A. Chalard et al. "Impact of the EMG normalization method on muscle activation and the antagonist-agonist co-contraction index during active elbow extension: Practical implications for post-stroke subjects". In: *Journal of Electromyography and Kinesiology* 51 (2020), p. 102403.
- [25] V. C. Cheung and K. Seki. "Approaches to revealing the neural basis of muscle synergies: A review and a critique". In: *Journal of Neurophysiology* 125 (5 2021), pp. 1580–1597.
- [26] V. C. Cheung et al. "Muscle synergy patterns as physiological markers of motor cortical damage". In: *Proceedings of the National Academy of Sciences of the United States of America* 109 (36 2012), pp. 14652–14656.
- [27] V. C. Cheung et al. "Stability of muscle synergies for voluntary actions after cortical stroke in humans". In: *Proceedings of the National Academy of Sciences of the United States of America* 106 (46 2009), p. 19563.
- [28] J. Cholewicki, S. M. McGill, and R. W. Norman. "Comparison of muscle forces and joint load from an optimization and EMG assisted lumbar spine model: towards development of a hybrid approach". In: *Journal of biomechanics* 28 (3 1995).
- [29] M. C. Cirstea and M. F. Levin. "Compensatory strategies for reaching in stroke". In: *Brain* 123 (5 2000), pp. 940–953.
- [30] J. J. Collins. "The redundant nature of locomotor optimization laws". In: *Journal of biomechanics* 28 (3 1995), pp. 251–267.
- [31] R. D. Crowninshield and R. A. Brand. "A physiologically based criterion of muscle force prediction in locomotion". In: *Journal of Biomechanics* 14 (11 1981), pp. 793–801.
- [32] C. Curreli et al. "Using Musculoskeletal Models to Estimate in vivo Total Knee Replacement Kinematics and Loads: Effect of Differences Between Models". In: *Frontiers in Bioengineering and Biotechnology* 9 (2021), p. 611.
- [33] A. D'Avella, P. Saltiel, and E. Bizzi. "Combinations of muscle synergies in the construction of a natural motor behavior". In: *Nature Neuroscience* 2003 6:3 6 (3 2003), pp. 300–308.
- [34] A. D'avella and M. C. Tresch. "Modularity in the motor system: decomposition of muscle patterns as combinations of time-varying synergies". In: *Advances in neural information processing systems* (2002).
- [35] A. D'Avella et al. "Control of fast-reaching movements by muscle synergy combinations". In: *The Journal of neuroscience : the official journal of the Society for Neuroscience* 26 (30 2006), pp. 7791–7810.
- [36] M. Damsgaard et al. "Analysis of musculoskeletal systems in the AnyBody Modeling System". In: *Simulation Modelling Practice and Theory* 14 (8 2006), pp. 1100–1111.

- [37] T. T. Dao. “Rigid musculoskeletal models of the human body systems: A review”. In: *Journal of Musculoskeletal Research* 19 (3 2016).
- [38] S. L. Delp et al. “OpenSim: open-source software to create and analyze dynamic simulations of movement”. In: *IEEE transactions on bio-medical engineering* 54 (11 2007), pp. 1940–1950.
- [39] J. P. A. Dewald et al. “Reorganization of flexion reflexes in the upper extremity of hemiparetic subjects”. In: *Muscle Nerve* 22 (1999), pp. 1209–1221.
- [40] C. R. Dickerson, D. B. Chaffin, and R. E. Hughes. “A mathematical musculoskeletal shoulder model for proactive ergonomic analysis”. In: *Computer methods in biomechanics and biomedical engineering* 10 (6 2007), pp. 389–400.
- [41] J. R. Dormand and P. J. Prince. “A family of embedded Runge-Kutta formulae”. In: *Journal of Computational and Applied Mathematics* 6 (1 1980), pp. 19–26.
- [42] J. Duchateau and R. M. Enoka. “Distribution of motor unit properties across human muscles”. In: *Journal of Applied Physiology* 132 (1 2022), pp. 1–13.
- [43] J. Duchateau and R. M. Enoka. “Human motor unit recordings: Origins and insight into the integrated motor system”. In: *Brain Research* 1409 (2011), pp. 42–61.
- [44] J. Dul et al. “Muscular synergism—I. On criteria for load sharing between synergistic muscles”. In: *Journal of biomechanics* 17 (9 1984), pp. 663–673.
- [45] E. Eisenberg, T. L. Hill, and Y. Chen. “Cross-bridge model of muscle contraction. Quantitative analysis.” In: *Biophysical Journal* 29 (2 1980), p. 195.
- [46] A. Erdemir et al. “Model-based estimation of muscle forces exerted during movements”. In: *Clinical Biomechanics* 22 (2 2007), pp. 131–154.
- [47] P. Favre, C. Gerber, and J. G. Snedeker. “Automated muscle wrapping using finite element contact detection”. In: *Favre, P; Gerber, C; Snedeker, J G (2010). Automated muscle wrapping using finite element contact detection. Journal of Biomechanics, 43(10):1931-1940.* 43 (10 2010), pp. 1931–1940.
- [48] B. Feinstein et al. “Morphologic studies of motor units in normal human muscles”. In: *Cells Tissues Organs* 23 (2 1955), pp. 127–142.
- [49] A. R. Fugl-Meyer et al. “A method for evaluation of physical performance”. In: *Scand J Rehabil Med* 7.1 (1975), pp. 13–31.
- [50] D. Gagnon et al. “An improved multi-joint EMG-assisted optimization approach to estimate joint and muscle forces in a musculoskeletal model of the lumbar spine”. In: *Journal of Biomechanics* 44 (8 2011), pp. 1521–1529.
- [51] F. Gao et al. “Computational method for muscle-path representation in musculoskeletal models”. In: *Biological Cybernetics* 87 (3 2002), pp. 199–210.

- [52] B. A. Garner and M. G. Pandy. “Estimation of Musculotendon Properties in the Human Upper Limb”. In: *Annals of Biomedical Engineering* 31:2 31 (2 2003), pp. 207–220.
- [53] B. A. Garner and M. G. Pandy. “Musculoskeletal model of the upper limb based on the visible human male dataset”. In: *Computer methods in biomechanics and biomedical engineering* 4 (2 2001), pp. 93–126.
- [54] B. A. Garner and M. G. Pandy. “The Obstacle-Set Method for Representing Muscle Paths in Musculoskeletal Models”. In: *Computer methods in biomechanics and biomedical engineering* 3 (1 2000), pp. 1–30.
- [55] F. Garro et al. “Neuromechanical Biomarkers for Robotic Neurorehabilitation”. In: *Frontiers in Neurorobotics* 15 (2021), p. 138.
- [56] C. Giang et al. “Motor improvement estimation and task adaptation for personalized robot-aided therapy: a feasibility study”. In: *BioMedical Engineering OnLine* 19 (1 2020).
- [57] D. J. Gladstone, C. J. Danells, and S. E. Black. “The fugl-meyer assessment of motor recovery after stroke: a critical review of its measurement properties”. In: *Neurorehabilitation and neural repair* 16 (3 2002), pp. 232–240.
- [58] S. K. Gollapudi and D. C. Lin. “Experimental determination of sarcomere force-length relationship in type-I human skeletal muscle fibers”. In: *Journal of biomechanics* 42 (13 2009), pp. 2011–2016.
- [59] T. Gordon et al. “The resilience of the size principle in the organization of motor unit properties in normal and reinnervated adult skeletal muscles”. In: *Canadian journal of physiology and pharmacology* 82 (8-9 2004), pp. 645–661.
- [60] A. G. Guggisberg et al. “Brain networks and their relevance for stroke rehabilitation”. In: *Clinical neurophysiology : official journal of the International Federation of Clinical Neurophysiology* 130 (7 2019), pp. 1098–1124.
- [61] K. Gustafsson. *Control of error and convergence in ODE solvers*. Tech. rep. Lund Univ.(Sweden). Dept. of Automatic Control, 1992.
- [62] R. Hainisch et al. “Method for determining musculotendon parameters in subject-specific musculoskeletal models of children developed from MRI data”. In: *Multibody System Dynamics* 28 (1-2 2012), pp. 143–156.
- [63] R. Happee. “Inverse dynamic optimization including muscular dynamics, a new simulation method applied to goal directed movements”. In: *Journal of Biomechanics* 27 (7 1994), pp. 953–960.
- [64] J. K. Harrison, K. S. McArthur, and T. J. Quinn. “Assessment scales in stroke: clinimetric and clinical considerations”. In: *Clinical interventions in aging* 8 (2013), pp. 201–211.
- [65] C. B. Hart and S. F. Giszter. “A Neural Basis for Motor Primitives in the Spinal Cord”. In: *Journal of Neuroscience* 30 (4 2010), pp. 1322–1336.

- [66] H. Hatze. “A myocybernetic control model of skeletal muscle”. In: *Biological Cybernetics* 25 (2 1977), pp. 103–119.
- [67] F. C. van der Helm. “A finite element musculoskeletal model of the shoulder mechanism”. In: *Journal of Biomechanics* 27 (5 1994), pp. 551–569.
- [68] F. C. van der Helm. “Analysis of the kinematic and dynamic behavior of the shoulder mechanism”. In: *Journal of Biomechanics* 27 (5 1994), pp. 527–550.
- [69] H. J. Hermens et al. “Development of recommendations for SEMG sensors and sensor placement procedures”. In: *Journal of electromyography and kinesiology : official journal of the International Society of Electrophysiological Kinesiology* 10 (5 2000), pp. 361–374.
- [70] W. Herzog. “Force-sharing among synergistic muscles”. In: *Exercise and Sport Sciences Reviews* 24 (1 1996), pp. 173–202.
- [71] A. V. Hill. “The Heat of Shortening and the Dynamic Constants of Muscle”. In: *Proceedings of the Royal Society B: Biological Sciences* 126 (843 1938), pp. 136–195.
- [72] H. X. Hoang et al. “A calibrated EMG-informed neuromusculoskeletal model can appropriately account for muscle co-contraction in the estimation of hip joint contact forces in people with hip osteoarthritis”. In: *Journal of Biomechanics* 83 (2019), pp. 134–142.
- [73] K. R. Holzbaur, W. M. Murray, and S. L. Delp. “A model of the upper extremity for simulating musculoskeletal surgery and analyzing neuromuscular control”. In: *Annals of Biomedical Engineering* 33 (6 2005), pp. 829–840.
- [74] F. Hug. “Can muscle coordination be precisely studied by surface electromyography?” In: *Journal of electromyography and kinesiology : official journal of the International Society of Electrophysiological Kinesiology* 21 (1 2011), pp. 1–12.
- [75] D. Ingram. “Musculoskeletal Model of the Human Shoulder for Joint Force Estimation”. PhD thesis. EPFL, 2015.
- [76] D. Ingram et al. “Muscle moment-arms: a key element in muscle-force estimation”. In: *Computer methods in biomechanics and biomedical engineering* 18 (5 2015), pp. 506–513.
- [77] Y. P. Ivanenko, R. E. Poppele, and F. Lacquaniti. “Five basic muscle activation patterns account for muscle activity during human locomotion”. In: *Journal of Physiology* 556 (1 2004), pp. 267–282.
- [78] E. Joos, F. Péan, and O. Goksel. “Reinforcement Learning of Musculoskeletal Control from Functional Simulations”. In: *Lecture Notes in Computer Science (including subseries Lecture Notes in Artificial Intelligence and Lecture Notes in Bioinformatics)* 12263 LNCS (2020), pp. 135–145.
- [79] G. C. Joyce and P. M. Rack. “Isotonic lengthening and shortening movements of cat soleus muscle”. In: *The Journal of physiology* 204 (2 1969), pp. 475–491.

- [80] D. Kaplan. *Knee Point - File Exchange - MATLAB Central*. 2023.
- [81] K. R. Kaufman et al. “Physiological prediction of muscle forces–I. Theoretical formulation”. In: *Neuroscience* 40 (3 1991), pp. 781–792.
- [82] A. Kian et al. “Static optimization underestimates antagonist muscle activity at the glenohumeral joint: A musculoskeletal modeling study”. In: *Journal of biomechanics* 97 (2019).
- [83] P. Kieliba et al. “How are Muscle Synergies Affected by Electromyography Pre-Processing?” In: *IEEE Transactions on Neural Systems and Rehabilitation Engineering* 26 (4 2018), pp. 882–893.
- [84] N. N. Kinany. “Central and peripheral mechanisms: a multimodal approach to understanding and restoring human motor control”. PhD thesis. 2020.
- [85] B. A. Knarr, J. A. Zeni, and J. S. Higginson. “Comparison of electromyography and joint moment as indicators of co-contraction”. In: *Journal of Electromyography and Kinesiology* 22 (4 2012), pp. 607–611.
- [86] P. Konrad. “The ABC of EMG A Practical Introduction to Kinesiological Electromyography”. In: *Noraxon Inc, USA* (2005).
- [87] H. I. Krebs et al. “Robotic measurement of arm movements after stroke establishes biomarkers of motor recovery”. In: *Stroke* 45 (1 2014), pp. 200–204.
- [88] A. M. Krylow and T. G. Sandercock. “Dynamic force responses of muscle involving eccentric contraction”. In: *Journal of Biomechanics* 30 (1 1997), pp. 27–33.
- [89] J. J. Kutch and F. J. Valero-Cuevas. “Challenges and New Approaches to Proving the Existence of Muscle Synergies of Neural Origin”. In: *PLOS Computational Biology* 8 (5 2012), e1002434.
- [90] G. Kwakkel, B. Kollen, and J. Twisk. “Impact of time on improvement of outcome after stroke”. In: *Stroke* 37 (9 2006), pp. 2348–2353.
- [91] M. Lamas et al. “Comparison of several muscle modeling alternatives for computationally intensive algorithms in human motion dynamics”. In: *Multibody System Dynamics* 54 (4 2022), pp. 415–442.
- [92] N. Lambert-Shirzad and H. M. Van der Loos. “On identifying kinematic and muscle synergies: a comparison of matrix factorization methods using experimental data from the healthy population”. In: *Journal of neurophysiology* 117.1 (2017), pp. 290–302.
- [93] I. Lamers et al. “Upper limb assessment in multiple sclerosis: a systematic review of outcome measures and their psychometric properties”. In: *Archives of physical medicine and rehabilitation* 95 (6 2014), pp. 1184–1200.
- [94] P. Langhorne, J. Bernhardt, and G. Kwakkel. “Stroke rehabilitation”. In: *Lancet (London, England)* 377 (9778 2011), pp. 1693–1702.

- [95] D. D. Lee and H. S. Seung. "Learning the parts of objects by non-negative matrix factorization". In: *Nature* 1999 401:6755 401 (6755 1999), pp. 788–791.
- [96] H. H. Lee et al. "Revisiting the Proportional Recovery Model in View of the Ceiling Effect of Fugl-Meyer Assessment". In: *Stroke* 52 (10 2021), pp. 3167–3175.
- [97] J. Lee and M. R. Muzio. "Neuroanatomy, extrapyramidal system". In: *Treasure Island (FL): StatPearls Publishing* (2022).
- [98] B. Lenzo, M. Bergamasco, and F. Salsedo. "Actuating method and device for human interaction multi-joint mechanisms". WO2013186701. 2015.
- [99] J. Liu et al. "The application of muscle wrapping to voxel-based finite element models of skeletal structures". In: *Biomechanics and Modeling in Mechanobiology* 11 (1-2 2012), pp. 35–47.
- [100] D. G. Lloyd and T. F. Besier. "An EMG-driven musculoskeletal model to estimate muscle forces and knee joint moments in vivo". In: *Journal of Biomechanics* 36 (6 2003), pp. 765–776.
- [101] G. E. Loeb and R. Davoodi. "Musculoskeletal Mechanics and Modeling". In: *Scholarpedia* 11 (11 2016), p. 12389.
- [102] A. Lohia and J. McKenzie. "Neuroanatomy, Pyramidal Tract Lesions". In: *StatPearls* (2022).
- [103] C. D. Luca. "Electromyography". In: *Encyclopedia of Medical Devices and Instrumentation* (2006).
- [104] I. Luis et al. "Evaluation of musculoskeletal models, scaling methods, and performance criteria for estimating muscle excitations and fiber lengths across walking speeds". In: *Frontiers in Bioengineering and Biotechnology* 10 (2022), p. 1865.
- [105] C. N. Maganaris and J. P. Paul. "Tensile properties of the in vivo human gastrocnemius tendon". In: *Journal of Biomechanics* 35 (12 2002), pp. 1639–1646.
- [106] S. P. Magnusson et al. "Load–displacement properties of the human triceps surae aponeurosis in vivo". In: *The Journal of Physiology* 531 (Pt 1 2001), p. 277.
- [107] M. Mancuso. "Evaluation and robotic simulation of the glenohumeral joint". PhD thesis. 2020.
- [108] M. Manto et al. "Consensus paper: roles of the cerebellum in motor control—the diversity of ideas on cerebellar involvement in movement". In: *Cerebellum (London, England)* 11 (2 2012), pp. 457–487.
- [109] R. Maruyama et al. "Detecting cells using non-negative matrix factorization on calcium imaging data". In: *Neural Networks* 55 (2014), pp. 11–19.

- [110] R. M. Maura et al. "Literature review of stroke assessment for upper-extremity physical function via EEG, EMG, kinematic, and kinetic measurements and their reliability". In: *Journal of NeuroEngineering and Rehabilitation* 20:1 20 (1 2023), pp. 1–32.
- [111] V. Mendez et al. "Current Solutions and Future Trends for Robotic Prosthetic Hands". In: *Annual Review of Control, Robotics, and Autonomous Systems* 4 (2021), pp. 595–627.
- [112] L. L. Menegaldo, A. D. T. Fleury, and H. I. Weber. "Moment arms and musculotendon lengths estimation for a three-dimensional lower-limb model". In: *Journal of Biomechanics* 37 (9 2004), pp. 1447–1453.
- [113] R. C. Miall. "Cortical motor control". In: *Neuroscience in the 21st Century: From Basic to Clinical* (2013), pp. 1187–1208.
- [114] M. Millard et al. "Flexing computational muscle: modeling and simulation of musculotendon dynamics". In: *Journal of biomechanical engineering* 135 (2 2013).
- [115] L. Modenese et al. "Estimation of musculotendon parameters for scaled and subject specific musculoskeletal models using an optimization technique". In: *Journal of Biomechanics* 49 (2 2016), pp. 141–148.
- [116] B. G. D. Monsabert et al. "Importance of Consistent Datasets in Musculoskeletal Modelling: A Study of the Hand and Wrist". In: *Annals of Biomedical Engineering* 46 (1 2018), p. 71.
- [117] A. Mousavi, H. Ehsani, and M. Rostami. "Compliant Vs. rigid tendon models: A simulation study on precision, computational efficiency and numerical stability". In: *2014 21st Iranian Conference on Biomedical Engineering, ICBME 2014* (2011), pp. 92–97.
- [118] T. Muraoka et al. "Estimation of passive ankle joint moment during standing and walking". In: *Journal of applied biomechanics* 21 (1 2005), pp. 72–84.
- [119] M. A. Murphy et al. "An overview of systematic reviews on upper extremity outcome measures after stroke". In: *BMC neurology* 15 (1 2015).
- [120] F. A. Mussa-Ivaldi and E. Bizzi. "Motor learning through the combination of primitives". In: *Philosophical Transactions of the Royal Society of London. Series B: Biological Sciences* 355 (1404 2000), pp. 1755–1769.
- [121] R. R. Neptune, D. J. Clark, and S. A. Kautz. "Modular control of human walking: a simulation study". In: *Journal of biomechanics* 42 (9 2009), pp. 1282–1287.
- [122] H. S. Neto et al. "Number and size of motor units in thenar muscles". In: *Clinical Anatomy* 17 (4 2004), pp. 308–311.
- [123] A. A. Nikooyan et al. "An EMG-driven musculoskeletal model of the shoulder". In: *Human Movement Science* 31 (2 2012), pp. 429–447.

- [124] S. Pandian and K. N. Arya. “Stroke-related motor outcome measures: Do they quantify the neurophysiological aspects of upper extremity recovery?” In: *Journal of Bodywork and Movement Therapies* 18 (3 2014), pp. 412–423.
- [125] C. Papazian et al. “Electromyography Recordings Detect Muscle Activity Before Observable Contractions in Acute Stroke Care”. In: *Archives of Rehabilitation Research and Clinical Translation* 3 (3 2021), p. 100136.
- [126] F. Péan. “Computational Modeling and Simulation of the Shoulder for Functional Analysis of Orthopedic Surgery Outcomes”. PhD thesis. 2021.
- [127] L. Pellegrino et al. “Stroke impairs the control of isometric forces and muscle activations in the ipsilesional arm”. In: *Scientific Reports* 2021 11:1 11 (1 2021), pp. 1–18.
- [128] A. O. Perotto. *Anatomical guide for the electromyographer: the limbs and trunk*. Charles C Thomas Publisher, 2011.
- [129] A. Picelli et al. “Rehabilitation and Biomarkers of Stroke Recovery: Study Protocol for a Randomized Controlled Trial”. In: *Frontiers in Neurology* 11 (2021), p. 1800.
- [130] C. Pierella et al. “A multimodal approach to capture post-stroke temporal dynamics of recovery”. In: *Journal of neural engineering* 17 (4 2020).
- [131] E. Pirondini et al. “Evaluation of the effects of the Arm Light Exoskeleton on movement execution and muscle activities: A pilot study on healthy subjects”. In: *Journal of NeuroEngineering and Rehabilitation* 13 (1 2016), pp. 1–21.
- [132] C. Pizzolato et al. “CEINMS: A toolbox to investigate the influence of different neural control solutions on the prediction of muscle excitation and joint moments during dynamic motor tasks”. In: *Journal of Biomechanics* 48 (14 2015), pp. 3929–3936.
- [133] J. A. Prinold et al. “Musculoskeletal shoulder models: A technical review and proposals for research foci”. In: *Proceedings of the Institution of Mechanical Engineers, Part H: Journal of Engineering in Medicine* 227 (10 2013), pp. 1041–1057.
- [134] C. Quental et al. “A multibody biomechanical model of the upper limb including the shoulder girdle”. In: *Multibody System Dynamics* 28 (1-2 2012), pp. 83–108.
- [135] M. F. Rabbi et al. “Non-negative matrix factorisation is the most appropriate method for extraction of muscle synergies in walking and running”. In: *Scientific Reports* 2020 10:1 10 (1 2020), pp. 1–11.
- [136] P. Raghavan. “Upper Limb Motor Impairment Post Stroke”. In: *Physical medicine and rehabilitation clinics of North America* 26 (4 2015), p. 599.

- [137] R. Raikova and H. Aladjov. “The influence of the way the muscle force is modeled on the predicted results obtained by solving indeterminate problems for a fast elbow flexion”. In: *Computer methods in biomechanics and biomedical engineering* 6 (3 2003), pp. 181–196.
- [138] J. Rasmussen, M. Damsgaard, and M. Voigt. “Muscle recruitment by the min/-max criterion – a comparative numerical study”. In: *Journal of biomechanics* 34 (3 2001), pp. 409–415.
- [139] J. Roh et al. “Alterations in upper limb muscle synergy structure in chronic stroke survivors”. In: *Journal of Neurophysiology* 109 (3 2013), pp. 768–781.
- [140] P. M. Rossini et al. “Post-stroke plastic reorganisation in the adult brain”. In: *The Lancet Neurology* 2 (8 2003), pp. 493–502.
- [141] K. S. Rudolph, M. J. Axe, and L. Snyder-Mackler. “Dynamic stability after ACL injury: who can hop?”. In: *Knee surgery, sports traumatology, arthroscopy: official journal of the ESSKA* 8 (5 2000), pp. 262–269.
- [142] A. M. Sabatini. “Identification of neuromuscular synergies in natural upper-arm movements”. In: *Biological Cybernetics* 86 (4 2002), pp. 253–262.
- [143] R. L. Sacco et al. “An Updated Definition of Stroke for the 21st Century”. In: *Stroke* 44 (7 2013), pp. 2064–2089.
- [144] P. Saltiel et al. “Muscle synergies encoded within the spinal cord: Evidence from focal intraspinal NMDA iontophoresis in the frog”. In: *Journal of Neurophysiology* 85 (2 2001), pp. 605–619.
- [145] E. Sarshari. “A Closed-Loop EMG-Assisted Shoulder Model”. PhD thesis. EPFL, 2018.
- [146] E. Sarshari et al. “A framework for forward-dynamics simulation of the human shoulder”. In: *11th Conference of the International Shoulder Group, ISG 2016* (2016).
- [147] E. Sarshari et al. “Muscle co-contraction in an upper limb musculoskeletal model: EMG-assisted vs. standard load-sharing”. In: *Computer methods in biomechanics and biomedical engineering* 24 (2 2020), pp. 137–150.
- [148] M. Sartori, D. Farina, and D. G. Lloyd. “Hybrid neuromusculoskeletal modeling to best track joint moments using a balance between muscle excitations derived from electromyograms and optimization”. In: *Journal of Biomechanics* 47 (15 2014), pp. 3613–3621.
- [149] M. Sartori, D. G. Llyod, and D. Farina. “Neural Data-Driven Musculoskeletal Modeling for Personalized Neurorehabilitation Technologies”. In: *IEEE transactions on bio-medical engineering* 63 (5 2016), pp. 879–893.
- [150] M. Sartori et al. “EMG-Driven Forward-Dynamic Estimation of Muscle Force and Joint Moment about Multiple Degrees of Freedom in the Human Lower Extremity”. In: *PLOS ONE* 7 (12 2012), e52618.

- [151] M. Sartori et al. “Estimation of musculotendon kinematics in large musculoskeletal models using multidimensional B-splines”. In: *Journal of Biomechanics* 45 (3 2012), pp. 595–601.
- [152] M. Sartori et al. “Robust simultaneous myoelectric control of multiple degrees of freedom in wrist-hand prostheses by real-time neuromusculoskeletal modeling”. In: *Journal of neural engineering* 15 (6 2018).
- [153] A. Scano et al. “Robotic assistance for upper limbs may induce slight changes in motor modules compared with free movements in stroke survivors: A cluster-based muscle synergy analysis”. In: *Frontiers in Human Neuroscience* 12 (2018), p. 290.
- [154] W. Senn et al. “Size principle and information theory”. In: *Biological cybernetics* 76 (1 1997), pp. 11–22.
- [155] W. Sheng et al. “Upper Limbs Muscle Co-contraction Changes Correlated With the Impairment of the Corticospinal Tract in Stroke Survivors: Preliminary Evidence From Electromyography and Motor-Evoked Potential”. In: *Frontiers in Neuroscience* 16 (2022), p. 717.
- [156] A. Shirazi-Adl et al. “Spinal muscle forces, internal loads and stability in standing under various postures and loads—application of kinematics-based algorithm”. In: *European Spine Journal* 14 (4 2005), p. 381.
- [157] T. Siebert et al. “Nonlinearities make a difference: comparison of two common Hill-type models with real muscle”. In: *Biological cybernetics* 98 (2 2008), pp. 133–143.
- [158] K. M. Steele, C. Papazian, and H. A. Feldner. “Muscle Activity After Stroke: Perspectives on Deploying Surface Electromyography in Acute Care”. In: *Frontiers in Neurology* 11 (2020), p. 576757.
- [159] K. M. Steele, M. C. Tresch, and E. J. Perreault. “Consequences of biomechanically constrained tasks in the design and interpretation of synergy analyses”. In: *Journal of neurophysiology* 113 (7 2015), pp. 2102–2113.
- [160] C. M. Stinear et al. “Advances and challenges in stroke rehabilitation”. In: *The Lancet. Neurology* 19 (4 2020), pp. 348–360.
- [161] Y. K. Tamilselvam et al. “Musculoskeletal model to predict muscle activity during upper limb movement”. In: *IEEE Access* 9 (2021), pp. 111472–111485.
- [162] A. Terrier et al. “A musculoskeletal shoulder model based on pseudo-inverse and null-space optimization”. In: *Medical engineering & physics* 32 (9 2010), pp. 1050–1056.
- [163] D. G. Thelen. “Adjustment of muscle mechanics model parameters to simulate dynamic contractions in older adults”. In: *Journal of biomechanical engineering* 125 (1 2003), pp. 70–77.

- [164] O. Till et al. "Characterization of isovelocity extension of activated muscle: A Hill-type model for eccentric contractions and a method for parameter determination". In: *Journal of Theoretical Biology* 255 (2 2008), pp. 176–187.
- [165] L. H. Ting and J. M. Macpherson. "A limited set of muscle synergies for force control during a postural task". In: *Journal of Neurophysiology* 93 (1 2005), pp. 609–613.
- [166] G. Torres-Oviedo, J. M. Macpherson, and L. H. Ting. "Muscle synergy organization is robust across a variety of postural perturbations". In: *Journal of Neurophysiology* 96 (3 2006), pp. 1530–1546.
- [167] M. C. Tresch, V. C. Cheung, and A. D'Avella. "Matrix factorization algorithms for the identification of muscle synergies: evaluation on simulated and experimental data sets". In: *Journal of neurophysiology* 95 (4 2006), pp. 2199–2212.
- [168] M. C. Tresch, P. Saltiel, and E. Bizzi. "The construction of movement by the spinal cord". In: *Nature Neuroscience* 1999 2:2 2 (2 1999), pp. 162–167.
- [169] P. Tropea et al. "Effects of early and intensive neuro-rehabilitative treatment on muscle synergies in acute post-stroke patients: A pilot study". In: *Journal of NeuroEngineering and Rehabilitation* 10 (1 2013), pp. 1–15.
- [170] C. W. Tsao et al. "Heart Disease and Stroke Statistics—2022 Update: A Report From the American Heart Association". In: *Circulation* 145 (8 2022), E153–E639.
- [171] J. D. Webb, S. S. Blemker, and S. L. Delp. "3D finite element models of shoulder muscles for computing lines of actions and moment arms". In: *Computer methods in biomechanics and biomedical engineering* 17 (8 2014), pp. 829–837.
- [172] J. M. Winters and L. Stark. "Analysis of fundamental human movement patterns through the use of in-depth antagonistic muscle models". In: *IEEE transactions on bio-medical engineering* 32 (10 1985), pp. 826–839.
- [173] R. D. Woittiez et al. "A three-dimensional muscle model: a quantified relation between form and function of skeletal muscles". In: *Journal of morphology* 182 (1 1984), pp. 95–113.
- [174] G. Wu et al. "ISB recommendation on definitions of joint coordinate systems of various joints for the reporting of human joint motion—Part II: shoulder, elbow, wrist and hand". In: *Journal of biomechanics* 38 (5 2005), pp. 981–992.
- [175] H. Yokoyama et al. "Cortical Correlates of Locomotor Muscle Synergy Activation in Humans: An Electroencephalographic Decoding Study". In: *iScience* 15 (2019), pp. 623–639.
- [176] G. I. Zahalak and S. P. Ma. "Muscle activation and contraction: constitutive relations based directly on cross-bridge kinetics". In: *Journal of biomechanical engineering* 112 (1 1990), pp. 52–62.

- [177] F. E. Zajac. “Muscle and tendon: properties, models, scaling, and application to biomechanics and motor control”. In: *Critical reviews in biomedical engineering* 17 (4 1989), pp. 359–411.
- [178] K. Zhao et al. “Evaluation of Methods for the Extraction of Spatial Muscle Synergies”. In: *Frontiers in Neuroscience* 16 (2022), p. 763.
- [179] M. Zheng et al. “Finite element models of the human shoulder complex: a review of their clinical implications and modelling techniques”. In: *International Journal for Numerical Methods in Biomedical Engineering* 33 (2 2017), e02777.

Tristan Barjavel



Rue des Entrepôts 6
1020 Renens

✉ tristan.barjavel@outlook.com
in linkedin.com/in/tbarjavel

☎ +41783199138

01.31.1992
French

Swiss B permit
Driving license



EDUCATION

- 2018 – Present** ● **Ph.D. in Mechanical Engineering**
ECOLE POLYTECHNIQUE FEDERALE DE LAUSANNE (EPFL), SWITZERLAND
Translational Neural Engineering Lab
Advisor: Prof. Silvestro Micera
- 2017** ● **MSc. in Mechanical Engineering**
ECOLE POLYTECHNIQUE FEDERALE DE LAUSANNE (EPFL), SWITZERLAND
Specialization : Biomechanics
Minor: Neuroprosthetics
- 2014** ● **BSc. in Mechanical Engineering**
ECOLE POLYTECHNIQUE FEDERALE DE LAUSANNE (EPFL), SWITZERLAND



WORK EXPERIENCE

- 2018- Present** ● **Ph.D Thesis: Understanding shoulder motor control and impairments**
ECOLE POLYTECHNIQUE FEDERALE DE LAUSANNE (EPFL), SWITZERLAND
TRANSLATION NEURAL ENGINEERING LAB OF PROF. SILVESTRO MICERA
Development of a numerical model of the human upper limb for muscle activation assessment and motor coordination understanding.
Clinical assessment of electromyography and kinematics of post-stroke patient using the ALEx robotic Exoskeleton
- 2016** ● **Intern – Swiss BioMotion Lab**
CHUV, LAUSANNE UNIVERSITY HOSPITAL
Lausanne, Switzerland
Introduction to analytical techniques of movement trajectories in hospitals and musculoskeletal diseases. View and reconstruction of the kinematics of the legs from a network of cameras.
- Summer 2012** ● **Internship – Atelier Gonin Moteur**
Lyon, France
Industrial internship:
-Understanding and Acquiring experience in machining
-Stock management
-high precision metrology



SKILLS

- Softwares** | C++, Python, Matlab, Simscape, ANSYS, COMSOL, Abaqus
Microsoft Office, Photoshop, LaTeX, Catia, SolidWorks, MSC software Adams,
- Languages** | French: mother language
English: full working proficiency
German: limited working proficiency
Chinese: elementary proficiency



CERTIFICATIONS

edX Certificate: MIT6.00.1x Computer Science and Programming using Python

AXELOS Global Best Practice: PRINCE2® 6th Edition Foundation in Project Management



PROJECTS

- Master Thesis: Design of a lower limb pediatric exoskeleton**
WYSS INSTITUTE FOR BIOLOGICALLY INSPIRED ENGINEERING AT HARVARD UNIVERSITY
MOTION ANALYSIS LABORATORY OF PROF. PAOLO BONATO, HARVARD MEDICAL SCHOOL, USA
Mechanical design and optimization of the exoskeleton's parts, control and sensing strategies. [09/2016-05/2017](#)
- Minor Project : Electrode design for retina electroporation optimization**
ECOLE POLYTECHNIQUE FEDERALE DE LAUSANNE (EPFL), SWITZERLAND
Using finite element analysis, model of the electric field for retinal electroporation with designed external electrodes, starting from anatomical data [Spring 2016](#)
- Semester Project : Lab In Tube**
ECOLE POLYTECHNIQUE FEDERALE DE LAUSANNE (EPFL), SWITZERLAND
Project management within a multidisciplinary team from the design to the production and implementation of miniaturized flexible microsenors in catheter's diameter tube to measure flow and temperature of blood like liquid. [Spring 2015](#)
- HYDROcontest: Design of the kit for the Hydrocontest competition**
HYDROS FOUNDATION
ECOLE POLYTECHNIQUE FEDERALE DE LAUSANNE (EPFL), SWITZERLAND
Design of the structure of the basic kit for the Hydrocontest project: a 1.5 meter motorboat race for student from different universities [Fall 2012](#)



IMPLICATIONS

- HACKAHEALTH GENEVA, SWITZERLAND : Board member. Search for sponsors and organizer of the annual Hackathon. [2019-present](#)
- HACKAHEALTH GENEVA - ECOLE POLYTECHNIQUE FEDERALE DE LAUSANNE (EPFL), SWITZERLAND: EPFL coordinator for the Assistive technologies challenge course. Creation of a university course based on the design of medical devices from a user-centric perspective. [2021](#)
- POLYSPORTS, LAUSANNE, SWITZERLAND : Sport accountant and then external communication manager for the PolySports, a sports competition between different student faculties. [2014-2016](#)
- ECOLE POLYTECHNIQUE FEDERALE DE LAUSANNE (EPFL), SWITZERLAND: Coach with a professional formation for freshmen in mechanical engineering [2011-2014](#)



CENTER OF INTERESTS

Handball: EPFL's team captain, **Sailing:** Windsurf, Catamaran, **Golf, Judo:** Brown Belt, **Cinema, Piano:** 5 years in a music school, **Cooking**

141

